



TECHNISCHE UNIVERSITÄT MÜNCHEN

Fakultät für Chemie

Lehrstuhl für Technische Chemie II

Zeolite catalyzed dehydration of substituted cyclic alcohols in aqueous phase

Peter Heinrich Hintermeier

Vollständiger Abdruck der von der Fakultät für Chemie der Technischen Universität München zur Erlangung des akademischen Grades eines

Doktors der Naturwissenschaften (Dr. rer. nat.)

genehmigten Dissertation.

Vorsitzender: Prof. Dr. Thomas Brück

Prüfer der Dissertation: 1. Prof. Dr. Johannes A. Lercher

2. Prof. Dr. Klaus Köhler

Die Dissertation wurde am 09.05.2017 bei der Technischen Universität München eingereicht und durch die Fakultät für Chemie am 01.06.2017 angenommen.

*„Nur wenige wissen, wie viel man
wissen muss, um zu wissen, wie
wenig man weiß“*

Werner Heisenberg (1901 - 1976)

Für meine Eltern

Abstract

The position of the alkyl and hydroxyl group decides on the dehydration mechanism of substituted cyclohexanols. Octahedrally coordinated aluminum in MFI zeolites with low Si/Al ratios (12 and 15) led to lower (ca. 10 kJ·mol⁻¹) activation barriers in case of the concerted elimination (*cis* 2-methylcyclohexanol), whereas the barrier was higher (ca. 10 kJ·mol⁻¹) for the dehydration pathway *via* carbocations (*cis/trans* 4-methylcyclohexanol). Increasing zeolite confinement (FAU → BEA → MFI) increased the turnover frequencies of the catalytically active hydronium ions. The resulting higher rates of a tertiary alcohol (1-methylcyclohexanol) are driven by decreasing enthalpies of activation (ΔH^{\ddagger}), whereas the higher TOFs in case of a primary alcohol (2-cyclohexylethanol) are entropically (ΔS^{\ddagger}) controlled.

Kurzzusammenfassung

Die Stellung der Alkyl- und Hydroxylgruppe entscheidet über den Mechanismus der Dehydratisierung von substituierten Cyclohexanolen. Oktaedrisch koordiniertes Aluminium in MFI Zeolithen mit niedrigem Si/Al-Verhältnis (12 und 15) führte zu niedrigeren (ca. 10 kJ·mol⁻¹) Aktivierungsbarrieren im Falle der konzertierten Eliminierung (*cis* 2-Methylcyclohexanol), während die Barriere höher (ca. 10 kJ·mol⁻¹) für den Reaktionspfad über Carbeniumionen (*cis/trans* 4-Methylcyclohexanol) war. Kleinere Zeolithporen (FAU → BEA → MFI) erhöhten die Wechselzahlen der katalytisch aktiven Hydroniumionen. Die resultierenden höheren Raten eines tertiären Alkohols (1-Methylcyclohexanol) sind durch niedrigere Aktivierungsenthalpien (ΔH^{\ddagger}) begründet, während die höheren Wechselzahlen im Falle eines primären Alkohols (2-Cyclohexylethanol) durch die Entropie (ΔS^{\ddagger}) begünstigt werden.

Danksagung

Zuerst möchte ich mich bei Prof. Dr. Johannes A. Lercher für die Aufnahme in seine Arbeitsgruppe (Lehrstuhl für Technische Chemie II) und die interessante Themenstellung bedanken. Besonders schätzte ich die Vielfalt des Forschungsthemas. Die gemeinsame Arbeitsatmosphäre war ebenso freundschaftlich wie lehrreich und interessant. Vielen Dank Johannes, ich habe in den vergangenen 3 ½ Jahren sehr viel von Dir gelernt und konnte mich immer auf Dich verlassen.

Weiterer Dank gilt Dr. Eszter Baráth, die im Rahmen ihrer Habilitation meine Dissertation betreute. Vielen Dank für die Zeit, in der wir gemeinsam freundschaftlich zusammengearbeitet haben. Danke auch an Dr. Donald Camaioni, Dr. Hui Shi, Dr. Mariefel Olarte (alle PNNL), Prof. Dr. Gary Haller und Dr. Yue Liu für die hilfreichen und konstruktiven Diskussionen. Außerdem möchte ich mich bei Apl. Prof. Dr. Andreas Jentys bedanken, der immer hilfreich mit guten Ideen zur Verfügung stand.

Dankeschön an Franz Xaver Hecht, der zu allen Problemen bezüglich Reaktoren oder Geräten immer eine Lösung fand. Vielen herzlichen Dank an Ulrike Sanwald und Stefanie Seibold für die Hilfsbereitschaft und die exzellente Organisation des Lehrstuhllalltags, an Bettina Federmann für die reibungslose und zuverlässige Abwicklung aller finanziellen Angelegenheiten, an Andreas Marx für die Hilfe bei Problemen rund um Computer und Elektronik, sowie an Martin Neukamm für die Verwaltung aller Chemikalien und die SEM- und AAS-Analytik.

Vielen Dank an meinen Projektkollegen Sebastian Eckstein, den ich als Freund und als Arbeitskollegen sehr schätze. Danke für die freundschaftliche, ehrliche und kreative Zusammenarbeit.

Vielen herzlichen Dank an alle Bürokollegen für die angenehme Atmosphäre und die gemeinsame lustige Zeit: Felix Kirchberger, Ferdinand Vogelgsang, Elisabeth Hanrieder, Sebastian Müller, Maximilian Werner Hahn, sowie den Bürogästen Bruno Dalla Costa und Sebastian Prodingler. Besonderer Dank geht an Matthias Steib, der vom ersten bis zum letzten Tag mein Schreibtischnachbar war.

Ich möchte mich bei allen Kollegen bedanken mit denen ich schöne und lustige Erlebnisse teilen durfte (Konferenzreisen, Fussball, Mittagspausen, etc.): Daniel Melzer, Andreas Ehrmaier, Kai Sanwald, Yuanshuai Liu, Stanislav Kasakov, Christian Gärtner, Martin Baumgärtl, Martina Braun, Manuel Wagenhofer, Manuel Weber, Sylvia Albersberger, Tobias Berto, Guoju Yang, Takaaki Ikuno, Moritz Schreiber, Sebastian Foraita, Sebastian Grundner, Edith Ball, Yu Lu, Bo Peng, Yuchun Zhi, Udishnu Sanyal, Marco Peroni, Christoph Denk, Verena Höpfl,

Teresa Schachtl, Ruixue Zhao, Yang Song, Yang Zhang, Wanqiu Lou, Navneet Gupta und Ricardo Bermejo Deval.

Vielen Dank an die Betreuer meiner Forschungs- und Abschlussarbeiten: Stefan Schallmoser, Linus Schulz, Sebastian Müller und Mark Maturi.

Ich möchte allen Forschungspraktikanten, Semesteranden und Bacheloranden für die Mithilfe bei den Experimenten danken. Besonderer Dank gilt den Masteranden Felix Kirchberger, Harry Renges, Paulina Waligorski und Philipp Pfauser. Vielen Dank für eure Unterstützung!

Vielen Dank für die wunderbare Studienzeit: Maxi, Patrick, Jan, Mähli, Tossi, Georg, Anna, Martin, Thomas, Manu, Rinat, Cons, Hannes, Hendrik, Rina, Anna, Marian, C. Streck, C. Baier und Stuff.

Danke an alle Aö-Freunde für die jahrelange und treue Freundschaft.

Vielen, vielen Dank für alles und die schöne gemeinsame Zeit, liebe Carolin.

Der größte Dank gilt meiner Familie, besonders meinen Eltern. Ohne eure Hilfe und Unterstützung hätte ich das alles mit Sicherheit nicht geschafft und wäre nicht da, wo ich heute stehe. Vielen herzlichen Dank für alles. Ihr seid die Besten!

Peter

List of abbreviations

A_{pre}	Pre-exponential factor of the Arrhenius equation
BAS	Brønsted acid site
BEA	Zeolite framework type code: Beta
c	Concentration
°C	Degree Celsius
CyOH	Cyclohexanol
E_a	Activation energy
EcyOH	Ethylcyclohexanol
EFAI	Extra-framework aluminum
FAU	Zeolite framework type code: Faujasite
ΔG^{\ddagger}	Standard Gibbs energy of activation
h	Planck's constant ($6.6261 \cdot 10^{-34}$ J·s)
ΔH^{\ddagger}	Standard enthalpy of activation
IR	Infrared
J	Joule
K	Equilibrium constant
k	Rate constant
k_B	Boltzmann's constant ($1.3807 \cdot 10^{-23}$ J·K ⁻¹)
kJ	Kilojoule
L	Liter
LAS	Lewis acid site
LTA	Zeolite framework type code: Linde Type A
M	Molar

m	Mass
mg	Milligram
mL	Milliliter
McyOH	Methylcyclohexanol
MFI	Zeolite framework type code: Mordenite framework inverted
mol	Molar amount ($6.022 \cdot 10^{23} \text{ mol}^{-1}$)
n	Reaction order
n	Molar amount
NMR	Nuclear Magnetic Resonance
p	Pressure
PcyOH	Propylcyclohexanol
ppm	Parts per million (10^{-6})
py	Pyridine
R	Universal gas constant ($8.3145 \text{ J} \cdot \text{K}^{-1} \cdot \text{mol}^{-1}$)
r	Reaction rate
S	Selectivity
s	Second
ΔS^{\ddagger}	Standard entropy of activation
SI	Supporting information
T	Temperature
t	Time
t_R	Reaction time
TOF	Turnover frequency
TPD	Temperature programmed desorption

ΔU^{\ddagger}	Standard internal energy of activation
V	Volume
ΔV^{\ddagger}	Standard volume of activation
X	Conversion
Y	Yield
ZSM-5	Zeolite Socony Mobil-5
2-CyEtOH	2-cyclohexylethanol

Table of Contents

1. Theoretical background	1
1.1. Research project and motivation	1
1.2. Elimination reactions in acid catalysis	5
1.3. Zeolite catalysts	6
1.4. Chemical kinetics and transition state theory.....	11
1.5. References	16
2. Hydronium ion catalyzed elimination pathways of substituted cyclohexanols	18
2.1. Introduction	19
2.2. Experimental	21
2.3. Results and discussion	24
2.4. Conclusions	35
2.5. References	36
2.6. Supporting information	38
3. Influence of acid site concentration and extra-framework aluminum in MFI zeolites on aqueous phase dehydration	53
3.1. Introduction	54
3.2. Experimental	55
3.3. Results and discussion	59
3.4. Conclusions	67
3.5. References	68
3.6. Supporting information	69
4. Impact of confinement on aqueous phase dehydration of substituted cyclic alcohols	90
4.1. Introduction	91
4.2. Experimental	92
4.3. Results and discussion	94

4.4. Conclusions	103
4.5. References	104
4.6. Supporting information	105
5. Summary	126
6. Zusammenfassung	129
7. List of publications	132
8. Curriculum vitae	133

1. Theoretical background

1.1. Research project and motivation

The overall aim of this research project was to gain a fundamental understanding of the catalytic key steps (hydrogenation, alkylation and dehydration) of biomass derived pyrolysis oil upgrading into transportation fuels (gasoline/diesel range).

Biomass mainly consists of cellulose (40 – 80%), hemicellulose (15 – 30%) as well as lignin (10 – 25%).^[1] Cellulose is a crystalline glucose polymer with an extended, flat, 2-D helical conformation, which consists of linear polysaccharides with β -1,4-linkages of D-glucopyranose monomers. The conformation of the chain is reinforced and maintained by hydrogen bonds.^[2] Hemicellulose is an amorphous and branched polymer consisting of five-carbon sugars (xylose and arabinose) and six-carbon sugars (galactose, glucose and mannose), which are highly substituted with acetic acid.^[3] This polysaccharide occurs in association with cellulose in the cell walls. Lignin is a highly branched, substituted, mononuclear aromatic polymer particularly present in the cell walls of woody biomass and often associated with cellulosic and hemicellulosic material.^[3] The irregular polymer formed by an enzyme-initiated free-radical polymerization of coniferyl, sinapyl and coumaryl alcohols.^[3] Softwood lignin mainly consists of coniferyl alcohol, whereas sinapyl alcohol is the major component of hardwood lignin. All three alcohol monomers are present in grass lignin.^[1]

A schematic representation of lignin is illustrated in **Figure 1.1**.^[4]

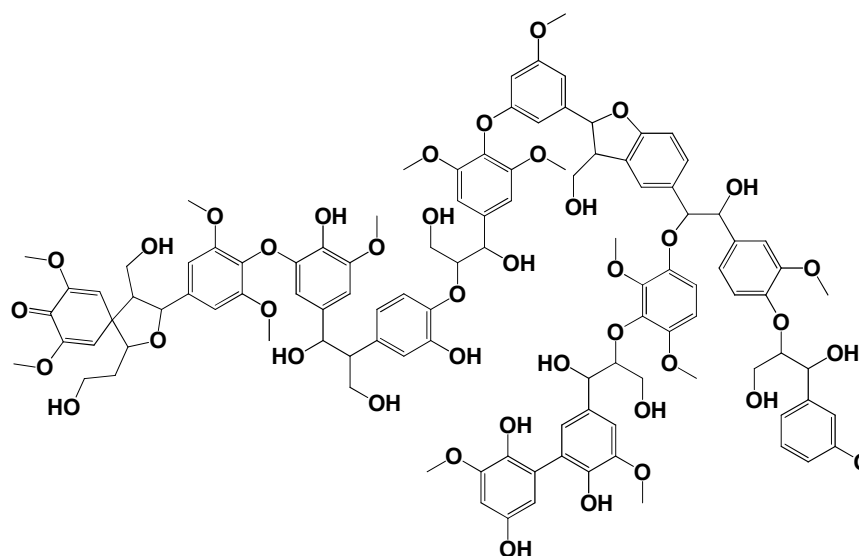


Figure 1.1. An exemplary excerpt of lignin (adapted from ref.^[4]).

Upgrading of lignin-derived biomass is a promising alternative in producing renewable fuels. Bio-oil is produced by converting solid biomass to liquid through solvolysis, hydrothermal liquefaction or fast pyrolysis.^[5] Although the products of high-pressure liquefaction possess properties more similar to transportation fuels, it is comparatively expensive due to the high capital cost.^[1] The obtained bio-crude still requires upgrading to produce hydrocarbons. Fast pyrolysis seems to be the more promising route mainly because of lower cost despite the need for further upgrading.^[6] Pyrolysis leads to liquid products of high yield (ca. 70%) by short residence times and fast heating in absence of oxygen at temperatures between 380 – 530 °C and pressures of 1 to 5 atm.^[1]

Nevertheless, bio-oil has several limitations, including high oxygen content, poor volatility, high viscosity, cold flow problems, corrosiveness (pH value of 2.5), high water content (difficulties in ignition) and coking of thermally unstable compounds.^[6] In general, bio-oil has a lower heating value (ca. 17 MJ·kg⁻¹) compared to conventional fuel oil (ca. 43 MJ·kg⁻¹).^[1]

The characteristics of the lignocellulose-based bio-oil significantly depend on the type of feedstock (e.g. wood, agricultural wastes and forest wastes), its water and protein content, heat transfer rate, residence time as well as reaction temperature. Generally, more than 400 different compounds can be found in bio-oil. These molecules are formed during pyrolysis by depolymerization and fragmentation reactions (e.g. hydrolysis, dehydration, isomerization, dehydrogenation, aromatization, retro-condensation and coking) from the three building blocks of lignocellulose: cellulose, hemicellulose and lignin.^[1, 7]

Compounds which are derived from lignin are mainly phenol derivatives like catechol or guaiacol. Sugars, furans and various small oxygenates are obtained by depolymerization of cellulose and hemicellulose. The decomposition of these oxygenates, sugars and furans form various acids (e.g. acetic acid), esters (e.g. butyrolactone), alcohols (e.g. methanol), ketones (e.g. acetone) and aldehydes (e.g. acetaldehyde).^[1, 8]

Storage of pyrolysis bio-oil is a critical issue due to multiple reactions occurring with time and temperature. Pyrolysis oil is chemically unstable and tends to polymerize, induced by ultraviolet light, oxygen exposure and elevated temperatures. These chemical modifications lead to an increasing viscosity and phase separation and deteriorate the quality of the obtained bio-oil.^[1, 6, 9]

Lignin requires at first a cleavage of the phenol linking C-O-C-bonds to be converted in a practical way.^[10] Pyrolysis oil contains a high proportion of water (ca. 30 wt.-%) and plenty of substituted phenolic compounds with methyl-, ethyl-, hydroxyl- or methoxy groups.^[11] **Figure 1.2.** represents a collection of prominent compounds found in pyrolysis oil.^[1, 4-7, 11]

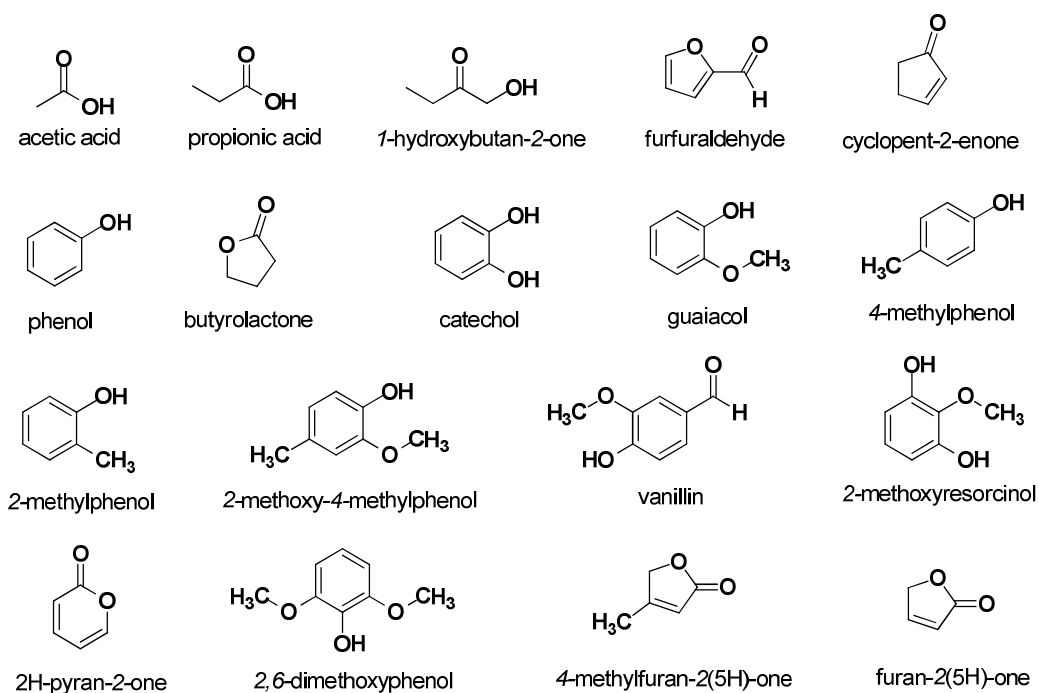
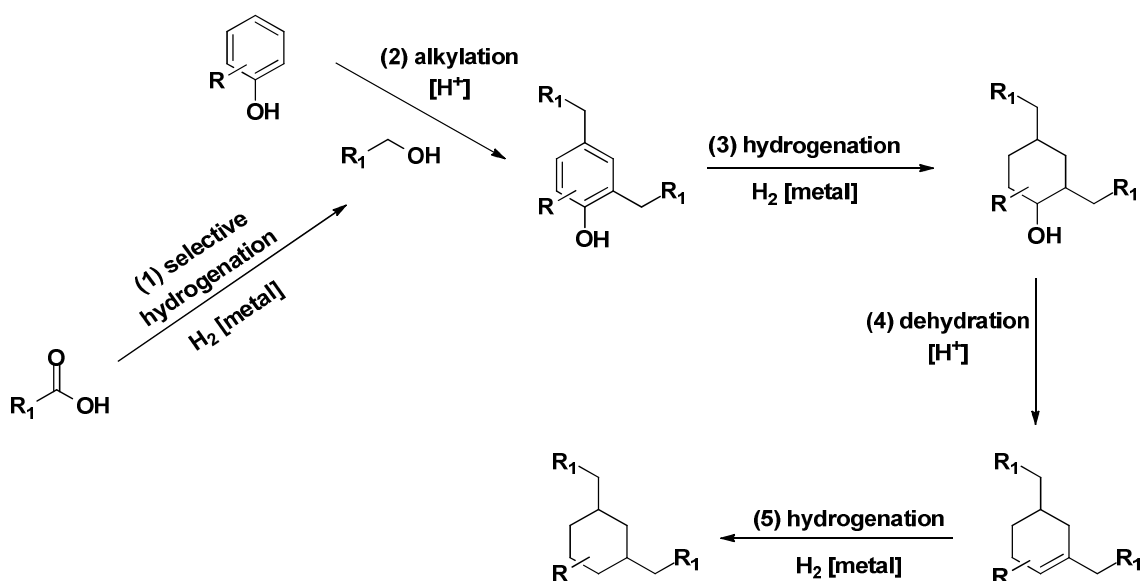


Figure 1.2. Representative model compounds found in pyrolysis oil (based on ref.^[1, 4-7]^[11])

The quantitative composition of pyrolysis oil depends on the process conditions (time, temperature, heating ramp, etc.) as well as on the feedstock (soft wood, hard wood, etc.). The sugars and highly reactive aldehydes tend to polymerize at low temperatures ($T < 100$ °C) in the presence of acid catalysts, which causes problems in further upgrading steps. The various phenolic compounds can be used as important chemicals or transportation fuels after hydrodeoxygenation. This includes the transformation of aromatic compounds into saturated cyclic alcohols *via* metal catalyzed hydrogenation and the removal of oxygen *via* acid catalyzed dehydration to produce olefinic cyclic compounds.

The research project's reaction cascade is schematically illustrated in **Scheme 1.1**. Based on the high water content of pyrolysis oil and a desired conversion without any purification, all reactions were investigated in aqueous phase.



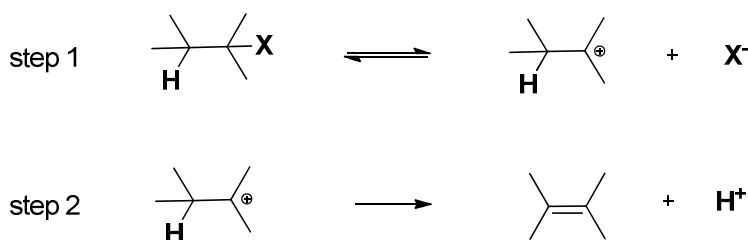
Scheme 1.1. The essential reaction steps of pyrolysis oil upgrading.

The ideal conception would be the performance of this reaction cascade in one batch with a bifunctional catalyst, which provides catalytically active metal as well as acid sites. Each reaction step was investigated separately in this project to determine chemical kinetics. The three key steps were (i) the valuable application of the short chain acids *via* reduction, (ii) the alkylation of the produced alcohols to phenolic compounds and (iii) the oxygen removal of the substituted and saturated cyclic alcohols.

The first part of the overall project (**Scheme 1.1.**, reaction **(1)**) was the reduction of short chain acids (e.g. acetic acid) on supported metal catalysts in the presence of hydrogen to obtain alcohols. A further task was the alkylation of phenolic compounds (e.g. phenol, guaiacol, catechol) with the produced alcohols (e.g. ethanol) *via* the zeolite catalyzed electrophilic aromatic substitution (**Scheme 1.1.**, reaction **(2)**). Main intention of this reaction was the maintenance of the carbon balance. In a next step, the alkylated phenolic compounds were hydrogenated in the presence of metal catalysts (**Scheme 1.1.**, reaction **(3)**). The acid catalyzed oxygen removal of substituted cyclohexanols (**Scheme 1.1.**, reaction **(4)**) is focus of this work. Based on the presence of 2- and 4-methylphenol and the favored *ortho* and *para* positions in the alkylation of phenolic compounds, especially 2- and 4-methylcyclohexanol as well as 2- and 4-ethylcyclohexanol will be discussed in detail in the upcoming chapters. Furthermore, the impact of catalyst properties like the Brønsted acid site concentration as well as the zeolite confinement on dehydration were investigated. The hydrogenation of the produced substituted cyclohexenes (**Scheme 1.1.**, reaction **(5)**) was not investigated in this project.

1.2. Elimination reactions in acid catalysis

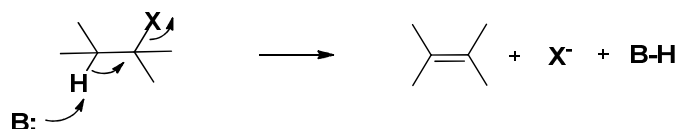
The E1 mechanism (elimination, monomolecular) is a two-step process in which generally the rate determining step is the formation of a carbocation with a subsequent elimination of a β -H (**Scheme 1.2.**).^[12]



Scheme 1.2. E1 elimination mechanism.^[12]

In general, the E1 mechanism proceeds without the addition of a base. The first step is the same as in nucleophilic substitution reactions (S_N1). In the second step the solvent usually abstracts the β -H, contrary to the S_N1 process where the positively charged carbon is attacked. In a pure E1 reaction (without ion pairs, etc.), the product generally is not stereospecific, since the carbocation is free to adopt its most stable conformation before the elimination of the proton.^[12]

In the E2 mechanism (elimination, bimolecular), the leaving group **X** as well as the β -H depart simultaneously. In general, the proton is pulled off by a base **B** (**Scheme 1.3.**).^[12]



Scheme 1.3. E2 elimination mechanism.^[12]

The E2 mechanism proceeds *via* one step and is second order from a kinetically point of view: first order in substrate and first order in base. It is analogous to the S_N2 mechanism and often competes with it. With respect to the substrate, the difference between the two pathways is whether the species with the unshared pair of electrons acts as a nucleophile and attacks the carbon or acts as a base and abstracts the hydrogen. The leaving group can be positive or neutral and the base may be negatively charged or neutral. In general, *anti*-elimination is favored in the E2 mechanism but among others, steric (inability to form the *anti*-periplanar transition state), conformational, and ion pairing cause *syn*-elimination to predominate in special cases.^[12]

There are general rules concerning the regiochemistry of the formed double bond. According to *Bredt's rule*^[13], the double bond is not formed between a bridgehead-carbon, except the ring sizes

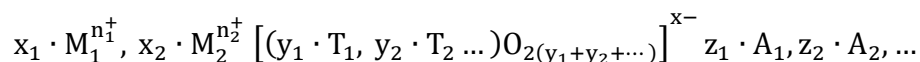
are large enough. In common, the conjugated product predominates: if there is already a double bond (C=C or C=O) or an aromatic ring in the molecule, the new C=C double bond forms in a way that it can be in conjugation. The selectivity within an E1 mechanism is determined by the relative stabilities of the possible alkenes. According to *Saytzeff's rule*^[14], the double bond is formed with the most highly substituted carbon (largest possible number of alkyl groups on the C=C carbons). If the new bond is formed with the least highly substituted carbon, the selectivity follows *Hofmann's rule*^[15]. In case of an anti E2 elimination, a *trans* β-H is required; if this is only accessible in one direction (in cyclic systems), the double bond will form this way. Syn E2 eliminations mainly lead to the *Hofmann-product*.^[12]

The impact of substrate structure on the elimination mechanism is induced by substituents on the α- and/or β-carbon either by stabilizing effects on the double bond, positive or negative charges or by steric effects. A further parameter, which has an influence on the mechanism, is the solvent, which might act as an attacking base (H₂O). Finally the leaving group can shift the reaction mechanism. Better leaving groups tend to drive the elimination *via* E1.^[12]

1.3. Zeolite catalysts

Aluminosilicate zeolites are microporous crystallized solids with a three-dimensional structure and a regular framework formed by linked TO₄-tetrahedra (T = Si, Al, ...), where each oxygen is shared between two T-elements. The channels and cavities with molecular sizes can host charge compensating cations, water or other molecules and salts.^[16]

The general composition of a zeolite can be described as follows:^[16]



The framework composition is defined in square brackets and the other terms represent the species in the micro pores:

- M₁, M₂,...: cations with charge n₁, n₂,..., which compensate the negative charge of the framework (x₁n₁ + x₂n₂ + ... = x)
- T₁, T₂,...: elements (Si, Al,...) in the tetrahedral (T-elements)
- A₁, A₂,...: water, molecules or ion pairs.^[16]

The field of zeolites applications in chemical industry and catalysis is manifold. A few examples are raw oil refining, petrochemical processes, production of fine chemicals, control and purification of exhaust gases, separation and adsorption processes. Zeolites can be tailored by synthesis according to the desired characteristics like crystal structure and size, porosity, pore diameter, a wide range of acidity, high hydrothermal stability and a high resistance against poisons. Also postsynthetic modifications like dealumination, silanization, ion exchange, impregnation and regeneration are possible.^[16]

A wide range of different zeolite structures can be produced by a high variety of template molecules used in synthesis. The different zeolite structure types can be distinguished according to the channel and pore dimensions as well as geometry, which decisively affect the shape selectivity. Today more than 170 different structure types are known. There are three groups, which can be distinguished according to their pore diameter (**Table 1.1.**)^[16]

	Small-pore zeolites	Medium-pore zeolites	Large-pore zeolites
Pore geometry	8-membered ring	10-membered ring	12-membered ring
Pore diameter	3.5 - 4.5 Å	4.5 - 6.0 Å	6.0 - 8.0 Å
Example	Zeolite A (LTA)	ZSM-5 (MFI)	Zeolite Y (FAU)

Table 1.1. Three classes of zeolites according to the pore geometry.^[16]

The sodalite cages of “Zeolite A” (LTA – “Linde type A” structure type, **Figure 1.3.**) are in a primitive cubic arrangement and joined *via* double 4-rings, which form α -cages in the center of the unit cell and a 3-dimensional, 8-ring channel system. In other words, the framework can be described as a primitive cubic arrangement of α -cages joined through single 8-rings, which produce a sodalite cage in the center. LTA is used as a desiccant as well as ion-exchanger in laundry detergents to prevent the formation of carbonates by trapping Mg^{2+} or Ca^{2+} .^[17]

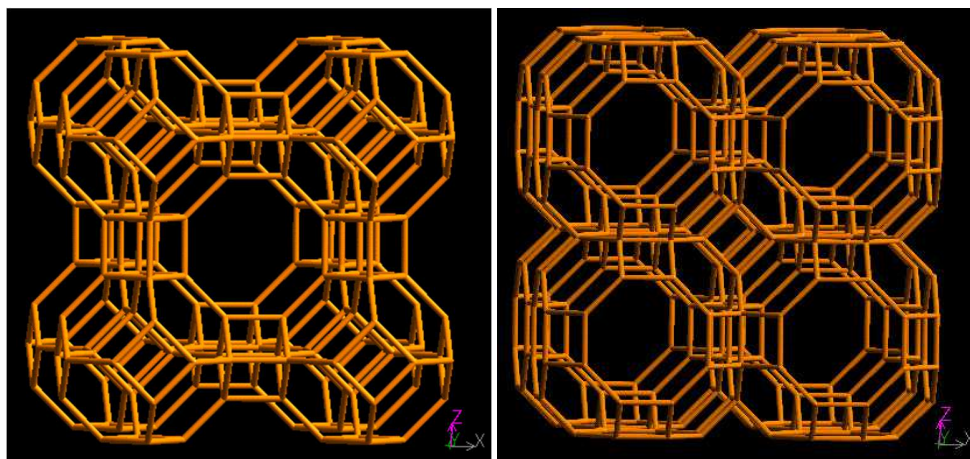


Figure 1.3. Structure and pore geometry of Zeolite A, LTA structure type (taken from ref.^[18]).

The sodalite cages in “Y-zeolite” (FAU – “*faujasite*” structure type, **Figure 1.4.**) are arranged in the same way as the carbon atoms in diamond, and are joined to one another *via* double 6-rings. These “supercages” have four, tetrahedrally-oriented, 12-ring pore openings and a 3-dimensional channel system.^[17] FAU is mainly used in the fluidized catalytic cracking (FCC) process where long hydrocarbons are cracked into lighter fractions.^[19]

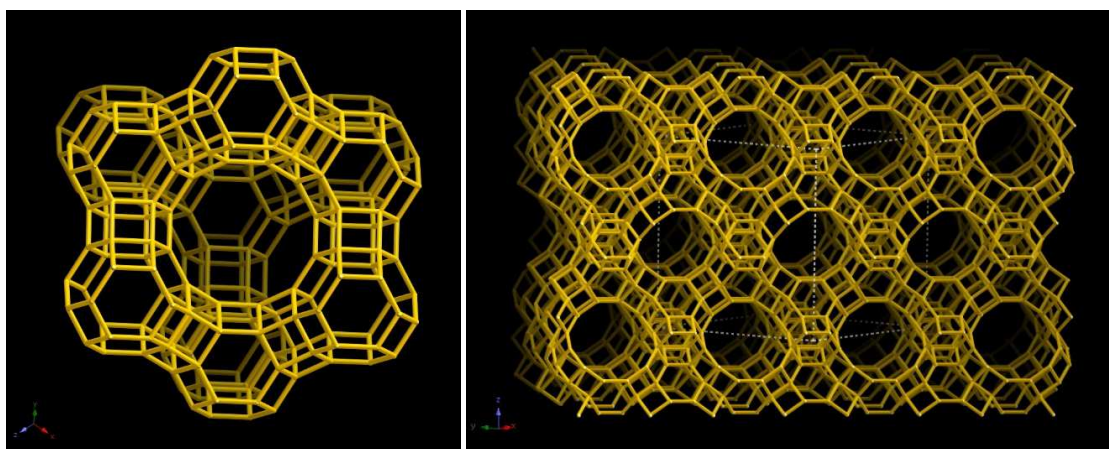


Figure 1.4. Structure and pore geometry of Y-Zeolite, FAU structure type (taken from ref.^[18]).

The well-defined layers of zeolite beta (BEA – “*beta*” structure type, **Figure 1.5.**) are stacked in a more or less random fashion. The four 5-ring units are joined *via* 4-rings to form layers with saddle-shaped 12-rings. Adjacent layers are related by a rotation of 90°. The disorder arises because this rotation can be in either a clockwise or a counterclockwise sense. If one rotation was maintained throughout the crystal, the structure would be ordered and chiral. All zeolite beta reported to date show extreme disorder and have a 3-dimensional 12-ring channel system independent of the

stacking sequence.^[17] BEA is industrially used for NO_x reduction in purification of exhaust gases in form of Fe-zeolites in selective catalytic reduction.^[20]

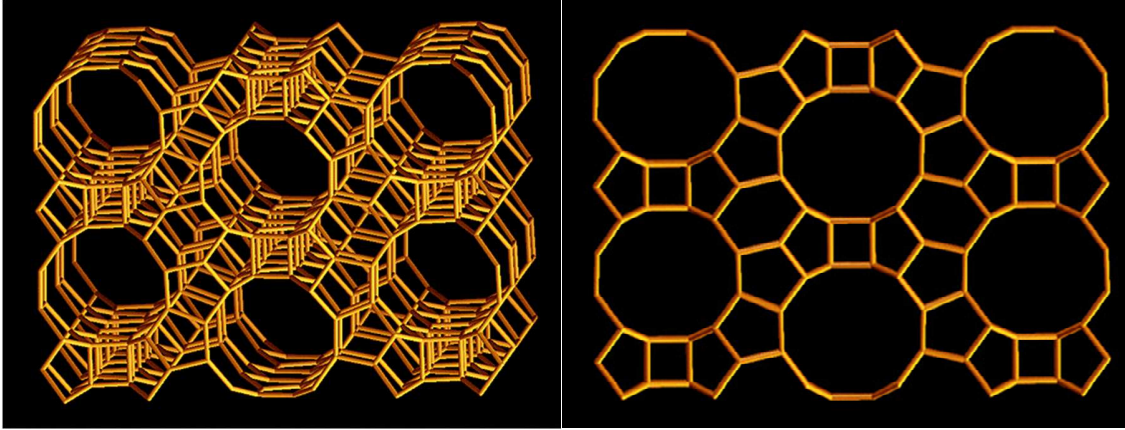


Figure 1.5. Structure and pore geometry of BEA zeolite, Beta structure type (taken from ref.^[18]).

In “ZSM-5” (MFI – “mordenite framework inverted” structure type, **Figure 1.6.**), the pentasil units are linked to form chains, which are linked by oxygen bridges to form corrugated sheets with 10-ring holes. These sheets are linked by oxygen bridges, which form a 3-dimensional structure. Straight 10-ring channels parallel to the corrugations and sinusoidal 10-ring channels perpendicular to the sheets are produced this way. The sinusoidal channels are linked to the straight channels and form a 3-dimensional 10-ring channel system.^[17] The industrial applications of MFI are manifold like isomerization of xylene, alkylation of benzene and the methanol-to-olefin (MTO) process, just to name a few.^[16]

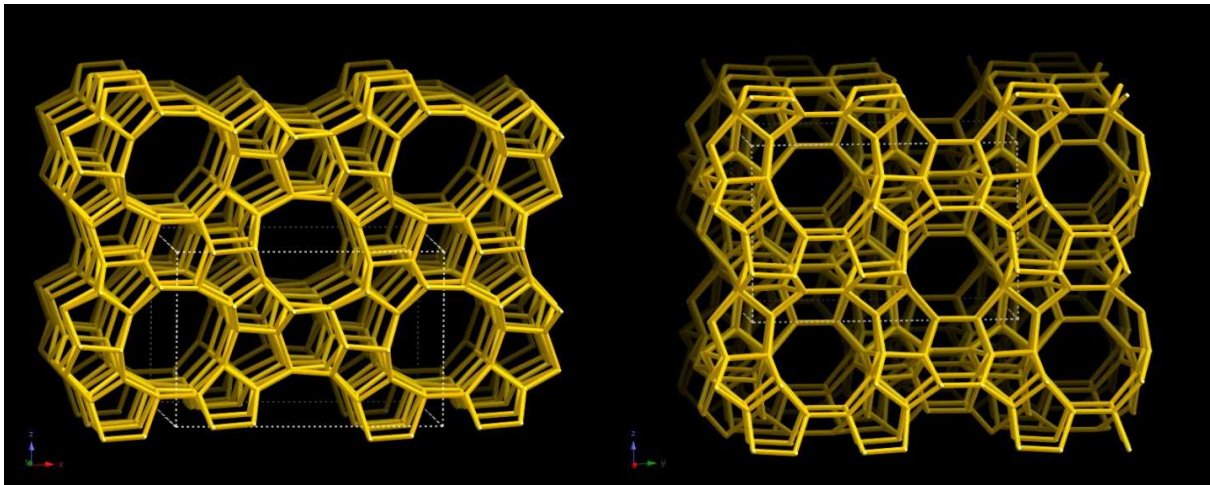


Figure 1.6. Structure and pore geometry of ZSM-5 zeolite, MFI structure type (taken from ref.^[18]).

The template molecules determine the unique zeolite specific character of shape selectivity. **Figure 1.7.** schematically illustrates the principle of shape selectivity, which includes three different types. *Reactant selectivity* is exemplarily illustrated by the preferred conversion of linear alkanes (*n*-heptane) compared to branched hydrocarbons (*iso*-heptane isomers) in catalytic cracking. Zeolite catalyzed alkylation of toluene with methanol to obtain the desired *para*-xylene is a typical example for *product selectivity*. The principle of *restricted transition state-type selectivity* is used in the *trans*-alkylation process of *meta*-xylene to obtain 1,2,4-trimethylbenzene and toluene.^[19]

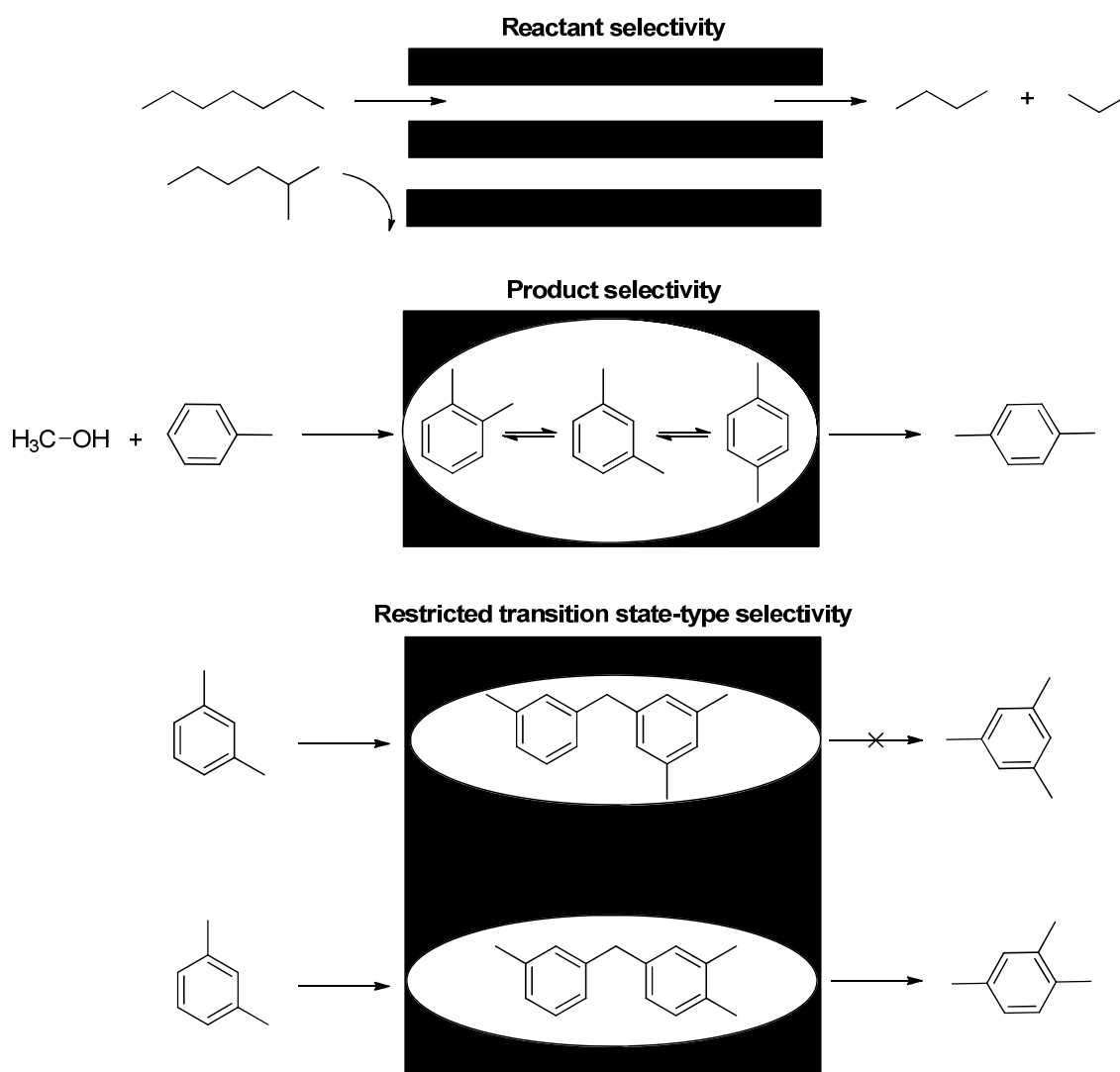


Figure 1.7. Schematic illustration of *reactant selectivity*, *product selectivity* and *restricted transition state-type selectivity* (adapted from ref.^[19]).

The acidity is another tunable factor, which is introduced to zeolite systems by the incorporation of Al^{3+} instead of Si^{4+} into the framework. According to *Löwenstein's rule* aluminosilicate zeolites are only stable if incorporated aluminum atoms are separated by at least one Si-bridge.^[16]

The term “*acid site density*” describes the zeolite’s concentration of acid sites ($\text{mol}\cdot\text{g}_{\text{cat}}^{-1}$, extensive property). Furthermore, the term “*acid strength*” describes the ability to protonate bases of different strengths (intensive property).^[16]

Acid site density can be adjusted by the module $\text{SiO}_2/\text{Al}_2\text{O}_3$ (also: Si/Al) of the reaction mixture’s composition. If the negative charge is compensated with H^+ (after ammonium exchange and calcination), two different types of acid sites are distinguishable: Brønsted and Lewis acid sites (**Figure 1.8.**). These acid sites react in the same way as inorganic acids: Brønsted acid sites are able to donate a proton and Lewis acid sites are species able to accept an electron pair to form a dative or coordinate bond.^[16]

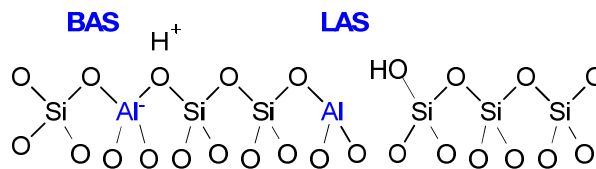


Figure 1.8. Illustration of Brønsted (BAS) and Lewis acid sites (LAS) in zeolites (adapted from ref.^[21]).

1.4. Chemical kinetics and transition state theory

The most important equations of chemical kinetics, which are used in the following chapters are shortly introduced in this section. The definitions of the terms *conversion*, *yield*, *selectivity*, *reaction rate* and *turnover frequency* are presented. Furthermore, the dependence of substrate concentration as well as temperature on reaction rates are elucidated. Finally, the concept of the transition state theory is concisely described.

The *conversion* X is defined as the amount of reactant, which was converted during the reaction period. The conversion is expressed as fraction of the initial amount of reactant $n_{\text{reactant},0}$ (**Equation 1.1.**)^[22]

$$X_{\text{reactant}} = \frac{n_{\text{reactant},0} - n_{\text{reactant}}}{n_{\text{reactant},0}}$$

Equation 1.1. Definition of the conversion (X_{reactant}).^[22]

The *yield* Y of a product is defined as the amount of product n_{product} , which was formed during the reaction time from the reactant $n_{\text{reactant},0}$. The yield is expressed as fraction of the maximum possible amount of substance (**Equation 1.2.**).^[22]

$$Y_{\text{product}} = \frac{n_{\text{product}} - n_{\text{product},0}}{n_{\text{reactant},0}} \cdot \frac{|v_{\text{reactant}}|}{\sum_i v_{\text{product}}}$$

Equation 1.2. Definition of the yield (Y_{product}).^[22]

The *selectivity* S of a product is the ratio of the yield and the conversion (**Equation 1.3.**).^[22]

$$S_{\text{product}} = \frac{n_{\text{product}} - n_{\text{product},0}}{\sum (n_{\text{product}} - n_{\text{product},0})} = \frac{Y_{\text{product}}}{X_{\text{reactant}}}$$

Equation 1.3. Definition of the selectivity S_{product} .^[22]

The *initial rates* r of the following dehydration reactions were determined *via* the differential method by plotting the conversion of the reactant X ($< 20\%$) versus the reaction time t_R . The slope of the straight line (gradient: $X \cdot t_R^{-1}$) is multiplied with the initial molar amount of reactant $n_{\text{reactant},0}$ and divided by the amount of catalyst m_{cat} (**Equation 1.4.**).^[22]

$$r = \frac{X \cdot n_{\text{reactant},0}}{t_R \cdot m_{\text{cat}}} \left[\frac{\text{mol}}{\text{s} \cdot \text{g}} \right]$$

Equation 1.4. Calculation of the reaction rate (r).^[22]

The *turnover frequency* TOF represents the number of converted molecules per time and per number of catalytically active centers. This number is calculated *via* normalizing the reaction rate [$\text{mol} \cdot \text{s}^{-1} \cdot \text{g}^{-1}$] to the concentration of Brønsted acid sites of the catalyst [$\text{mol} \cdot \text{g}^{-1}$] (**Equation 1.5.**).^[22]

$$TOF = \frac{r}{c(H^+)} \left[\frac{\text{mol}_{\text{reactant}}}{\text{mol}_{H^+} \cdot \text{s}} \right] \text{ or } \left[\frac{1}{\text{s}} \right]$$

Equation 1.5. Calculation of the turnover frequency (TOF).^[22]

It is important to know the reaction rate's dependence of the reactant concentration. The rate equation is the product of the rate constant k and the concentration of the reactant c to the power of the reaction order n (**Equation 1.6.**).^[22]

$$r = k \cdot c^n$$

Equation 1.6. Definition of the rate equation.^[22]

The rate equation has to be linearized in the following way to determine the order of a chemical reaction:

$$\ln(r) = \ln(k) + n \cdot \ln(c)$$

Equation 1.7. Linearization of the rate equation.^[22]

The double-logarithmic plot of the reaction rate $\ln(r)$ versus the initial concentration of reactant $\ln(c)$, gives a straight line. The slope corresponds to the reaction order n and the intercept of the y-axis represents $\ln(k)$.^[22]

The influence of temperature on the rates of chemical reactions is determined by the Arrhenius equation (**Equation 1.8.**). The rate constant k is the product of the pre-exponential factor A_{pre} and an exponential factor, which involves the temperature T , the universal gas constant R and the activation energy E_a .^[23]

$$k = A_{pre} \cdot e^{-\frac{E_a}{R \cdot T}}$$

Equation 1.8. The definition of the Arrhenius equation.^[23]

The Arrhenius equation has to be linearized in the following way to determine the activation energy E_a of a reaction:

$$\ln(k) = \ln(A_{pre}) - \frac{E_a}{R \cdot T}$$

Equation 1.9. Linearization of the Arrhenius equation.^[23]

If the logarithmic reaction constant $\ln(k)$ is plotted versus $(R \cdot T)^{-1}$, the slope of the straight line represents the activation barrier E_a and the intercept of the y-axis is $\ln(A_{pre})$.^[23]

The conventional transition state theory is a theory of reaction rates and was published by Eyring, Evans and Polanyi in 1935. This theory is based on four assumptions. 1) The reactant molecules which passed the barrier and formed products cannot turn back to reactants again. 2) The energy of the reactant molecules corresponds to the Maxwell-Boltzmann distribution. The equilibrium theory for the activated complexes (molecular species at the top of the barrier) can be used even if the whole system is not in equilibrium. 3) It is allowed to separate the motion of the system over the col from all other motions associated with the activated complex. 4) A chemical reaction can be treated as a classical motion over the barrier and quantum effects are ignored. All these assumptions are valid for the calculation of the equilibrium constants using statistical mechanics.^[23]

The equilibrium constant K_c^\ddagger for the formation of the activated complex X^\ddagger of the reactants A and B can be written as:

$$K_c^\ddagger = \left(\frac{[X^\ddagger]}{[A] \cdot [B]} \right)_{eq}$$

Equation 1.10. Equilibrium constant of the activated complex X^\ddagger .^[23]

The rate constant k can now be expressed as:

$$k = \frac{k_B \cdot T}{h} \cdot K_c^\ddagger$$

Equation 1.11. Rate constant k as a function of the equilibrium constant of the activated complex K_c^\ddagger .^[23]

K_c^\ddagger can be expressed in terms of the standard Gibbs energy ΔG^{\ddagger} during the formation of the activated complex from the reactants:

$$k = \frac{k_B \cdot T}{h} \cdot e^{-\frac{\Delta G^{\ddagger}}{R \cdot T}}$$

Equation 1.12. The rate constant as a function of the standard Gibbs energy of activation ΔG^{\ddagger} .^[23]

If the standard Gibbs energy of activation ΔG^{\ddagger} is expressed as a function of enthalpy and entropy, the following equation results:

$$k = \frac{k_B \cdot T}{h} \cdot e^{-\frac{(\Delta H^{\ddagger} - T \cdot \Delta S^{\ddagger})}{R \cdot T}}$$

Equation 1.13. Expression of the rate constant in terms of the standard enthalpy ΔH^{\ddagger} and standard entropy of activation ΔS^{\ddagger} .^[23]

The equation must be arranged in the following way to determine ΔH^{\ddagger} and ΔS^{\ddagger} of a reaction:

$$\ln \left(\frac{k \cdot h}{k_B \cdot T} \right) \cdot R = \Delta S^{\ddagger} - \frac{\Delta H^{\ddagger}}{T}$$

Equation 1.14. Linearization of Equation 1.13. to determine ΔH^{\ddagger} and ΔS^{\ddagger} .^[23]

ΔH^{\ddagger} and ΔS^{\ddagger} can be determined graphically by plotting $\ln(k \cdot h \cdot k_B^{-1} \cdot T^{-1}) \cdot R$ versus T^{-1} . The slope of the straight line corresponds to the standard enthalpy of activation and the standard entropy of activation is the intercept of the y-axis. Often it is useful to express the equations in terms of the activation energy E_a :

$$E_a = R \cdot T + \Delta U^{\ddagger}$$

Equation 1.15. E_a as a function of the standard internal energy of activation ΔU^{\ddagger} .^[23]

Based on the fact, that ΔU^{\ddagger} is the difference of ΔH^{\ddagger} (standard internal energy of activation) and $p \cdot \Delta V^{\ddagger}$ (standard volume of activation), the following expression results:

$$E_a = R \cdot T + \Delta H^{\ddagger} - p \cdot \Delta V^{\ddagger}$$

Equation 1.16. More detailed expression of the activation energy E_a .^[23]

For unimolecular reactions with no change in number of molecules or for reactions in solution (condensed systems) the term $p \cdot \Delta V^{\ddagger}$ is zero or negligible. Therefore, the correlation between the activation energy and the standard enthalpy of activation can be concluded:

$$E_a = \Delta H^{\ddagger} + R \cdot T$$

Equation 1.17. Correlation between E_a and ΔH^{\ddagger} for reactions in condensed systems.^[23]

1.5. References

- [1] G. W. Huber, S. Iborra, A. Corma, *Chemical reviews* **2006**, *106*, 4044-4098.
- [2] S. Malherbe, T. E. Cloete, *Reviews in Environmental Science and Biotechnology* **2002**, *1*, 105-114.
- [3] D. Mohan, C. U. Pittman, P. H. Steele, *Energy & fuels* **2006**, *20*, 848-889.
- [4] H. Nimz, *Angewandte Chemie* **1974**, *86*, 336-344.
- [5] a) D. Carpenter, T. L. Westover, S. Czernik, W. Jablonski, *Green Chemistry* **2014**, *16*, 384-406; b) A. Corma, S. Iborra, A. Velty, *Chemical Reviews* **2007**, *107*, 2411-2502; c) D. A. Ruddy, J. A. Schaidle, J. R. Ferrell III, J. Wang, L. Moens, J. E. Hensley, *Green Chemistry* **2014**, *16*, 454-490; d) J. Zakzeski, P. C. Bruijninx, A. L. Jongerius, B. M. Weckhuysen, *Chemical reviews* **2010**, *110*, 3552-3599.
- [6] S. Czernik, A. Bridgwater, *Energy & Fuels* **2004**, *18*, 590-598.
- [7] a) A. V. Bridgwater, *Biomass and bioenergy* **2012**, *38*, 68-94; b) J. J. Bozell, G. R. Petersen, *Green Chemistry* **2010**, *12*, 539-554.
- [8] a) C. A. Mullen, A. A. Boateng, *Energy & Fuels* **2008**, *22*, 2104-2109; b) C. A. Mullen, A. A. Boateng, K. B. Hicks, N. M. Goldberg, R. A. Moreau, *Energy & fuels* **2009**, *24*, 699-706; c) R. A. Sheldon, *Green Chemistry* **2014**, *16*, 950-963; d) C. Branca, P. Giudicianni, C. Di Blasi, *Industrial & Engineering Chemistry Research* **2003**, *42*, 3190-3202.
- [9] J. P. Diebold, *A review of the chemical and physical mechanisms of the storage stability of fast pyrolysis bio-oils*, National Renewable Energy Laboratory Golden, CO, **2000**.
- [10] J. He, C. Zhao, J. A. Lercher, *Journal of the American Chemical Society* **2012**, *134*, 20768-20775.
- [11] C. Zhao, J. A. Lercher, *Angewandte Chemie* **2012**, *51*, 5935-5940.
- [12] M. B. Smith, J. March, *Advanced Organic Chemistry*, 6. Edition, Wiley, New York, **2007**, 1477-1558.
- [13] J. Brecht, H. Thoutet, J. Schmitz, *Justus Liebigs Annalen der Chemie* **1924**, *437*, 1-13.
- [14] A. Saytzeff, *Justus Liebigs Annalen der Chemie* **1875**, *179*, 296-301.
- [15] A. Hofmann, *Justus Liebigs Annalen der Chemie* **1851**, *79*, 11-39.
- [16] J. Weitkamp, L. Puppe, *Catalysis and zeolites: fundamentals and applications*, 1. Edition, Springer Science & Business Media, Berlin, **2013**.
- [17] P. Jacobs, E. Flanigen, J. Jansen, H. van Bekkum, *Introduction to zeolite science and practice*, Vol. 137, 2. Edition, Elsevier, Amsterdam, **2001**.
- [18] C. Baerlocher, L. B. McCusker, *Database of Zeolite Structures*, www.iza-structure.org/databases/, accessed: 12/2016.
- [19] J. A. Moulijn, M. Makkee, A. E. Van Diepen, *Chemical process technology*, 1. Edition, John Wiley & Sons, Weinheim, **2001**.

- [20] a) O. Mihai, C. R. Widyastuti, S. Andonova, K. Kamasamudram, J. Li, S. Y. Joshi, N. W. Currier, A. Yezerets, L. Olsson, *Journal of Catalysis* **2014**, *311*, 170-181; b) S. A. Skarlis, D. Berthout, A. Nicolle, C. Dujardin, P. Granger, *Applied Catalysis B: Environmental* **2014**, *148*, 446-465; c) S. Shwan, R. Nedyalkova, J. Jansson, J. Korsgren, L. Olsson, M. Skoglundh, *Industrial & Engineering Chemistry Research* **2012**, *51*, 12762_12772; d) A. M. Frey, S. Mert, J. Due-Hansen, R. Fehrmann, C. H. Christensen, *Catalysis letters* **2009**, *130*, 1-8.
- [21] G. Woolery, G. Kuehl, H. Timken, A. Chester, J. Vartuli, *Zeolites* **1997**, *19*, 288-296.
- [22] M. Baerns, A. Behr, A. Brehm, J. Gmehling, H. Hofmann, U. Onken, *Technische Chemie, 1. Edition*, John Wiley & Sons, Weinheim, **2006**.
- [23] K. J. Laidler, *Chemical Kinetics: Theories of Reaction Rates; 3. Edition*, Harper & Row, New York, **1987**; 89-115.

2. Hydronium ion catalyzed elimination pathways of substituted cyclohexanols

This chapter is based on:

Peter H. Hintermeier, Sebastian Eckstein, Mariefel V. Olarte, Donald M. Camaioni, Eszter Baráth and Johannes A. Lercher, “*Hydronium ion catalyzed elimination pathways of substituted cyclohexanols*“, ready for submission.

P.H.H. performed experiments, analyzed the data and wrote the manuscript. M.V.O. (project coordination), S.E., D.M.C. and E.B. contributed in preparing the manuscript by fruitful discussions. J.A.L. is the principal investigator of this project.

Abstract

Hydronium ions in the pores of zeolite HZSM-5 show high catalytic activity in the elimination of water from cyclohexanol in aqueous phase. Substitution induces subtle changes in rates and reaction pathways, which are concluded to be related to the nature of the transition states. The reaction pathways of 2-, 3-, 4-methylcyclohexanol (2-McyOH, 3-McyOH, 4-McyOH), 2-, 4-ethylcyclohexanol (2-EcyOH, 4-EcyOH), 2-*n*-propylcyclohexanol (2-PcyOH) and cyclohexanol (CyOH) were quantitatively and qualitatively explored. Kinetic analysis shows an increasing character of E2 mechanism with closer positioning of the alkyl- and the hydroxyl-group. 4-McyOH dehydration proceeds *via* an E1 type reaction, while (*cis*) 2-McyOH preferentially reacts *via* an E2 pathway. The entropy of activation decreased with increasing alkyl chain length (ca. $-20 \text{ J}\cdot\text{K}^{-1}\cdot\text{mol}^{-1}$ per CH_2 -unit) for 2-substituted alcohols and is concluded to result from constraints influencing the configurational entropy of the transition states.

2.1. Introduction

Decentralized synthesis of energy carriers will require to perform both metal as well as acid-base catalyzed reactions at much milder temperatures and higher selectivities than hitherto possible. To achieve such transformative catalysis, the reaction pathways of potential intermediates have to be understood at a molecular level.

Elimination reactions in the gas phase such as the dehydration of (cyclic) alcohols on acidic catalysts has been extensively studied, not only because of the significant synthetic interest, but also because it helped to elucidate fundamental mechanistic principles.^[1-3] A seminal study of Macht *et al.* reported that 1- and 2-butanol on Keggin-type polyoxometalate (POM) catalysts involve late carbenium-ion-type transition states in the kinetically relevant elimination step.^[4] Similar catalysis was also observed for zeolites.^[5] The presence of H₂O led, however, to the formation of stable and less reactive coordination complexes of water and alcohol.^[5] This suggests that the local environment and the interactions between reactant influence the reaction pathways. The deprotonation energy of the acid catalyst and the protonation enthalpies of the alcohols and the stability of these complexes determine the enthalpies and entropies of activation along the elimination reaction path.^[5] Therefore, the structure and the degree of substitution of the alcohol markedly influence the elimination pathway, as both affect the stabilization of ground and transition states.^[4]

Dehydration in aqueous phase is catalyzed by hydrated hydronium ions, independent whether they are provided by molecular or solid acids. For solids, the hydronium ions remain associated with the surface or pores of the solid acid, as charge separation prevents complete delocalization. Water on surface of non-porous solid acids such as POMs or in zeolite pores abstract protons and stabilize hydrated hydronium ions (H₃O⁺).^[5] The solvated proton is hypothesized to have two structures for its first coordination shell, i.e. a triple hydrated hydronium ion (H₃O⁺(H₂O)₃), the Eigen-type cluster^[6a] or a dihydrate (H₅O₂⁺) named as Zundel cation.^[6b] Recent studies suggest that the Zundel cation is an intermediate between two distorted Eigen cation driven by a reorganization of two hydration shells.^[7]

The presence of zeolite constraints enhance the dehydration rates compared to reactions in aqueous solutions of acids. While significantly higher dehydration rates of cyclohexanol (CyOH) by hydronium ions in a zeolite BEA compared to phosphoric acid are found, the principal E1 mechanism is preserved unchanged (schematic reaction pathways, **Figure 2.1.**)^[8]

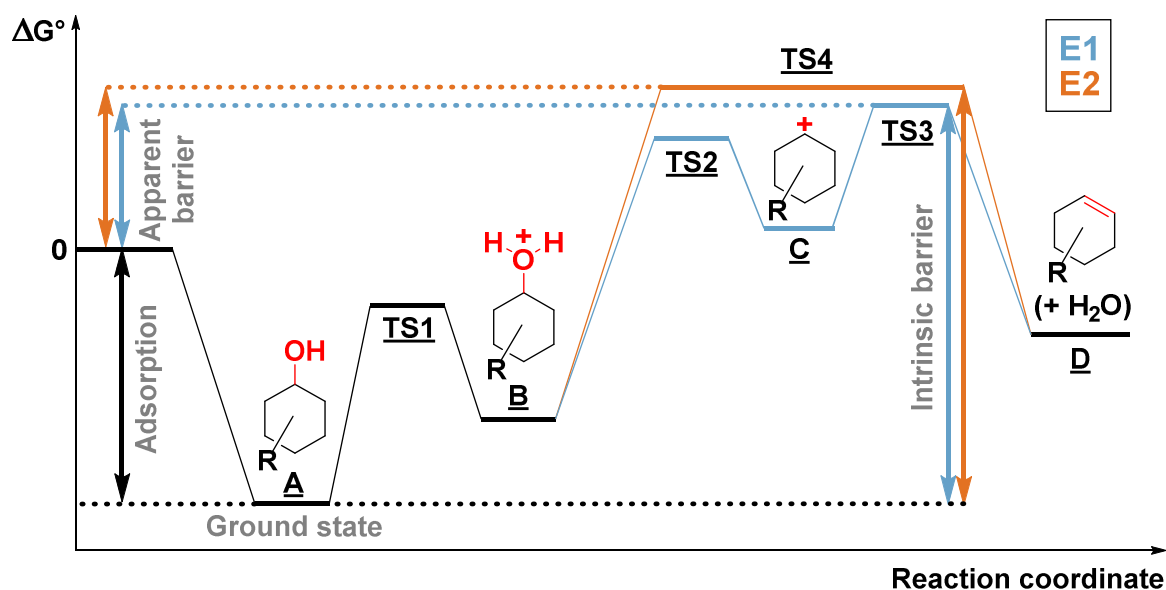


Figure 2.1. Schematic energy diagram of possible dehydration pathways (E1 and E2) on solid acid catalysts (adapted from ref.^[8]).

Upon adsorption, the alcohol and the hydronium ion associate in an exothermic step (**A**). Because of the additional stabilization by the zeolite pores this leads to a zero order for each of the alcohols studied. As a note in passing, we would like to emphasize that the exact coordination of the alcohol has not been experimentally shown so far. The subsequent protonation (**B**) is correlated with an increase in ΔG° passing the first transition state (**TS1**). Then, the E1-type elimination proceeds via a stepwise cleavage of the $C_\alpha-O$ (**TS2**) and $C_\beta-H$ bonds (**TS3**) with a stable intermediate (carbenium ion; **C**). A simultaneous cleavage of the $C_\alpha-O$ and $C_\beta-H$ bonds (**TS4**) forming the $C=C$ double bond and water (**D**) would follow in an E2-type elimination pathway.^[8, 9]

The alkyl substituents of cyclohexanols influence the hydronium ion catalyzed dehydration, leading to different reactivity of the isomers.^[10a,b] The differences of the reaction rates on $\gamma-Al_2O_3$ ^[10d] for various alcohols suggest that varying interactions with the reactive surface environment and variations in the reaction path induce the differences in catalytic activity.

In order to tailor catalysts for complex functionalized alcohols, we explore here the impact of the substituents of cyclohexanol on the reaction pathways and rates of hydronium catalyzed dehydration. We use the confines of the MFI structure, as these confines led to the highest rates for simple alcohols^[11] and were expected to exert marked influence on catalytic activity and selectivity. Varying the size (chain length) and the position of the alkyl substituent relative to the OH-group was chosen as approach to qualitatively and quantitatively analyze dehydration pathways.

2.2. Experimental

Chemicals. The following chemicals were used: cyclohexanol (99%, *Sigma-Aldrich*), 4-methylcyclohexanol (mixture of *cis* and *trans* (25%:75%), 98%, *Sigma-Aldrich*), *cis* 4-methylcyclohexanol (> 98%, *Tokyo Chemical Industry*), *trans* 4-methylcyclohexanol (> 98%, *Tokyo Chemical Industry*), 3-methylcyclohexanol (mixture of *cis* and *trans* (43%:57%), > 98%, *Tokyo Chemical Industry*), 2-methylcyclohexanol (mixture of *cis* and *trans* (48%:52%), 99%, *Sigma-Aldrich*), *cis* 2-methylcyclohexanol (98%, *Sigma-Aldrich*), *trans* 2-methylcyclohexanol (99%, *Sigma-Aldrich*), 4-ethylcyclohexanol (mixture of *cis* and *trans* (31%:69%), > 97%, *Tokyo Chemical Industry*), 2-ethylcyclohexanol (mixture of *cis* and *trans* (75%:25%) > 97%, *Tokyo Chemical Industry*), 2-propylcyclohexanol (mixture of *cis* and *trans* (57%:43%), > 90%, *Tokyo Chemical Industry*), sodium sulfate (ACS reagent, > 99%, *Sigma-Aldrich*) ethyl acetate (*Chromasolv*, 99.9%, *Sigma-Aldrich*), phosphoric acid (85% solution, *Sigma-Aldrich*) and sodium chloride (*ReagentPlus*, > 99%, *Sigma-Aldrich*). Hydrogen gas was obtained from *Westfalen* (> 99.999%). Deionized water was treated with an *Easypure-II* system from *WERNER* to obtain ultrapure water (18.2 M Ω ·cm).

Zeolite Catalyst. Zeolite MFI (Si/Al = 45) was obtained from *CLARIANT AG* in H-form and was treated at 550 °C (rate: 10 °C·min⁻¹) for six hours in 100 mL·min⁻¹ synthetic air (80% nitrogen, 20% oxygen; > 99%).

Catalyst stability experiments. 1.0 g of catalyst was stirred in the batch reactor at 190 °C and 50 bar for 14 hours. As an internal standard MgO was physically mixed with the parent and the treated zeolite in a 1:1 wt.% ratio. The MFI (22.5 and 25.0 θ) and MgO reflexes (60.0 – 65.0 θ) of the treated sample were integrated with GRAMS/Al (*Version 9.00R2 32*, Thermo Fisher Scientific) and compared to the parent MFI sample.

Reaction procedure. All reactions were performed with the same molar amount of reactant, catalyst and solvent. In 100 mL ultrapure water 0.05 mol of substrate (5.01 g cyclohexanol, 5.71 g of 1-/2-/3-/4-methylcyclohexanol, 6.41 g of 2-/4-ethylcyclohexanol and 7.11 g of 2-propylcyclohexanol) and 50 mg of MFI zeolite were dissolved and suspended, respectively. The molar amount of reactant of pure *cis* or *trans* 2-methylcyclohexanol was 4.38 mmol (0.5 g) in 100 mL water. In case of phosphoric acid, 5.0 mmol (342 μ L or 0.58 g of 85% H₃PO₄), or 1.7 mmol (114 μ L, 0.19 g of 85% H₃PO₄) were used in 100 mL water depending on reaction temperature.

The autoclave (300 mL) was loaded with 100 mL water, 50 mg MFI zeolite catalyst and 0.05 mol of (substituted) cyclohexanol substrate. The reactor was purged two times (20 bar) with hydrogen

and was heated to the desired temperature at a pressure of 20 bar hydrogen at the start without stirring. Ten degrees below the reaction temperature the total pressure of the reactor was adjusted to 50 bar with hydrogen gas and as soon as the reaction temperature was reached the stirring rate was set to 700 rpm. After the reaction time, the reactor was cooled using an ice bath. The pressure within the reactor was released below a temperature of 5 °C to prevent the loss of volatile products (cyclohexene). The reaction mixture was extracted with 3 x 20 mL ethyl acetate. To improve the phase separation of the organic and the aqueous phases, a small amount of sodium chloride was added to the reaction mixture. After extraction, the organic phase was dried over sodium sulfate. The carbon-balance was monitored by an internal standard (dodecane).

Reactor. All reactions were performed in an autoclave (300 mL) from *Parr Instruments Co.* (type: *PST FS*, material: HASTELLOY C) with a temperature and stirring controlling device (*Parr Instruments Co. 4848 Reactor Controller*).

GC-MS. Quantification and qualification of the dehydration reactions was analyzed by GC/MS (*Agilent Technologies 7890 B GC*, column: *Agilent 19091S-433UI INV02* (30 m x 250 µm x 0.25 µm), heating program: 10 °C·min⁻¹ from 80 °C to 280 °C). Data was analyzed with *MassHunter Workstation Software, Qualitative Analysis, Version B.06.00, Agilent Technologies (2012)*.

AAS. The Si and Al content of the MFI zeolite sample was determined by atomic absorption spectroscopy (AAS) on a *UNICAM 939 AA-Spectrometer*.

N₂ physisorption. The specific surface area and pore volume of the zeolite were determined by nitrogen physisorption. The isotherms were measured at liquid nitrogen temperature (-196 °C) using a *PMI Automatic Sorptometer*. The catalyst was activated in vacuum at 200 °C for two hours before measurement. Apparent surface area was calculated by applying the *Brunauer-Emmett-Teller (BET)* theory, and the *t-plot method* was used to determine the pore volumes.

SEM. The scanning electron microscopy (SEM) images were recorded on a *JEOL 500 SEM-microscopy* (accelerating voltage: 25 kV). The samples were prepared by depositing a drop of an ultrasonicated methanol suspension of the solid material onto a carbon-coated Cu grid.

XRD. The crystal structures of the zeolites were analyzed by X-ray powder diffraction (XRD) using a *Philips X'Pert Pro system*, with Cu-K_α radiation operating at 45 kV/40 mA. The sample was measured with a scanning rate of 0.017°/s in the range from 5 to 70° (2θ).

IR. Infrared spectroscopy of adsorbed pyridine was performed with a *Perkin–Elmer 2000* spectrometer at a resolution of 4 cm^{-1} . The catalyst sample was prepared as wafer and activated in vacuum (ca. 10^{-6} mbar) at $450\text{ }^{\circ}\text{C}$ for one hour (heating rate = $10\text{ }^{\circ}\text{C}\cdot\text{min}^{-1}$). After this, at $150\text{ }^{\circ}\text{C}$ the sample was equilibrated with 0.1 mbar of pyridine for 30 min followed by outgassing for one hour. A spectrum with the chemisorbed pyridine was recorded thereafter. Adsorbed pyridine was desorbed finally by heating up to $450\text{ }^{\circ}\text{C}$ at $10\text{ }^{\circ}\text{C}\cdot\text{min}^{-1}$ for half an hour. Again the spectra were recorded at equilibrium. For quantification, molar integral extinction coefficients of $0.73\text{ cm}\cdot\mu\text{mol}^{-1}$ and $0.96\text{ cm}\cdot\mu\text{mol}^{-1}$ were used for *Brønsted* and *Lewis* acid sites respectively.

$^1\text{H-NMR}$. $^1\text{H-NMR}$ spectra with water signal suppression were recorded at $30\text{ }^{\circ}\text{C}$ using an *Avance III HD 500 System* (Bruker Biospin, Rheinstetten, Germany) with an Ultra-Shield 500 MHz magnet (11.75 T) and a BBI 500 S2 probe head (5 mm, inverse 1H/X with Z-gradient). The resonance frequency of ^1H was 500.13 MHz. Longitudinal relaxation times (T_1) were determined by the inversion recovery pulse method. Relaxation delay and acquisition time were set to 26 s and 4.1 s, respectively. Typically, 64 or 128 scans, with 64 k data points were collected. An exponential window function with a line broadening of 0.2 Hz was applied prior to Fourier transformation and the spectra were manually phased, baseline corrected and integrated using *Mestre-C 8.1.1* software package. Quantification of *cis/trans* isomers was done on the basis of the integrated signal intensities.

$\text{NH}_3\text{-TPD}$. Temperature-programmed desorption (TPD) of ammonia was performed in a 6-fold parallel reactor system. The catalysts were activated under reduced pressure at $450\text{ }^{\circ}\text{C}$ (heating rate: $5\text{ }^{\circ}\text{C}\cdot\text{min}^{-1}$) for one hour. NH_3 was adsorbed for one hour with partial pressures of 1 mbar at $100\text{ }^{\circ}\text{C}$, respectively. Subsequently, the samples were evacuated for two hours in order to remove physisorbed probe molecules. For the temperature-programmed desorption experiments, six samples were sequentially heated from 100 to $770\text{ }^{\circ}\text{C}$ with a heating rate of $10\text{ }^{\circ}\text{C}\cdot\text{min}^{-1}$ to desorb ammonia. The rates of desorbing species were monitored by mass spectrometry (*Balzers QME 200*). For the quantification of the amount of acidity, a standard MFI zeolite with known acid site concentration was used to calibrate the signal.

2.3. Results and Discussion

Characterization and stability of HZSM-5 zeolite

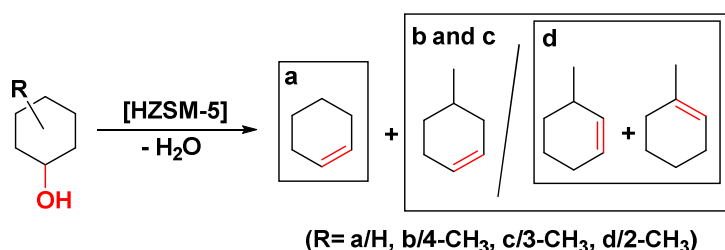
The most important physicochemical properties of the MFI zeolite, i.e. the micropore volume and the concentration of acid sites are compiled in **Table S2.1**. The concentration of Brønsted ($360 \mu\text{mol}\cdot\text{g}^{-1}$) and Lewis acid sites ($45 \mu\text{mol}\cdot\text{g}^{-1}$) were determined by IR spectra of adsorbed pyridine. The crystal size of the MFI zeolite was estimated to be between 100 and 150 nm (SI, **SEM-Image S2.1** and **S2.2**).

Both, the position and intensity of XRD peaks assured that, the microcrystalline structure was maintained during the catalytic experiments (SI, **Figure S2**). The acid site concentration also did not decrease markedly. Thus, we conclude that the zeolite was stable under the conditions used for the presented experiments.

Dehydration of alkylcyclohexanols in aqueous phase

The dehydration of alkyl cyclohexanols substituted at the 2-, 3-, or 4-positions led to various alkenes (**Scheme 2.1**). The product selectivities are compiled in **Table 2.1**. Main products were isomers of alkylcyclohexenes and, at higher temperatures, additional small amounts of ring-contracted alkylcyclopentenenes (selectivity < 2%).

The more highly substituted double-bond product, e.g., 1-methylcyclohexene, (*Saytzeff*-product^[12]) dominated (ca. 80% for 2-McyOH); the product with the less substituted double bond, e.g., 3-methylcyclohexene (*Hofmann*-product) was always found in lower concentrations (ca. 13% for 2-McyOH).^[13]



Scheme 2.1. Dehydration products of 2-, 3-, 4-McyOH and CyOH.

We want to emphasize that dehydration in aqueous phase is a reversible reaction.^[8] The addition product 1-methylcyclohexanol (1-McyOH; selectivity < 6%) is attributed to the hydration of 1-methylcyclohexene *via* the formation of a tertiary carbenium ion following *Markovnikov's rule*.^[14]

Table 2.1. Selectivity [%] of the dehydration products of 2-, 3-, 4-McyOH and CyOH.

Reactant	cyclohexene	4-, 3-methyl-cyclohexene	1-methyl-cyclohexene	1-methyl-cyclohexanol
CyOH	100	-	-	-
2-McyOH	-	14	80	6
3-McyOH	-	70	28	2
4-McyOH	-	72	26	2

Selectivity in %, ca. 10 % conversion, 170 °C, MFI zeolite.

Dehydration of 2-, 3-, 4-McyOH and CyOH

In a first step 2-, 3-, 4-McyOH and CyOH as a benchmark substrate were kinetically investigated in condensed aqueous phase dehydration. A reaction order of zero in alcohol was determined for 2-, 4-McyOH as well as CyOH (SI, **Figures** and **Tables S2.2. – S2.4.**), which implies that the reaction enthalpies and entropies represent intrinsic values.^[15] **Figure 2.2.** illustrates the temperature dependence of the dehydration rates catalyzed by hydronium ions in zeolite MFI.

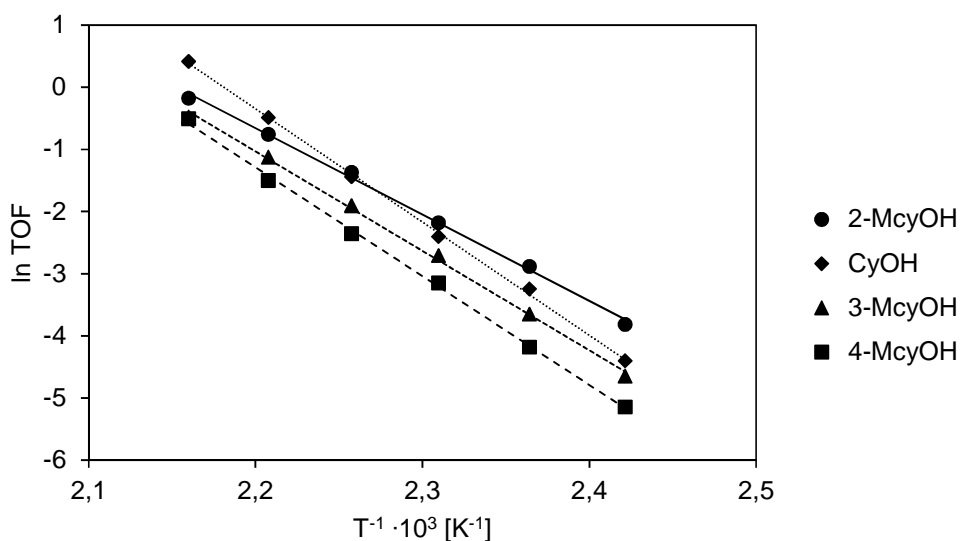


Figure 2.2. Arrhenius plots for the dehydration of 2-, 3-, 4-McyOH (*cis/trans* mixtures) and CyOH (MFI).

The corresponding activation energies (E_a), the turnover frequencies, enthalpies (ΔH^{\ddagger}) as well as entropies of activation (ΔS^{\ddagger}) of all methyl-substituted reactants and CyOH are compiled in **Table 2.2.** The differences in E_a , ΔH^{\ddagger} and ΔS^{\ddagger} among the substrates with varying substituent position are significant.

Table 2.2. Comparison of E_a^{intr} , ΔH^{\ddagger} , ΔS^{\ddagger} , and TOF for the dehydration of CyOH and McyOHs (MFI).^a

Entry	Substrate	E_a^{intr}	ΔH^{\ddagger} [kJ·mol ⁻¹]	ΔS^{\ddagger} [J·mol ⁻¹ ·K ⁻¹]	TOF (170 °C) [s ⁻¹]
1	CyOH	152 (±2)	148 (±2)	+74 (± 6)	0.24 (±0.02)
2	4-McyOH	146 (±3)	142 (±3)	+53 (± 6)	0.10 (±0.02)
3	3-McyOH	133 (±3)	129 (±3)	+28 (± 7)	0.15 (±0.01)
4	2-McyOH	116 (±3)	112 (±3)	-8 (± 7)	0.25 (±0.01)

a) Conditions: 120 – 160 °C, 0.5 M (*cis/trans* mixtures), 100 mL H₂O, 50 bar.

Compared to CyOH, the introduction of a methyl-group in position 4 affects ΔS^{\ddagger} more than ΔH^{\ddagger} (**Table 2.2., Entries 1 and 2**). The slightly higher enthalpy of activation (148 vs. 142 kJ·mol⁻¹) for CyOH is overcompensated by a higher entropy of activation (+74 vs. +53 J·K⁻¹·mol⁻¹) such that the rates and TOFs at every reaction temperature are higher than those of 4-McyOH.

We would like to emphasize that the activation parameters for 3-McyOH (**Table 2.2., Entry 3**) differed significantly from both CyOH and 4-McyOH. The activation enthalpy (129 kJ·mol⁻¹) and the entropy (+28 J·K⁻¹·mol⁻¹) were both significantly lower compared to the two previously discussed substrates. Although the entropy was lower (+28 vs. +53 J·K⁻¹·mol⁻¹), the reduced activation enthalpy (129 vs. 142 kJ·mol⁻¹) resulted in higher TOFs compared to 4-McyOH (**Table 2.2., Entries 2 and 3**). The magnitude of the enthalpic and entropic barriers of 3-McyOH dehydration were between those of 2- and 4-methylcyclohexanol (**Table 2.2., Entry 2, 3 and 4**).

Dehydration of 2-McyOH (**Table 2.2., Entry 4**) led to a low enthalpy (116 kJ·mol⁻¹) and a negative entropy of activation ΔS^{\ddagger} (-8 J·K⁻¹·mol⁻¹). The differences of 30 kJ·mol⁻¹ in ΔH^{\ddagger} and ca. 60 J·K⁻¹·mol⁻¹ in ΔS^{\ddagger} between 2- and 4-McyOH are remarkable (**Table 2.2., Entry 2 and 4**). The higher reactivity of the *cis* isomer in a *cis/trans* mixture (1:1) of 2-McyOH point to an important steric effect of the substituent.^[10c] **Table 2.3.** compiles the kinetic data of the hydronium ion catalyzed dehydration of *cis* and *trans* isomers of 2-McyOH and 4-McyOH.

Table 2.3. Comparison of E_a^{intr} , ΔH^{\ddagger} , ΔS^{\ddagger} , and TOF for the dehydration of 2- and 4-McyOH isomers (MFI).^a

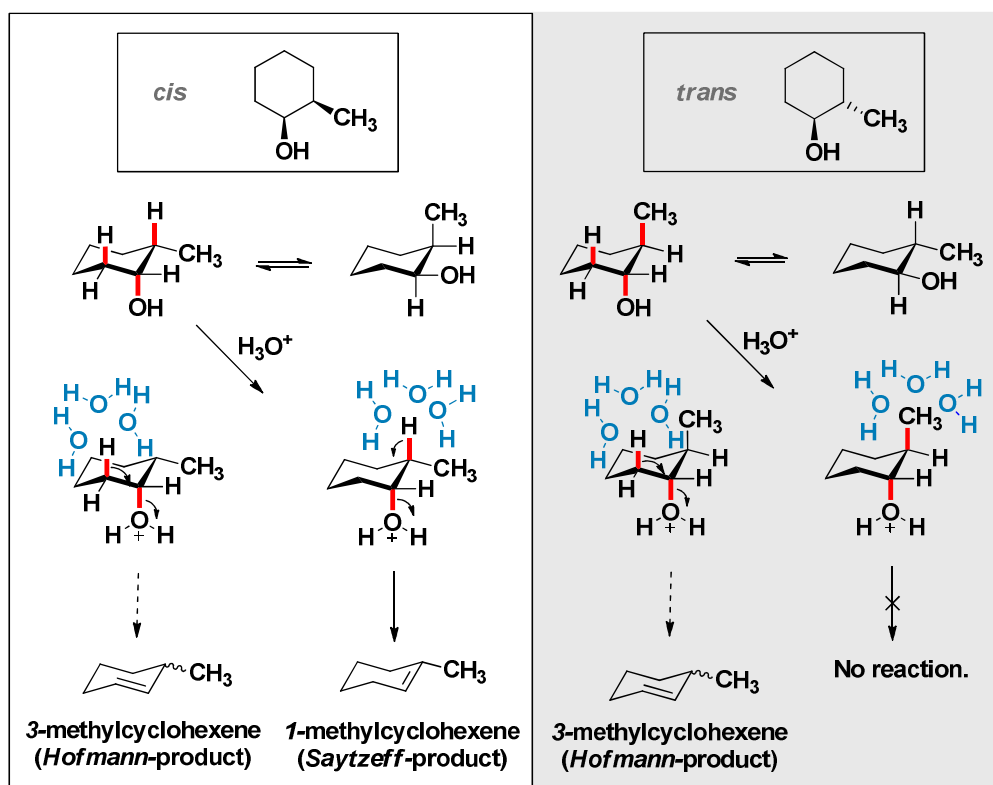
Entry	Substrate	E_a^{intr}	ΔH^{\ddagger} [kJ·mol ⁻¹]	ΔS^{\ddagger} [J·mol ⁻¹ ·K ⁻¹]	TOF (140 °C) [s ⁻¹]
1	<i>trans</i> 4-McyOH	148 (± 2)	144 (± 2)	+59 (± 4)	5.4 (±2) · 10 ⁻³
2	<i>cis</i> 4-McyOH	148 (± 2)	145 (± 2)	+58 (± 2)	4.4 (±1) · 10 ⁻³
3	<i>trans</i> 2-McyOH	144 (± 2)	141 (± 2)	+43 (± 2)	2.1 (±1) · 10 ⁻³
4	<i>cis</i> 2-McyOH	114 (± 3)	111 (± 3)	-14 (± 7)	1.2 (±1) · 10 ⁻²

a) Conditions: 120 – 160 °C, 0.05 M, 100 mL H₂O, 50 bar.

Cis and *trans* isomers of 4-McyOH showed the same reactivity in dehydration (**Table 2.3., Entry 1 and 2**). Not only the rates per active site (TOFs: $5.4 \cdot 10^{-3} \text{ s}^{-1}$ and $4.4 \cdot 10^{-3} \text{ s}^{-1}$), but also ΔH^{\ddagger} (144 and 145 $\text{kJ} \cdot \text{mol}^{-1}$) as well as ΔS^{\ddagger} (+58 and +59 $\text{J} \cdot \text{K}^{-1} \cdot \text{mol}^{-1}$) were nearly identical (**Table 2.3., Entry 2**).

Significant differences were observed, however, between the two isomers of 2-McyOH (**Table 2.3., Entry 3**). Dehydration of *trans* 2-McyOH surprisingly showed the same order of magnitude in TOF ($2.1 \cdot 10^{-3} \text{ s}^{-1}$) and similar enthalpy of activation (141 $\text{kJ} \cdot \text{mol}^{-1}$) as the isomers of 4-McyOH. The reactivity of *cis* 2-McyOH (**Table 2.3., Entry 4**) was about one order of magnitude higher ($1.2 \cdot 10^{-2} \text{ s}^{-1}$), most markedly induced by a lower activation enthalpy. Therefore, the *cis* isomer represents the reactivity of the 2-McyOH *cis/trans* mixture.

In order to explain the differences in reactivity, let us analyze the products in detail. Elimination of water via an E1 type mechanism should not discriminate between *cis* and *trans* isomers of the alcohol.^[16] Therefore, we hypothesize that the elimination occurs in a concerted reaction step (E2 mechanism) with 2-McyOH. Dehydration via this route requires an anti-periplanar configuration of the protonated hydroxyl-group and the adjacent β -H (**Scheme 2.2.**)^[16]



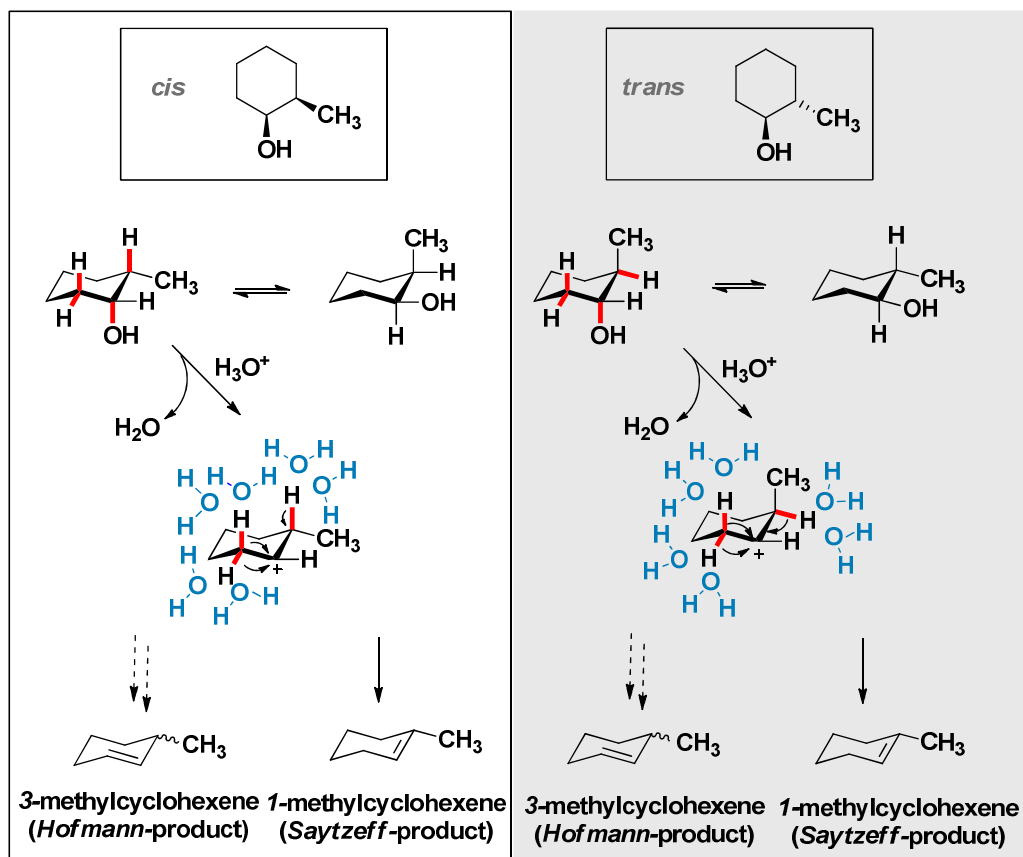
Scheme 2.2. E2 dehydration pathways for *cis* and *trans* 2-McyOH.

In case of *cis* 2-McyOH both reaction products can be formed, the *Saytzeff*-product with the more highly substituted double bond (energetically favored) and the *Hofmann*-product (energetically less favored). By contrast, for *trans* 2-McyOH the formation of the *Saytzeff*-product is not possible via an E2 mechanism. Thus, the pathway leading to the *Hofmann*-product is the only accessible. The higher activation barrier of *trans* 2-McyOH is attributed to the formation of the more energetically demanding *Hofmann*-product.

As outlined above, the anti-periplanar orientation of both leaving groups is not required in an E1 elimination (**Scheme 2.3.**). The resulting higher number of abstractable β -protons favors the formation of the *Hofmann*-product statistically (2:1) for both isomers of 2-McyOH (**Table 2.4.**).

Table 2.4. *Saytzeff/Hofmann*-product ratios for the dehydration of *cis* and *trans* 2-McyOH (MFI).

Substrate	120 °C	140 °C	160 °C
<i>cis</i> 2-McyOH (<i>Saytzeff/Hofmann</i>)	14.4	13.6	11.2
<i>trans</i> 2-McyOH (<i>Saytzeff/Hofmann</i>)	1.7	1.5	1.6

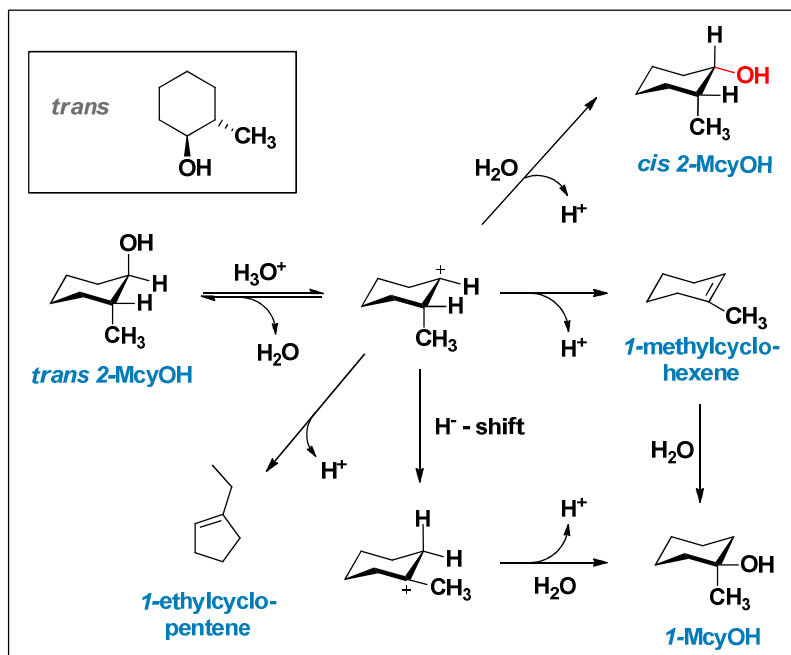


Scheme 2.3. E1 dehydration pathways for *cis* and *trans* 2-McyOH.

The substantial excess of the *Saytzeff*-product (11- to 14-fold) with *cis* 2-McyOH allows to conclude, therefore, that the elimination occurs concertedly, i.e., without the possibility of isomerization of an intermediately formed carbenium ion by hydride shift. On first sight, one could argue that the lower activation energy is caused by the fact that charged species are avoided in the reaction path on the expense of a lower entropy of activation. However, we would tend to rule out this argument, as it would also suggest that a concerted pathway should have been dominating for the non-substituted alcohol.^[8] Therefore, we hypothesize that the concerted elimination requires the steric proximity of the bonds to be broken. The proton to be transferred and the proton to be accepted can be seen in such a case to be catalyzed by one dynamic ensemble, a hydrated hydronium ion. In the case of *cis* 2-McyOH, the repulsion of the leaving and the methyl group destabilizes the transition state making the simultaneous elimination more favorable. In case of *trans* 2-McyOH the larger distance to the methyl group does not permit this. Independent of the orientation, elimination of water from 4-McyOH also does not allow this elimination. In consequence, the coincidence of the easier C-O bond breaking and the proximity of the acid and base site (the same hydronium cluster is proton donating (acid) and proton accepting (base) site) make the overall reaction energetically more favorable and concerted. In turn, the concerted action requires more stringent boundary conditions for the transition state, in line with the lower entropy of activation. For the other cases, cleaving water in the absence of steric repulsive effects is energetically less favorable, but the stepwise E1 mechanism leads intrinsically to higher entropies.

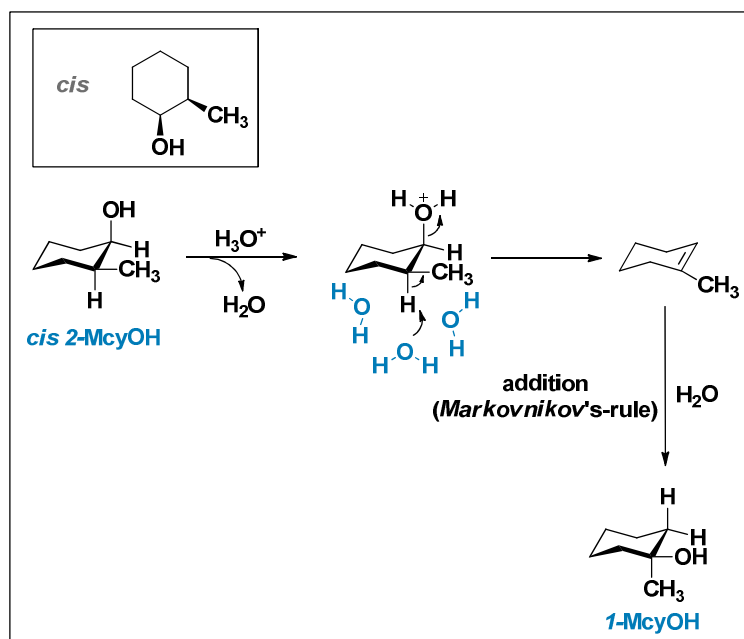
Scheme 2.4. and **Scheme 2.5.** illustrate the pathways leading to the observed product distributions. Dehydration of *trans* 2-McyOH results in a slight excess of the *Saytzeff*-olefin. The statistic distribution of products is in line with a pathway *via* carbocation. In contrast, the high excess of the *Saytzeff*-product for *cis* 2-McyOH is characteristic for a concerted reaction pathway.

Following the product yields as a function of conversion, further supports the mechanistic picture. For *trans* 2-McyOH (SI, **Chromatogram S2.1.**) dehydration conversion was positively correlated with the formation of the *cis* isomer. The formation of ethylcyclopentene was already detected at low conversions ($X < 3\%$), as it is characteristic for the presence of a carbenium ion. For *cis* 2-McyOH (SI, **Chromatogram S2.2.**), however, neither the fraction of *trans* 2-McyOH changed with conversion nor was ethylcyclopentene observed. In all cases, the amount of 1-McyOH increased with rising conversion.



Scheme 2.4. Reaction pathways of *trans* 2-McyOH via a carbocation.

1-McyOH can be either formed by the addition of water to the olefinic product *via* the most stable carbenium ion according to *Markovnikov's rule* or the secondary carbocation can be transformed into a tertiary carbocation by a hydride-shift and a subsequent attack of water (**Scheme 2.4.** and **Scheme 2.5.**).



Scheme 2.5. E2 dehydration pathway of *cis* 2-McyOH.

A separate set of experiments using $^1\text{H-NMR}$ to analyze the products support these conclusions (SI, **Table S2.22.**). Conversion of *cis* 2-McyOH did not lead to the *trans* isomer (**Scheme 2.5.**), whereas the experiments with pure *trans* 2-McyOH formed the *cis* isomer with increasing reaction time (**Scheme 2.4.**). The *cis* and *trans* isomers of 4-McyOH are also interconverted as a function of reaction time, by rehydration of 4-methylcyclohexyl cation as well as the product 4-methylcyclohexene.

Together with the information of product distribution of the pure isomers, the activation parameters like E_a , ΔH^{\ddagger} and ΔS^{\ddagger} (**Table 2.2.** and **2.3.**) can be evaluated in more detail. The variation in activation energy of about $30 \text{ kJ}\cdot\text{mol}^{-1}$ among both 2-McyOH isomers seems to be the consequence of two different dehydration routes. The negative entropy of activation ($\Delta S^{\ddagger} = -8 \text{ J}\cdot\text{K}^{-1}\cdot\text{mol}^{-1}$) in case of *cis* 2-McyOH is assumed to represent an early and substrate-like transition state. The low entropy of activation is associated with the constrained and highly ordered E2 arrangement consisting of the substrate, the proton (converting R-OH into the reactive leaving group R-OH₂⁺) and the water cluster (β -H abstracting base). Contrary to this, the positive entropy of activation in case of *trans* 2-McyOH ($\Delta S^{\ddagger} = +42 \text{ J}\cdot\text{K}^{-1}\cdot\text{mol}^{-1}$) is interpreted as a late and product-like transition state with a stepwise C-O cleavage and a consecutive proton abstraction.

The difference between the two dehydration paths of the isomers of 2-McyOH is illustrated by **Figure 2.1.** The enthalpically favored pathway (E2) prevents the formation of a carbenium ion and stabilizes the complex early transition state. In case of *trans* 2-McyOH the concerted pathway leading to the thermodynamically favored *Saytzeff*-product is forbidden by absence of the anti-periplanar orientation of the molecular orbitals. As a result, the dehydration follows the enthalpically less favored, stepwise reaction sequence *via* the carbenium ion.

Interestingly, the isomers of 4-McyOH are not restricted in possible dehydration pathways nevertheless seem to react *via* E1 ($\Delta S^{\ddagger} = +53 \text{ J}\cdot\text{K}^{-1}\cdot\text{mol}^{-1}$ and $\Delta H^{\ddagger} = 142 \text{ kJ}\cdot\text{mol}^{-1}$), comparable to the data of *trans* 2-McyOH. Same is assumed for CyOH ($\Delta S^{\ddagger} = +74 \text{ J}\cdot\text{K}^{-1}\cdot\text{mol}^{-1}$ and $\Delta H^{\ddagger} = 148 \text{ kJ}\cdot\text{mol}^{-1}$) with slight deviation occurring from the absence of the methyl substituent. In contrast to the 2-McyOH *cis/trans* mixture, which is kinetically determined by the *cis* isomer (E2), the activation parameters of 3-McyOH ($\Delta S^{\ddagger} = +29 \text{ J}\cdot\text{K}^{-1}\cdot\text{mol}^{-1}$ and $\Delta H^{\ddagger} = 128 \text{ kJ}\cdot\text{mol}^{-1}$) led to average values which are located between both extreme cases (E1 and E2) (**Table 2.2.**).

Experiments with heavy water and deuterated cyclohexanol previously showed that the C-H bond cleavage is the rate determining step within the E1 route.^[6] This implies that independently of the elimination mechanism, the step of proton abstraction is a kinetically relevant step. Therefore, it can be assumed, that the acidity of the β -H of alcohol is critical in determining the reaction

pathway. The chemical shifts in $^1\text{H-NMR}$ of the $\beta\text{-H}$ (attached to same C-atom as CH_3 -group) leading to the *Saytzeff*-product differ remarkably among *cis* 2-McyOH (ca. 1.70 – 1.60 ppm) and the *trans* isomer (ca. 1.35 – 1.15 ppm).^[17]

To explore whether the differences in activation enthalpy and entropy results primarily from the molecular structure or additionally from the zeolite confinement, dehydration kinetics of 2- and 4-McyOH were analyzed in the presence of hydronium ions generated by a molecular acid (H_3PO_4) under identical reaction conditions. Contrary to the MFI catalyzed reactions, the reaction orders were first order in substrate (SI, **Figure** and **Table S2.9.** and **S2.12.**). **Table 2.5.** compiles TOF, E_a^{app} , ΔS^{\ddagger} and ΔH^{\ddagger} for the dehydration of *trans* 2-McyOH and *cis* 2-McyOH.

A comparison of the reaction rates normalized to the concentrations of hydronium ions from H_3PO_4 (calculated according to Rudolph *et al.*^[18]) quantifies the difference in reactivity between the *cis* (TOF: $1.8 \cdot 10^{-4} \text{ s}^{-1}$) and the *trans* (TOF: $1.9 \cdot 10^{-5} \text{ s}^{-1}$) isomer of 2-McyOH, like in zeolite catalysis, to one order of magnitude (**Table 2.5., Entry 1** and **2**). In line with this, a significantly higher activation barrier ($E_a^{\text{app}} = 167 \text{ kJ}\cdot\text{mol}^{-1}$) for *trans* 2-McyOH was determined compared to the *cis* isomer ($E_a^{\text{app}} = 133 \text{ kJ}\cdot\text{mol}^{-1}$). Similar to the zeolite results presented above, the entropy of activation was higher for the *trans* isomer (*cis*: $\Delta S^{\ddagger} = +4 \text{ J}\cdot\text{K}^{-1}\cdot\text{mol}^{-1}$; *trans*: $\Delta S^{\ddagger} = +43 \text{ J}\cdot\text{K}^{-1}\cdot\text{mol}^{-1}$).

Table 2.5. Homogeneously catalyzed dehydration (H_3PO_4): comparison of TOF, E_a^{app} , ΔH^{\ddagger} and ΔS^{\ddagger} .

Entry	Substrate	E_a^{app} [kJ·mol ⁻¹]	ΔH^{\ddagger} [kJ·mol ⁻¹]	ΔS^{\ddagger} [J·K ⁻¹ ·mol ⁻¹]	TOF (140 °C) ^c [s ⁻¹]
1 ^a	<i>cis</i> 2-McyOH	133 (±3)	129 (±3)	+4 (±7)	$1.8 (\pm 0.1) \cdot 10^{-4}$
2 ^b	<i>trans</i> 2-McyOH	167 (±3)	163 (±3)	+43 (±6)	$1.9 (\pm 0.2) \cdot 10^{-5}$

a) Conditions: 150 – 190 °C, 0.2 M (cis/trans mixture), 50 bar, 3 mM H_3PO_4 . b) Conditions: 170 – 210 °C, 44 mM alcohol, 50 bar, 50 mM/17 mM H_3PO_4 . c) Conditions: 44 mM alcohol, 50 bar, 73 H_3PO_4 .

$^1\text{H-NMR}$ analysis (SI, **Table S2.22.**) after catalytic conversion of pure isomers with hydronium ions generated by H_3PO_4 gave the same results as for hydronium ions generated by HZSM-5. Dehydration of *cis* 2-McyOH did not form the *trans* isomer (E2), whereas the *trans* 2-McyOH produced the corresponding other isomer (E1 *via* carbenium ion). Therefore, it is concluded that the dehydration mechanism does not depend on the steric constraints of the hydronium ion. The selectivity observed with phosphoric acid is comparable to zeolite catalysis, with *Saytzeff*-/*Hofmann*-product ratios between 1.3 and 1.5 for *trans* 2-McyOH and between 14 and 19 for *cis* 2-McyOH. The differences between both isomers of 2-McyOH in TOF (about one order of magnitude) as well as in enthalpic (ca. $30 \text{ kJ}\cdot\text{mol}^{-1}$) and entropic barriers (ca. $40 \text{ J}\cdot\text{K}^{-1}\cdot\text{mol}^{-1}$)

were constant and independent of the environment of the hydronium ion (**Table 2.3.**, **Entry 3** and **4**; **Table 2.5.**, **Entry 1** and **2**).

Thus, we conclude that the specific activity of the isomers does not depend on the environment of the hydrated hydronium ion. It appears to be solely dependent on the steric factors outlined above. The two orders of magnitude higher rate of reaction, normalized to the concentration of hydronium ions shows that both pathways benefit equally from steric constraints.

Impact of larger alkyl-substituents

As we showed that the environment has a positive influence and may constrain the ground and transition states of reacting substrates in their interactions with hydrated hydronium ions, we explored the impact of increasing steric limitations by replacing the methyl substituent with an ethyl- and propyl-group for 2- and 4-substituted CyOHs. Turnover frequencies, entropy and enthalpy of activation for the ethyl- and propyl-substituted cyclohexanols are compiled in **Table 2.6**. The dehydration reactions catalyzed by MFI were zero order with respect to the alcohol.

Similar to methyl-substituted cyclohexanols, all substrates formed alkyl cyclohexenes and only trace quantities of five-membered ring products (mainly at higher temperatures). The *Saytzeff*-isomer was the major olefinic product for all 2-substituted substrates. For 2-EcyOH the excess was 9 – 14 fold, similar to the selectivity of 2-McyOH. Interestingly, the *Saytzeff/Hofmann* isomer ratios for 2-PcyOH were lower, i.e., between 4 and 7. In case of 4-substituted cyclohexanols, the primary products were 4-alkylcyclohexenes, although 3- and 1-alkylcyclohexenes were observed in small concentrations.

Table 2.6. Comparison of E_a^{intr} , ΔH^{\ddagger} , ΔS^{\ddagger} and TOF for the dehydration of larger alkyl-substituents (MFI).^a

Entry	Substrate	E_a^{intr}	ΔH^{\ddagger} [kJ·mol ⁻¹]	ΔS^{\ddagger} [J·mol ⁻¹ ·K ⁻¹]	TOF (170 °C) [s ⁻¹]
1	4-McyOH	146 (±3)	142 (±3)	+53 (±6)	0.10 (±0.02)
2	4-EcyOH	143 (±3)	139 (±3)	+50 (±7)	0.15 (±0.01)
3	2-McyOH	116 (±3)	112 (±3)	-8 (±7)	0.25 (±0.01)
4	2-EcyOH	107 (±2)	104 (±2)	-25 (±4)	0.28 (±0.01)
5	2-PcyOH	104 (±2)	101 (±2)	-43 (±7)	0.07 (±0.01)

a) Conditions: 140 – 190 °C, 0.5 M (*cis/trans* mixture), 50 bar.

Increasing the substitution size did not strongly influence the rates or enthalpies and entropies of activation in position 4. We conclude, therefore, that the size of an *n*-alkyl group hardly influences the ground and transition state along the reaction pathway.

The *n*-propyl-substituent in position 2, had a greater impact on the TOF (0.07 s^{-1} ; **Table 2.6., Entry 5**) lowering it approximately four fold. The decrease in the reaction entropy with chain length is attributed to a rather limited configurational entropy in the transition state.

Correlating all enthalpies and entropies one notes a compensation effect (**Figure 2.3.**), independent of the specific nature of the mechanism. Such a strict correlation beyond the observed mechanistic details suggests that the change of the mechanism is gradual. The differentiation may be related to a rather late (product-like) transition state with a high entropy and an early (reactant-like) transition state with a low entropy for the E2 like elimination. Especially remarkable is the significant difference between *cis* and *trans* 2-McyOH. It highlights how a combination of several factors determines the catalytic conversion, i.e., (i) the position of the alkyl-substituents, (ii) their steric configuration to the OH group, and (iii) their size.

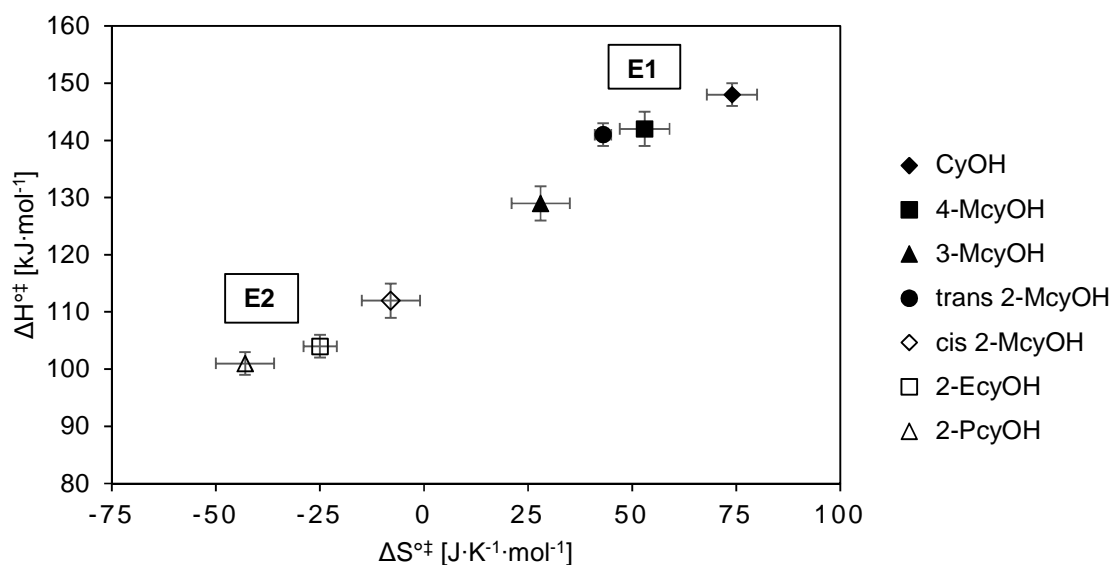


Figure 2.3. Correlation of enthalpy and entropy of the zeolite catalyzed dehydration.

2.4. Conclusions

Elimination of water from secondary methyl substituted cyclohexanols catalyzed by hydronium ions in the medium pore zeolite ZSM-5 depends on the position and the size of the alkyl substitution. Methyl substitution closer to the hydroxyl-group leads to a concerted (E2-type) elimination, while those with a higher distance between methyl and OH-group tend to eliminate water in an E1-type pathway. The two pathways are characterized by differences in enthalpies and entropies of activation, with the E2 pathway showing lower enthalpies and higher entropies than elimination *via* the E1 pathway.

The differences between the two mechanisms are reflected in the higher selectivity to the *Saytzeff*-product (approximately 14/1) for the E2 pathway as observed in case of *cis* 2-McyOH. In general, higher enthalpy leads to lower rates of reaction. However, two remarkable exceptions were observed. One is the higher rate of dehydration of unsubstituted cyclohexanol, which is attributed to the much higher entropy (rather free rotation in the pores) compared to the substituted cyclohexanols. The other case is the elimination of 2-PcyOH, which has a particularly low entropy (rather limited configurational entropy in the transition state).

Independent of the dehydration mechanism, catalysis of hydronium ions generated by H₃PO₄ in water always led to TOFs that were two orders of magnitude lower and higher activation barriers compared to hydronium ions in the confines of MFI pores.

The results show, how the chemical nature of the reacting substrate can experience local differences despite the identical nature of the catalytically active site. The steric constraints and the chemical activity of the active site determine the rate constants. While we begin to understand these localized activities of sites in a system resembling the confines of enzyme pockets, the presented study also points to the complexity and challenges to quantitatively describe and understand the conversions on a molecular scale.

2.5. References

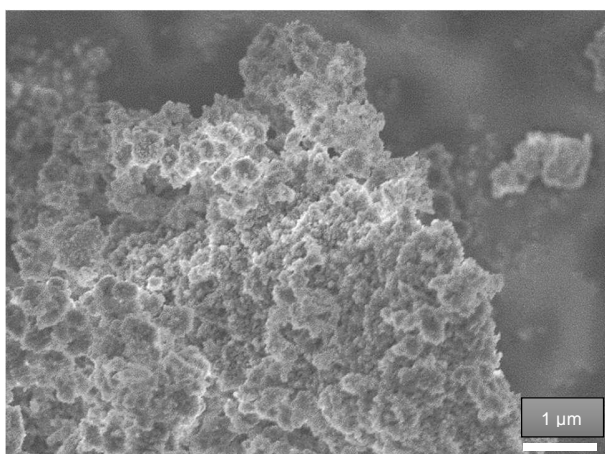
- [1] a) H. Noller, K. Thomke, *Journal of Molecular Catalysis* **1979**, 6, 375-392. b) H. Noller, W. Kladnig, *Catalysis Reviews Science and Engineering* **1976**, 13, 149-207. c) P. Salvador, W. Kladnig, *Journal of the Chemical Society Faraday Transactions 1: Physical Chemistry in Condensed Phases* **1977**, 73, 1153-1168. d) K. Thomke, H. Noller, *Zeitschrift für Naturforschung B* **1972**, 27, 1462-1464.
- [2] a) J. He, C. Zhao, J. A. Lercher, *Journal of Catalysis* **2014**, 309, 362-375. b) C. Zhao, W. Song, J. A. Lercher, *ACS Catalysis* **2012**, 2, 2714-2723. c) C. Zhao, J. A. Lercher, *Angewandte Chemie International Edition* **2012**, 24, 6037-6042. d) C. Zhao, Y. Kou, A. A. Lemonidou, X. Li, J. A. Lercher, *Angewandte Chemie International Edition* **2009**, 22, 4047-4050. e) C. Zhao, S. Kasakov, J. He, J. A. Lercher, *Journal of Catalysis* **2012**, 296, 12-23. f) C. Zhao, J. He, A. A. Lemonidou, X. Li, J. A. Lercher, *Journal of Catalysis* **2011**, 280, 8-16. g) C. Zhao, D. M. Camaioni, J. A. Lercher, *Journal of Catalysis* **2012**, 288, 92-103. h) A. Vjunov, M. Y. Hu, J. Feng, D. M. Camaioni, D. Mei, J. C. Hu, C. Zhao, J. A. Lercher, *Angewandte Chemie International Edition* **2014**, 53, 479-482.
- [3] a) F. Bautista, J. Campelo, A. Garcia, D. Luna, J. Marinas, R. Quiros, A. Romero, *Applied Catalysis A: General* **2003**, 243, 93-107. b) A. Clearfield, D. S. Thakur, *Journal of Catalysis* **1980**, 65, 185-194. c) R. A. Johnstone, J.-Y. Liu, D. Whittaker, *Journal of the Chemical Society Perkin Transactions 2* **1998**, 1287-1288. d) D. Thakur, A. Clearfield, *Journal of Catalysis* **1981**, 69, 230-233.
- [4] a) J. Macht, M. J. Janik, M. Neurock, E. Iglesia, *Journal of the American Chemical Society* **2008**, 130, 10369-10379. b) M. J. Janik, J. Macht, E. Iglesia, M. Neurock, *Journal of Physical Chemistry C* **2009**, 113, 1872-1885.
- [5] a) Y. Zhi, H. Shi, L. Mu, Y. Liu, D. Mei, D. M. Camaioni, J. A. Lercher, *Journal of the American Chemical Society* **2015**, 137, 15781-15794. b) D. Mei, J. A. Lercher, *American Institute of Chemical Engineers Journal* **2017**, 63, 172-184.
- [6] a) M. Eigen, *Angewandte Chemie International Edition* **1964**, 3, 1-19. b) G. Zundel, *Angewandte Chemie International Edition* **1969**, 8, 499-509.
- [7] a) W. Kulig, N. Agmon, *Nature Chemistry* **2013**, 5, 29-35. b) O. Markovitch, N. Agmon, *Journal of Physical Chemistry A* **2007**, 111, 2253-2256. c) N. Agmon, S. Y. Goldberg, D. Huppert, *Journal of Molecular Liquids* **1995**, 64, 161-195. d) N. Agmon, *Chemical Physics Letters* **1995**, 244, 456-462. e) O. Markovitch, *Journal of Physical Chemistry B* **2008**, 112, 9456-9466. f) D. Marx, M. E. Tuckerman, J. Hutter, M. Parrinello, *Nature* **1999**, 397, 601-604.
- [8] Y. Liu, A. Vjunov, H. Shi, S. Eckstein, D. Camaioni, D. Mei, E. Barath, J. A. Lercher, *Nature Communications* **2016**, DOI: 10.1038/ncomms14113.
- [9] A. Thibblin, *Chemical Society Reviews* **1993**, 22, 427-433.

- [10] a) M. M. Clennan, E. L. Clennan, *Journal of Chemical Education* **2011**, *88*, 646-648. b) J. B. Friesen, R. Schretzman, *Journal of Chemical Education* **2011**, *88*, 1141-1147. c) D. Todd, *Journal of Chemical Education* **1994**, *71*, 440-440. d) K. Kochloefl, M. Kraus, C. Chin-Shen, L. Beranek, V. Bažant, *Collection of Czechoslovak Chemical Communications* **1962**, *27*, 1199-1209.
- [11] H. Shi, S. Eckstein, A. Vjunov, D. Camaioni, J. A. Lercher, *Nature Communications* **2017**, DOI: 10.1038/ncomms15442.
- [12] A. Saytzeff, *Justus Liebigs Annalen der Chemie* **1875**, *179*, 296-301.
- [13] A. Hofmann, *Justus Liebigs Annalen der Chemie* **1851**, *79*, 11-39.
- [14] W. Markownikoff, *Justus Liebigs Annalen der Chemie* **1870**, *153*, 228-259.
- [15] K. J. Laidler, *Chemical Kinetics: Theories of Reaction Rates; 3. Edition*, Harper & Row, New York, **1987**; 89-115.
- [16] M. B. Smith, J. March, *Advanced Organic Chemistry, 6. Edition*, Wiley, New York, **2007**, 1477-1558.
- [17] National Institute of Advanced Industrial Science and Technology, <https://sdfs.db.aist.go.jp>, accessed: 04/2017.
- [18] W. W. Rudolph, *Journal of Solution Chemistry* **2012**, *41*, 630-645.

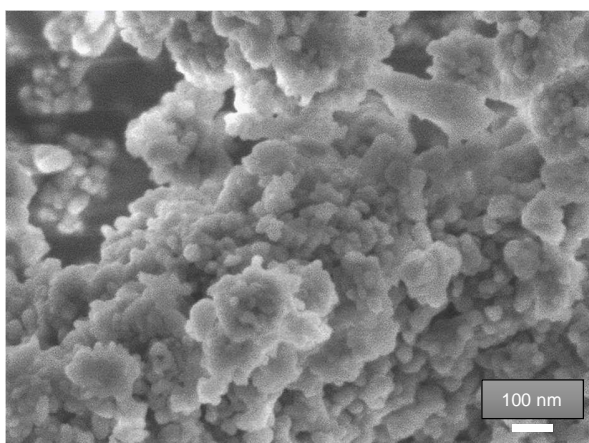
2.6. Supporting information

Table S2.1. Characterization of the investigated **MFI-45** zeolite (Si/Al = 45).

Property	Unit	Value
Particle size	[nm]	100 - 150
Surface area - total	[m ² ·g ⁻¹]	389
Surface area – micro pores	[m ² ·g ⁻¹]	302
Surface area – meso pores	[m ² ·g ⁻¹]	87
C (acid sites) TPD	[μmol·g ⁻¹]	400
C (Brønsted acid sites) IR	[μmol·g ⁻¹]	360
C (Lewis acid sites) IR	[μmol·g ⁻¹]	45



SEM-Image S2.1. MFI-45 (Si/Al = 45).



SEM-Image 2.2. MFI-45 (Si/Al = 45).

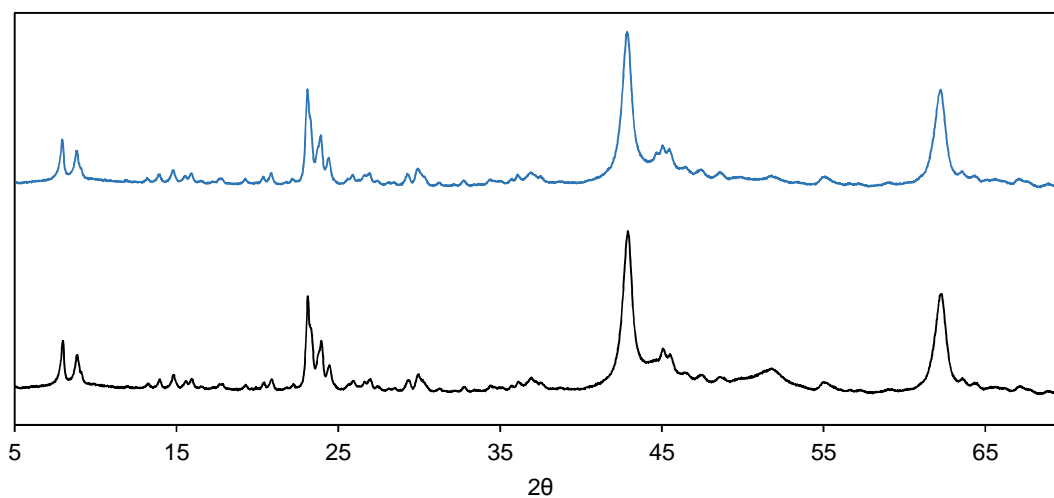
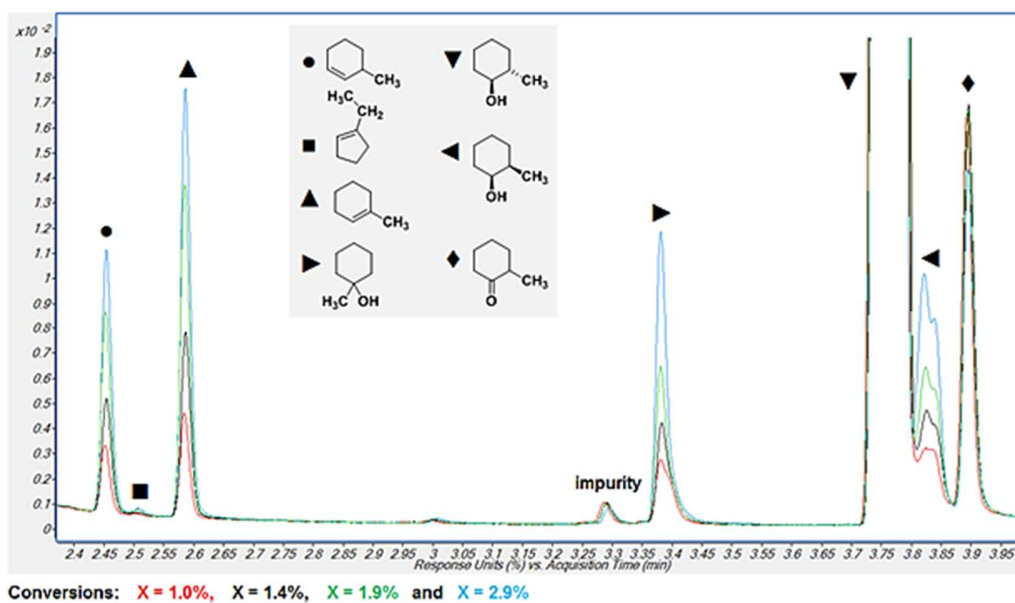
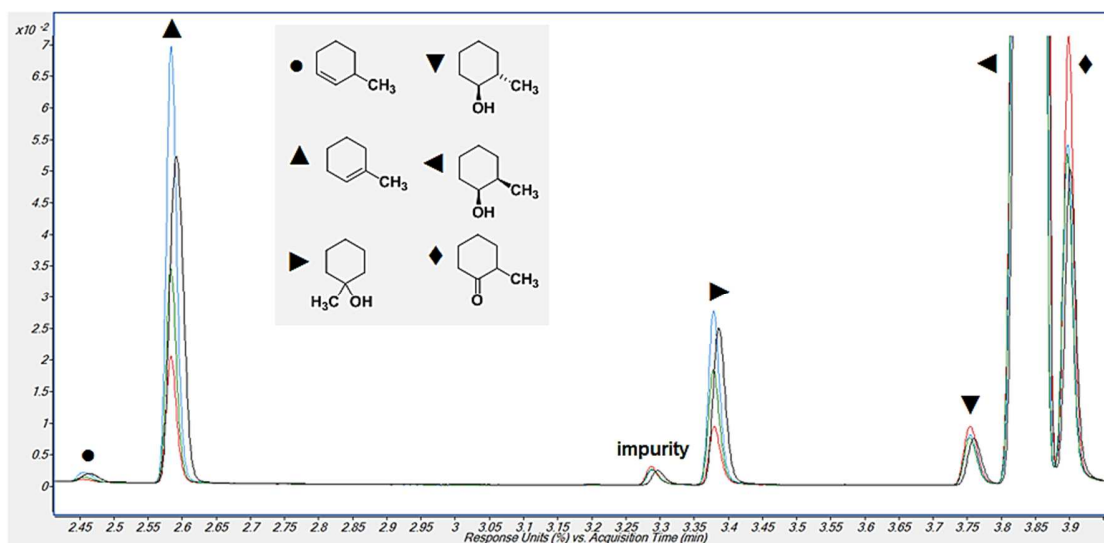


Figure S2.1. X-Ray diffraction pattern of the treated (blue; 190 °C, 14h) and parent (black) **MFI-45** (internal standard MgO).



Chromatogram S2.1. Dehydration of *trans* 2-McyOH forms *cis* 2-McyOH via rehydration (initial impurity of *cis* 2-McyOH: ca. 1%). ● Hofmann-product; ■ 1-ethylcyclopent-1-ene; ▲ Saytzeff-product; ► 1-McyOH; ▼ *trans* 2-McyOH; ◄ *cis* 2-McyOH; ◆ 2-methyl-cyclohexan-1-one (impurity).

2. Hydronium ion catalyzed elimination pathways of substituted cyclohexanols



Conversions: $X = 1.7\%$, $X = 3.6\%$, $X = 5.8\%$ and $X = 6.1\%$

Chromatogram S2.2. Dehydration of *cis*-2-McyOH does not form *trans*-2-McyOH (initial impurity of *trans*-2-McyOH: ca. 1%). ● Hofmann-product; ▲ Saytzeff-product; ► 1-McyOH; ▼ *trans*-2-McyOH (impurity); ◄ *cis*-2-McyOH; ◆ 2-methyl-cyclohexan-1-one (impurity).

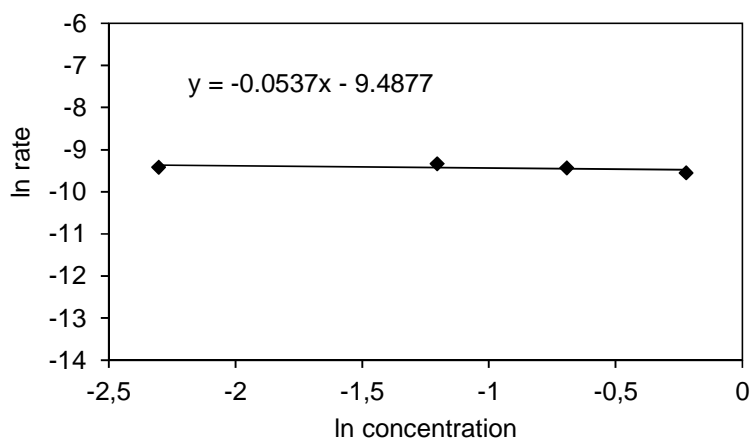


Figure S2.2. Reaction order of **CyOH** dehydration (170 °C, 50 bar, **MFI-45**).

Table S2.2. Dehydration rates and initial concentrations of **CyOH** dehydration (170 °C, 50bar, **MFI-45**).

rate [mol·g ⁻¹ ·s ⁻¹]	n [mol]	c [mol·L ⁻¹]	ln rate	ln c
7.2·10 ⁻⁵	0.08	0.80	-9.54	-0.22
8.1·10 ⁻⁵	0.05	0.50	-9.43	-0.69
8.9·10 ⁻⁵	0.03	0.30	-9.33	-1.20
8.2·10 ⁻⁵	0.01	0.10	-9.41	-2.30

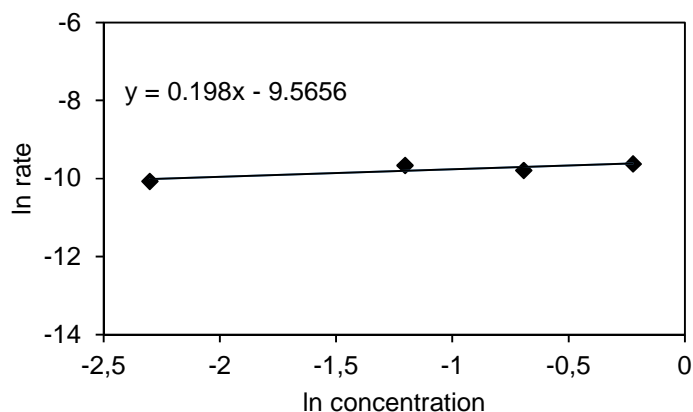


Figure S2.3. Reaction order of **2-McyOH** dehydration (170 °C, 50 bar, **MFI-45**).

Table S2.3. Dehydration rates and initial concentration of **2-McyOH** (170 °C, 50 bar, **MFI-45**).

rate [mol·g ⁻¹ ·s ⁻¹]	n [mol]	c [mol·L ⁻¹]	ln rate	ln c
6.7·10 ⁻⁵	0.08	0.80	- 9.62	-0.22
5.6·10 ⁻⁵	0.05	0.50	- 9.79	-0.69
6.4·10 ⁻⁵	0.03	0.30	- 9.66	-1.20
4.2·10 ⁻⁵	0.01	0.10	-10.07	-2.30

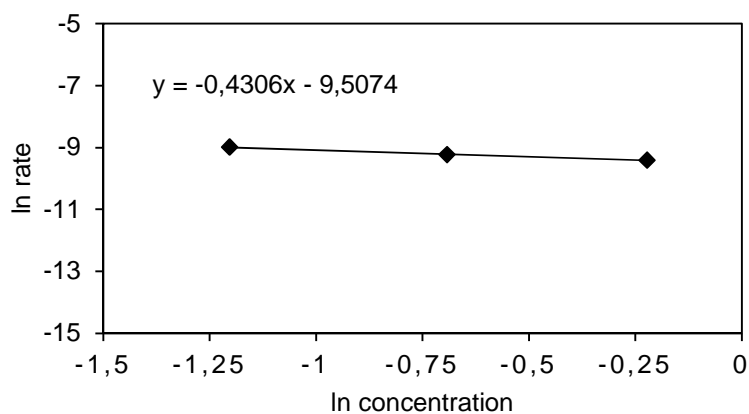


Figure S2.4. Reaction order of **4-McyOH** dehydration (180 °C, 50 bar, **MFI-45**).

Table S2.4. Dehydration rates and initial concentration of **4-McyOH** (180 °C, 50 bar, **MFI-45**).

rate [mol·g ⁻¹ ·s ⁻¹]	n [mol]	c [mol·L ⁻¹]	ln rate	ln c
8.2·10 ⁻⁵	0.08	0.80	- 9.41	-0.22
9.9·10 ⁻⁵	0.05	0.50	- 9.22	-0.69
1.3·10 ⁻⁴	0.03	0.30	- 8.98	-1.20

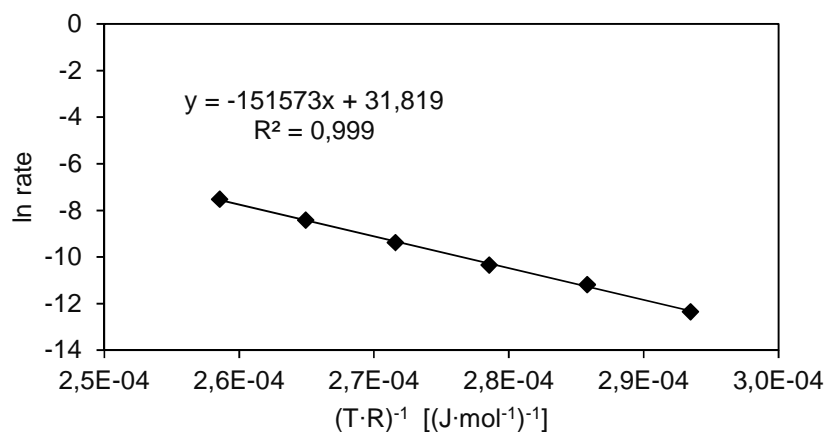


Figure S2.5. Arrhenius-plot: **CyOH** (0.5 M) dehydration ($E_a \approx 152$ kJ/mol), **MFI-45**.

Table S2.5. **CyOH** (0.5 M) dehydration rates at different reaction temperatures, **MFI-45**.

T [°C]	T [K]	TOF [s ⁻¹]	rate [mol·g ⁻¹ ·s ⁻¹]	(T·R) ⁻¹ [(J·mol ⁻¹) ⁻¹]	ln rate
140	413	1.2·10 ⁻²	4.4·10 ⁻⁶	2.91·10 ⁻⁴	-12.3
150	423	3.9·10 ⁻²	1.4·10 ⁻⁵	2.84·10 ⁻⁴	-11.2
160	433	9.1·10 ⁻²	3.3·10 ⁻⁵	2.78·10 ⁻⁴	-10.3
170	443	2.4·10 ⁻¹	8.6·10 ⁻⁵	2.71·10 ⁻⁴	-9.4
180	453	6.2·10 ⁻¹	2.2·10 ⁻⁴	2.65·10 ⁻⁴	-8.4
190	463	1.5	5.5·10 ⁻⁴	2.60·10 ⁻⁴	-7.5

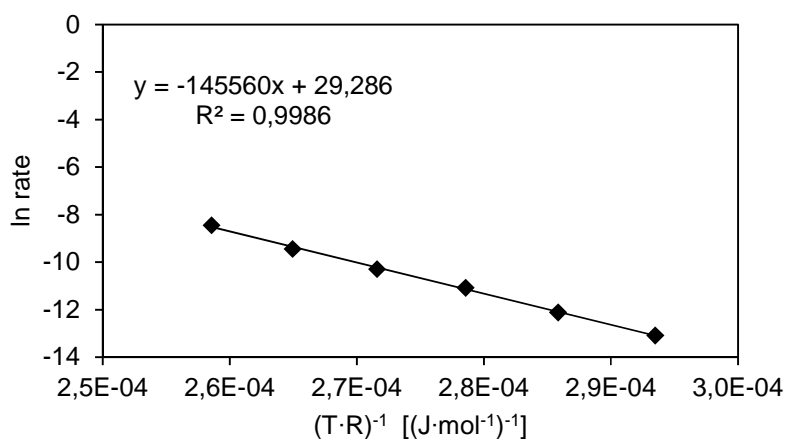
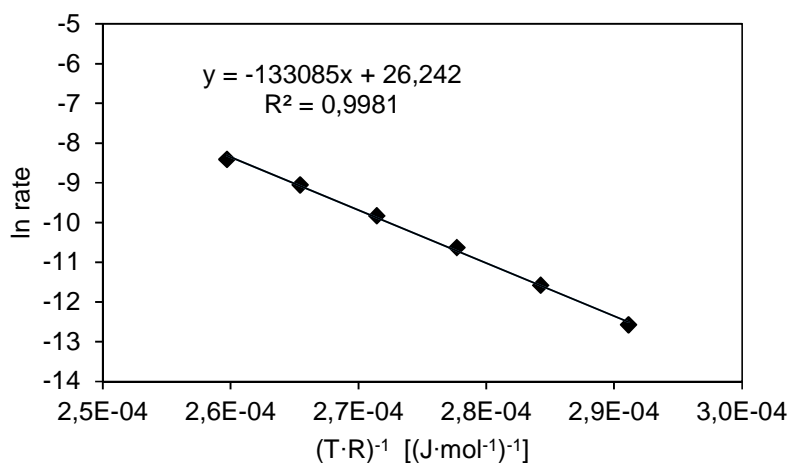


Figure S2.6. Arrhenius-plot: **4-McyOH** (0.5 M) dehydration ($E_a \approx 146$ kJ/mol), **MFI-45**.

Table S2.6. 4-McyOH (0.5 M) dehydration rates at different reaction temperatures, MFI-45.

T [°C]	T [K]	TOF [s ⁻¹]	rate [mol·g ⁻¹ ·s ⁻¹]	(T·R) ⁻¹ [(J·mol ⁻¹) ⁻¹]	ln rate
140	413	5.8·10 ⁻³	2.1·10 ⁻⁶	2.91·10 ⁻⁴	-13.1
150	423	1.5·10 ⁻²	5.5·10 ⁻⁶	2.84·10 ⁻⁴	-12.1
160	433	4.3·10 ⁻²	1.6·10 ⁻⁵	2.78·10 ⁻⁴	-11.1
170	443	9.5·10 ⁻²	3.4·10 ⁻⁵	2.71·10 ⁻⁴	-10.3
180	453	2.2·10 ⁻¹	8.1·10 ⁻⁵	2.65·10 ⁻⁴	-9.4
190	463	6.0·10 ⁻¹	2.2·10 ⁻⁴	2.60·10 ⁻⁴	-8.4

**Figure S2.7.** Arrhenius-plot: 3-McyOH (0.5 M) dehydration ($E_a \approx 133$ kJ/mol), MFI-45.**Table S2.7.** 3-McyOH (0.5 M) dehydration rates at different reaction temperatures, MFI-45.

T [°C]	T [K]	TOF [s ⁻¹]	rate [mol·g ⁻¹ ·s ⁻¹]	(T·R) ⁻¹ [(J·mol ⁻¹) ⁻¹]	ln rate
140	413	9.6·10 ⁻³	3.5·10 ⁻⁶	2.91·10 ⁻⁴	-12.6
150	423	2.6·10 ⁻²	9.4·10 ⁻⁶	2.84·10 ⁻⁴	-11.6
160	433	6.7·10 ⁻²	2.4·10 ⁻⁵	2.78·10 ⁻⁴	-10.6
170	443	1.5·10 ⁻¹	5.4·10 ⁻⁵	2.71·10 ⁻⁴	-9.3
180	453	3.3·10 ⁻¹	1.2·10 ⁻⁴	2.65·10 ⁻⁴	-9.1
190	463	6.2·10 ⁻¹	2.2·10 ⁻⁴	2.60·10 ⁻⁴	-8.4

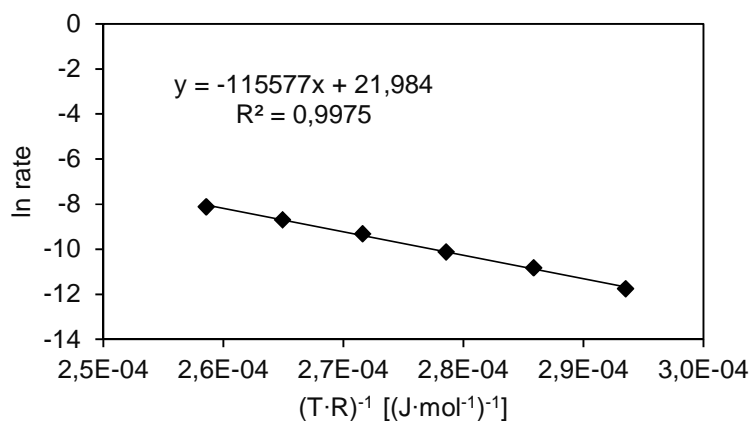


Figure S2.8. Arrhenius-plot: **2-McyOH** (0.5 M) dehydration ($E_a \approx 116$ kJ/mol), **MFI-45**.

Table S2.8. **2-McyOH** (0.5 M) dehydration rates at different reaction temperatures, **MFI-45**.

T [°C]	T [K]	TOF [s ⁻¹]	rate [mol·g ⁻¹ ·s ⁻¹]	(T·R) ⁻¹ [(J·mol ⁻¹) ⁻¹]	ln rate
140	413	2.2·10 ⁻²	7.9·10 ⁻⁶	2.91·10 ⁻⁴	-11.7
150	423	5.6·10 ⁻²	2.0·10 ⁻⁵	2.84·10 ⁻⁴	-10.8
160	433	1.1·10 ⁻¹	4.0·10 ⁻⁵	2.78·10 ⁻⁴	-10.1
170	443	2.5·10 ⁻¹	9.2·10 ⁻⁵	2.71·10 ⁻⁴	-9.3
180	453	4.7·10 ⁻¹	1.7·10 ⁻⁴	2.65·10 ⁻⁴	-8.7
190	463	8.4·10 ⁻¹	3.0·10 ⁻⁴	2.60·10 ⁻⁴	-8.1

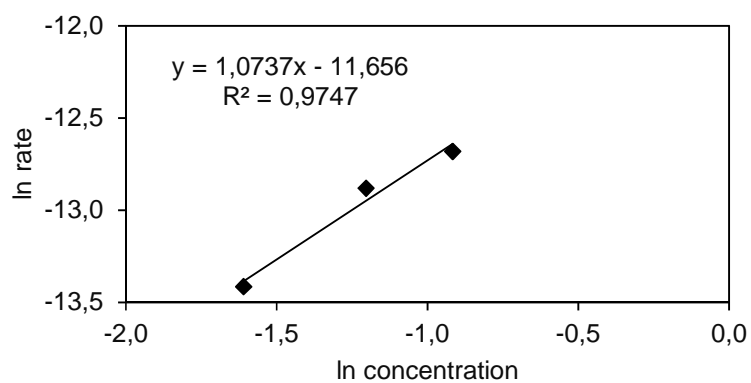


Figure S2.9. Reaction order of **cis 2-McyOH** dehydration (170 °C, 50 bar, **H₃PO₄**).

Table S2.9. Dehydration rates and initial concentrations of **cis 2-McyOH** (170 °C, 50bar, **H₃PO₄**).

c [mol·L ⁻¹]	rate [mol·s ⁻¹]	TOF [s ⁻¹]	n H ⁺ [mol]	ln TOF	ln c	ln rate
0.2	1.5·10 ⁻⁶	9.9·10 ⁻³	1.51·10 ⁻⁴	-4.61	-1.61	-13.41
0.3	2.6·10 ⁻⁶	1.7·10 ⁻²	1.51·10 ⁻⁴	-4.08	-1.20	-12.88
0.4	3.1·10 ⁻⁶	2.1·10 ⁻²	1.51·10 ⁻⁴	-3.88	-0.92	-12.68

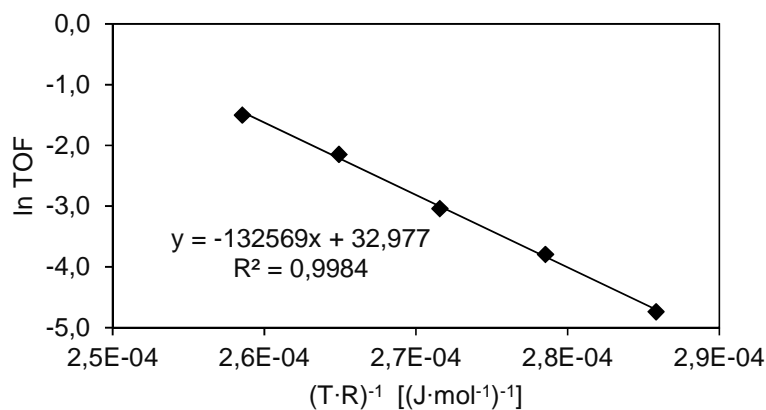


Figure S2.10. Arrhenius-plot: *cis* 2-McyOH (0.2 M) dehydration ($E_a \approx 133$ kJ/mol), H_3PO_4 .

Table S2.10. *Cis* 2-McyOH (0.2 M) dehydration rates at different reaction temperatures, H_3PO_4 .

T [°C]	T [K]	rate [mol·s ⁻¹]	TOF [s ⁻¹]	n H ⁺ [mmol]	ln TOF	(T·R) ⁻¹ [(J·mol ⁻¹) ⁻¹]
150	423	$3.2 \cdot 10^{-7}$	$8.8 \cdot 10^{-3}$	$1.83 \cdot 10^{-1}$	-4.74	$2.84 \cdot 10^{-4}$
160	433	$7.5 \cdot 10^{-7}$	$2.3 \cdot 10^{-2}$	$1.66 \cdot 10^{-1}$	-3.79	$2.78 \cdot 10^{-4}$
170	443	$1.4 \cdot 10^{-6}$	$4.8 \cdot 10^{-2}$	$1.51 \cdot 10^{-1}$	-3.04	$2.71 \cdot 10^{-4}$
180	453	$3.2 \cdot 10^{-6}$	$1.2 \cdot 10^{-1}$	$1.36 \cdot 10^{-1}$	-2.14	$2.65 \cdot 10^{-4}$
190	463	$5.5 \cdot 10^{-6}$	$2.2 \cdot 10^{-1}$	$1.23 \cdot 10^{-1}$	-1.50	$2.60 \cdot 10^{-4}$

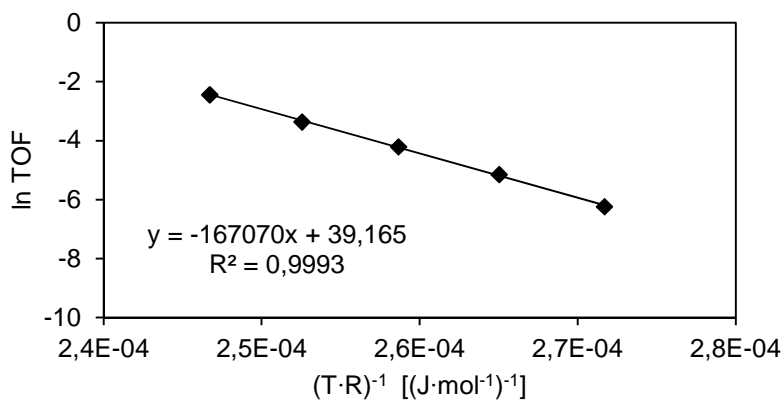


Figure S2.11. Arrhenius-plot: *trans* 2-McyOH (0.04 M) dehydration ($E_a \approx 167$ kJ/mol), H_3PO_4 .

Table S2.11. *Trans* 2-McyOH (0.04 M) dehydration rates at different reaction temperatures, H_3PO_4 .

T [°C]	T [K]	rate [mol·s ⁻¹]	TOF [s ⁻¹]	ln TOF	(T·R) ⁻¹ [(J·mol ⁻¹) ⁻¹]
170	443	$5.3 \cdot 10^{-8}$	$2.0 \cdot 10^{-3}$	-6.24	$2.72 \cdot 10^{-4}$
180	453	$1.4 \cdot 10^{-7}$	$5.8 \cdot 10^{-3}$	-5.15	$2.66 \cdot 10^{-4}$
190	463	$3.3 \cdot 10^{-7}$	$1.5 \cdot 10^{-2}$	-4.21	$2.60 \cdot 10^{-4}$
200	473	$4.1 \cdot 10^{-7}$	$3.5 \cdot 10^{-2}$	-3.36	$2.54 \cdot 10^{-4}$
210	483	$9.2 \cdot 10^{-7}$	$8.7 \cdot 10^{-2}$	-2.44	$2.49 \cdot 10^{-4}$

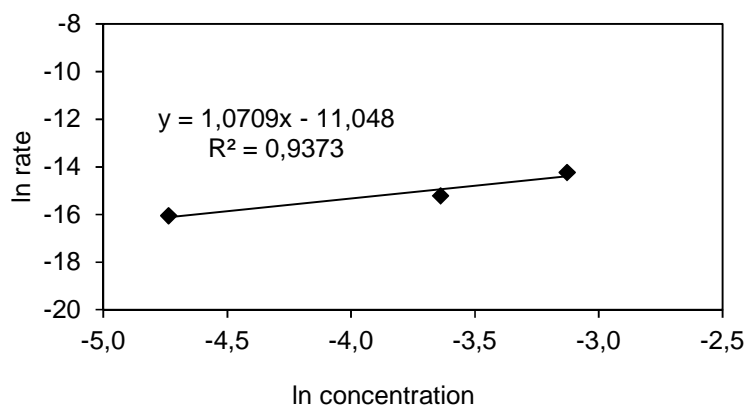


Figure S2.12. Reaction order for *trans* 2-McyOH dehydration, H₃PO₄.

Table S2.12. *Trans* 2-McyOH dehydration rates for different initial concentrations, H₃PO₄.

rate [mol·g ⁻¹ ·s ⁻¹]	n [mmol]	c [mmol·L ⁻¹]	ln rate	ln c
1.58·10 ⁻⁷	0.9	8.8	- 16.0	- 4.7
2.26·10 ⁻⁷	2.6	26.3	- 15.2	- 3.6
6.66·10 ⁻⁷	4.4	43.8	- 14.2	- 3.1

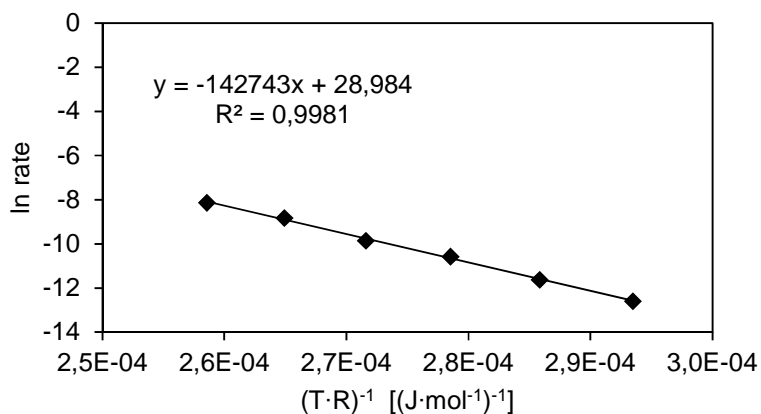


Figure S2.13. Arrhenius-plot: 4-EcyOH (0.5 M) dehydration ($E_a \approx 143$ kJ/mol), MFI-45.

Table S2.13. 4-EcyOH (0.5 M) dehydration rates at different reaction temperatures, MFI-45.

T [°C]	T [K]	TOF [s ⁻¹]	rate [mol·s ⁻¹]	(T·R) ⁻¹ [(J·mol ⁻¹) ⁻¹]	ln rate
140	413	9.5·10 ⁻³	3.4·10 ⁻⁶	2.91·10 ⁻⁴	-12.6
150	423	2.5·10 ⁻²	9.1·10 ⁻⁶	2.84·10 ⁻⁴	-11.6
160	433	7.2·10 ⁻²	2.6·10 ⁻⁵	2.78·10 ⁻⁴	-10.6
170	443	1.5·10 ⁻¹	5.3·10 ⁻⁵	2.71·10 ⁻⁴	-9.6
180	453	4.1·10 ⁻¹	1.5·10 ⁻⁴	2.65·10 ⁻⁴	-8.8
190	463	8.2·10 ⁻¹	2.9·10 ⁻⁴	2.60·10 ⁻⁴	-8.1

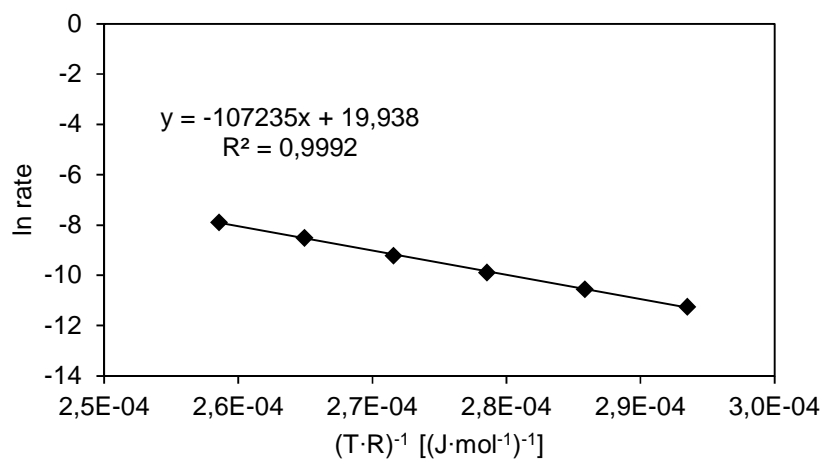


Figure S2.14. Arrhenius-plot: **2-EcyOH** (0.5 M) dehydration ($E_a \approx 107$ kJ/mol), **MFI-45**.

Table S2.14. **2-EcyOH** (0.5 M) dehydration rates at different reaction temperatures, **MFI-45**.

T [°C]	T [K]	TOF [s ⁻¹]	rate [mol·g ⁻¹ ·s ⁻¹]	(T·R) ⁻¹ [(J·mol ⁻¹) ⁻¹]	ln rate
140	413	3.6·10 ⁻²	1.3·10 ⁻⁵	2.91·10 ⁻⁴	-11.2
150	423	7.3·10 ⁻²	2.6·10 ⁻⁵	2.84·10 ⁻⁴	-10.6
160	433	1.4·10 ⁻¹	5.1·10 ⁻⁵	2.78·10 ⁻⁴	-9.9
170	443	2.8·10 ⁻¹	1.0·10 ⁻⁴	2.71·10 ⁻⁴	-9.2
180	453	5.6·10 ⁻¹	2.0·10 ⁻⁴	2.65·10 ⁻⁴	-8.5
190	463	1.0	3.8·10 ⁻⁴	2.60·10 ⁻⁴	-7.9

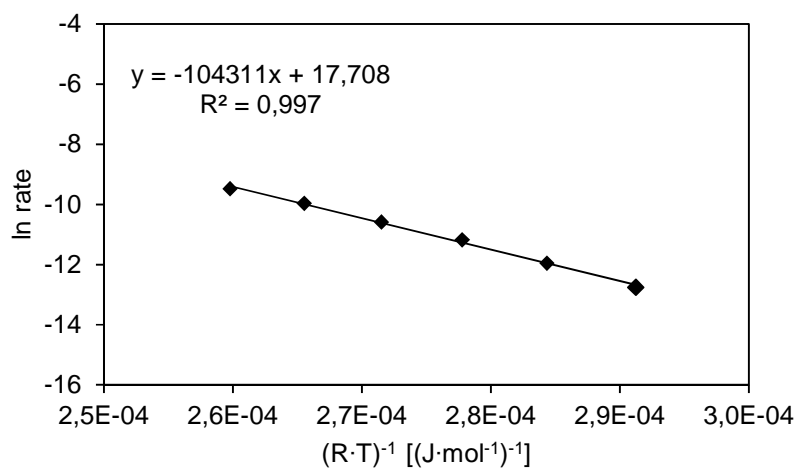


Figure S2.15. Arrhenius-plot: **2-PcyOH** (0.5 M) dehydration ($E_a \approx 104$ kJ/mol), **MFI-45**.

Table S2.15. 2-PcyOH (0.5 M) dehydration rates at different reaction temperatures, MFI-45.

T [°C]	T [K]	TOF [s ⁻¹]	rate [mol·g ⁻¹ ·s ⁻¹]	(T·R) ⁻¹ [(J·mol ⁻¹) ⁻¹]	ln rate
140	413	8.1·10 ⁻³	2.9·10 ⁻⁶	2.91·10 ⁻⁴	-12.7
150	423	1.8·10 ⁻²	6.5·10 ⁻⁶	2.84·10 ⁻⁴	-12.0
160	433	3.4·10 ⁻²	1.4·10 ⁻⁵	2.78·10 ⁻⁴	-11.2
170	443	7.1·10 ⁻²	2.5·10 ⁻⁵	2.71·10 ⁻⁴	-10.6
180	453	1.3·10 ⁻¹	4.7·10 ⁻⁵	2.65·10 ⁻⁴	-10.0
190	463	2.1·10 ⁻¹	7.7·10 ⁻⁵	2.60·10 ⁻⁴	-9.5

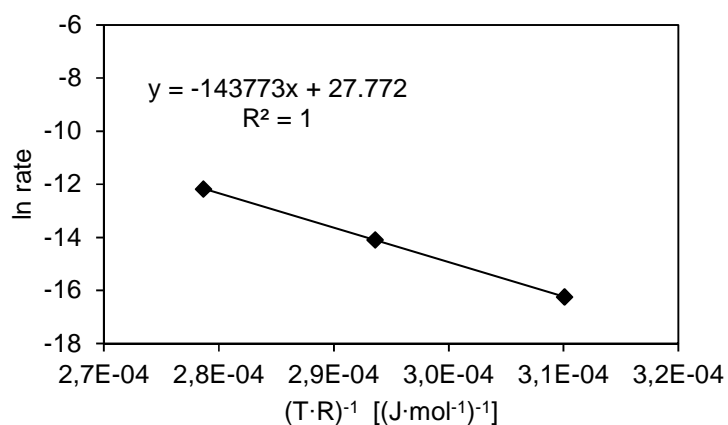
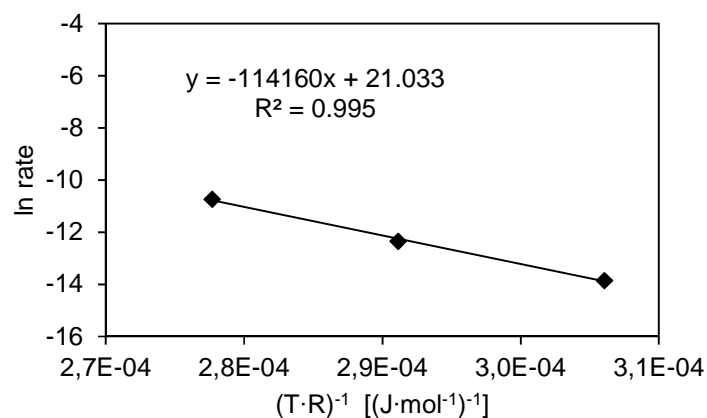
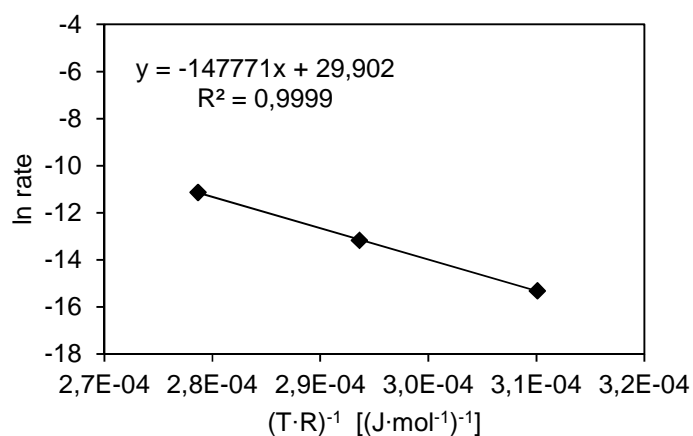
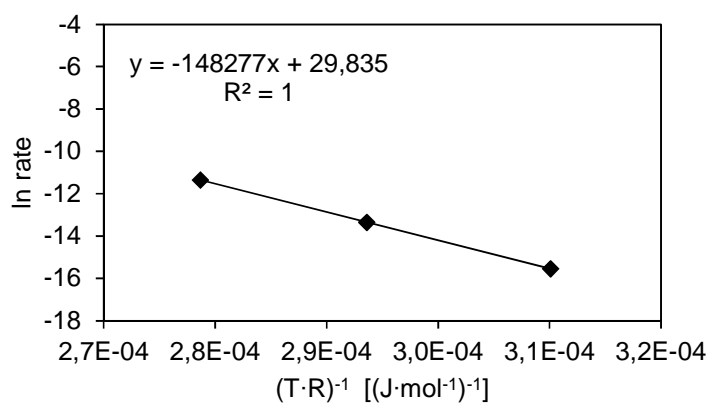
**Figure S2.16.** Arrhenius-plot: pure isomers of 2-methylcyclohexanol (0.04 M), *cis* 2-McyOH (top; $E_a = 114$ kJ/mol) and *trans* 2-McyOH (bottom; $E_a \approx 144$ kJ/mol), MFI-45.

Table S2.16. *cis* 2-McyOH (0.04 M, top) and *trans* 2-McyOH (0.04 M, bottom) dehydration rates, MFI-45.

T [°C]	T [K]	TOF [s ⁻¹]	rate [mol·g ⁻¹ ·s ⁻¹]	(T·R) ⁻¹ [(J·mol ⁻¹) ⁻¹]	ln rate
120	393	2.7·10 ⁻³	9.7·10 ⁻⁷	3.06·10 ⁻⁴	-13.8
140	413	1.2·10 ⁻²	4.4·10 ⁻⁶	2.91·10 ⁻⁴	-12.3
160	433	6.1·10 ⁻²	2.5·10 ⁻⁵	2.78·10 ⁻⁴	-10.6

T [°C]	T [K]	TOF [s ⁻¹]	rate [mol·g ⁻¹ ·s ⁻¹]	(T·R) ⁻¹ [(J·mol ⁻¹) ⁻¹]	ln rate
120	393	2.5·10 ⁻⁴	8.9·10 ⁻⁸	3.06·10 ⁻⁴	-16.2
140	413	2.1·10 ⁻³	7.6·10 ⁻⁷	2.91·10 ⁻⁴	-14.1
160	433	1.4·10 ⁻²	5.2·10 ⁻⁶	2.78·10 ⁻⁴	-12.2

**Figure S2.17.** Arrhenius-plot: pure isomers of 4-methylcyclohexanol (0.04 M), *cis* 4-McyOH (top; $E_a = 148$ kJ/mol) and *trans* 4-McyOH (bottom; $E_a \approx 148$ kJ/mol), MFI-45.

2. Hydronium ion catalyzed elimination pathways of substituted cyclohexanols

Table S2.17. *cis* 4-McyOH (0.04 M, top) and *trans* 2-McyOH dehydration rates (0.04 M, bottom) at different reaction temperatures, MFI-45.

T [°C]	T [K]	TOF [s ⁻¹]	rate [mol·g ⁻¹ ·s ⁻¹]	(T·R) ⁻¹ [(J·mol ⁻¹) ⁻¹]	ln rate
120	393	4.9·10 ⁻⁴	1.8·10 ⁻⁷	3.06·10 ⁻⁴	-15.6
140	413	4.4·10 ⁻³	1.6·10 ⁻⁶	2.91·10 ⁻⁴	-13.4
160	433	3.3·10 ⁻²	1.2·10 ⁻⁵	2.78·10 ⁻⁴	-11.4

T [°C]	T [K]	TOF [s ⁻¹]	rate [mol·g ⁻¹ ·s ⁻¹]	(T·R) ⁻¹ [(J·mol ⁻¹) ⁻¹]	ln rate
120	393	6.2·10 ⁻⁴	2.2·10 ⁻⁷	3.06·10 ⁻⁴	-15.3
140	413	5.4·10 ⁻³	1.9·10 ⁻⁶	2.91·10 ⁻⁴	-13.2
160	433	4.1·10 ⁻²	1.5·10 ⁻⁵	2.78·10 ⁻⁴	-11.1

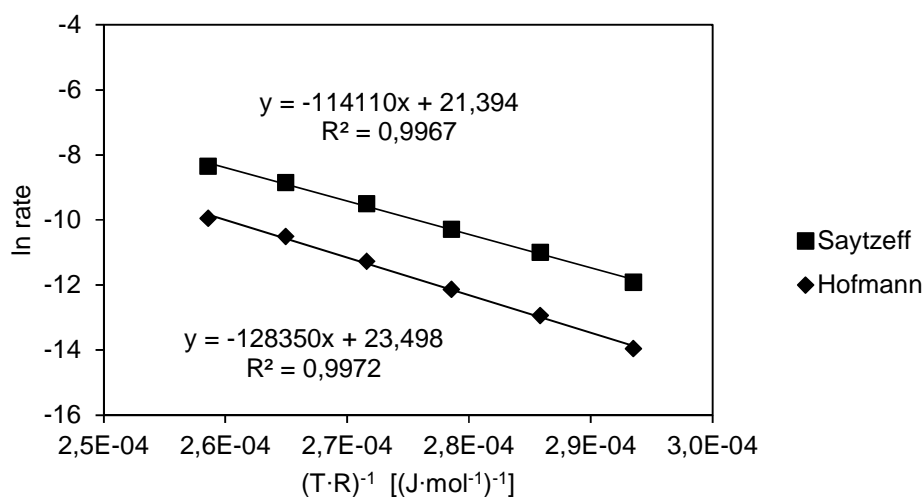


Figure S2.18. Arrhenius-plot: Hofmann- and Saytzeff-products of 2-McyOH (0.5 M), MFI-45.

Table S2.18. Dehydration rates leading to Hofmann- and Saytzeff-products of 2-McyOH (0.5 M), MFI-45.

T [°C]	T [K]	rate Hofmann	rate Saytzeff	(T·R) ⁻¹ [(J·mol ⁻¹) ⁻¹]	ln rate Hofmann	ln rate Saytzeff
140	413	8.7·10 ⁻⁷	6.7·10 ⁻⁶	2.91·10 ⁻⁴	-13.95	-11.91
150	423	2.4·10 ⁻⁶	1.7·10 ⁻⁵	2.84·10 ⁻⁴	-12.94	-10.99
160	433	5.4·10 ⁻⁶	3.4·10 ⁻⁵	2.78·10 ⁻⁴	-12.13	-10.29
170	443	1.3·10 ⁻⁵	7.5·10 ⁻⁵	2.71·10 ⁻⁴	-11.27	-9.49
180	453	2.7·10 ⁻⁵	1.4·10 ⁻⁴	2.65·10 ⁻⁴	-10.51	-8.85
190	463	4.8·10 ⁻⁵	2.4·10 ⁻⁴	2.60·10 ⁻⁴	-9.95	-8.347

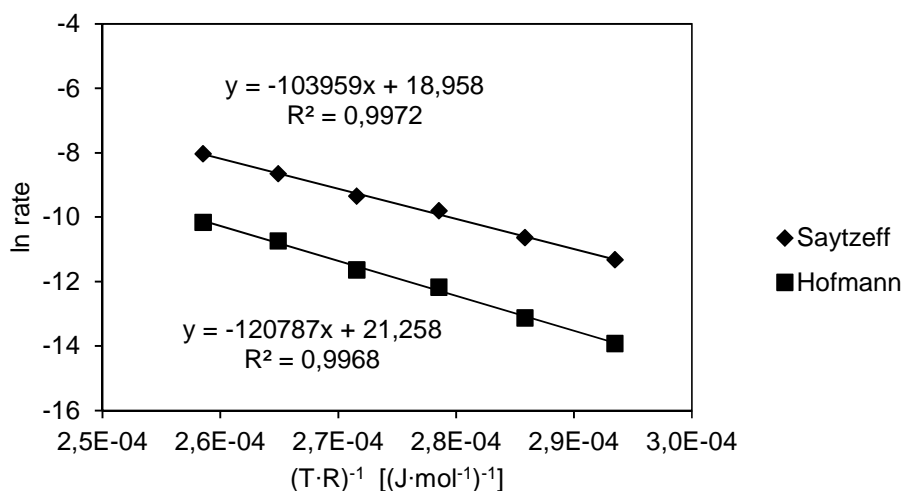


Figure S2.19. Arrhenius-plot: Hofmann- and Saytzeff-products of **2-EcyOH** (0.5 M), **MFI-45**.

Table S2.19. Dehydration rates leading to Hofmann- and Saytzeff-products of **2-EcyOH** (0.5 M), **MFI-45**.

T [°C]	T [K]	rate Hofmann	rate Saytzeff	$(T \cdot R)^{-1}$ [(J·mol ⁻¹) ⁻¹]	ln rate Saytzeff	ln rate Hofmann
140	413	$9.1 \cdot 10^{-7}$	$1.2 \cdot 10^{-5}$	$2.91 \cdot 10^{-4}$	-11.31	-13.92
150	423	$2.0 \cdot 10^{-6}$	$2.4 \cdot 10^{-5}$	$2.84 \cdot 10^{-4}$	-10.63	-13.12
160	433	$5.2 \cdot 10^{-6}$	$5.6 \cdot 10^{-5}$	$2.78 \cdot 10^{-4}$	-9.80	-12.17
170	443	$8.9 \cdot 10^{-6}$	$8.8 \cdot 10^{-5}$	$2.71 \cdot 10^{-4}$	-9.34	-11.63
180	453	$2.2 \cdot 10^{-5}$	$1.8 \cdot 10^{-4}$	$2.65 \cdot 10^{-4}$	-8.65	-10.72
190	463	$3.9 \cdot 10^{-5}$	$3.3 \cdot 10^{-4}$	$2.60 \cdot 10^{-4}$	-8.02	-10.15

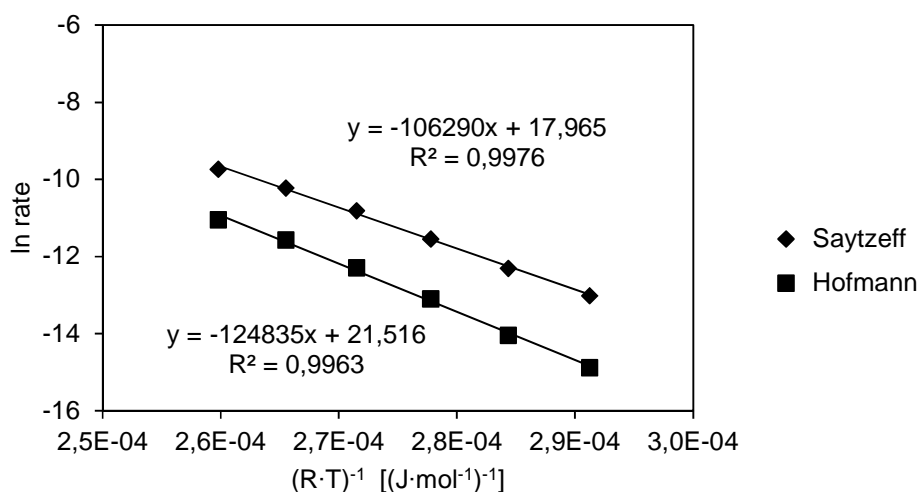


Figure S2.20. Arrhenius-plot: Hofmann- and Saytzeff-products of **2-PcyOH** (0.5 M), **MFI-45**.

Table S2.20. Dehydration rates leading to *Hofmann*- and *Saytzeff*-products of **2-PcyOH** (0.5 M), **MFI-45**.

T [°C]	T [K]	rate <i>Saytzeff</i>	rate <i>Hofmann</i>	$(T \cdot R)^{-1}$ [$(\text{J} \cdot \text{mol}^{-1})^{-1}$]	ln rate <i>Saytzeff</i>	ln rate <i>Hofmann</i>
140	413	$2.2 \cdot 10^{-6}$	$3.5 \cdot 10^{-7}$	$2.91 \cdot 10^{-4}$	-13.01	-14.88
150	423	$4.6 \cdot 10^{-6}$	$8.0 \cdot 10^{-7}$	$2.84 \cdot 10^{-4}$	-12.30	-14.04
160	433	$9.7 \cdot 10^{-6}$	$2.1 \cdot 10^{-6}$	$2.78 \cdot 10^{-4}$	-11.54	-13.09
170	443	$2.0 \cdot 10^{-5}$	$4.6 \cdot 10^{-6}$	$2.72 \cdot 10^{-4}$	-10.81	-12.28
180	453	$3.7 \cdot 10^{-5}$	$9.5 \cdot 10^{-6}$	$2.66 \cdot 10^{-4}$	-10.22	-11.56
190	463	$5.9 \cdot 10^{-5}$	$1.6 \cdot 10^{-5}$	$2.60 \cdot 10^{-4}$	-9.73	-11.04

Table S2.21. Comparison of ΔH^{\ddagger} and ΔS^{\ddagger} of *Saytzeff*- and *Hofmann*-products, **MFI-45** and **H₃PO₄**.

Cat.	Substrate	<i>Saytzeff</i> -product		<i>Hofmann</i> -product	
		ΔH^{\ddagger} [kJ·mol ⁻¹]	ΔS^{\ddagger} [J·K ⁻¹ ·mol ⁻¹]	ΔH^{\ddagger} [kJ·mol ⁻¹]	ΔS^{\ddagger} [J·K ⁻¹ ·mol ⁻¹]
H ₃ PO ₄	2-McyOH ^a	130 (±1)	+18 (±3)	144 (±1)	+28 (±1)
MFI	2-McyOH ^b	110 (±3)	-13 (±8)	125 (±3)	+5 (±8)
MFI	2-EcyOH ^b	100 (±3)	-33 (±6)	117 (±3)	-14 (±8)
MFI	2-PcyOH ^b	103 (±3)	-41 (±6)	121 (±4)	-12 (±9)

Table S2.22. ¹H-NMR analysis of experiments with pure isomers: *cis/trans* 2- and *cis/trans* 4-McyOH, **MFI-45** and **H₃PO₄**.

Substrate	Catalyst	Conversion [%]	<i>Cis</i> or <i>trans</i> isomer, initial impurity [%]	<i>Cis</i> or <i>trans</i> isomer, final composition [%]	Assigned Mechanism
<i>cis</i> 2-McyOH	H ₃ PO ₄	14.2	1 ^a	1 ^a	E2
<i>cis</i> 2-McyOH	H ₃ PO ₄	12.3	2 ^a	1 ^a	E2
<i>cis</i> 4-McyOH	H ₃ PO ₄	61.9	1 ^a	69 ^a	E1
<i>trans</i> 4-McyOH	H ₃ PO ₄	21.1	1 ^b	4 ^b	E1
<i>trans</i> 2-McyOH	H ₃ PO ₄	29.9	3 ^b	6 ^b	E1
<i>cis</i> 2-McyOH	MFI	39.7	1 ^a	2 ^a	E2
<i>trans</i> 2-McyOH	MFI	64.0	0 ^b	5 ^b	E1
<i>cis</i> 4-McyOH	MFI	17.1	1 ^a	9 ^a	E1
<i>trans</i> 4-McyOH	MFI	20.1	1 ^b	3 ^b	E1

^a *Trans* isomer. ^b *Cis* isomer.

3. Influence of acid site concentration and extra-framework aluminum in MFI zeolites on aqueous phase dehydration

This chapter is based on:

Peter H. Hintermeier, Sebastian Eckstein, Yue Liu, Eszter Baráth and Johannes A. Lercher, “*Influence of acid site density and extra-framework aluminum on aqueous phase dehydration in MFI zeolites*“, in preparation.

P.H.H. performed experiments, analyzed the data and wrote the manuscript. S.E. performed the adsorption experiments and analysis. S.E., Y. L. and E.B. contributed in preparing the manuscript by fruitful discussions. J.A.L. is the principal investigator of this project.

Abstract

This chapter highlights the impact of acid site concentration and extra-framework aluminum (EFAl) in HZSM-5 zeolites on aqueous phase dehydration *via* E1 (4-methylcyclohexanol; 4-McyOH) and E2 (2-methylcyclohexanol; 2-McyOH) elimination pathways. Eight MFI zeolites of different Si/Al ratios (12, 15, 23, 32, 40, 45, 60 and 193) were tested in aqueous phase dehydration of 2- and 4-McyOH. The two catalysts with the highest concentration of Aluminum led to *lower* (by 10 kJ·mol⁻¹) activation barriers in 2-McyOH dehydration compared to all other MFI zeolites. In contrast, the activation barrier for 4-McyOH dehydration was *higher* (by 10 kJ·mol⁻¹) on these two MFI zeolites (Si/Al = 12 and 15) compared to the zeolites of higher Si/Al ratios. The removal of EFAl revealed that this octahedrally coordinated Al species has a positive enthalpic effect in a concerted dehydration pathway (E2) and a negative effect on the activation barrier of a stepwise mechanism *via* carbocations (E1), respectively.

3.1. Introduction

The influence of Brønsted acid site concentration on zeolite catalyzed reactions is controversially discussed over decades. On the one hand, all catalytically active centers are of identical composition and therefore should have the same intrinsic acidity, independent of their environment. Based on this assumption only the total number of acid sites should be relevant for catalysis, but not the location or the spatial proximity of the active sites. Haag *et al.* showed that there is a linear correlation between activity and aluminum content of MFI zeolites in *n*-hexane cracking.^[1] On the other hand, there are quantum chemical studies which report that the environment of the Al atoms in MFI zeolites influences the intrinsic acidity and activity of Brønsted acid sites.^[2] Gounder and Iglesia experimentally observed a variation of turnover frequencies by a factor of 5 in propane cracking catalyzed by MFI zeolites of different Al content, without any systematic correlation or trend.^[3] A widely accepted hypothesis is that the acid strength of a Brønsted acid site (BAS) in high aluminum containing zeolites is lower compared to acid sites in zeolites with higher Si/Al ratios.^[4] The correlation of increasing aluminum content and decreasing activity was exemplarily shown for *n*-heptane cracking with FAU zeolites.^[5]

Not only the activity, but also the selectivity can be affected by the acid site strength of the catalytically active centers. Interesting changes in selectivity were reported for high aluminum MFI zeolites in catalytic cracking of 1-butene.^[6] This effect was attributed to “paired Al sites”, which are Brønsted acid sites in close proximity.^[7] The formation of aromatic compounds was significantly higher for zeolites with a high fraction of Al pairs and designated to an enhancement of hydrogen transfer reaction rates.^[6] A similar correlation between reactivity and density of Brønsted acid sites was reported for the isomerization of *n*-butane over MOR zeolites.^[8]

Besides the density or the spatial distance between Brønsted acid sites, also the location within the zeolite channels and pores is assumed to have an influence on catalysis. Janda and Bell reported that the elevated activity in *n*-butane cracking and dehydrogenation in MFI zeolites of increasing Al concentration is a result of a higher concentration of BAS at the intersections (ca. 9 Å) of the straight and sinusoidal channels (ca. 5.4 Å).^[9]

An increasing amount of aluminum does not exclusively lead to a higher number of incorporated (tetrahedral) aluminum, but also leads to a growth of extra-framework aluminum (octahedrally coordinated Al).^[4] This species appears in form of AlOOH, Al(OH)₃, aluminum-oxo and aluminum-hydroxyl clusters as well as bulk aluminum oxide aggregates.^[10] It is of high importance to rationalize the impact of EFAl species on acid catalyzed reactions. Neither the impact of Brønsted acid site concentration, nor the role of Lewis acid sites (LAS) in acid catalyzed reactions are

entirely understood. The catalytically active species in acid catalyzed aqueous phase reactions is “H₃O⁺”. Since these reactions can be catalyzed by inorganic Brønsted acids (HCl, H₂SO₄, HNO₃, etc.) in homogeneous catalysis, a major contribution or significant influence of Lewis acid sites is not expected. On the other hand, a “synergy-effect” of BAS and LAS was reported by solid state NMR analysis in case of dealuminated FAU^[11] and MOR^[12] zeolites. Furthermore, the interaction of EFAl and BAS was reported as “super acid site”^[13] and observed in propane cracking catalyzed by FAU zeolites.^[14]

A significant influence of extra-framework aluminum on *n*-pentane cracking rates was reported for MFI zeolites with Si/Al < 20.^[10] It was assumed, that EFAl in close spatial distance to BAS, remarkably effects the intrinsic acidity of these sites. After removal of the octahedrally coordinated aluminum (with ammonium hexafluorosilicate; AHFS) the reaction rates as well as the activation barriers were in the same range as the parent zeolites with Si/Al > 20 with negligible amount of EFAl.^[10] Also for FAU zeolites with EFAl, higher isomerization and hydrogen transfer rates were observed in *n*-heptane cracking.^[15] The observed effect was attributed to an inductive influence due to a close relation between EFAl and BAS.^[16]

To the best of our knowledge, the influence of BAS density and extra-framework aluminum has not been explored for acid catalyzed reactions in aqueous systems yet. This report reveals the impact of these parameters on E1 as well as on E2 dehydration pathways.

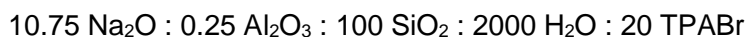
3.2. Experimental

Chemicals. The following chemicals were used: 4-methylcyclohexanol (mixture of *cis* and *trans* (25%:75%), 98%, *Sigma-Aldrich*), 2-methylcyclohexanol (mixture of *cis* and *trans* (48%:52%), 99%, *Sigma-Aldrich*), sodium sulfate (ACS reagent, > 99%, *Sigma-Aldrich*) ethyl acetate (*Chromasolv*, 99.9%, *Sigma-Aldrich*). Hydrogen gas was obtained from *Westfalen* (> 99.999%). Deionized water was treated with an *Easypure-II* system from *WERNER* to obtain ultrapure water (18.2 MΩ·cm).

Zeolite catalysts. All zeolites are referred to as MFI-X, where “X” is the Si/Al ratio as determined by atomic absorption spectroscopy. Zeolite MFI-45 (Si/Al = 45) and MFI-60 (Si/Al = 60) was obtained from *CLARIANT AG* in H-form. MFI-193 was synthesized according to the recipe described below. The MFI zeolites CBV8014 (referred to MFI-40; Si/Al = 40), CBV3024E (referred to MFI-15; Si/Al = 15) and CBV2314 (referred to as MFI-12; Si/Al = 11.5) were obtained from *ZEOLYST* in H-form. For removal of EFAl, the parent zeolites were treated with AHFS according

to the method given below. All zeolites were treated at 550 °C (rate: 10 °C·min⁻¹) for six hours in 100 mL·min⁻¹ synthetic air (80% nitrogen, 20% oxygen; > 99%) before they were tested.

Zeolite synthesis of MFI-193. The MFI zeolite (desired Si/Al ratio: 200) had the following gel-composition:



At first, 1.38 g NaOH was dissolved in 35.34 g H₂O. Step by step 8.55 g tetrapropylammonium bromide, 0.25 g Al₂(SO₄)₃·H₂O and 32.1 g LUDOX-30 (*Sigma-Aldrich*, AS-30) were added to the solution under vigorously stirring. The zeolite gel was stirred over night at room temperature to increase homogeneity. The gel crystallized during 60 hours of slow axial rotation (30 rpm) in autoclaves at 170 °C. After drying overnight, the template was removed by thermal treatment at 550 °C (heating rate: 10 °C·min⁻¹) for six hours and 100 mL·min⁻¹ flow of synthetic air.

Catalytically active H-form was obtained after NH₄⁺-exchange, where approximately 2 g of Na-form MFI-193 were stirred with 50 mL of 1M NH₄NO₃ (*Sigma-Aldrich*, >99%) solution at 80 °C for 2 h. The treated zeolite was centrifuged and washed with deionized water. The exchange procedure was repeated two further times before the zeolite was dried overnight and calcined as described above.

AHFS treatment procedure.^[10] Approximately 2 g of zeolite was added to a solution of (NH₄)₂SiF₆ (ca. 80 mL) and stirred in a polypropylene-bottle for five hours. The solution contained a 4-fold excess of AHFS with respect to the Al content of the zeolite. In case of MFI-15 (CBV3024E; 2.76 wt.% Al corresponding to 2.1 mmol) this was 1.50 g (8.4 mmol) AHFS. For the modification of MFI-12 (CBV2314; 3.63 wt.% Al corresponding to 2.7 mmol), 1.92 g (10.8 mmol) AHFS was used. After the treatment, the samples were washed six times in hot deionized water (80 °C) and calcined for 5 h in a stream of synthetic air (100 mL·min⁻¹, heating rate: 10 °C·min⁻¹) at 550 °C. All samples modified by AHFS are referred to as MFI-X_AHFS, where "X" is the Si/Al ratio before treatment as determined by atomic absorption spectroscopy.

Reaction procedure. All reactions were performed with the same molar amount of reactant, catalyst and solvent. In 100 mL ultrapure water 0.05 mol of substrate (5.71 g of 2-/4-methylcyclohexanol) and 50 mg of MFI-45 zeolite, MFI-193, MFI-15 (CBV3024E), MFI-12 (CBV2314), MFI-15_AHFS (CBV3024E treated with AHFS) and MFI-12_AHFS (CBV2314 treated with AHFS) were dissolved and suspended, respectively.

Catalytic reactions. The autoclave (300 mL) was loaded with 100 mL water, the given amount of zeolite catalyst (see above) and 0.05 mol of substituted cyclohexanol substrate. The reactor was

purged two times up to 20 bar with hydrogen and was heated to the desired temperature with a heating rate of 10 °C per minute under a starting pressure of 20 bar hydrogen without stirring. Ten degrees below the reaction temperature the total pressure of the reactor was adjusted to 50 bar with hydrogen gas and as soon as the reaction temperature was reached the stirring rate was set to 700 rpm.

After the reaction time, the reactor was cooled down from reaction temperature to room temperature within two minutes using an ice bath. The pressure within the reactor was released at a temperature of 5 °C to prevent the loss of volatile products (cyclohexene). The reaction mixture was extracted with 3 x 20 mL ethyl acetate. To improve the phase separation of the organic and the aqueous phases, a small amount of sodium chloride was added to the reaction mixture. After extraction, the organic phase was dried over sodium sulfate. The carbon-balance was monitored by an internal standard (dodecane).

Used equipment

Reactor. All reactions were performed in an autoclave (300 mL) from *Parr Instruments Co.* (type: *PST FS*, material: HASTELLOY C) with a temperature and stirring controlling device (*Parr Instruments Co. 4848 Reactor Controller*).

GC-MS. Quantification and qualification of the dehydration reactions was analyzed by GC/MS (*Agilent Technologies 7890 B GC*, column: *Agilent 19091S-433UI INV02* (30 m x 250 µm x 0.25 µm), heating program: 10 °C·min⁻¹ from 80 °C to 280 °C). Data was analyzed with *MassHunter Workstation Software, Qualitative Analysis, Version B.06.00, Agilent Technologies (2012)*.

AAS. The Si and Al content of the zeolite samples was measured by atomic absorption spectroscopy (AAS) on a *UNICAM 939 AA-Spectrometer*.

N₂ physisorption. The BET specific surface area and pore volume of the zeolite were determined by nitrogen physisorption. The isotherms were measured at liquid nitrogen temperature (-196 °C) using a *PMI Automatic Sorptometer*. The catalyst was activated in vacuum at 200 °C for two hours before measurement. Apparent surface area was calculated by applying the *Brunauer-Emmett-Teller (BET)* theory, and the *t-plot method* was used to determine the pore volumes.

SEM. The scanning electron microscopy (SEM) images were recorded on a *JEOL 500 SEM-microscopy* (accelerating voltage: 25 kV). The samples were prepared by depositing a drop of an ultrasonicated methanol suspension of the solid material onto a carbon-coated Cu grid.

XRD. The crystal structures of the zeolites were analyzed by X-ray powder diffraction (XRD) using a *Phillips X'Pert Pro system*, with Cu-K α radiation operating at 45 kV/40 mA. The sample was measured with a scanning rate of 0.017°/s in the range from 5 to 70° (2 θ).

MAS ^{27}Al -NMR. Magic angle spinning spectra were recorded on a *Bruker Avance AMX-500* spectrometer. Samples were packed after hydration at 42 mbar H $_2$ O into ZrO $_2$ -rotos, which were spun at 10 kHz. Al(NO $_3$) \cdot 9H $_2$ O was used as reference. For measuring the 1D spectrum, an excitation pulse with power level of 7 dB and a length of 0.7 μ s was applied. Relaxation time was set to 2.0 s and 2000 scans were recorded. The data was processed and after Fourier transformation using *Bruker's software Topspin*.

IR. Infrared spectroscopy of adsorbed pyridine was performed with a *Perkin–Elmer 2000* spectrometer at a resolution of 4 cm $^{-1}$. The catalyst sample was prepared as wafer and activated in vacuum (ca. 10 $^{-6}$ mbar) at 450 °C for one hour (heating rate = 10 °C \cdot min $^{-1}$). After cooling to 150 °C, the sample was equilibrated with 0.1 mbar of pyridine for 30 min followed by outgassing for one hour. A spectrum with the chemisorbed pyridine was recorded thereafter. Adsorbed pyridine was desorbed finally by heating up to 450 °C with 10 °C \cdot min $^{-1}$ for half an hour, the spectra were recorded at equilibrium. For quantification, molar integral extinction coefficients of 0.73 cm \cdot μ mol $^{-1}$ and 0.96 cm \cdot μ mol $^{-1}$ were used for *Brønsted* and *Lewis* acid sites respectively.

NH $_3$ -TPD. Temperature-programmed desorption (TPD) of ammonia was performed in a 6-fold parallel reactor system. The catalysts were activated under reduced pressure at 450 °C (heating rate: 5 °C \cdot min $^{-1}$) for one hour. NH $_3$ was adsorbed for one hour with partial pressures of 1 mbar at 100 °C, respectively. Subsequently, the samples were evacuated for two hours to remove physisorbed probe molecules. For the temperature-programmed desorption experiments, six samples were sequentially heated from 100 to 770 °C with a heating rate of 10 °C \cdot min $^{-1}$ to desorb ammonia. The rates of desorbing species were monitored by mass spectrometry (*Balzars QME 200*). For the quantification of the amount of acidity, a standard MFI-zeolite with known acid site concentration was used to calibrate the signal.

3.3. Results and Discussion

Characterization of MFI zeolites (MFI-193, MFI-60, MFI-45, MFI-40, MFI-15, MFI-12, MFI-15_AHFS and MFI-12_AHFS)

The concentrations of BAS ($1141 - 90 \mu\text{mol}\cdot\text{g}^{-1}$) and LAS ($199 - 15 \mu\text{mol}\cdot\text{g}^{-1}$) of MFI zeolites with varying Si/Al ratios ($\text{Si}/\text{Al} = 12 - 193$) are compiled in **Table 3.1.** To analyze the impact of extra-framework aluminum on aqueous phase dehydration, the two most acidic samples of considerable amount EFAl (MFI-12 and MFI-15) were treated with AHFS to remove the octahedrally coordinated Al species.^[10, 17]

Table 3.1. Characterization of the investigated MFI zeolites.

Entry	Zeolite	Si/Al	Surface area [$\text{m}^2\cdot\text{g}^{-1}$]	C (BAS) ^a [$\mu\text{mol}\cdot\text{g}^{-1}$]	C (LAS) ^a [$\mu\text{mol}\cdot\text{g}^{-1}$]	C (BAS+LAS) ^b [$\mu\text{mol}\cdot\text{g}^{-1}$]
1	MFI-193	193	379	90	15	105
2	MFI-60	60	460	226	82	279
3	MFI-45	45	389	360	45	400
4	MFI-40	40	478	310	79	408
5	MFI-15_AHFS	32	378	470	60	516
6	MFI-12_AHFS	23	398	627	114	862
7	MFI-15	15	419	781	158	755
8	MFI-12	12	432	1141	199	(827)

^a determined by IR spectroscopy (pyridine), ^b determined by TPD (NH_3).

The surface areas (**Table 3.1.**) as well as the crystal sizes (SI, **SEM Image S3.1. – S3.6.**) of all investigated MFI zeolites were comparable. The concentrations of Brønsted and Lewis acid sites determined by IR spectroscopy are in agreement with the results of the temperature programmed desorption of NH_3 (**Table 3.1.**). As the BAS of zeolites transform in hydronium ions when immersed in water,^[18] the concentrations of accessible hydronium ions were experimentally verified in aqueous phase (SI, **Tables and Figures S3.21. – S3.28.**) by adding different amounts of pyridine as a poisoning agent to the reaction mixture of zeolite, substrate and water. The determined concentrations of acid sites under reaction conditions (quantified by the correlation of dehydration rates and amount of pyridine) were found to be the same for both model compounds and comparable to the acid site concentrations in **Table 3.1.**

After the AHFS-treatment, the number of EFAl was remarkably reduced which was verified by IR spectroscopy (**Table 3.1.** and **Figure 3.1.**) and ^{27}Al -MAS-NMR (**Figure 3.2.**). The concentration of LAS was significantly reduced to ca. one third in case of the zeolite MFI-15 (c (LAS): $158 \rightarrow 60 \mu\text{mol}\cdot\text{g}^{-1}$) and to nearly a half in case of MFI-12 (c (LAS): $199 \rightarrow 114 \mu\text{mol}\cdot\text{g}^{-1}$).

Unfortunately, also the concentration of BAS decreased remarkably after the AHFS-treatment for both modified samples MFI-12 (c (BAS): 1141 \rightarrow 627 $\mu\text{mol}\cdot\text{g}^{-1}$) and MFI-15 (c (BAS): 781 \rightarrow 470 $\mu\text{mol}\cdot\text{g}^{-1}$). Infrared spectra of the parent and the treated samples of MFI-15 and MFI-12 show the disappearance of the bands at 3780 and 3660 cm^{-1} and indicate a successful removal of EFAI and Al-OH species, respectively (**Figure 3.1.**).

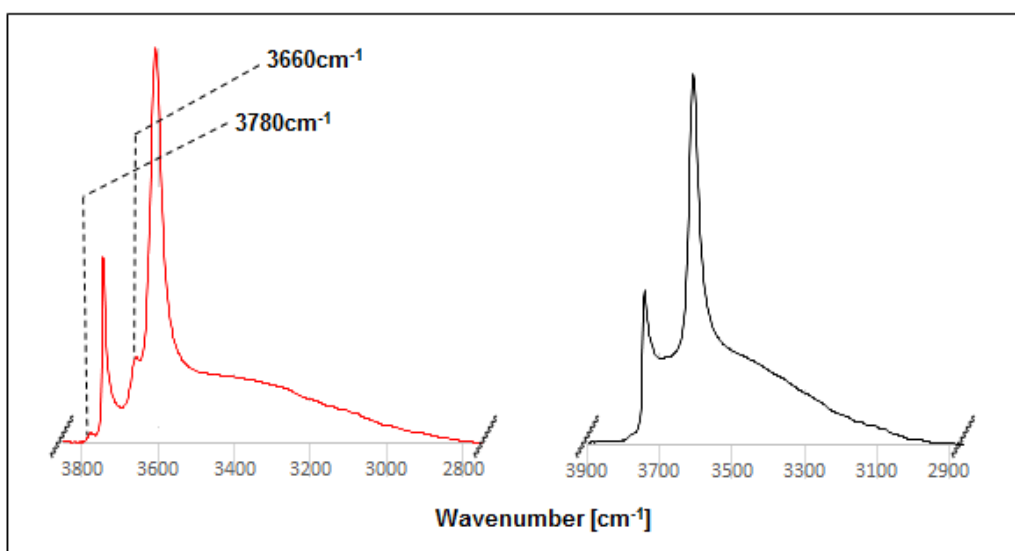


Figure 3.1. Infrared spectra of the parent MFI-12 (●) and the treated MFI-12_AHFS (●).

The ²⁷Al-MAS-NMR spectra of MFI-15 before and after AHFS-treatment confirm that the octahedrally coordinated aluminum species (**Figure 3.2.**) were removed to a large extent.

In addition, the reduced concentration of BAS after AHFS-treatment is also evident from **Figure 3.2.** in view of the lower intensity of the tetrahedrally coordinated aluminum at 55 ppm. All other MFI zeolites did not contain considerable concentrations of EFAI according to the ²⁷Al-MAS-NMR measurements (see SI, **NMR-S3.1** and **NMR-S3.2.**).

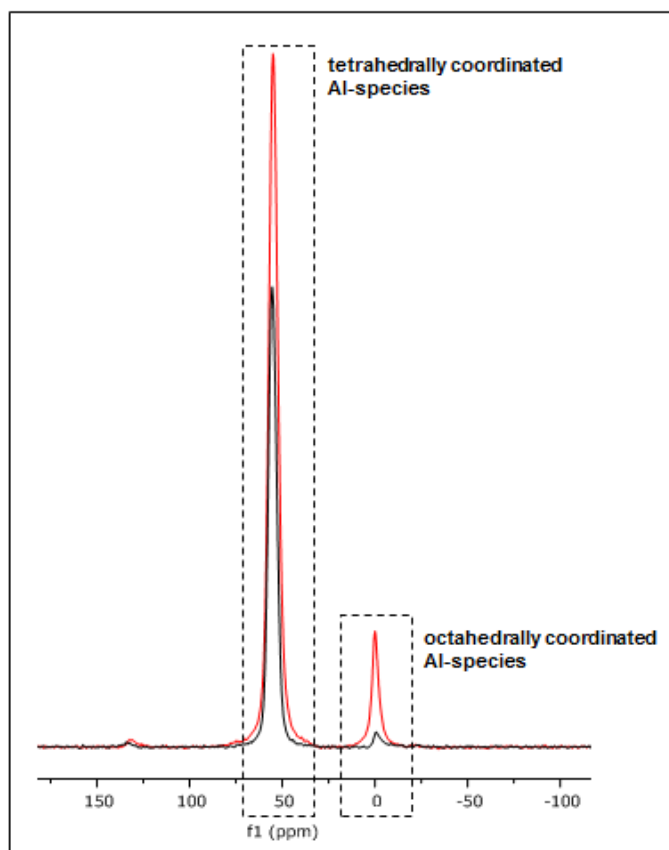


Figure 3.2. ^{27}Al -MAS-NMR spectra of the parent MFI-15 (●) and the treated MFI-15_AHFS (●).

Dehydration of 2- and 4-methylcyclohexanol catalyzed by parent and AHFS-treated MFI zeolites

Previous investigations revealed that there are two possible dehydration pathways for methylcyclohexanols. The product distribution and the activation parameters (ΔH^{\ddagger} and ΔS^{\ddagger}) led to the conclusion that *trans* 2-McyOH and 4-McyOH (*cis* and *trans*) are dehydrated in a stepwise manner *via* carbenium ions (E1). A concerted dehydration mechanism (E2) is in effect for the dehydration of *cis* 2-McyOH. The *cis* isomer shows a $30 \text{ kJ}\cdot\text{mol}^{-1}$ lower activation barrier than the *trans* isomer and therefore is exclusively converted in a racemic mixture of both isomers. The reaction order in 2- and 4-methylcyclohexanol was determined to be zero for MFI zeolites (SI, **Figures** and **Tables S3.1. – S3.4.**).

Dehydration of cis/trans 4-methylcyclohexanol via the E1 dehydration pathway

The impact of acid site concentrations on the dehydration rates and activation parameters of 4-McyOH represents their influence on the E1 pathway. **Table 3.2.** compiles the turnover frequencies (150 °C) obtained by MFI zeolites of different aluminum concentrations.

Table 3.2. TOFs (150 °C) for 4-McyOH dehydration with MFI zeolites.

Zeolite	MFI-193	MFI-60	MFI-45	MFI-40	MFI-15	MFI-12	MFI-15_AHFS	MFI-12_AHFS
TOF [s ⁻¹]	0.009	0.029	0.015	0.034	0.005	0.004	0.007	0.006

The dependence of TOF on the BAS concentration is shown in **Figure 3.3.** The highest TOF appeared on zeolites with concentrations between 200 and 300 $\mu\text{mol BAS per g}$ (MFI-40 and MFI-60).

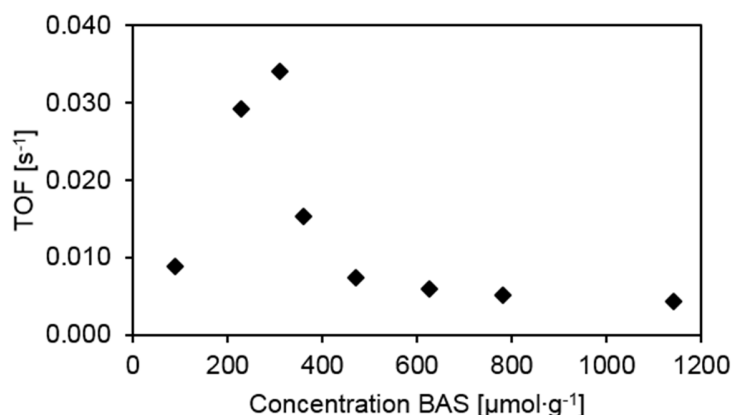


Figure 3.3. TOF as a function of BAS concentration in dehydration of 4-McyOH at 150 °C.

According to **Figure 3.3.** an optimum concentration of BAS exists showing the maximum in catalytic activity. The higher the concentration of aluminum, the higher is the polarity of the zeolite. As adsorption experiments (SI, **Figure** and **Table S3.29.**) showed, an increasing Al concentration results in an increasing uptake of water (less uptake of cyclohexanol) in the zeolite pores. In contrast, Al poor samples are less polar and the concentration of alcohol in the zeolite pores is significantly higher (less water). In aqueous phase, water molecules participate in protonation (in form of hydronium ions ^[18]) as well as in the second and kinetically relevant step of β -H abstraction (as a base) in the E1 pathway.^[19] As the concentration of alcohol and the concentration of water in the zeolite pores determine the reaction rate, there is an optimum proportion of both concentrations leading to a maximal turnover frequency for zeolites of moderate Al content. A similar correlation of TOF and Al content of MFI zeolites (maximum TOF at higher Al concentrations) was reported in *n*-butane cracking.^[9]

The activation barrier as well as the enthalpy and entropy of activation obtained with the investigated MFI zeolites are compiled in **Table 3.3.** Despite the different dehydration rates, the enthalpies and entropies of activation are comparable for the zeolites with Si/Al \geq 40 (**Table 3.3. Entry 1 – 4:** $\Delta H^{\ddagger} = 145 - 147 \text{ kJ}\cdot\text{mol}^{-1}$ and $\Delta S^{\ddagger} = 48 - 60 \text{ J}\cdot\text{K}^{-1}\cdot\text{mol}^{-1}$). A significant deviation was observed in case of MFI-12 and MFI-15 (**Table 3.3. Entry 7 – 8:** $E_a = 160$ and $156 \text{ kJ}\cdot\text{mol}^{-1}$) with a 10 to $15 \text{ kJ}\cdot\text{mol}^{-1}$ higher activation barrier compared to all other zeolites of moderate to low acidity. The same trend was observed for the activation entropy with values of 66 and $77 \text{ J}\cdot\text{K}^{-1}\cdot\text{mol}^{-1}$.

Table 3.3. E_a , ΔH^{\ddagger} and ΔS^{\ddagger} for 4-McyOH dehydration over MFI zeolites.

Entry	Zeolite	Si/Al	E_a [kJ·mol ⁻¹]	ΔH^{\ddagger} [kJ·mol ⁻¹]	ΔS^{\ddagger} [J·K ⁻¹ ·mol ⁻¹]
1	MFI-193	193	145 (± 3)	141 (± 3)	+48 (± 7)
2	MFI-60	60	147 (± 3)	143 (± 3)	+60 (± 6)
3	MFI-45	45	146 (± 3)	142 (± 3)	+53 (± 6)
4	MFI-40	40	145 (± 4)	141 (± 4)	+56 (± 10)
5	MFI-15_AHFS	32	149 (± 3)	145 (± 3)	+53 (± 6)
6	MFI-12_AHFS	23	150 (± 4)	146 (± 4)	+55 (± 9)
7	MFI-15	15	160 (± 4)	157 (± 4)	+77 (± 8)
8	MFI-12	11.5	156 (± 3)	153 (± 3)	+66 (± 7)

After AHFS-treatment the two most acidic zeolites showed lower activation barriers and entropies (**Table 3.3. Entry 5 – 6:** $\Delta H^{\ddagger} = 149/150 \text{ kJ}\cdot\text{mol}^{-1}$ and $\Delta S^{\ddagger} = 53/55 \text{ J}\cdot\text{K}^{-1}\cdot\text{mol}^{-1}$), which became close to the parent zeolites without significant concentration of EFAl. Janda and Bell observed a similar phenomenon for rates and barriers in protolytic alkane cracking: a high TOF was not associated with a low activation barrier.^[9] The observations were attributed to a shift towards higher entropies of the transition state resulting of preferential cracking at the BAS located in the intersections of the straight and sinusoidal channels in zeolites of high Al concentration.^[9] A similar dependence of rate constants and activation barriers on the Al concentration was reported by Schallmoser *et al.* in *n*-pentane cracking.^[10] The presence of EFAl in MFI zeolites (Si/Al < 20) effected a shift towards higher entropy values suggesting a later transition state (elongated C-C bond, product-like). The resulting higher activation barrier (although higher reaction rates) was assumed to be overcompensated by a higher entropy of the transition state.^[10]

A comparison of the experimental data obtained by MFI-12 and MFI-15 and their EFAl-free counterparts (MFI-12_AHFS and MFI-15_AHFS) leads to the assumption that the EFAl species

causes the higher values in ΔH^{\ddagger} and ΔS^{\ddagger} . Catalytic cracking and dehydration proceed *via* positively charged intermediates (penta-coordinated carbonium or carbenium ions). According to the higher enthalpic barriers (by 10 kJ·mol⁻¹) it is hypothesized that the presence of EFAl destabilizes the positively charged intermediates. Following this, an enthalpic destabilization induced by EFAl should not be observable in the absence of carbocations which is the case for a concerted dehydration mechanism (E2).

Dehydration of (cis) 2-methylcyclohexanol via the E2 dehydration pathway

The dehydration of (*cis*) 2-McyOH on MFI zeolites of different Al content reveal the impact of EFAl on the concerted elimination mechanism. **Table 3.4.** compiles the TOFs at 150 °C obtained by the same MFI zeolites used in dehydration of 4-McyOH. The determined TOFs exclusively result from the significantly more reactive *cis* isomer.

Table 3.4. TOFs (150 °C) for 2-McyOH dehydration with MFI zeolites.

Zeolite	MFI-193	MFI-60	MFI-45	MFI-40	MFI-15	MFI-12	MFI-15_AHFS	MFI-12_AHFS
TOF [s ⁻¹]	0.02	0.08	0.06	0.09	0.05	0.02	0.02	0.03

The correlation of TOF and the BAS concentration of all investigated MFI zeolites in dehydration of (*cis*) 2-McyOH (**Figure 3.4.**) led to a similar trend as in the previous case (4-McyOH). This is not surprising due to the fact that also in a concerted E2 dehydration pathway, the β -H abstraction (and simultaneous C-O bond cleavage) is the kinetic relevant step. The highest TOF in the dehydration of (*cis*) 2-McyOH was obtained by BAS concentrations between 200 and 300 $\mu\text{mol}\cdot\text{g}^{-1}$. Contrary to **Figure 3.3.**, the TOFs observed by the two AHFS-treated zeolites (c (BAS) \approx 500 and 600 $\mu\text{mol}\cdot\text{g}^{-1}$) were slightly smaller and indicate a second, but significantly smaller climax (local maximum) at around 800 $\mu\text{mol}\cdot\text{g}^{-1}$.

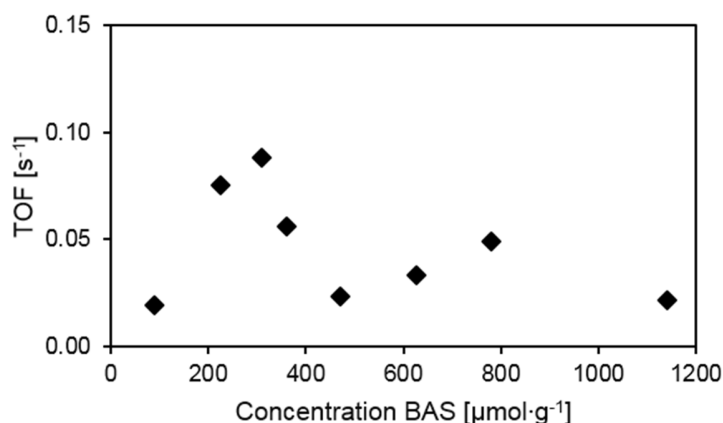


Figure 3.4. TOF as a function of BAS concentration in dehydration of 2-McyOH at 150 °C.

The activation barriers as well as the enthalpies and entropies of activation are compiled in **Table 3.5**. The activation energy for the concerted pathway (E2) of *cis* 2-McyOH (*trans* 2-McyOH proceeds *via* E1; $E_a = 144 \text{ kJ}\cdot\text{mol}^{-1}$) is between 112 and 118 $\text{kJ}\cdot\text{mol}^{-1}$ for the zeolites of moderate acidity (**Table 3.5. Entry 1 – 4**).

Table 3.5. E_a , ΔH^{\ddagger} and ΔS^{\ddagger} for *cis* 2-McyOH dehydration over MFI zeolites.

Entry	Zeolite	Si/Al	E_a [$\text{kJ}\cdot\text{mol}^{-1}$]	ΔH^{\ddagger} [$\text{kJ}\cdot\text{mol}^{-1}$]	ΔS^{\ddagger} [$\text{J}\cdot\text{K}^{-1}\cdot\text{mol}^{-1}$]
1	MFI-193	193	114 (± 4)	111 (± 4)	-19 (± 10)
2	MFI-60	60	118 (± 2)	115 (± 2)	+2 (± 4)
3	MFI-45	45	116 (± 3)	112 (± 3)	-8 (± 7)
4	MFI-40	40	112 (± 4)	108 (± 4)	-12 (± 8)
5	MFI-15_AHFS	32	124 (± 4)	121 (± 4)	-5 (± 8)
6	MFI-12_AHFS	23	114 (± 3)	110 (± 3)	-15 (± 6)
7	MFI-15	15	106 (± 2)	102 (± 2)	-30 (± 4)
8	MFI-12	11.5	106 (± 2)	102 (± 2)	-39 (± 4)

The determined activation parameters obtained by the two zeolites containing the highest amount of Al (MFI-15 and MFI-12) deviate from all other investigated zeolites in the concerted dehydration pathway (**Table 3.5. Entry 7 – 8**). The result of ca. 10 $\text{kJ}\cdot\text{mol}^{-1}$ lower activation barriers ($E_a = 106 \text{ kJ}\cdot\text{mol}^{-1}$) for zeolites with considerable amount of EFAI is contrary to the observations for the E1 pathway, where the barriers were about the same extent higher. In addition, the effect on the entropy of activation is reverse compared to the stepwise mechanism: ΔS^{\ddagger} decreased remarkably in the presence of octahedrally coordinated aluminum species ($\Delta S^{\ddagger} = -30$ and $-39 \text{ J}\cdot\text{K}^{-1}\cdot\text{mol}^{-1}$) compared to the samples without EFAI

($\Delta S^{\ddagger} = +2, -8, -12$ and $-19 \text{ J}\cdot\text{K}^{-1}\cdot\text{mol}^{-1}$). The removal of EFAl gave proof of its significant impact on activation parameters, as the enthalpic ($\Delta H^{\ddagger} = 110$ and $121 \text{ kJ}\cdot\text{mol}^{-1}$) and entropic ($\Delta S^{\ddagger} = -5$ and $-15 \text{ J}\cdot\text{K}^{-1}\cdot\text{mol}^{-1}$) barriers increased to comparable values obtained by the zeolites of higher Si/Al ratios.

As the dehydration experiments of 2- and 4-McyOH revealed, the presence of extra-framework aluminum has a remarkable impact on ΔH^{\ddagger} and ΔS^{\ddagger} of the stepwise (E1) as well as of the concerted (E2) dehydration pathway. According to the experimental data, a considerable amount of EFAl effects the enthalpy of pathways *via* a positively charged intermediate negatively (ca. $10 \text{ kJ}\cdot\text{mol}^{-1}$ higher), whereas the concerted elimination route is positively influenced (ca. $10 \text{ kJ}\cdot\text{mol}^{-1}$ lower).

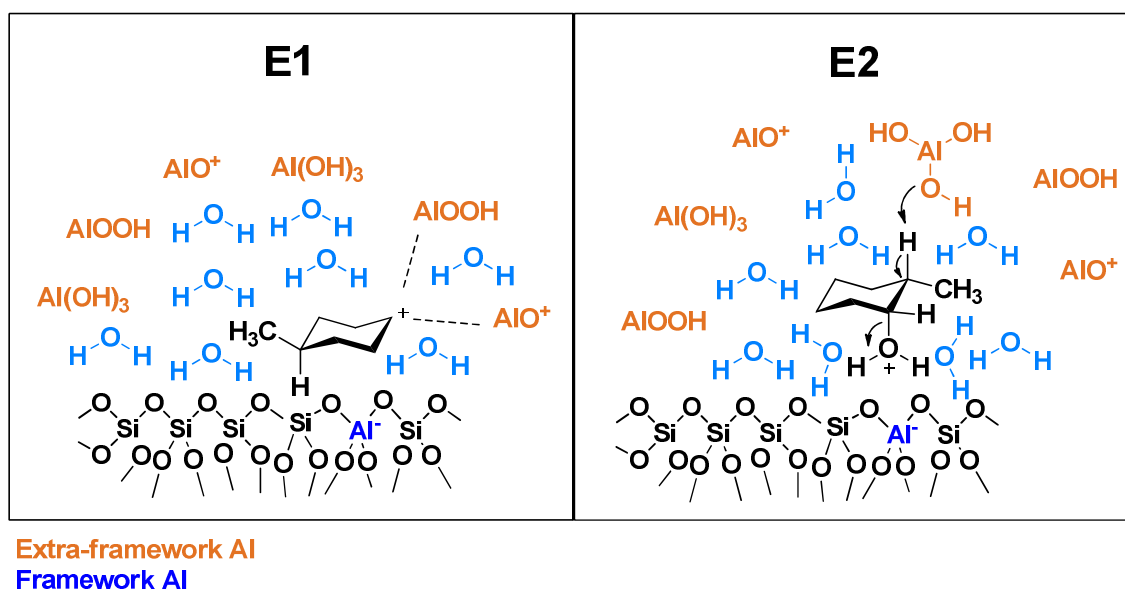


Figure 3.5. Hypothesized interaction of the EFAl species in E1 and E2 dehydration pathways.

It is assumed that the octahedrally coordinated Al in form of AlOOH or $\text{Al}(\text{OH})_3$ interacts as a base in β -proton abstraction in an E2 pathway (**Figure 3.5.**). A shift to lower values of ΔS^{\ddagger} is attributed to this mechanistic participation of EFAl in the rather complex transition state of the concerted elimination consisting of the proton, the alcohol and the abstracting base (water and EFAl species). On the other hand, the higher enthalpic barriers in an E1 dehydration pathway are assumed to result of a destabilization of the positively charged carbenium ion by the Lewis acidic character of the EFAl (**Figure 3.5.**). In addition, ΔS^{\ddagger} was shifted to higher values, which illustrates a later transition state. The removal of EFAl led to a disappearance of the reported effects on ΔH^{\ddagger} and ΔS^{\ddagger} .

3.4. Conclusions

The impact of Brønsted acid site concentration and the influence of extra-framework Al on the aqueous phase dehydration of 2- and 4-methylcyclohexanol was investigated. The highest dehydration rates were obtained by zeolites of moderate Si/Al ratios. This is attributed to an optimum proportion of alcohol as well as water in the zeolite pores as both determine the reaction rate.

MFI zeolites with considerable amount of EFAl (Si/Al = 11.5 and 15) effected remarkably ΔH^{\ddagger} and ΔS^{\ddagger} of both E1 and E2 dehydration pathways.

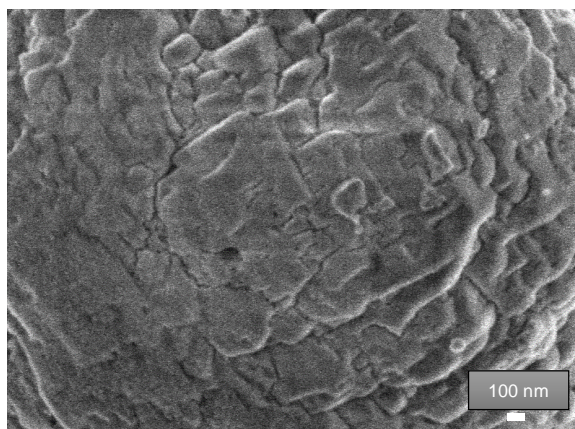
The presence of aluminium oxide clusters led to higher (by ca. $10 \text{ kJ}\cdot\text{mol}^{-1}$) enthalpic barriers in the dehydration of 4-McyOH (E1 route). This result is attributed to the destabilization of the carbenium ion intermediate by the Lewis acidic character of octahedrally coordinated Al in form of AlOOH or Al(OH)₃. Higher values of ΔS^{\ddagger} (by $5 - 30 \text{ J}\cdot\text{K}^{-1}\cdot\text{mol}^{-1}$) indicate a shift towards later (product-like) transition states.

The smaller activation barrier of ca. $10 \text{ kJ}\cdot\text{mol}^{-1}$ in the dehydration of (*cis*) 2-McyOH (E2 pathway) is assigned to the active participation of the Lewis acidic EFAl species in β -proton abstraction. This interaction is expressed by a shift to smaller values of ΔS^{\ddagger} (by $10 - 40 \text{ J}\cdot\text{K}^{-1}\cdot\text{mol}^{-1}$) illustrating the complex (reactant-like) transition state consisting of proton, alcohol and base (water and EFAl) in the concerted dehydration mechanism.

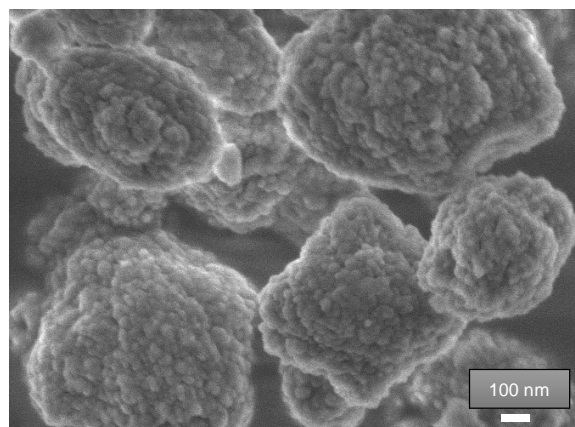
3.5. References

- [1] a) D. Olson, W. Haag, R. Lago, *Journal of Catalysis* **1980**, *61*, 390-396; b) W. Haag, R. Lago, P. Weisz, **1984**; c) W. Haag, *Studies in Surface Science and Catalysis* **1994**, *84*, 1375-1394.
- [2] V. Kazanskii, *Accounts of chemical research* **1991**, *24*, 379-383.
- [3] R. Gounder, E. Iglesia, *Journal of the American Chemical Society* **2009**, *131*, 1958-1971.
- [4] A. Corma, *Chemical Reviews* **1995**, *95*, 559-614.
- [5] J. Meusinger, A. Corma, *Journal of catalysis* **1996**, *159*, 353-360.
- [6] P. Sazama, J. Dedecek, V. Gabova, B. Wichterlova, G. Spoto, S. Bordiga, *Journal of Catalysis* **2008**, *254*, 180-189.
- [7] a) J. Dědeček, Z. Sobalik, B. Wichterlová, *Catalysis Reviews* **2012**, *54*, 135-223; b) J. Dědeček, B. Wichterlová, *The Journal of Physical Chemistry B* **1997**, *101*, 10233-10240; c) J. Dědeček, D. Kaucký, B. Wichterlová, O. Gonsiorová, *Physical Chemistry Chemical Physics* **2002**, *4*, 5406-5413; d) V. Gábová, J. Dědeček, J. Čejka, *Chemical Communications* **2003**, 1196-1197.
- [8] M.-T. Tran, N. Gnep, G. Szabo, M. Guisnet, *Journal of catalysis* **1998**, *174*, 185-190.
- [9] A. Janda, A. T. Bell, *Journal of the American Chemical Society* **2013**, *135*, 19193-19207.
- [10] S. Schallmoser, T. Ikuno, M. Wagenhofer, R. Kolvenbach, G. Haller, M. Sanchez-Sanchez, J. Lercher, *Journal of Catalysis* **2014**, *316*, 93-102.
- [11] S. Li, A. Zheng, Y. Su, H. Zhang, L. Chen, J. Yang, C. Ye, F. Deng, *Journal of the American Chemical Society* **2007**, *129*, 11161-11171.
- [12] Z. Yu, S. Li, Q. Wang, A. Zheng, X. Jun, L. Chen, F. Deng, *The Journal of Physical Chemistry C* **2011**, *115*, 22320-22327.
- [13] C. Mirodatos, D. Barthomeuf, *Journal of the Chemical Society, Chemical Communications* **1981**, 39-40.
- [14] S. M. Almutairi, B. Mezari, G. A. Filonenko, P. C. Magusin, M. S. Rigutto, E. A. Pidko, E. J. Hensen, *ChemCatChem* **2013**, *5*, 452-466.
- [15] Q. Wang, G. Giannetto, M. Guisnet, *Journal of Catalysis* **1991**, *130*, 471-482.
- [16] L. Fernandes, J. Monteiro, E. F. Sousa-Aguiar, A. Martinez, A. Corma, *Journal of Catalysis* **1998**, *177*, 363-377.
- [17] a) A. Gola, B. Rebours, E. Milazzo, J. Lynch, E. Benazzi, S. Lacombe, L. Delevoye, C. Fernandez, *Microporous and mesoporous materials* **2000**, *40*, 73-83; b) C. S. Triantafyllidis, A. G. Vlessidis, L. Nalbandian, N. P. Evmiridis, *Microporous and Mesoporous Materials* **2001**, *47*, 369-388; c) R. López-Fonseca, B. De Rivas, J. Gutiérrez-Ortiz, J. González-Velasco, *Studies in Surface Science and Catalysis* **2002**, *144*, 717-722.
- [18] a) M. Eigen, *Angewandte Chemie* **1963**, *75*, 489-508; b) G. Zundel, *Angewandte Chemie International Edition* **1969**, *8*, 499-509.
- [19] Y. Liu, A. Vjunov, H. Shi, S. Eckstein, D. Camaioni, D. Mei, E. Barath, J. A. Lercher, *Nature Communications* **2016**, DOI: 10.1038/ncomms14113.

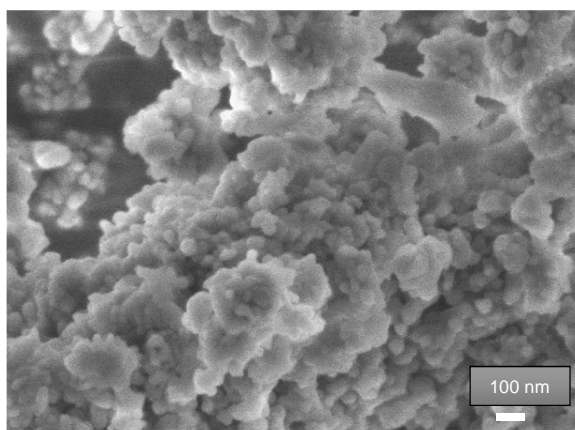
3.6. Supporting Information



SEM Image S3.1. MFI-193 (Si/Al = 193).

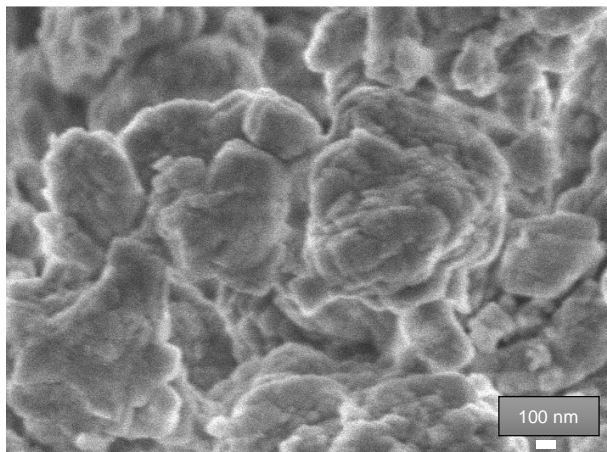


SEM Image S3.2. MFI-60 (Si/Al = 60).

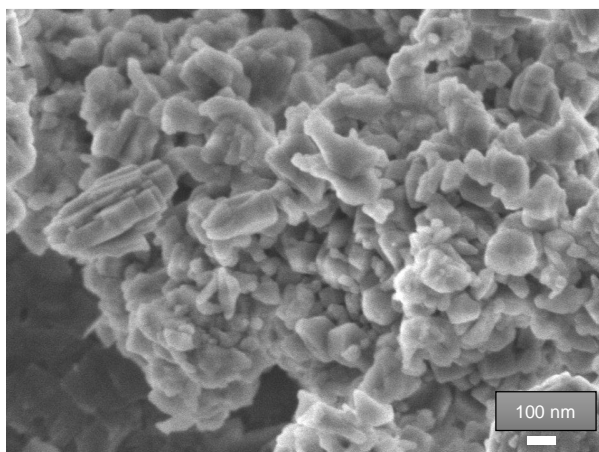


SEM Image S3.3. MFI-45 (Si/Al = 45).

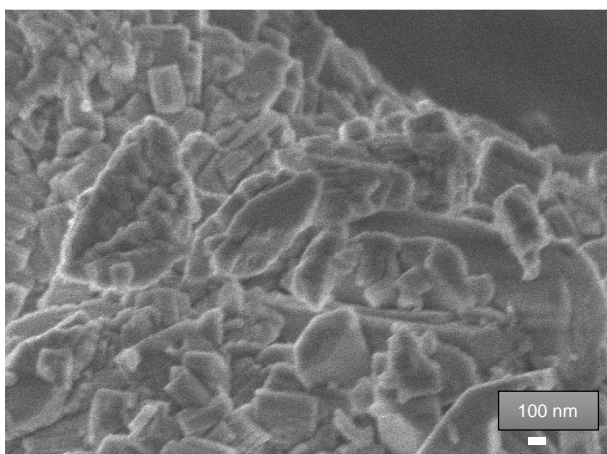
3. Influence of acid site concentration and EFAI in MFI zeolites on aqueous phase dehydration



SEM Image S3.4. MFI-40 (Si/Al = 40).

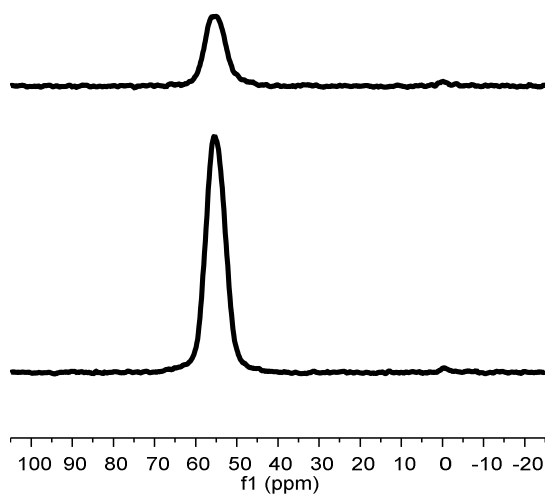


SEM Image S3.5. MFI-15 (Si/Al = 15).

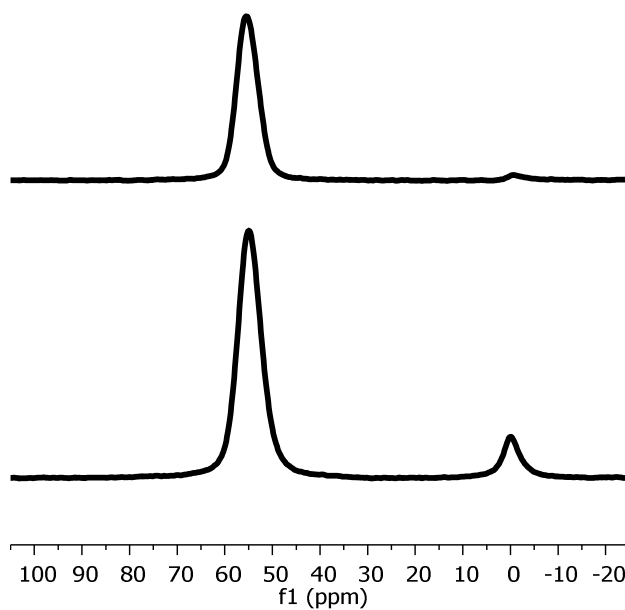


SEM Image S3.6. MFI-12 (Si/Al = 11.5).

^{27}Al -MAS-NMR



NMR-S3.1. ^{27}Al -MAS-NMR-Spectra of **MFI-193** (top) and **MFI-45** (bottom).



NMR-S3.2. ^{27}Al -MAS-NMR-Spectra of **MFI-12_AHFS** (top) and **MFI-12** (bottom).

Reaction orders of aqueous phase dehydration

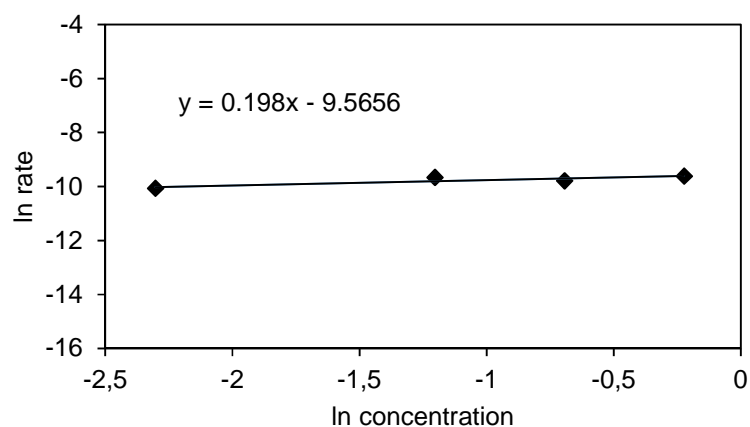


Figure S3.1. Reaction order: **2-methylcyclohexanol** dehydration (170 °C, 50 bar, **MFI-45**).

Table S3.1. Dehydration rates and initial concentrations of **2-methylcyclohexanol** (170 °C, 50 bar, **MFI-45**).

rate [mol·g ⁻¹ ·s ⁻¹]	n [mol]	c [mol·L ⁻¹]	ln rate	ln c
4.24·10 ⁻⁵	0.01	0.10	-10.07	-2.30
6.36·10 ⁻⁵	0.03	0.30	-9.66	-1.20
5.60·10 ⁻⁵	0.05	0.50	-9.79	-0.69
6.66·10 ⁻⁵	0.08	0.80	-9.62	-0.22

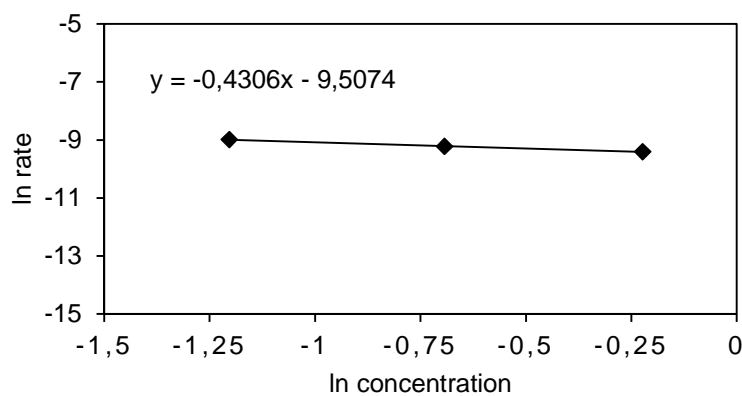


Figure S3.2. Reaction order: **4-methylcyclohexanol** dehydration (180 °C, 50 bar, **MFI-45**).

Table S3.2. Dehydration rates and initial concentration of **4-methylcyclohexanol** (180 °C, 50 bar, **MFI-45**).

rate [mol·g ⁻¹ ·s ⁻¹]	n [mol]	c [mol·L ⁻¹]	ln rate	ln c
1.25·10 ⁻⁴	0.03	0.30	-8.98	-1.20
9.91·10 ⁻⁵	0.05	0.50	-9.22	-0.69
8.22·10 ⁻⁵	0.08	0.80	-9.41	-0.22

3. Influence of acid site concentration and EFAI in MFI zeolites on aqueous phase dehydration

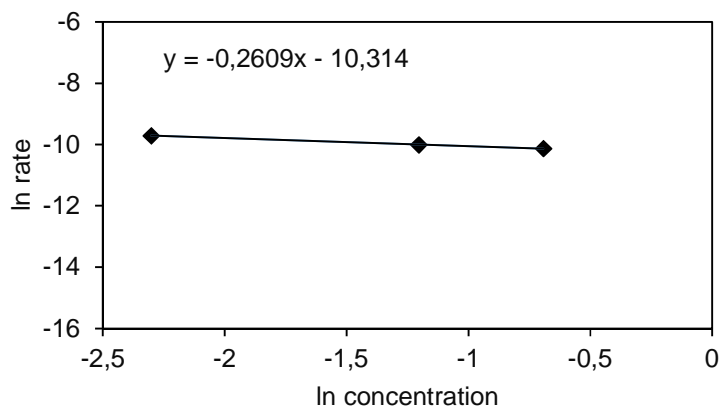


Figure S3.3. Reaction order: **4-methylcyclohexanol** dehydration (180 °C, 50 bar, **MFI-12**).

Table S3.3. Dehydration rates and initial concentrations of **4-methylcyclohexanol** (180 °C, 50 bar, **MFI-12**).

rate [mol·g ⁻¹ ·s ⁻¹]	n [mol]	c [mol·L ⁻¹]	ln rate	ln c
6.07·10 ⁻⁵	0.01	0.10	- 9.71	-2.30
4.50·10 ⁻⁵	0.03	0.30	- 10.00	-1.20
4.00·10 ⁻⁵	0.05	0.50	- 10.13	-0.69

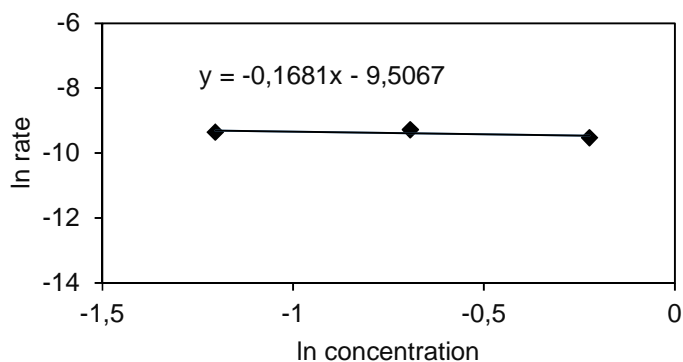


Figure S3.4. Reaction order: **2-methylcyclohexanol** dehydration (170 °C, 50 bar, **MFI-12**).

Table S3.4. Dehydration rates and initial concentrations of **2-methylcyclohexanol** (180 °C, 50 bar, **MFI-12**).

rate [mol·g ⁻¹ ·s ⁻¹]	n [mol]	c [mol·L ⁻¹]	ln rate	ln c
8.63·10 ⁻⁵	0.03	0.30	- 9.36	-1.20
9.35·10 ⁻⁵	0.05	0.50	- 9.28	-0.69
7.28·10 ⁻⁵	0.08	0.80	- 9.53	-0.22

Dehydration of 2- and 4-methylcyclohexanol (MFI-193, MFI-60, MFI-45, MFI-40, MFI-15 and MFI-12)

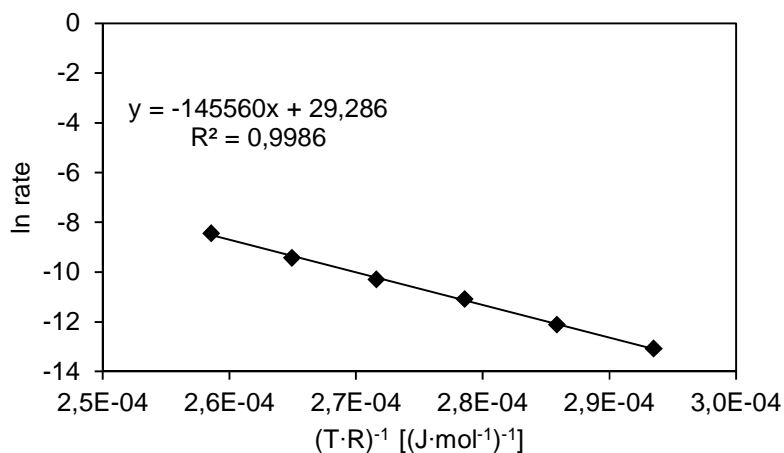


Figure S3.5. Arrhenius-plot: 4-methylcyclohexanol (0.5 M) dehydration ($E_a \approx 146$ kJ/mol), MFI-45.

Table S3.5. 4-methylcyclohexanol (0.5 M) dehydration rates at different reaction temperatures, MFI-45.

T [°C]	T [K]	TOF [s ⁻¹]	rate [mol·g ⁻¹ ·s ⁻¹]	(T·R) ⁻¹ [(J·mol ⁻¹) ⁻¹]	ln rate
140	413	$5.8 \cdot 10^{-3}$	$2.1 \cdot 10^{-6}$	$2.91 \cdot 10^{-4}$	-13.1
150	423	$1.5 \cdot 10^{-2}$	$5.5 \cdot 10^{-6}$	$2.84 \cdot 10^{-4}$	-12.1
160	433	$4.3 \cdot 10^{-2}$	$1.6 \cdot 10^{-5}$	$2.78 \cdot 10^{-4}$	-11.1
170	443	$9.5 \cdot 10^{-2}$	$3.4 \cdot 10^{-5}$	$2.71 \cdot 10^{-4}$	-10.3
180	453	$2.2 \cdot 10^{-1}$	$8.1 \cdot 10^{-5}$	$2.65 \cdot 10^{-4}$	-9.4
190	463	$6.0 \cdot 10^{-1}$	$2.2 \cdot 10^{-4}$	$2.60 \cdot 10^{-4}$	-8.4

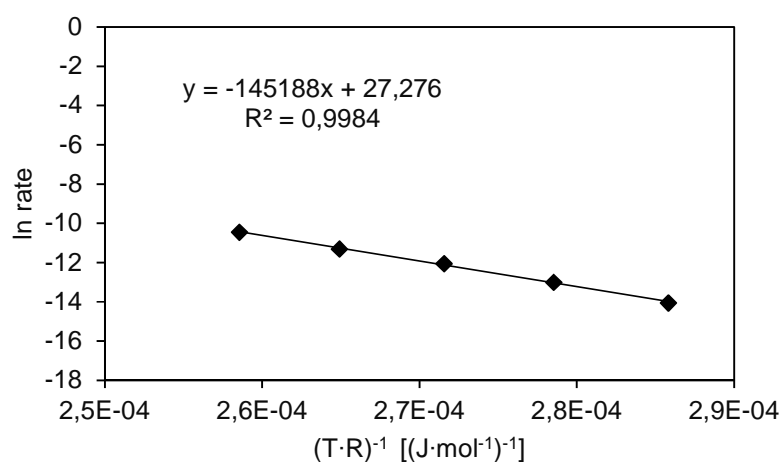
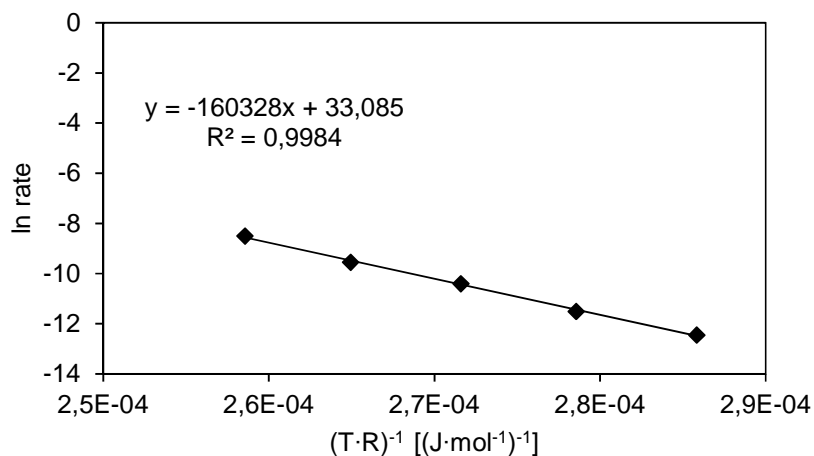


Figure S3.6. Arrhenius-plot: 4-methylcyclohexanol (0.5 M) dehydration ($E_a \approx 145$ kJ/mol), MFI-193.

Table S3.6. 4-methylcyclohexanol (0.5 M) dehydration rates at different reaction temperatures, **MFI-193**.

T [°C]	T [K]	TOF [s ⁻¹]	rate [mol·g ⁻¹ ·s ⁻¹]	(T·R) ⁻¹ [(J·mol ⁻¹) ⁻¹]	ln rate
150	423	8.8·10 ⁻³	7.9·10 ⁻⁷	2.84·10 ⁻⁴	-14.1
160	433	2.5·10 ⁻²	2.3·10 ⁻⁶	2.78·10 ⁻⁴	-13.0
170	443	6.5·10 ⁻²	5.8·10 ⁻⁶	2.71·10 ⁻⁴	-12.1
180	453	1.4·10 ⁻¹	1.2·10 ⁻⁵	2.65·10 ⁻⁴	-11.3
190	463	3.2·10 ⁻¹	2.9·10 ⁻⁵	2.60·10 ⁻⁴	-10.4

**Figure S3.7.** Arrhenius-plot: 4-methylcyclohexanol (0.5 M) dehydration ($E_a \approx 160$ kJ/mol), **MFI-15**.**Table S3.7.** 4-methylcyclohexanol (0.5 M) dehydration rates at different reaction temperatures, **MFI-15**.

T [°C]	T [K]	TOF [s ⁻¹]	rate [mol·g ⁻¹ ·s ⁻¹]	(T·R) ⁻¹ [(J·mol ⁻¹) ⁻¹]	ln rate
150	423	5.1·10 ⁻³	4.0·10 ⁻⁶	2.84·10 ⁻⁴	-12.4
160	433	1.3·10 ⁻²	1.0·10 ⁻⁵	2.78·10 ⁻⁴	-11.5
170	443	3.9·10 ⁻²	3.1·10 ⁻⁵	2.71·10 ⁻⁴	-10.4
180	453	9.2·10 ⁻²	7.2·10 ⁻⁵	2.65·10 ⁻⁴	-9.5
190	463	2.6·10 ⁻¹	2.0·10 ⁻⁴	2.60·10 ⁻⁴	-8.5

3. Influence of acid site concentration and EFAI in MFI zeolites on aqueous phase dehydration

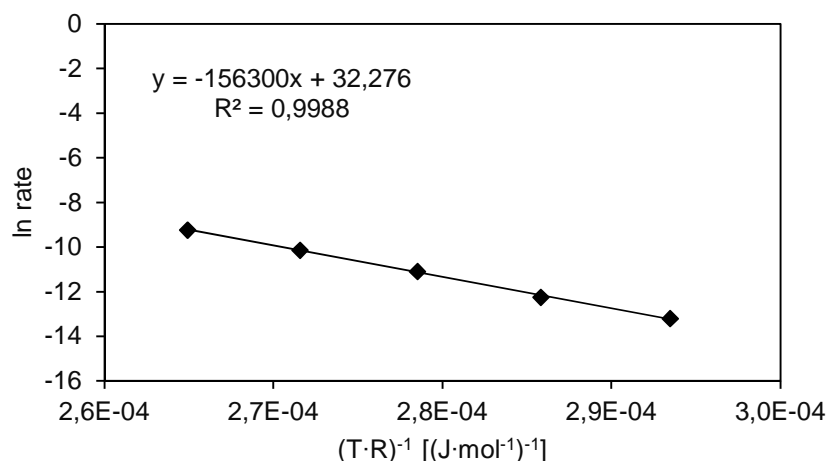


Figure S3.8. Arrhenius-plot for **4-methylcyclohexanol** (0.5 M) dehydration ($E_a \approx 156$ kJ/mol), **MFI-12**.

Table S3.8. **4-methylcyclohexanol** (0.5 M) dehydration rates at different reaction temperatures, **MFI-12**.

T [°C]	T [K]	TOF [s ⁻¹]	rate [mol·g ⁻¹ ·s ⁻¹]	(T·R) ⁻¹ [(J·mol ⁻¹) ⁻¹]	ln rate
140	413	3.6·10 ⁻³	1.9·10 ⁻⁶	2.91·10 ⁻⁴	-13.2
150	423	4.2·10 ⁻³	4.8·10 ⁻⁶	2.84·10 ⁻⁴	-12.2
160	433	1.3·10 ⁻²	1.5·10 ⁻⁵	2.78·10 ⁻⁴	-11.1
170	443	3.5·10 ⁻²	4.0·10 ⁻⁵	2.71·10 ⁻⁴	-10.1
180	453	8.7·10 ⁻²	9.9·10 ⁻⁵	2.65·10 ⁻⁴	-9.2

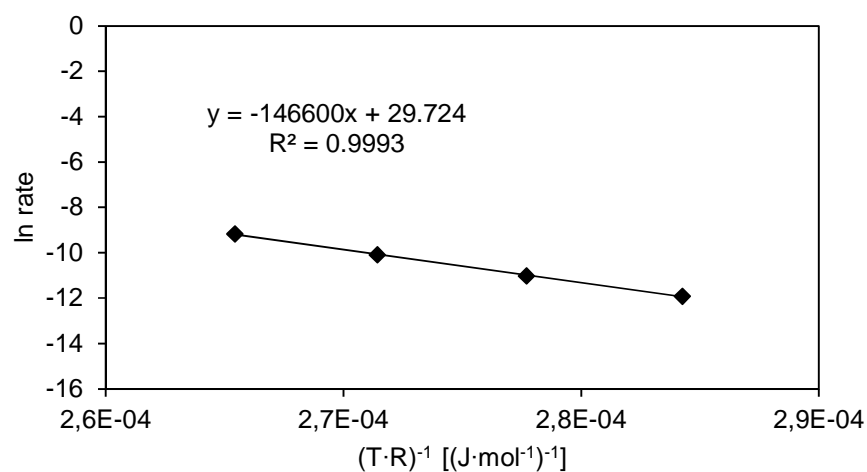
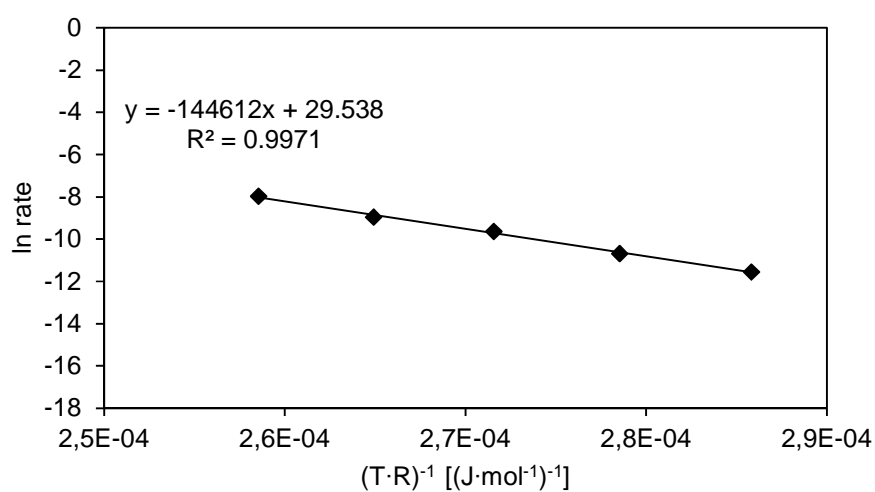


Figure S3.9. Arrhenius-plot: **4-methylcyclohexanol** (0.5 M) dehydration ($E_a \approx 147$ kJ/mol), **MFI-60**.

Table S3.9. 4-methylcyclohexanol (0.5 M) dehydration rates at different reaction temperatures, **MFI-60**.

T [°C]	T [K]	TOF [s ⁻¹]	rate [mol·g ⁻¹ ·s ⁻¹]	(T·R) ⁻¹ [(J·mol ⁻¹) ⁻¹]	ln rate
150	423	2.9·10 ⁻²	6.7·10 ⁻⁶	2.84·10 ⁻⁴	-11.9
160	433	7.2·10 ⁻²	1.6·10 ⁻⁵	2.78·10 ⁻⁴	-11.0
170	443	1.8·10 ⁻¹	4.2·10 ⁻⁵	2.71·10 ⁻⁴	-10.1
180	453	4.6·10 ⁻¹	1.1·10 ⁻⁴	2.65·10 ⁻⁴	-9.2

**Figure S3.10.** Arrhenius-plot: 4-methylcyclohexanol (0.5 M) dehydration ($E_a \approx 145$ kJ/mol), **MFI-40**.**Table S3.10.** 4-methylcyclohexanol (0.5 M) dehydration rates at different reaction temperatures, **MFI-40**.

T [°C]	T [K]	TOF [s ⁻¹]	rate [mol·g ⁻¹ ·s ⁻¹]	(T·R) ⁻¹ [(J·mol ⁻¹) ⁻¹]	ln rate
150	423	3.4·10 ⁻²	9.7·10 ⁻⁶	2.84·10 ⁻⁴	-11.5
160	433	8.1·10 ⁻²	2.3·10 ⁻⁵	2.78·10 ⁻⁴	-10.7
170	443	2.3·10 ⁻¹	6.6·10 ⁻⁵	2.71·10 ⁻⁴	-9.6
180	453	4.6·10 ⁻¹	1.3·10 ⁻⁴	2.65·10 ⁻⁴	-9.0
190	463	1.2	3.5·10 ⁻⁴	2.60·10 ⁻⁴	-8.0

3. Influence of acid site concentration and EFAl in MFI zeolites on aqueous phase dehydration

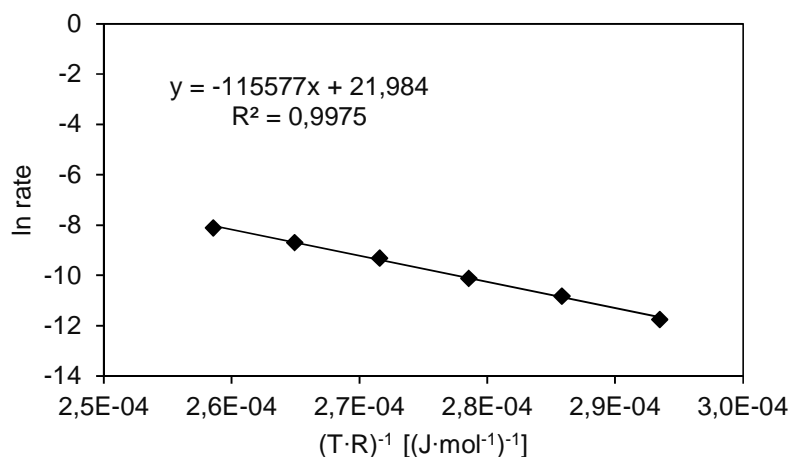


Figure S3.11. Arrhenius-plot: **2-methylcyclohexanol** (0.5 M) dehydration ($E_a \approx 116$ kJ/mol), **MFI-45**.

Table S3.11. **2-methylcyclohexanol** (0.5 M) dehydration rates at different reaction temperatures, **MFI-45**.

T [°C]	T [K]	TOF [s ⁻¹]	rate [mol·g ⁻¹ ·s ⁻¹]	(T·R) ⁻¹ [(J·mol ⁻¹) ⁻¹]	ln rate
140	413	2.2·10 ⁻²	7.9·10 ⁻⁶	2.91·10 ⁻⁴	-11.7
150	423	5.6·10 ⁻²	2.0·10 ⁻⁵	2.84·10 ⁻⁴	-10.8
160	433	1.1·10 ⁻¹	4.0·10 ⁻⁵	2.78·10 ⁻⁴	-10.1
170	443	2.5·10 ⁻¹	9.2·10 ⁻⁵	2.71·10 ⁻⁴	-9.3
180	453	4.7·10 ⁻¹	1.7·10 ⁻⁴	2.65·10 ⁻⁴	-8.7
190	463	8.4·10 ⁻¹	3.0·10 ⁻⁴	2.60·10 ⁻⁴	-8.1

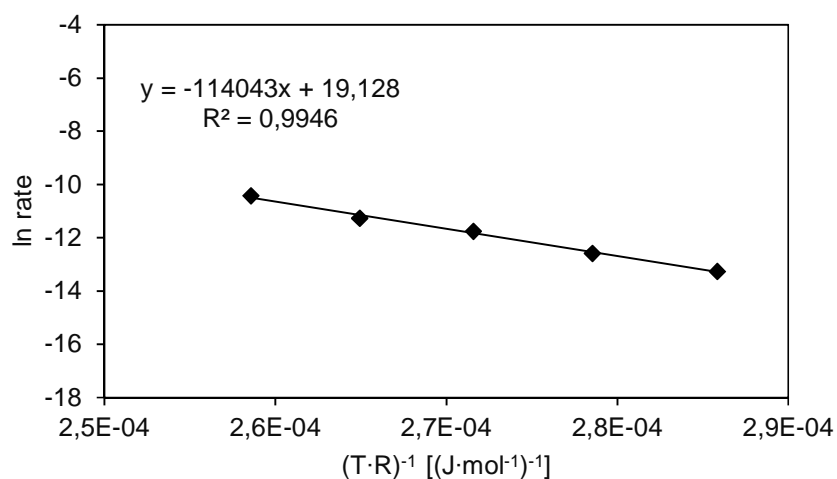
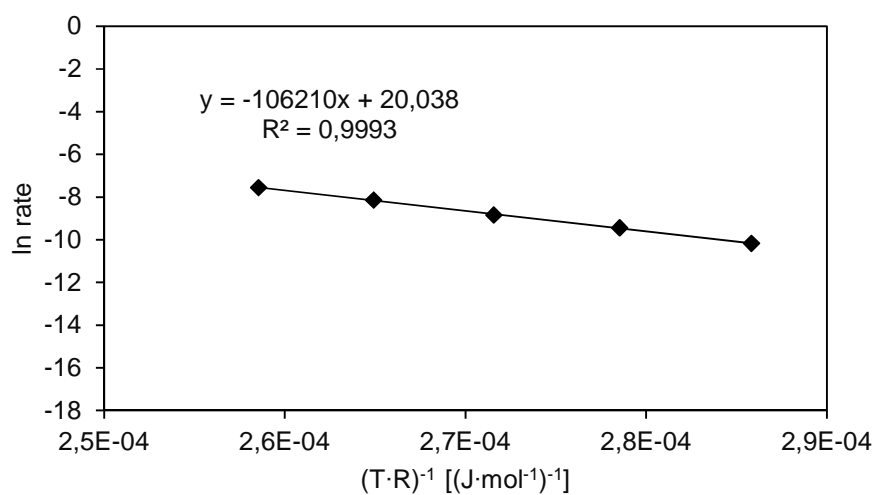


Figure S3.12. Arrhenius-plot: **2-methylcyclohexanol** (0.5 M) dehydration ($E_a \approx 114$ kJ/mol), **MFI-193**.

Table S3.12. 2-methylcyclohexanol (0.5 M) dehydration rates at different reaction temperatures, **MFI-193**.

T [°C]	T [K]	TOF [s ⁻¹]	rate [mol·g ⁻¹ ·s ⁻¹]	(T·R) ⁻¹ [(J·mol ⁻¹) ⁻¹]	ln rate
150	423	1.9·10 ⁻²	1.7·10 ⁻⁶	2.84·10 ⁻⁴	-13.3
160	433	3.8·10 ⁻²	3.4·10 ⁻⁶	2.78·10 ⁻⁴	-12.6
170	443	8.7·10 ⁻²	7.9·10 ⁻⁶	2.71·10 ⁻⁴	-11.8
180	453	1.5·10 ⁻¹	1.3·10 ⁻⁵	2.65·10 ⁻⁴	-11.3
190	463	3.3·10 ⁻¹	3.0·10 ⁻⁵	2.60·10 ⁻⁴	-10.4

**Figure S3.13.** Arrhenius-plot: 2-methylcyclohexanol (0.5 M) dehydration ($E_a \approx 106$ kJ/mol), **MFI-15**.**Table S3.13.** 2-methylcyclohexanol (0.5 M) dehydration rates at different reaction temperatures, **MFI-15**.

T [°C]	T [K]	TOF [s ⁻¹]	rate [mol·g ⁻¹ ·s ⁻¹]	(T·R) ⁻¹ [(J·mol ⁻¹) ⁻¹]	ln rate
150	423	4.9·10 ⁻²	3.9·10 ⁻⁵	2.84·10 ⁻⁴	-10.2
160	433	1.0·10 ⁻¹	8.0·10 ⁻⁵	2.78·10 ⁻⁴	-9.4
170	443	1.9·10 ⁻¹	1.5·10 ⁻⁴	2.71·10 ⁻⁴	-8.8
180	453	3.8·10 ⁻¹	3.0·10 ⁻⁴	2.65·10 ⁻⁴	-8.1
190	463	6.6·10 ⁻¹	5.3·10 ⁻⁴	2.60·10 ⁻⁴	-7.6

3. Influence of acid site concentration and EFAl in MFI zeolites on aqueous phase dehydration

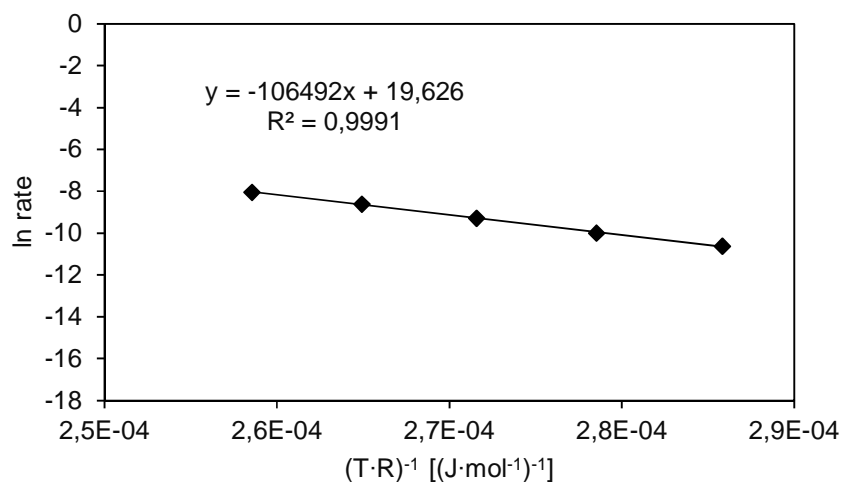


Figure S3.14. Arrhenius-plot: 2-methylcyclohexanol (0.5 M) dehydration ($E_a \approx 106$ kJ/mol), **MFI-12**.

Table S3.14. 2-methylcyclohexanol (0.5 M) dehydration rates at different reaction temperatures, **MFI-12**.

T [°C]	T [K]	TOF [s ⁻¹]	rate [mol·g ⁻¹ ·s ⁻¹]	$(T \cdot R)^{-1} [(J \cdot mol^{-1})^{-1}]$	ln rate
150	423	$2.1 \cdot 10^{-2}$	$2.5 \cdot 10^{-5}$	$2.84 \cdot 10^{-4}$	-10.6
160	433	$4.0 \cdot 10^{-2}$	$4.6 \cdot 10^{-5}$	$2.78 \cdot 10^{-4}$	-10.0
170	443	$8.2 \cdot 10^{-2}$	$9.4 \cdot 10^{-5}$	$2.71 \cdot 10^{-4}$	-9.3
180	453	$1.6 \cdot 10^{-1}$	$1.8 \cdot 10^{-4}$	$2.65 \cdot 10^{-4}$	-8.6
190	463	$2.8 \cdot 10^{-1}$	$3.2 \cdot 10^{-4}$	$2.60 \cdot 10^{-4}$	-8.0

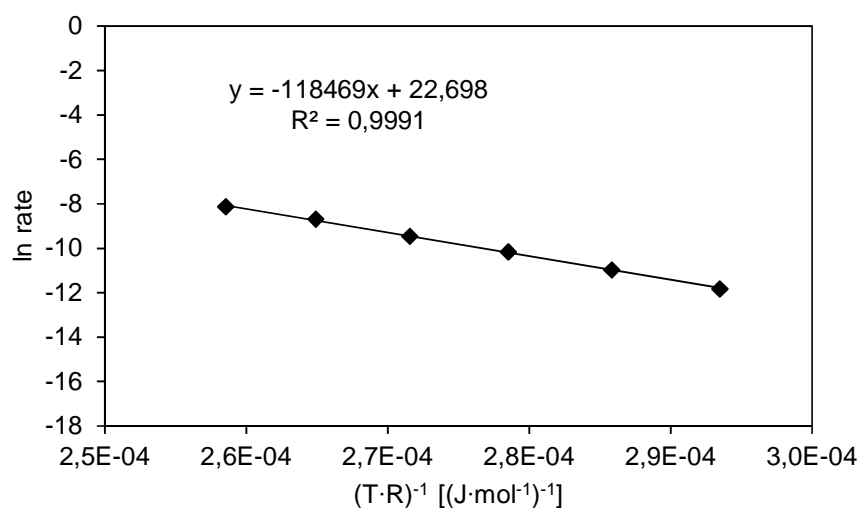


Figure S3.15. Arrhenius-plot: 2-methylcyclohexanol (0.5 M) dehydration ($E_a \approx 118$ kJ/mol), **MFI-60**.

3. Influence of acid site concentration and EFAI in MFI zeolites on aqueous phase dehydration

Table S3.15. 2-methylcyclohexanol (0.5 M) dehydration rates at different reaction temperatures, MFI-60.

T [°C]	T [K]	TOF [s ⁻¹]	rate [mol·g ⁻¹ ·s ⁻¹]	(T·R) ⁻¹ [(J·mol ⁻¹) ⁻¹]	ln rate
140	413	2.9·10 ⁻²	7.3·10 ⁻⁶	2.91·10 ⁻⁴	-11.8
150	423	7.5·10 ⁻²	1.7·10 ⁻⁵	2.84·10 ⁻⁴	-11.0
160	433	1.7·10 ⁻¹	3.9·10 ⁻⁵	2.78·10 ⁻⁴	-10.2
170	443	3.4·10 ⁻¹	7.8·10 ⁻⁵	2.71·10 ⁻⁴	-9.5
180	453	6.2·10 ⁻¹	1.7·10 ⁻⁴	2.65·10 ⁻⁴	-8.7
190	463	1.4	3.0·10 ⁻⁴	2.60·10 ⁻⁴	-8.1

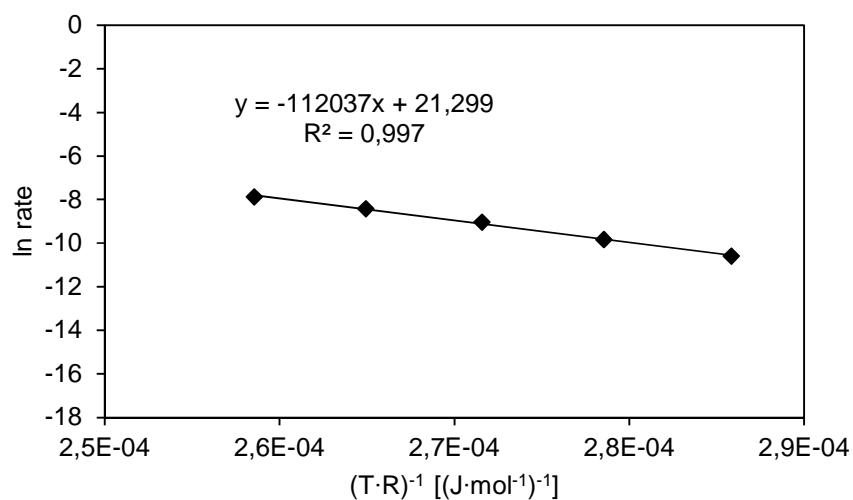


Figure S3.16. Arrhenius-plot: 2-methylcyclohexanol (0.5 M) dehydration ($E_a \approx 112$ kJ/mol), MFI-40.

Table S3.16. 2-methylcyclohexanol (0.5 M) dehydration rates at different reaction temperatures, MFI-40.

T [°C]	T [K]	TOF [s ⁻¹]	rate [mol·g ⁻¹ ·s ⁻¹]	(T·R) ⁻¹ [(J·mol ⁻¹) ⁻¹]	ln rate
150	423	8.8·10 ⁻²	2.5·10 ⁻⁵	2.84·10 ⁻⁴	-10.6
160	433	1.9·10 ⁻¹	5.4·10 ⁻⁵	2.78·10 ⁻⁴	-9.8
170	443	4.2·10 ⁻¹	1.2·10 ⁻⁴	2.71·10 ⁻⁴	-9.0
180	453	7.9·10 ⁻¹	2.2·10 ⁻⁴	2.65·10 ⁻⁴	-8.4
190	463	1.3	3.8·10 ⁻⁴	2.60·10 ⁻⁴	-7.9

Dehydration of 2- and 4-methylcyclohexanol with AHFS treated zeolites (MFI-15_AHFS and MFI-12_AHFS)

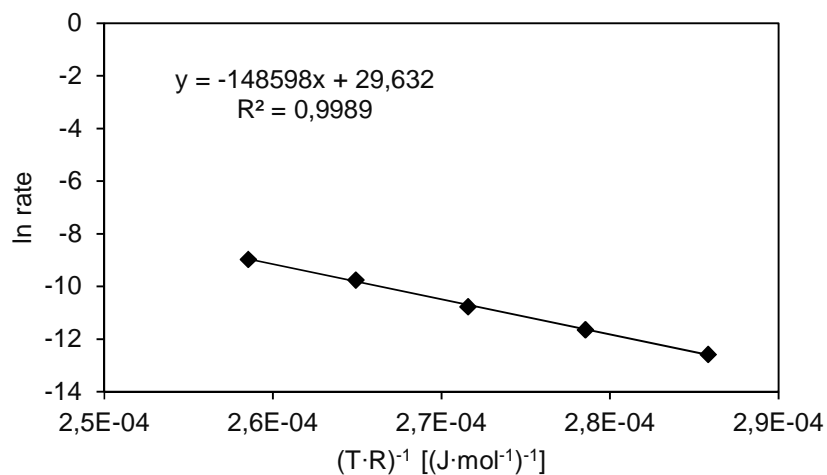


Figure S3.17. Arrhenius-plot: 4-methylcyclohexanol (0.5 M) dehydration ($E_a \approx 149$ kJ/mol), MFI-15_AHFS.

Table S3.17. 4-methylcyclohexanol (0.5 M) dehydration rates at different reaction temperatures, MFI-15_AHFS.

T [°C]	T [K]	TOF [s ⁻¹]	rate [mol·g ⁻¹ ·s ⁻¹]	$(T \cdot R)^{-1} [(J \cdot mol^{-1})^{-1}]$	ln rate
150	423	$7.3 \cdot 10^{-3}$	$3.4 \cdot 10^{-6}$	$2.84 \cdot 10^{-4}$	-12.6
160	433	$1.9 \cdot 10^{-2}$	$8.8 \cdot 10^{-6}$	$2.78 \cdot 10^{-4}$	-11.6
170	443	$4.5 \cdot 10^{-2}$	$2.1 \cdot 10^{-5}$	$2.71 \cdot 10^{-4}$	-10.8
180	453	$1.2 \cdot 10^{-1}$	$5.6 \cdot 10^{-5}$	$2.65 \cdot 10^{-4}$	-9.8
190	463	$2.7 \cdot 10^{-1}$	$1.3 \cdot 10^{-4}$	$2.60 \cdot 10^{-4}$	-9.0

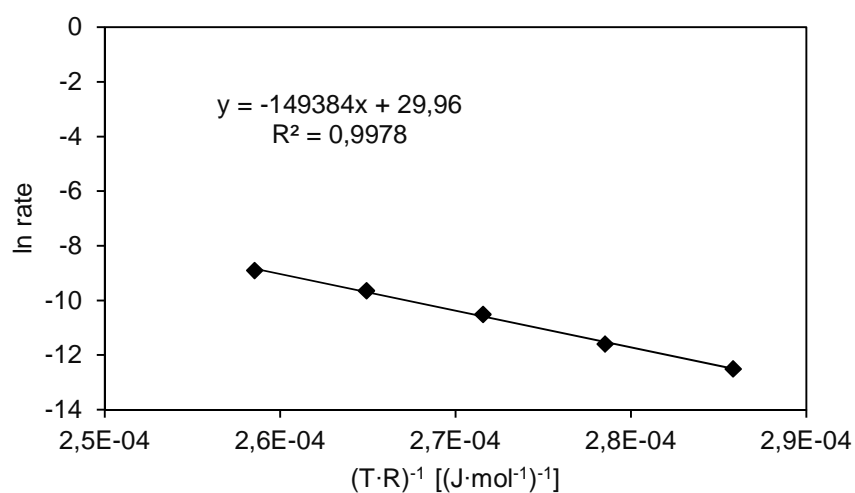
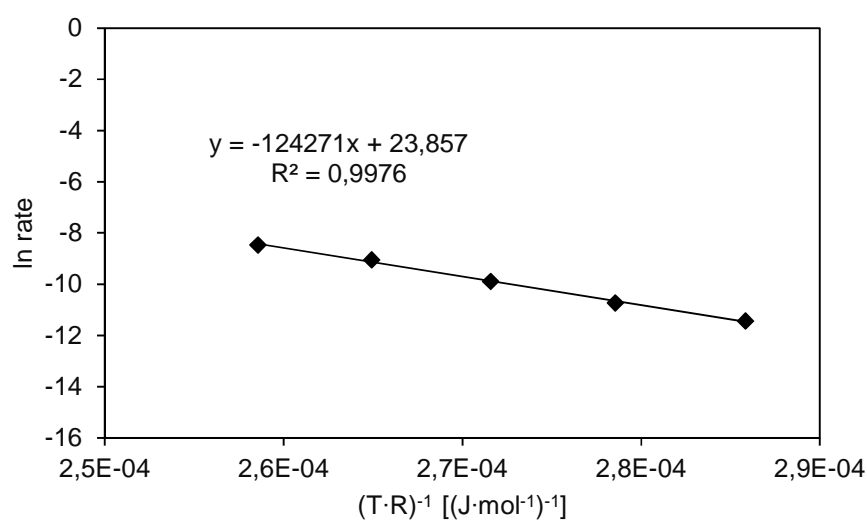


Figure S3.18. Arrhenius-plot: 4-methylcyclohexanol (0.5 M) dehydration ($E_a \approx 149$ kJ/mol), MFI-12_AHFS.

Table S3.18. 4-methylcyclohexanol (0.5 M) dehydration rates at different reaction temperatures, MFI-12_AHFS.

T [°C]	T [K]	TOF [s ⁻¹]	rate [mol·g ⁻¹ ·s ⁻¹]	(T·R) ⁻¹ [(J·mol ⁻¹) ⁻¹]	ln rate
150	423	5.9·10 ⁻³	3.7·10 ⁻⁶	2.84·10 ⁻⁴	-12.5
160	433	1.5·10 ⁻²	9.3·10 ⁻⁶	2.78·10 ⁻⁴	-11.6
170	443	4.4·10 ⁻²	2.8·10 ⁻⁵	2.71·10 ⁻⁴	-10.5
180	453	1.0·10 ⁻¹	6.5·10 ⁻⁵	2.65·10 ⁻⁴	-9.6
190	463	2.2·10 ⁻¹	1.4·10 ⁻⁴	2.60·10 ⁻⁴	-8.9

**Figure S3.19.** Arrhenius-plot: 2-methylcyclohexanol (0.5 M) dehydration ($E_a \approx 124$ kJ/mol), MFI-15_AHFS.**Table S3.19.** 2-methylcyclohexanol (0.5 M) dehydration rates at different reaction temperatures, MFI-15_AHFS.

T [°C]	T [K]	TOF [s ⁻¹]	rate [mol·g ⁻¹ ·s ⁻¹]	(T·R) ⁻¹ [(J·mol ⁻¹) ⁻¹]	ln rate
150	423	2.3·10 ⁻²	1.1·10 ⁻⁵	2.84·10 ⁻⁴	-11.4
160	433	4.7·10 ⁻²	2.2·10 ⁻⁵	2.78·10 ⁻⁴	-10.7
170	443	1.1·10 ⁻¹	5.1·10 ⁻⁵	2.71·10 ⁻⁴	-9.9
180	453	2.5·10 ⁻¹	1.2·10 ⁻⁴	2.65·10 ⁻⁴	-9.1
190	463	4.5·10 ⁻¹	2.1·10 ⁻⁴	2.60·10 ⁻⁴	-8.5

3. Influence of acid site concentration and EFAl in MFI zeolites on aqueous phase dehydration

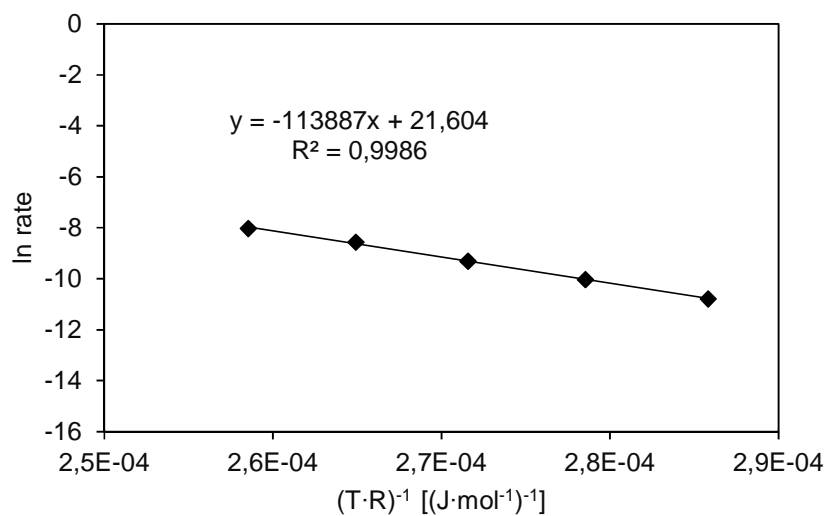


Figure S3.20. Arrhenius-plot: 2-methylcyclohexanol (0.5 M) dehydration ($E_a \approx 114$ kJ/mol), MFI-12_AHFS.

Table S3.20. 2-methylcyclohexanol (0.5 M) dehydration rates at different reaction temperatures, MFI-12_AHFS.

T [°C]	T [K]	TOF [s^{-1}]	rate [$\text{mol} \cdot \text{g}^{-1} \cdot \text{s}^{-1}$]	$(T \cdot R)^{-1}$ [$(\text{J} \cdot \text{mol}^{-1})^{-1}$]	ln rate
150	423	$3,3 \cdot 10^{-2}$	$2,1 \cdot 10^{-5}$	$2,84 \cdot 10^{-4}$	-10,8
160	433	$7,1 \cdot 10^{-2}$	$4,4 \cdot 10^{-5}$	$2,78 \cdot 10^{-4}$	-10,0
170	443	$1,5 \cdot 10^{-1}$	$9,1 \cdot 10^{-5}$	$2,71 \cdot 10^{-4}$	-9,3
180	453	$3,1 \cdot 10^{-1}$	$1,9 \cdot 10^{-4}$	$2,65 \cdot 10^{-4}$	-8,6
190	463	$5,2 \cdot 10^{-1}$	$3,3 \cdot 10^{-4}$	$2,60 \cdot 10^{-4}$	-8,0

In-situ probing of acid sites: Poisoning experiments with pyridine in liquid phase under reaction conditions.

These experiments were carried out at 170 °C with 0.05 mol **4-methylcyclohexanol**, 100 mL H₂O, 50 bar and 50 mg **MFI-45**.

- Determination of acid sites – MFI-45

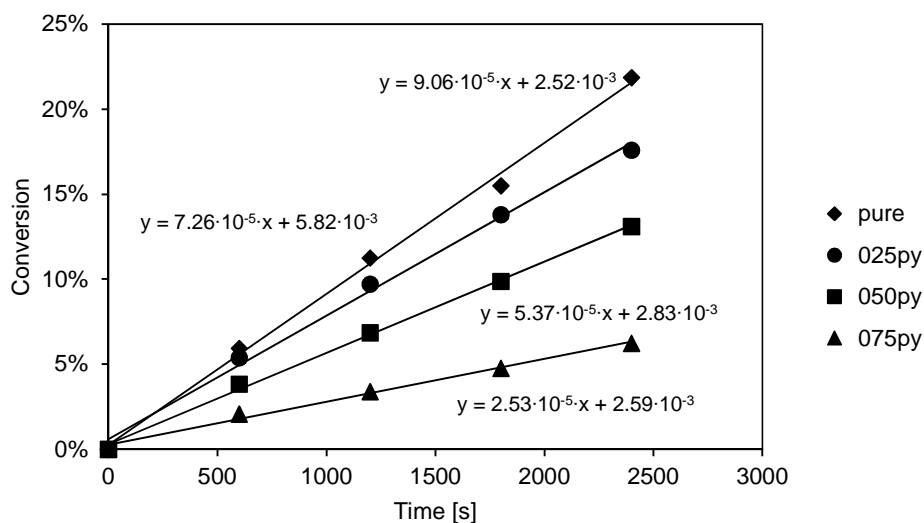


Figure S3.21. Determination of acid sites in dehydration of **4-MCH** with **MFI-45**. 025py = 90 μmol pyridine per g, 050py = 180 μmol pyridine per g, 075py = 270 μmol pyridine per g.

Table S3.21. Kinetic data of the poisoning experiments for **4-MCH** dehydration, **MFI-45**.

t [min]	t [s]	Pure X [%]	025py X [%]	050py X [%]	075py X [%]
10	600	5.9	5.4	3.8	2.1
20	1200	11.3	9.7	6.8	3.4
30	1800	15.5	13.8	9.9	4.8
40	2400	21.9	17.6	13.1	6.2

3. Influence of acid site concentration and EFAl in MFI zeolites on aqueous phase dehydration

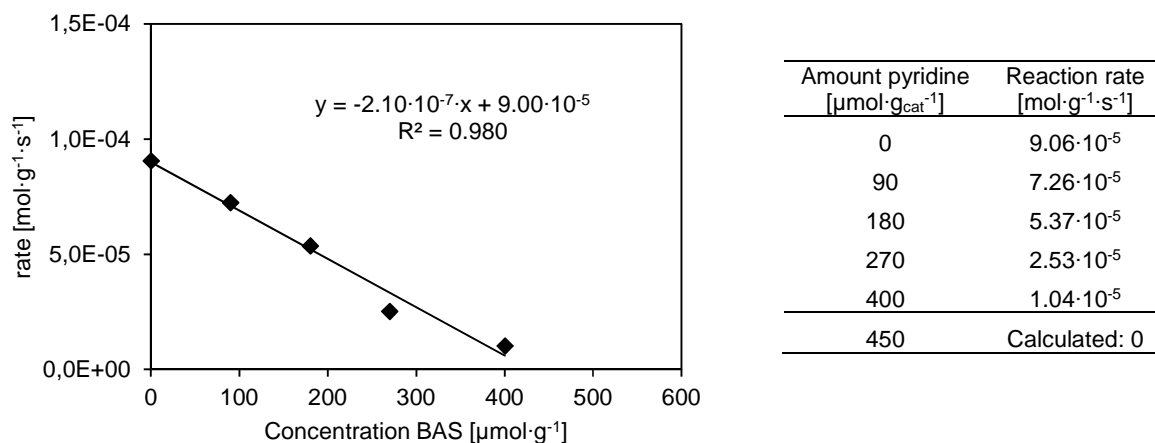


Figure and Table S3.22. Correlation of reaction rates and amount of pyridine per g **MFI-45** zeolite. Calculated maximal acid sites: 450 μmol per g **MFI-45**.

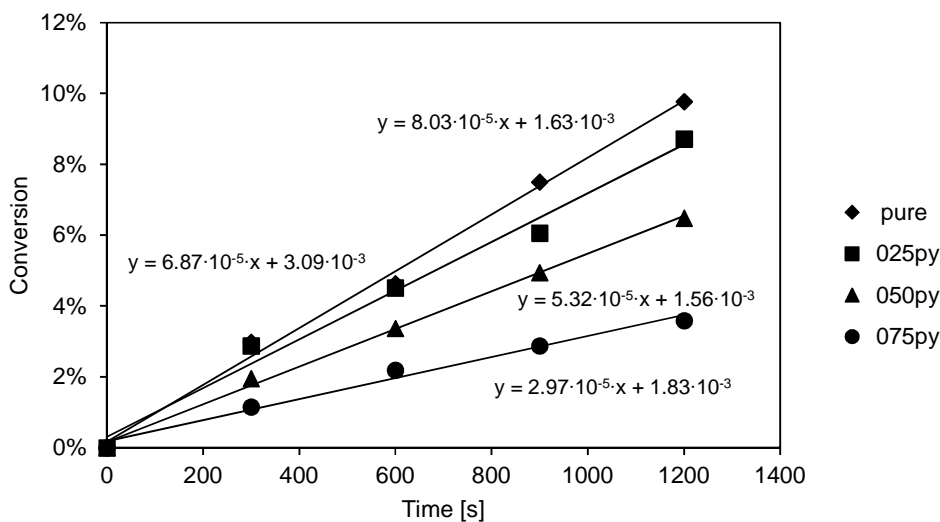


Figure S3.23. Determination of acid sites in dehydration of **2-MCH** with **MFI-45**. 025py = 90 μmol pyridine per g, 050py = 180 μmol pyridine per g, 075py = 270 μmol pyridine per g.

Table S3.23. Kinetic data of the poisoning experiments for **4-MCH** dehydration, **MFI-45**.

t [min]	t [s]	Pure X [%]	025py X [%]	050py X [%]	075py X [%]
5	300	3.0	2.9	1.9	1.2
10	600	4.6	4.5	3.4	2.2
15	900	7.5	6.1	4.9	2.9
20	1200	9.8	8.7	6.5	3.6

3. Influence of acid site concentration and EFAl in MFI zeolites on aqueous phase dehydration

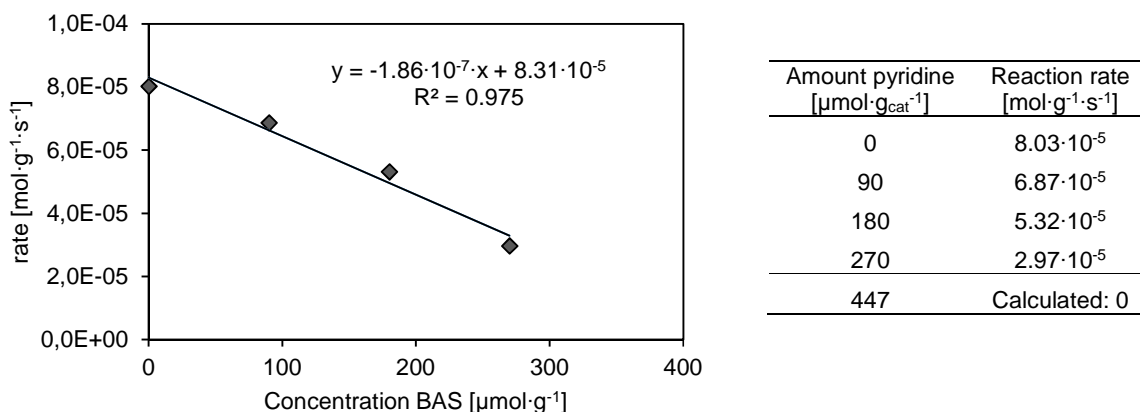


Figure and Table S3.24. Correlation of reaction rates and amount of pyridine per g **MFI-45** zeolite. Calculated maximal acid sites: 447 μmol per g **MFI-45**.

- Determination of acid sites – MFI-12

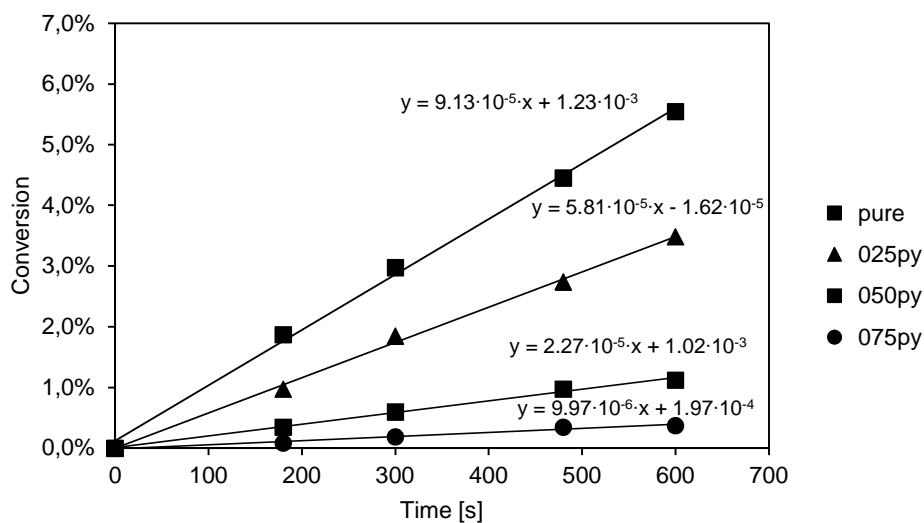


Figure S3.25. In-operando determination of acid sites in dehydration of **4-MCH** with **MFI-12**. 025py = 350 μmol pyridine per g, 050py = 700 μmol pyridine per g, 075py = 1050 μmol pyridine per g.

Table S3.25. Kinetic data of the poisoning experiments of **4-methylcyclohexanol** dehydration with **MFI-12**.

t [min]	t [s]	Pure X [%]	025py X [%]	050py X [%]	075py X [%]
3	180	1.9	1.0	0.4	0.1
5	300	3.0	1.8	0.6	0.2
8	480	4.5	2.7	1.0	0.3
10	600	5.5	3.5	1.1	0.4

3. Influence of acid site concentration and EFAI in MFI zeolites on aqueous phase dehydration

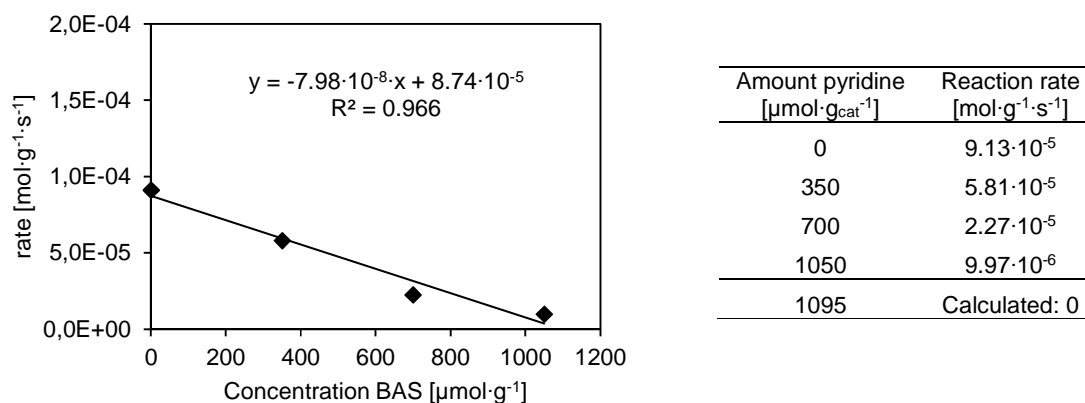


Figure and Table S3.26. Correlation of reaction rates and amount of pyridine per g **MFI-12** zeolite. Calculated maximal acid sites: 1095 μmol per g **MFI-12**.

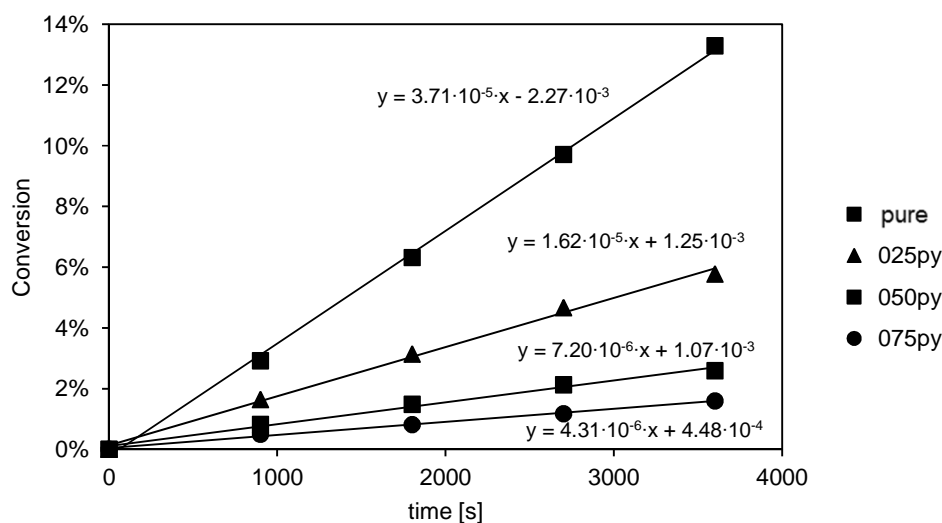
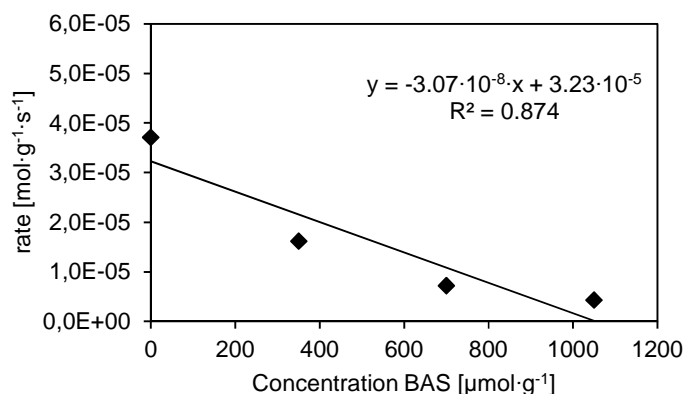


Figure S3.27. Determination of acid sites in dehydration of **2-MCH** with **MFI-12**. 025py = 350 μmol pyridine per g, 050py = 700 μmol pyridine per g, 075py = 1050 μmol pyridine per g.

Table S3.27. Kinetic data of the poisoning experiments of **4-methylcyclohexanol** dehydration with **MFI-12**.

t [min]	t [s]	Pure X [%]	025py X [%]	050py X [%]	075py X [%]
15	900	2.9	1.6	0.8	0.5
30	1800	6.3	3.1	1.5	0.8
45	2700	9.7	4.7	2.1	1.2
60	3600	13.3	5.8	2.6	1.6

3. Influence of acid site concentration and EFAI in MFI zeolites on aqueous phase dehydration

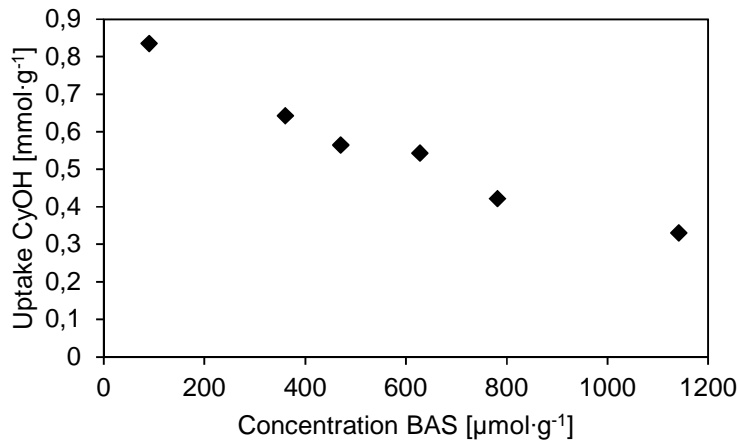


Amount pyridine [$\mu\text{mol}\cdot\text{g}_{\text{cat}}^{-1}$]	Reaction rate [$\text{mol}\cdot\text{g}^{-1}\cdot\text{s}^{-1}$]
0	$3.71\cdot 10^{-5}$
350	$1.62\cdot 10^{-5}$
700	$7.20\cdot 10^{-6}$
1050	$4.31\cdot 10^{-6}$
1052	Calculated: 0

Figure and Table S3.28. Correlation of reaction rates and amount of pyridine per g **MFI-12** zeolite. Calculated maximal acid sites: 1095 μmol per g **MFI-12**.

Cyclohexanol adsorption on MFI zeolites

Figure and Table S3.29. Cyclohexanol adsorption (25 °C) on MFI zeolites with varying concentration of BAS.



	MFI-193	MFI-45	MFI-15_AHFS	MFI-12_AHFS	MFI-15	MFI-12
Concentration BAS [$\mu\text{mol}\cdot\text{g}^{-1}$]	90	360	470	627	781	1141
Micropore volume [$\text{mL}\cdot\text{g}^{-1}$]	0.101	0.120	0.138	0.160	0.175	0.178
Uptake CyOH (25 °C) [$\text{mmol}\cdot\text{g}^{-1}$]	0.836	0.643	0.565	0.543	0.422	0.331

4. Impact of confinement on aqueous phase dehydration of substituted cyclic alcohols

This chapter is based on:

Peter H. Hintermeier, Sebastian Eckstein, Eszter Baráth and Johannes A. Lercher, "*Impact of confinement on aqueous phase dehydration of substituted cyclic alcohols*", in preparation.

P.H.H. performed experiments, analyzed the data and wrote the manuscript. S.E. and E.B. contributed in preparing the manuscript by fruitful discussions. J.A.L. is the principal investigator of this project.

Abstract

This chapter highlights the impact of zeolite confinement (MFI, BEA and FAU) on the dehydration of substituted cyclic alcohols in aqueous phase. *Cis* and *trans* 2-methylcyclohexanol (2-McyOH) serve as representative secondary alcohols following either a concerted or a stepwise elimination mechanisms. Furthermore, the impact of catalyst confinement on an E1 dehydration pathway was exemplarily investigated for 1-methylcyclohexanol (1-McyOH) as a tertiary alcohol and 2-cyclohexylethanol (2-CyEtOH) as a primary alcohol proceeding *via* a concerted elimination pathway. A comparison of TOF, E_a , ΔH^{\ddagger} and ΔS^{\ddagger} obtained by MFI, BEA, FAU zeolites and H_3PO_4 revealed that the increasing dehydration rates with increasing confinement are either enthalpically (E1) or entropically (E2) controlled.

4.1. Introduction

Reaction pathways in zeolites are significantly influenced by the confinement^{[1],[2]} Parameters like the selectivity of reactants, products and transition states are crucially influenced by the environment of the catalytically active sites in zeolite channels.^[3] Besides chemical reactions (cleavage and formation of bonds) also the adsorption of alkanes on zeolites is remarkably affected by the pore dimensions. Increasing confinement correlates with increasing heats of adsorption and losses in entropy.^[4]

Acid catalyzed reactions in zeolites (e.g. cracking, dehydration^[5] or alkene oligomerization) are significantly influenced by the catalyst confinement.^[6] The impact of pore and channel dimensions on the product selectivity was exemplarily shown for the transformation of glucose to aromatic compounds.^[7] Medium pore size zeolites showed the best results for this reaction. The large pore zeolites formed coke with a high selectivity, whereas those with small channels mainly produced CO and CO₂ instead of aromatic compounds.^[7]

Especially the influence of confinement on cracking of alkanes over MOR, MFI and FAU zeolites was investigated in detail.^[6] The location of the catalytically active sites in zeolites is decisive and the spatial constraints decide about the stability of reactants and cationic transition states. The turnover rates for monomolecular propane and *n*-butane cracking were significantly higher in 8-membered ring side pockets than in the 12-membered ring main channels of H-MOR zeolite. It was assumed that entropic gains compensate for enthalpy and cause an overall lower free energy for the transition states in smaller side pockets. In such cases, the higher energetic transition states reflect higher values for entropy and illustrate late and product-like transition states. The formation of a cationic transition state/intermediate in a zeolite is rather fundamentally influenced by enthalpy and entropy factors than by simplified considerations of size and shape.^[8]

As the confinement of zeolites has a significant impact on reaction rates and activation barriers in gaseous phase, this chapter focuses on the acid catalyzed dehydration in condensed aqueous phase. The efficiency of hydronium ions in confines is remarkably higher than in homogeneous systems as reported in a previous study.^[9] Shi *et al.* investigated aqueous phase dehydration of cyclohexanol with different zeolite frameworks (MFI, BEA and FAU) as well as hetero polyacids (polyoxometalates).^[10] The higher dehydration rates result of greater enthalpic stabilization of the transition states (relative to the H-bonded alcohols) in smaller pores (e.g. MFI zeolite) which overcompensated the loss in entropy in such tighter confines.^[10]

This study investigates the impact of zeolite confinement on the dehydration of primary, secondary and tertiary alcohols proceeding either *via* E1 or E2 dehydration routes.

4.2. Experimental

Chemicals

The following chemicals were used: 2-methylcyclohexanol (mixture of *cis* and *trans* (48%:52%), 99%, *Sigma-Aldrich*), *trans* 2-methylcyclohexanol (99%, *Sigma-Aldrich*), 1-methylcyclohexanol (96%, *Sigma-Aldrich*), 2-cyclohexylethanol (99%, *Sigma-Aldrich*), sodium sulfate (ACS reagent, > 99%, *Sigma-Aldrich*) ethyl acetate (*Chromasolv*, 99.9%, *Sigma-Aldrich*), phosphoric acid (85% solution, *Sigma-Aldrich*) and sodium chloride (*ReagentPlus*, > 99%, *Sigma-Aldrich*). Hydrogen gas was obtained from *Westfalen* (> 99.999%). Deionized water was treated with an *Easypure-II* system from *WERNER* to obtain ultrapure water (18.2 M Ω ·cm).

Zeolite catalysts

Zeolites MFI (Si/Al = 45), BEA (Si/Al = 15) and BEA (Si/Al = 83) were obtained from *CLARIANT AG* in H-form. FAU (Si/Al = 3; *CBV600*) and FAU (Si/Al = 15; *CBV720*) were obtained from *ZEOLYST* in H-form. All zeolites were treated at 550 °C (rate: 10 °C·min⁻¹) for six hours in 100 mL·min⁻¹ synthetic air (80% nitrogen, 20% oxygen; > 99%).

Reaction procedure

All reactions were performed with reactant, catalyst and solvent. In 100 mL ultrapure water 0.05 mol of substrate (5.71 g) of 1-/2-methylcyclohexanol and 0.01/0.02 mol (1.28/2.56 g) of 2-cyclohexylethanol and between 50 and 200 mg zeolite were dissolved and suspended, respectively. The molar amount of reactant of pure *trans* 2-methylcyclohexanol was 4.38 mmol (0.5 g) in 100 mL water. For the homogeneously catalyzed experiments 1-methylcyclohexanol (0.05 mol) and 0.05 mmol phosphoric acid (3.5 μ L, 0.006 g of 85 wt.-% H₃PO₄) were used in 100 mL water depending on the reaction temperature. For experiments with 2-cyclohexylethanol (0.02 mol) 0.07 mol (5 mL, 8.4 g of 85 wt.-% H₃PO₄) phosphoric acid were used.

The autoclave (300 mL) was loaded with 100 mL water, zeolite catalyst and substituted cyclohexanol substrate. The reactor was purged two times with hydrogen (20 bar) and was heated to the reaction temperature (80 – 200 °C) with a heating rate of 10 °C per minute with 20 bar at the beginning and without stirring. Ten degrees below the reaction temperature the total pressure of the reactor was adjusted to 50 bar with hydrogen gas and as soon as the reaction temperature was reached the stirring rate was set to 700 rpm. After the reaction time, the reactor was cooled down to room temperature with an ice bath. The pressure within the reactor was released below 5 °C to prevent the loss of volatile products. The reaction mixture was extracted with 3 x 20 mL ethyl acetate. To improve the phase separation of the organic and the aqueous phases, a small amount of sodium chloride was added to the reaction mixture. After extraction, the organic phase

was dried over sodium sulfate. The carbon balance was monitored by an internal standard (dodecane).

Catalytic reactions and equipment

Reactor. All reactions were performed in an autoclave (300 mL) from *Parr Instruments Co.* (type: *PST FS*, material: HASTELLOY C) with a temperature and stirring controlling device (*Parr Instruments Co. 4848 Reactor Controller*).

GC-MS. Quantification and qualification of the dehydration reactions was analyzed by GC/MS (*Agilent Technologies 7890 B GC*, column: *Agilent 19091S-433UI INV02* (30 m x 250 μm x 0.25 μm), heating program: 10 $^{\circ}\text{C}\cdot\text{min}^{-1}$ from 80 $^{\circ}\text{C}$ to 280 $^{\circ}\text{C}$). Data was analyzed with *MassHunter Workstation Software, Qualitative Analysis, Version B.06.00, Agilent Technologies (2012)*.

AAS. The Si and Al content of the MFI-90 zeolite sample was measured by atomic absorption spectroscopy (AAS) on a *UNICAM 939 AA-Spectrometer*.

N₂ physisorption. The BET specific surface area and pore volume of the zeolite were determined by nitrogen physisorption. The isotherms were measured at liquid nitrogen temperature (-196 $^{\circ}\text{C}$) using a *PMI Automatic Sorptometer*. The catalyst was activated in vacuum at 200 $^{\circ}\text{C}$ for two hours before measurement. Apparent surface area was calculated by applying the *Brunauer-Emmett-Teller (BET)* theory, and the *t-plot method* was used to determine the pore volumes.

SEM. The scanning electron microscopy (SEM) images were recorded on a *JEOL 500 SEM-microscopy* (accelerating voltage: 25 kV). The samples were prepared by depositing a drop of an ultrasonicated methanol suspension of the solid material onto a carbon-coated Cu grid.

IR. Infrared spectroscopy of adsorbed pyridine was performed with a *Perkin-Elmer 2000* spectrometer at a resolution of 4 cm^{-1} . The catalyst sample was prepared as wafer and activated in vacuum (ca. 10^{-6} mbar) at 450 $^{\circ}\text{C}$ for one hour (heating rate = 10 $^{\circ}\text{C}\cdot\text{min}^{-1}$). After this, the sample was equilibrated with 0.1 mbar of pyridine for 30 minutes followed by outgassing for one hour at 150 $^{\circ}\text{C}$. A spectrum with the chemisorbed pyridine was recorded thereafter. Adsorbed pyridine was desorbed finally at 450 $^{\circ}\text{C}$ with 10 $^{\circ}\text{C}\cdot\text{min}^{-1}$ for half an hour. A spectrum was recorded at equilibrium. For quantification, molar integral extinction coefficients of 0.73 $\text{cm}\cdot\mu\text{mol}^{-1}$ and 0.96 $\text{cm}\cdot\mu\text{mol}^{-1}$ were used for *Brønsted* and *Lewis* acid sites, respectively.

¹H-NMR. ¹H-NMR spectra with water signal suppression were recorded at 30 $^{\circ}\text{C}$ using an Avance III HD 500 System (Bruker Biospin, Rheinstetten, Germany) with an UltraShield 500 MHz magnet

(11.75 T) and a BBI 500 S2 probe head (5 mm, inverse 1H/X with Z-gradient). The resonance frequency of ^1H was 500.13 MHz. Longitudinal relaxation times (T_1) were determined by the inversion recovery pulse method. Relaxation delay and acquisition time were set to 26 s and 4.1 s, respectively. Typically, 64 or 128 scans, with 64 k data points were collected. An exponential window function with a line broadening of 0.2 Hz was applied prior to Fourier transformation and the spectra were manually phased, baseline corrected and integrated using *Mestre-C 8.1.1* software package. Quantification of *cis/trans* isomers was based on the integrated signal intensities.

NH₃-TPD. Temperature programmed desorption (TPD) of ammonia was performed in a 6-fold parallel reactor system. The catalysts were activated under reduced pressure at 450 °C (heating rate: 5 °C·min⁻¹) for one hour. NH₃ was adsorbed for one hour with partial pressures of 1 mbar at 100 °C, respectively. Subsequently, the samples were evacuated for two hours to remove physisorbed probe molecules. For the TPD experiments, six samples were sequentially heated from 100 to 770 °C with a heating rate of 10 °C·min⁻¹ to desorb ammonia. The rates of desorbing species were monitored by mass spectrometry (*Balzers QME 200*). For the quantification of the amount of acidity, a standard MFI zeolite with known acid site concentration was used to calibrate the signal.

4.3. Results and Discussion

Characterization of zeolites (MFI, BEA and FAU)

Three zeolite frameworks of different pore or channel dimensions (MFI, BEA and FAU) were investigated to reveal the impact of confinement on acid catalyzed dehydration pathways of substituted cyclic alcohols. The Si/Al ratios of the catalysts were chosen according to the highest stability of zeolites in hot liquid water, quantified by XRD after reaction conditions and in accordance with the results of Lutz *et al.*^[11] BEA zeolites with moderate Al content are the most suitable for catalysis in aqueous phase. FAU zeolites with a high amount of aluminum showed the highest resistance to water at higher temperatures. The MFI structure is the most stable zeolite type, almost independent of the Si/Al ratio. **Table 4.1.** compiles the properties of the examined MFI (Si/Al = 45), BEA (Si/Al = 83) and FAU (Si/Al = 3) zeolites.

As a result of the high aluminum content in the investigated FAU zeolite, the concentration of total acid sites ($c(\text{BAS}) = 335 \mu\text{mol}\cdot\text{g}^{-1}$ and $c(\text{LAS}) = 294 \mu\text{mol}\cdot\text{g}^{-1}$) is relatively high (**Table 4.1. Entry 3**). Nevertheless, the number of catalytically active species BAS is comparable

to the investigated MFI ($c(\text{LAS}) = 45 \mu\text{mol}\cdot\text{g}^{-1}$ and $c(\text{BAS}) = 360 \mu\text{mol}\cdot\text{g}^{-1}$; **Table 4.1. Entry 1**). The concentration of acid sites in BEA zeolite is low ($c(\text{LAS}) = 20 \mu\text{mol}\cdot\text{g}^{-1}$ and $c(\text{BAS}) = 120 \mu\text{mol}\cdot\text{g}^{-1}$) based on the high Si/Al ratio (**Table 4.1. Entry 2**).

Table 4.1. Characterization of the investigated MFI, BEA and FAU zeolite.

Entry	Zeolite	Si/Al	Concentration (BAS) ^a [$\mu\text{mol}\cdot\text{g}^{-1}$]	Concentration (LAS) ^a [$\mu\text{mol}\cdot\text{g}^{-1}$]	Concentration (BAS+LAS) ^b [$\mu\text{mol}\cdot\text{g}^{-1}$]
1	MFI	45	360	45	400
2	BEA	83	120	20	156
3	FAU	3	335	294	685

^a determined by IR spectroscopy (pyridine), ^b determined by TPD (NH_3).

Based on the different Si/Al ratios of the chosen zeolites, the dehydration data obtained by FAU and BEA zeolites of Si/Al = 15 are compiled in the Supporting Information (SI, **Figures S4.2., S4.10., S4.11.** and **Tables S4.3., S4.11., S4.12.**). Despite the remarkable differences regarding the acid site concentrations, the determined activation barriers were comparable for zeolites of the same framework type.

Dehydration of cis and trans 2-methylcyclohexanol: impact of confinement on different dehydration pathways

Based on a comparison of dehydration rates, selectivity, reaction progress (formation of the other isomer), ΔS^\ddagger and ΔH^\ddagger it was previously shown that the two isomers of 2-McyOH proceed *via* two different dehydration mechanisms. While the *trans* isomer is converted stepwise *via* a carbenium ion intermediate (E1), the dehydration of the *cis* isomer proceeds *via* a concerted pathway (E2). The impact of zeolite confinement on the turnover frequencies of the hydronium ions was investigated by a gradual decrease of the channel and pore diameter. Therefore, the determined dehydration rates and activation parameters obtained by MFI zeolite (10-membered ring pores) are compared to data of BEA (12-membered ring pores) and FAU zeolite (12-membered ring pores with super-cages). Activation barriers and turnover frequencies for the homogeneously catalyzed (H_3PO_4) dehydration of *cis* and *trans* 2-McyOH were reported in Chapter 2. Enthalpy and entropy of activation illustrate the impact of zeolite confinement on the transition states. Based on zero order regime in zeolite catalysis, all presented numbers are intrinsic activation parameters.

Dehydration of trans 2-methylcyclohexanol

The conversion of *trans* 2-methylcyclohexanol, exemplarily represents predominantly the dehydration pathway *via* carbenium ion intermediates. The turnover frequencies obtained by MFI,

BEA and FAU are compiled in **Table 4.2.** The dehydration rates per hydronium ion at 180 °C were about two orders of magnitude higher in MFI ($3.2 \cdot 10^{-2} \text{ s}^{-1}$) or BEA ($3.3 \cdot 10^{-2} \text{ s}^{-1}$) zeolites compared to FAU zeolite ($2.9 \cdot 10^{-4} \text{ s}^{-1}$). The correlation between the turnover frequencies and the inverse reaction temperature for the different catalysts is illustrated in **Figure 4.1.**

Table 4.2. Activation parameters and TOFs for the dehydration of *trans* 2-McyOH catalyzed by MFI, BEA and FAU.

Entry	Zeolite	E_a^{intr} [kJ·mol ⁻¹]	ΔH^{\ddagger} [kJ·mol ⁻¹]	ΔS^{\ddagger} [J·K ⁻¹ ·mol ⁻¹]	TOF (180 °C) [s ⁻¹]
1	FAU	189 (±7)	185 (±7)	+92 (±14)	$2.9 (\pm 1) \cdot 10^{-4}$
2	BEA	182 (±5)	178 (±5)	+116 (±11)	$3.3 (\pm 1) \cdot 10^{-2}$
3	MFI	144 (±1)	140 (±1)	+43 (±2)	$3.2 (\pm 1) \cdot 10^{-2}$

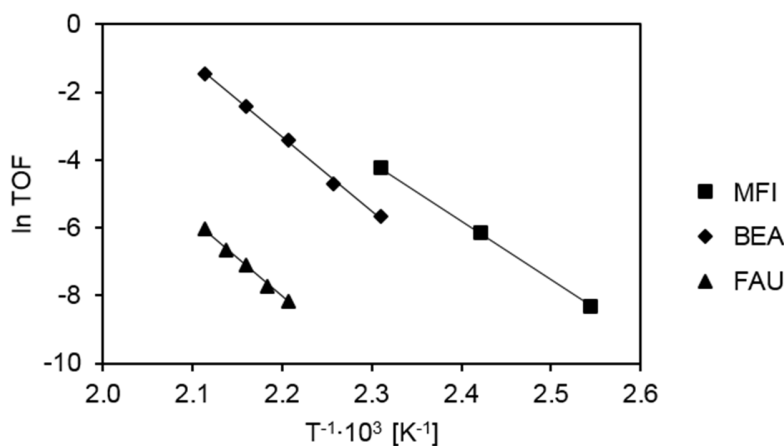


Figure 4.1. Correlation of TOF and the inverse reaction temperature for *trans* 2-McyOH dehydration.

The spatial constrain by smaller reaction channels within the zeolite led to decreasing entropic contributions in the transition state (FAU: +92 → BEA: +116 → MFI: +43 J·K⁻¹·mol⁻¹, **Table 4.2.**). The comparably high positive values illustrate the late and product-like transition state of an E1 pathway with a stepwise cleavage of the C-O and C-H bonds. The higher turnover frequencies in smaller zeolite channels are enthalpically motivated, as the enthalpies of activation were gradually decreasing (FAU: 185 → BEA: 178 → MFI: 140 kJ·mol⁻¹, **Table 4.2.**). The slightly higher entropy and the smaller enthalpic barrier in BEA zeolite seem to be the reasons for the significantly higher TOF compared to FAU zeolite. The decreasing enthalpic barriers are attributed to an increasing stabilization of the intermediate in smaller zeolite pores. The positively charged carbenium ion is assumed to be balanced by the negative charges of the lattice, which is more efficient in tighter confines according to the experimental data. This underlines the high efficiency of enzymes, which perfectly stabilize (charged) intermediates/transition states by a perfectly tailored environment.^[12]

Dehydration of *cis* 2-methylcyclohexanol

The dehydration experiments of *cis* 2-methylcyclohexanol reveal the impact of confinement on the concerted elimination mechanism. **Table 4.3.** compiles the TOF and the activation parameters obtained by MFI, BEA and FAU zeolites. The trend of increasing dehydration rates for *cis* 2-McyOH (**Table 4.3.**) with increasing zeolite confinement is similar to the observations of the *trans* isomer. The turnover frequency was accelerated about one order of magnitude in the pores of BEA ($6.2 \cdot 10^{-1} \text{ s}^{-1}$) compared to FAU ($3.5 \cdot 10^{-2} \text{ s}^{-1}$). Surprisingly, the TOF at 170 °C obtained by BEA was about a factor of 2 higher compared to the dehydration rates per hydronium ion in MFI zeolite ($2.7 \cdot 10^{-1} \text{ s}^{-1}$). **Figure 4.2.** illustrates the TOFs as a function of the inverse reaction temperature of the tested zeolites.

Table 4.3. Activation parameters and TOFs for the dehydration of *cis* 2-McyOH catalyzed by MFI, BEA and FAU.

Entry	Zeolite	E_a^{intr} [kJ·mol ⁻¹]	ΔH^{\ddagger} [kJ·mol ⁻¹]	ΔS^{\ddagger} [J·K ⁻¹ ·mol ⁻¹]	TOF (170°C) [s ⁻¹]
1	FAU	144 (±3)	141 (±3)	+42 (±7)	$3.5 (\pm 1) \cdot 10^{-2}$
2	BEA	141 (±3)	137 (±3)	+56 (±6)	$6.2 (\pm 1) \cdot 10^{-1}$
3	MFI	116 (±3)	112 (±3)	-8 (±7)	$2.7 (\pm 1) \cdot 10^{-1}$

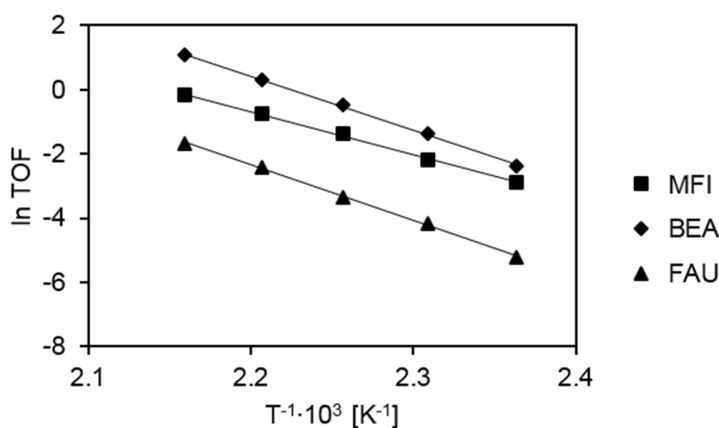


Figure 4.2. Correlation of TOF and inverse reaction temperature for *cis* 2-McyOH dehydration.

The enthalpic barriers of activation were decreasing with increasing confinement (FAU: 141 → BEA: 137 → MFI: 112 kJ·mol⁻¹, **Table 4.3.**). The increasing zeolite confinement caused a remarkable drop in the entropy of activation for MFI (FAU: +42 → BEA: +56 → MFI: -8 J·K⁻¹·mol⁻¹, **Table 4.3.**), which is attributed to a more confined transition state. The comparable low or even negative entropies illustrate the complex structure of an early and substrate-like transition state within a concerted elimination pathway, which consists of the proton,

the alcohol as well as water molecules forming the β -H abstracting base. The distinctly higher turnover frequency in BEA zeolite compared to FAU is attributed to the entropic benefit as well as a slightly reduced enthalpic barrier of activation. A further decrease of the zeolite pore diameter (MFI) led to a significant drop of the enthalpy. This observation leads to the conclusion that also the transition state of a concerted dehydration pathway is enthalpically favored in smaller reaction channels. The higher enthalpic barrier in BEA compared to MFI (by 25 $\text{kJ}\cdot\text{mol}^{-1}$), was over-compensated by a significant higher activation entropy (by 60 $\text{J}\cdot\text{K}^{-1}\cdot\text{mol}^{-1}$), which led to higher dehydration rates per hydronium ion. The absence of a carbocation and the participating role of water (β -H abstraction) within the concerted dehydration mechanism are important details in explaining the higher efficiency of the larger pore zeolite BEA compared to MFI. **Table 4.4.** compiles ΔH^{\ddagger} and ΔS^{\ddagger} of both elimination pathways.

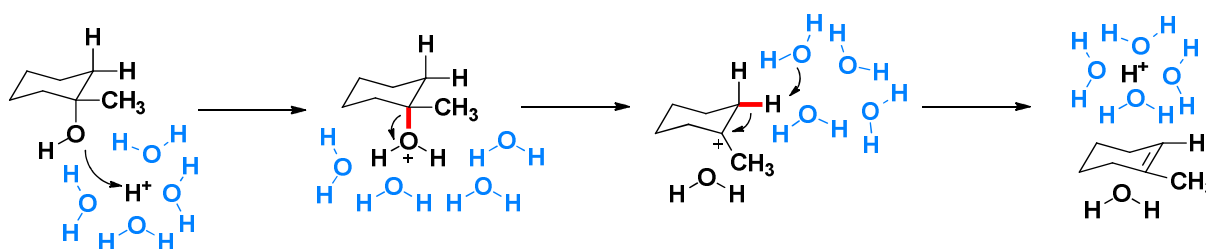
Table 4.4. Comparison of E1 and E2 dehydration pathways catalyzed by MFI, BEA and FAU zeolites.

Zeolite	Parameter	E1 (<i>trans</i> 2-McyOH)	E2 (<i>cis</i> 2-McyOH)	Δ (E1-E2)
FAU	ΔH^{\ddagger} [$\text{kJ}\cdot\text{mol}^{-1}$]	185 (± 7)	141 (± 3)	44
	ΔS^{\ddagger} [$\text{J}\cdot\text{K}^{-1}\cdot\text{mol}^{-1}$]	+92 (± 14)	+42 (± 7)	50
BEA	ΔH^{\ddagger} [$\text{kJ}\cdot\text{mol}^{-1}$]	178 (± 5)	137 (± 3)	41
	ΔS^{\ddagger} [$\text{J}\cdot\text{K}^{-1}\cdot\text{mol}^{-1}$]	+116 (± 11)	+56 (± 6)	60
MFI	ΔH^{\ddagger} [$\text{kJ}\cdot\text{mol}^{-1}$]	140 (± 1)	112 (± 3)	28
	ΔS^{\ddagger} [$\text{J}\cdot\text{K}^{-1}\cdot\text{mol}^{-1}$]	+43 (± 1)	-8 (± 7)	51

All determined enthalpies and entropies of activation for the E2 pathway are throughout lower compared to the E1 reaction route independent of the investigated zeolite framework. Enthalpic stabilization of the transition states induced by confinement led to larger differences between the E1 and the E2 pathway in large pore zeolites. Whereas the gap between both pathways was quantified by 28 $\text{kJ}\cdot\text{mol}^{-1}$ for MFI, it was significantly higher for BEA ($\Delta\Delta H^{\ddagger} = 41 \text{ kJ}\cdot\text{mol}^{-1}$) and FAU ($\Delta\Delta H^{\ddagger} = 44 \text{ kJ}\cdot\text{mol}^{-1}$). The entropic differences among both reaction routes were relatively constant with values between 50 and 60 $\text{J}\cdot\text{K}^{-1}\cdot\text{mol}^{-1}$.

Impact of confinement on the dehydration of a tertiary and a primary alcohol

The reactivity *via* E1 and E2 dehydration routes of a tertiary (1-McyOH) as well as a primary alcohol (2-CyhexEtOH) were investigated as a function of zeolite confinement (MFI, BEA and FAU) and compared to homogeneous catalysis (H_3PO_4). The dehydration of the tertiary alcohol proceeds most likely stepwise, based on the high stability of a tertiary carbenium ion (**Scheme 4.1.**). The primary alcohol is expected to react *via* a concerted dehydration mechanism, avoiding the energetically labile primary carbocation (**Scheme 4.2.**). Activation barriers and transition state considerations give additional information about the proceeding pathways of the acid catalyzed oxygen removal reaction.

Dehydration of 1-methylcyclohexanol: reactivity of a tertiary alcohol

Scheme 4.1. Dehydration of 1-methylcyclohexanol *via* a tertiary carbocation intermediate (E1).

Table 4.5. compiles the activation parameters and TOFs for the dehydration of 1-methylcyclohexanol. As observed for the secondary alcohol, the dehydration rate of the tertiary alcohol increased with increasing confinement. The turnover frequency at 110 °C was about two times higher in FAU zeolite ($2.1 \cdot 10^{-2} \text{ s}^{-1}$) compared to H_3PO_4 ($7.3 \cdot 10^{-3} \text{ s}^{-1}$). The TOFs further increased about one order of magnitude in case of BEA zeolite ($3.0 \cdot 10^{-1} \text{ s}^{-1}$). Same as for *trans* 2-methylcyclohexanol, the dehydration rates obtained by BEA zeolite were comparable to those of MFI ($1.2 \cdot 10^{-1} \text{ s}^{-1}$). The turnover frequencies as a function of the inverse reaction temperature are illustrated in **Figure 4.3.**

Table 4.5. Activation parameters and TOFs for the dehydration of 1-McyOH catalyzed by MFI, BEA, FAU and H_3PO_4 .

Entry	Zeolite	E_a [kJ·mol ⁻¹]	ΔH^{\ddagger} [kJ·mol ⁻¹]	ΔS^{\ddagger} [J·K ⁻¹ ·mol ⁻¹]	TOF (110 °C) [s ⁻¹]
1	H_3PO_4	170 (±5)	167 (±5)	+148 (±12)	$7.3 (\pm 1) \cdot 10^{-3}$
2	FAU	151 (±3)	148 (±3)	+108 (±6)	$2.1 (\pm 1) \cdot 10^{-2}$
3	BEA	131 (±3)	128 (±3)	+76 (±7)	$3.0 (\pm 1) \cdot 10^{-1}$
4	MFI	116 (±2)	113 (±2)	+30 (±5)	$1.2 (\pm 1) \cdot 10^{-1}$

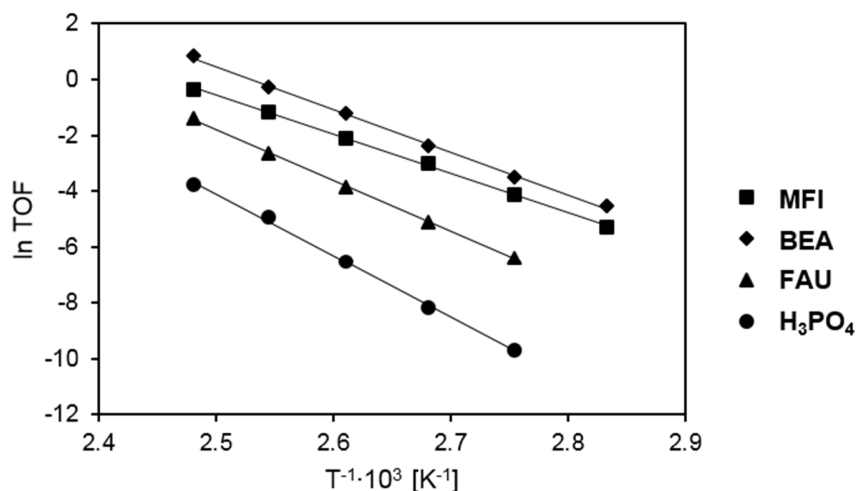


Figure 4.3. Correlation of TOF and the inverse reaction temperature for 1-McyOH dehydration.

The regimes of first order in alcohol for H₃PO₄ and zero order in alcohol for zeolite catalyzed experiments were determined and compiled in the Supporting information (SI, **Figures S4.1. – S4.7.** and **Tables S4.2. – S4.8.**).

With increasing confinement, the enthalpic barriers decreased constantly by 15 – 20 kJ·mol⁻¹ (H₃PO₄: 167 → FAU: 148 → BEA: 128 → MFI: 113 kJ·mol⁻¹). The same trend was observed for the entropy of activation (H₃PO₄: +148 → FAU: +108 → BEA: +76 → MFI: +30 J·K⁻¹·mol⁻¹), which dropped in steps of 30 – 50 J·K⁻¹·mol⁻¹ with decreasing channel diameters. According to the high entropy values, which illustrate a late and product-like transition state (like in case of *trans*-2-McyOH), the dehydration pathway *via* the stable tertiary carbocation seems to be corroborated. Smaller reaction channels in zeolite pores restrict the transition state (decreasing ΔS^{\ddagger}) and reduce the mobility of the substrate and the leaving H₂O molecule. Larger pores cannot accomplish enthalpic stabilization like it is the case in highly confined catalyst environments.

Figure 4.4. illustrates the correlation of ΔH^{\ddagger} and ΔS^{\ddagger} for the E1 dehydration of the tertiary alcohol 1-McyOH. The correlation of enthalpy and entropy of activation shows a linear trend with decreasing diameters of the zeolite pores. Reasonably, the increasing catalyst confinement leads to a restricted transition state, which is expressed in lower values of ΔS^{\ddagger} . At the same time the smaller zeolite channels enthalpically favor the E1 dehydration pathway, which is attributed to the increasing ionic stabilization of the carbenium ion by the zeolite lattice. Analysis of ΔH^{\ddagger} and ΔS^{\ddagger} leads to the conclusion that the higher TOFs with increasing confinement are enthalpically motivated.

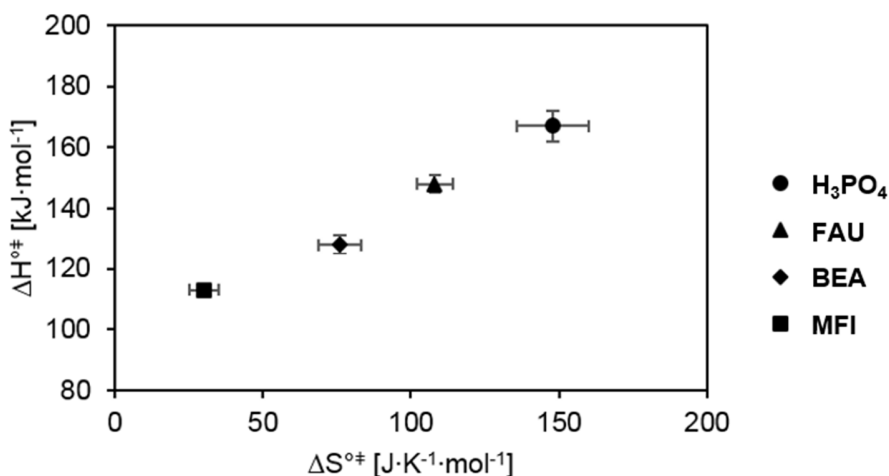
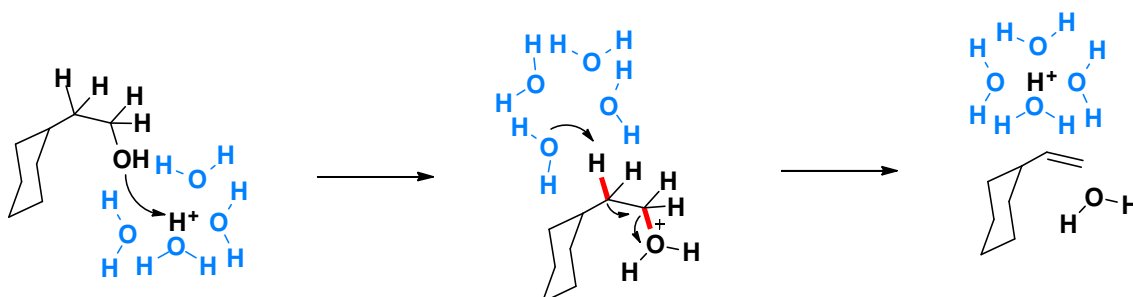


Figure 4.4. Correlation of ΔH^{\ddagger} and ΔS^{\ddagger} for the dehydration of 1-McyOH.

Dehydration of 2-cyclohexylethanol: reactivity of a primary alcohol

The primary alcohol 2-cyclohexylethanol serves as a model compound to understand the impact of confinement on a concerted dehydration pathway (**Scheme 4.2**).

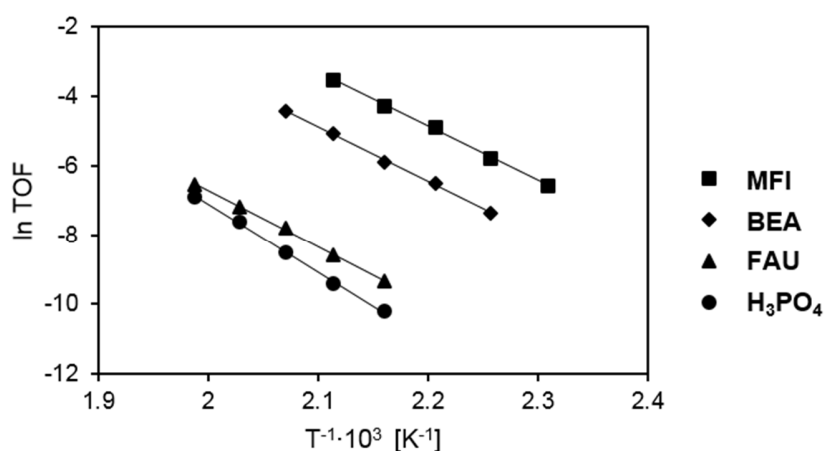


Scheme 4.2. Dehydration of 2-CyEtOH via a concerted elimination pathway (E2).

Based on the poor energetic stability of a primary carbenium ion intermediate, a concerted elimination mechanism for the dehydration of 2-CyEtOH is highly assumed. As for all previously presented studies, the TOFs for the dehydration of the primary alcohol increased with increasing confinement (**Table 4.6**). Compared to hydronium ions provided by H₃PO₄ (3.7·10⁻⁵ s⁻¹), the TOF at 190 °C doubled within the channels of FAU zeolite (8.7·10⁻⁵ s⁻¹). A further reduction of the channel diameters led to an increased dehydration rate per hydronium ion of more than one order of magnitude in case of BEA (2.8·10⁻³ s⁻¹) and even more than two orders of magnitude for MFI zeolite (1.4·10⁻² s⁻¹) compared to FAU. **Figure 4.5** illustrates the correlation of the TOFs and the inverse reaction temperature of the investigated catalysts.

Table 4.6. Activation parameters and TOFs for 2-CyEtOH dehydration catalyzed by MFI, BEA, FAU and H₃PO₄.

Entry	Zeolite	E _a [kJ·mol ⁻¹]	ΔH [‡] [kJ·mol ⁻¹]	ΔS [‡] [J·K ⁻¹ ·mol ⁻¹]	TOF (190 °C) [s ⁻¹]
1	H ₃ PO ₄	163 (±3)	159 (±3)	+9 (±7)	3.7 (±1) · 10 ⁻⁵
2	FAU	136 (±3)	132 (±3)	-40 (±6)	8.7 (±2) · 10 ⁻⁵
3	BEA	131 (±3)	127 (±3)	-22 (±6)	2.8 (±1) · 10 ⁻³
4	MFI	130 (±3)	127 (±3)	-10 (±6)	1.4 (±1) · 10 ⁻²

**Figure 4.5.** Correlation of TOF and inverse reaction temperature for 2-CyEtOH dehydration with different catalysts.

The enthalpic barrier for the dehydration of the primary alcohol in the absence of confines was 159 kJ·mol⁻¹ (**Table 4.6.**). All enthalpies of activation catalyzed by zeolite were comparable and about 30 kJ·mol⁻¹ lower (ΔH[‡] = 127 – 132 kJ·mol⁻¹) independent of the zeolite framework. The same enthalpic barriers are attributed to the absence of the carbenium ion within the concerted dehydration pathway. The results are contrary to those of the E1 route, where a direct proportionality between confinement and enthalpy was observed.

Significant changes in the entropies of activation were observed in zeolite catalyzed experiments.

Figure 4.6. illustrates the correlation of ΔH[‡] and ΔS[‡] for the concerted dehydration of 2-cyclohexylethanol. The low or even negative values for the entropy of activation reconfirm a complex arrangement of the proton, the alcohol and the β-H abstracting base (H₂O molecules) in an early transition state. The entropy of activation (ΔS[‡] = +9 J·K⁻¹·mol⁻¹) was significantly higher in the absence of constraints, as experiments with H₃PO₄ revealed.

Surprisingly, the transition state was entropically favored with decreasing channel diameters (FAU: -40 → BEA: -22 → MFI: -10 J·K⁻¹·mol⁻¹). Constant enthalpic barriers and rising entropic gains elucidate that the rising TOFs (with increasing confinement) are entropically controlled in an

E2 pathway. Higher values for ΔS^{\ddagger} in smaller zeolite pores are attributed to less complex transition states expressed by a reduced number of H_2O molecules forming the $\beta\text{-H}$ abstracting base in zeolite channels of increasing confinement.

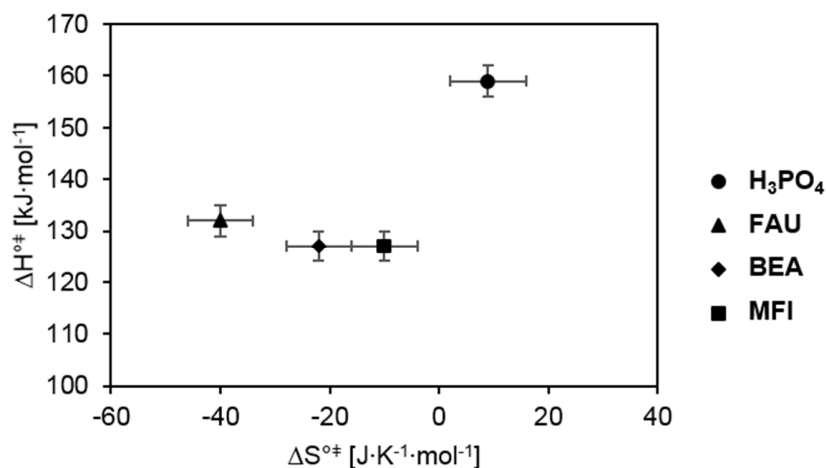


Figure 4.6. Correlation of ΔH^{\ddagger} and ΔS^{\ddagger} for the dehydration of 2-CyEtOH.

4.4. Conclusions

The impact of confinement on acid catalyzed E1 and E2 dehydration pathways of secondary alcohols (*cis* and *trans* 2-methylcyclohexanol) was investigated with zeolites of different channel diameters (MFI, BEA and FAU). The stepwise elimination route *via* the carbocation intermediate (*trans* 2-McyOH) led to significantly higher enthalpic barriers (by 30 – 40 $\text{kJ}\cdot\text{mol}^{-1}$) and higher entropies (by 50 – 60 $\text{J}\cdot\text{K}^{-1}\cdot\text{mol}^{-1}$) compared to the concerted elimination (*cis* 2-McyOH). Higher turnover frequencies with increasing zeolite confinement result from smaller enthalpic barriers, which are attributed to an increasing ionic stabilization of the carbocation in smaller zeolite channels.

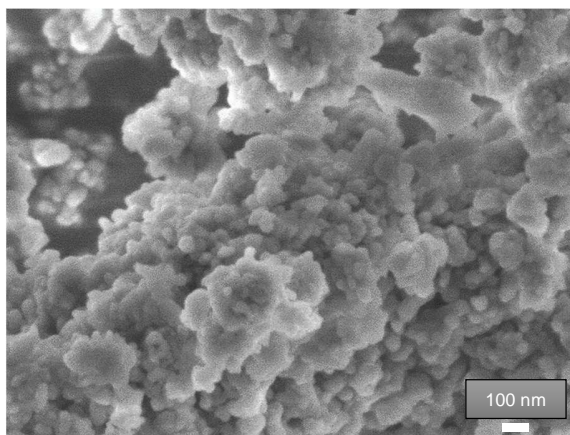
Furthermore, the dehydration of a primary (2-cyclohexylethanol) and a tertiary alcohol (1-methylcyclohexanol) was investigated as a parameter of confinement. Dehydration of both alcohols led to significantly higher rates in smaller zeolite pores. The rate enhancement of the tertiary alcohol (E1) is enthalpically motivated (decreasing ΔH^{\ddagger}) and assigned to an increasing stabilization of the carbocation. The increasing TOFs in the concerted dehydration of the primary alcohol (E2) with increasing confinement are entropically driven. While ΔH^{\ddagger} was constant for all framework types ΔS^{\ddagger} increased gradually with decreasing zeolite channel diameter. The entropic

gain is assigned to a decreasing complexity of the transition state in the concerted E2 dehydration pathway.

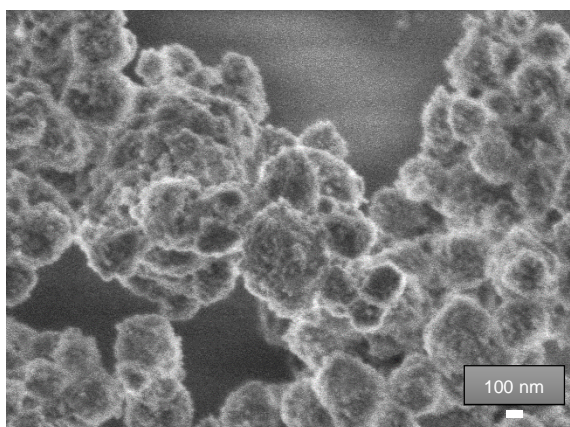
4.5. References

- [1] G. Sastre, A. Corma, *Journal of Molecular Catalysis A: Chemical* **2009**, *305*, 3-7.
- [2] a) D. Lesthaeghe, V. Van Speybroeck, M. Waroquier, *Physical Chemistry Chemical Physics* **2009**, *11*, 5222-5226; b) T. Yumura, M. Takeuchi, H. Kobayashi, Y. Kuroda, *Inorganic chemistry* **2008**, *48*, 508-517.
- [3] a) M. Stratakis, D. Kalaitzakis, D. Stavroulakis, G. Kosmas, C. Tsangarakis, *Organic letters* **2003**, *5*, 3471-3474; b) C. Tsangarakis, M. Stratakis, *European journal of organic chemistry* **2006**, *2006*, 4435-4439; c) J. Sivaguru, T. Poon, R. Franz, S. Jockusch, W. Adam, N. J. Turro, *Journal of the American Chemical Society* **2004**, *126*, 10816-10817; d) V. Ramamurthy, *Journal of Photochemistry and Photobiology C: Photochemistry Reviews* **2000**, *1*, 145-166.
- [4] a) F. Eder, J. Lercher, *The Journal of Physical Chemistry B* **1997**, *101*, 1273-1278; b) F. Eder, J. A. Lercher, *Zeolites* **1997**, *18*, 75-81; c) F. Eder, M. Stockenhuber, J. Lercher, *The Journal of Physical Chemistry B* **1997**, *101*, 5414-5419.
- [5] a) M. Makarova, C. Williams, V. Romannikov, K. Zamaraev, J. Thomas, *Journal of the Chemical Society, Faraday Transactions* **1990**, *86*, 581-584; b) M. Makarova, E. Paukshtis, J. Thomas, C. Williams, K. Zamaraev, *Journal of Catalysis* **1994**, *149*, 36-51.
- [6] R. Gounder, E. Iglesia, *Chemical Communications* **2013**, *49*, 3491-3509.
- [7] J. Jae, G. A. Tompsett, A. J. Foster, K. D. Hammond, S. M. Auerbach, R. F. Lobo, G. W. Huber, *Journal of Catalysis* **2011**, *279*, 257-268.
- [8] R. Gounder, E. Iglesia, *Journal of the American Chemical Society* **2009**, *131*, 1958-1971.
- [9] Y. Liu, A. Vjunov, H. Shi, S. Eckstein, D. Camaioni, D. Mei, E. Barath, J. A. Lercher, *Nature Communications* **2016**, DOI: 10.1038/ncomms14113.
- [10] H. Shi, S. Eckstein, A. Vjunov, D. Camaioni, J. A. Lercher, *Nature Communications* **2017**, DOI: 10.1038/ncomms15442.
- [11] W. Lutz, H. Toufar, R. Kurzhals, M. Suckow, *Adsorption* **2005**, *11*, 405-413.
- [12] a) K. P. Jensen, U. Ryde, *Journal of the American Chemical Society* **2005**, *127*, 9117-9128; b) F. Wen, N. U. Nair, H. Zhao, *Current opinion in biotechnology* **2009**, *20*, 412-419.

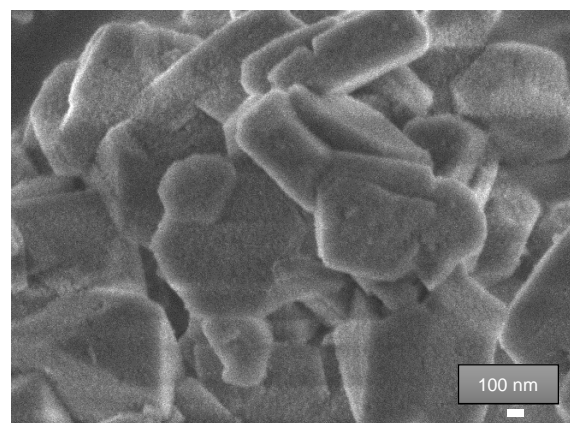
4.6. Supporting Information



SEM Image S4.1. MFI-45 (Si/Al = 45).



SEM Image S4.2. BEA-83 (Si/Al = 83).



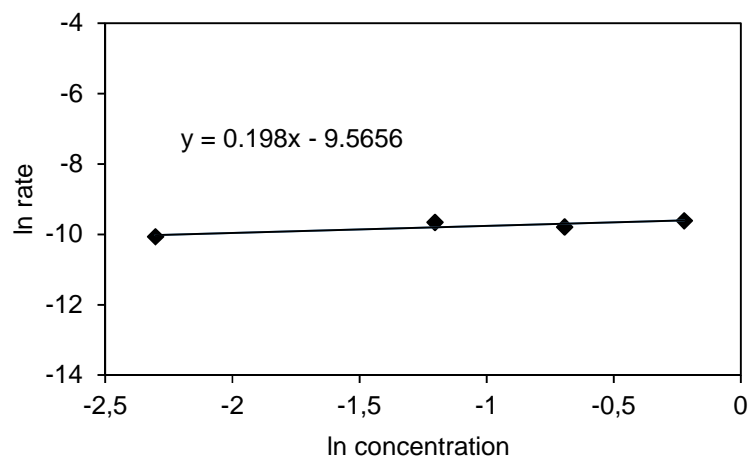
SEM Image S4.3. FAU-3 (Si/Al = 3).

Table S4.1. Surface area and concentration of acid sites of investigated zeolites.

Zeolite	Si/Al	Surface area [m ² ·g ⁻¹]	Micro-pores [m ² ·g ⁻¹]	Concentration (BAS) ^a [μmol·g ⁻¹]	Concentration (LAS) ^a [μmol·g ⁻¹]	Concentration (BAS+LAS) ^b [μmol·g ⁻¹]
MFI-45	45	389	302	360	45	400
BEA-83	83	523	132	120	20	156
BEA-15	15	509	59	282	322	591
FAU-15	15	765	157	387	176	547
FAU-3	3	631	50	335	294	685

^a = IR spectroscopy (pyridine), ^b = Temperature programmed desorption (NH₃).

Reaction order of aqueous phase dehydration

**Figure S4.1.** Reaction order *cis* 2-methylcyclohexanol dehydration (170 °C, 50 bar, MFI-45).**Table S4.2.** Dehydration rates and concentration *cis* 2-methylcyclohexanol dehydration (170 °C, 50 bar, MFI-45).

rate [mol·g ⁻¹ ·s ⁻¹]	n [mol]	c [mol·L ⁻¹]	ln rate	ln c
4.2·10 ⁻⁵	0.01	0.1	-10.07	-2.30
6.4·10 ⁻⁵	0.03	0.3	-9.66	-1.20
5.6·10 ⁻⁵	0.05	0.5	-9.79	-0.69
6.7·10 ⁻⁵	0.08	0.8	-9.62	-0.22

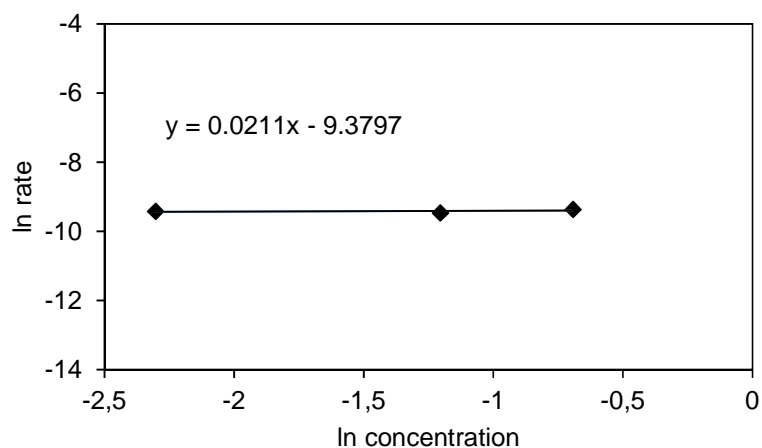


Figure S4.2. Reaction order *cis* 2-methylcyclohexanol dehydration (160 °C, 50 bar, BEA-15).

Table S4.3. Dehydration rates and initial concentrations of *cis* 2-methylcyclohexanol (160 °C, 50 bar, BEA-15).

rate [mol·g ⁻¹ ·s ⁻¹]	n [mol]	c [mol·L ⁻¹]	ln rate	ln c
8.2·10 ⁻⁵	0.01	0.1	- 9.41	-2.30
7.8·10 ⁻⁵	0.03	0.3	- 9.46	-1.20
8.6·10 ⁻⁵	0.05	0.5	- 9.36	-0.69

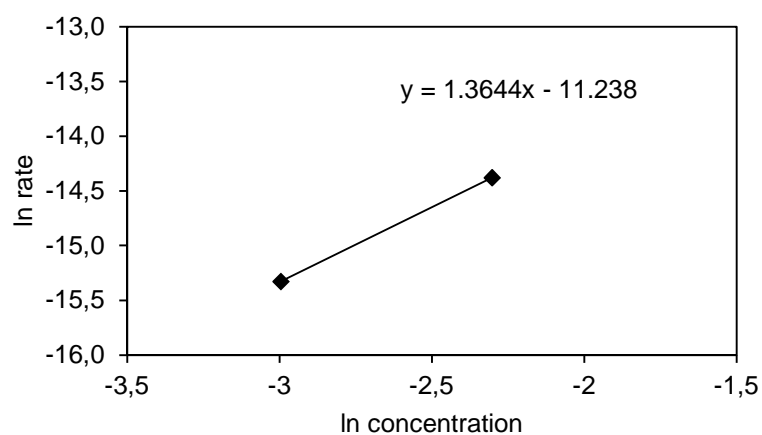


Figure S4.3. Reaction order: 1-methylcyclohexanol dehydration (110 °C, 50 bar, H₃PO₄).

Table S4.4. 1-methylcyclohexanol dehydration rates and different initial concentrations (110 °C, 50 bar, H₃PO₄).

rate [mol·g ⁻¹ ·s ⁻¹]	n [mol]	c [mol·L ⁻¹]	ln rate	ln c
5.7·10 ⁻⁷	0.010	0.10	- 14.4	- 2.30
2.2·10 ⁻⁷	0.005	0.05	- 15.3	- 3.00

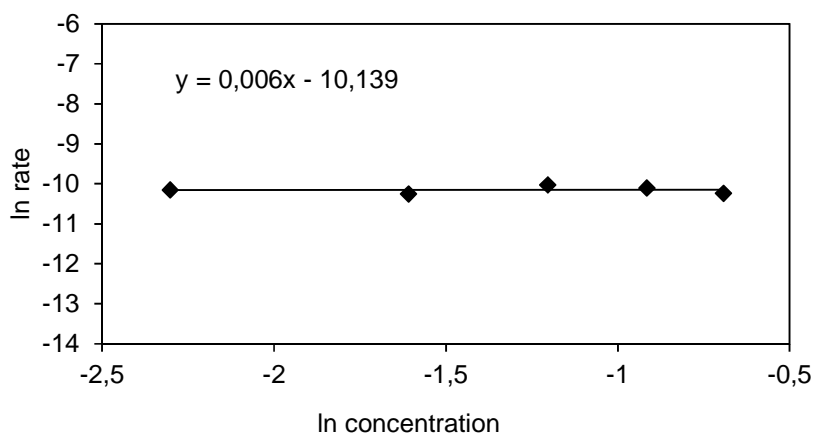


Figure S4.4. Reaction order: **1-methylcyclohexanol** dehydration (110 °C, **BEA-83**).

Table S4.5. **1-methylcyclohexanol** dehydration rates and different initial concentrations (110 °C, **BEA-83**).

rate [mol·g ⁻¹ ·s ⁻¹]	n [mol]	c [mol·L ⁻¹]	ln c	ln rate
3.9·10 ⁻⁵	0.01	0.1	-2.30	-10.15
3.6·10 ⁻⁵	0.02	0.2	-1.61	-10.24
4.5·10 ⁻⁵	0.03	0.3	-1.20	-10.02
4.1·10 ⁻⁵	0.04	0.4	-0.92	-10.10
3.6·10 ⁻⁵	0.05	0.5	-0.69	-10.23

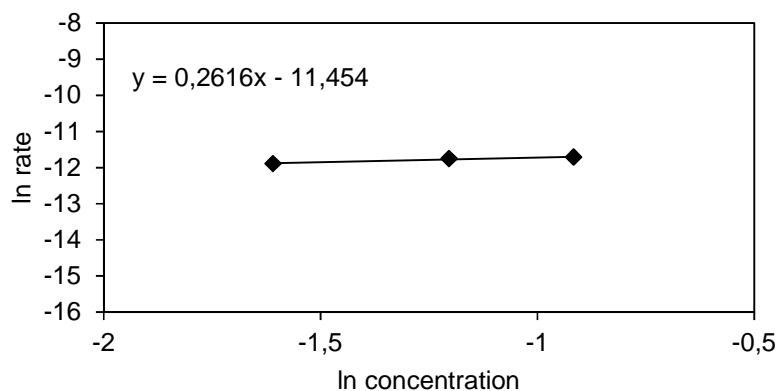


Figure S4.5. Reaction order: **1-methylcyclohexanol** dehydration (110 °C, 50 bar, **FAU-3**).

Table S4.6. **1-methylcyclohexanol** dehydration rates and different initial concentrations (110 °C, 50 bar, **FAU-3**).

rate [mol·g ⁻¹ ·s ⁻¹]	n [mol]	c [mol·L ⁻¹]	ln c	ln rate
6.9·10 ⁻⁶	0.02	0.2	-1.61	-11.88
7.9·10 ⁻⁶	0.03	0.3	-1.20	-11.75
8.2·10 ⁻⁶	0.04	0.4	-0.92	-11.71

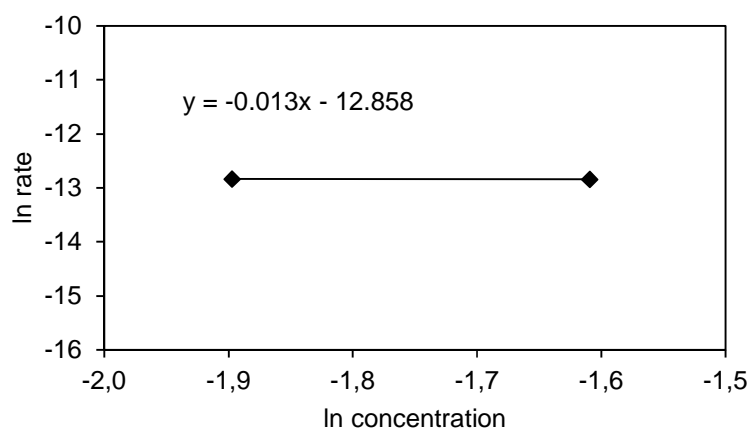


Figure S4.6. Reaction order: **2-cyclohexylethanol** dehydration (180 °C, 50 bar, **MFI-45**).

Table S4.7. **2-cyclohexylethanol** dehydration rates and different initial concentrations (180 °C, 50 bar, **MFI-45**).

n [mol]	c [mol·L ⁻¹]	rate [mol·g ⁻¹ ·s ⁻¹]	ln rate	ln c
0.015	0.15	2.7·10 ⁻⁶	-12.83	-1.90
0.020	0.20	2.7·10 ⁻⁶	-12.84	-1.61

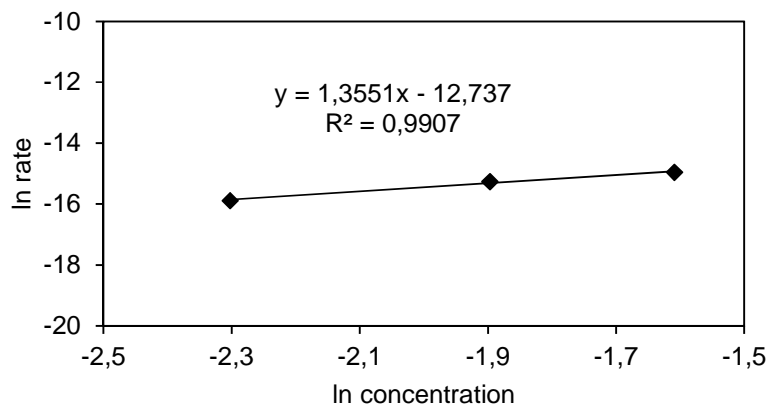
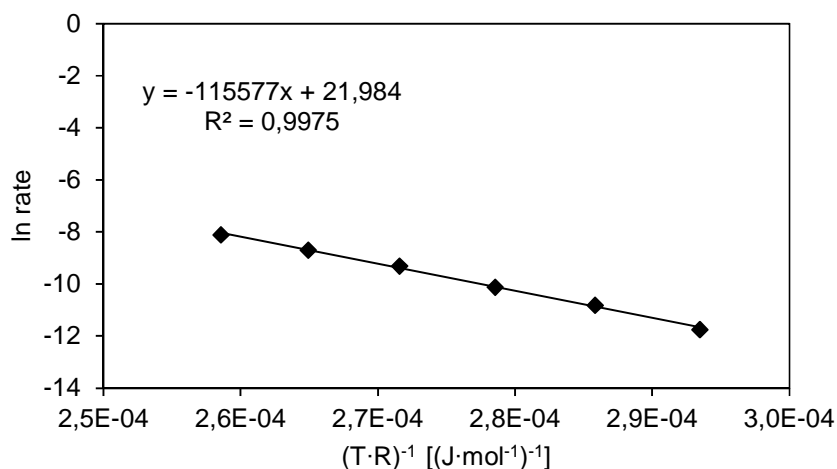


Figure S4.7. Reaction order: **2-cyclohexylethanol** dehydration (210 °C, 50 bar, **H₃PO₄**).

Table S4.8. **2-cyclohexylethanol** dehydration rates and different initial concentrations (210 °C, 50 bar, **H₃PO₄**).

n [mol]	c [mol·L ⁻¹]	rate [mol·s ⁻¹]	TOF real [s ⁻¹]	ln c	ln TOF	ln rate
0.020	0.20	3.2·10 ⁻⁷	1.0·10 ⁻³	-1.61	-6.89	-14.95
0.015	0.15	2.4·10 ⁻⁷	1.0·10 ⁻³	-1.90	-6.91	-15.26
0.010	0.10	1.3·10 ⁻⁷	8.0·10 ⁻⁴	-2.30	-7.13	-15.88

Dehydration of *cis* 2-methylcyclohexanolFigure S4.8. Arrhenius-plot: *Cis* 2-methylcyclohexanol (0.5 M) dehydration ($E_a \approx 116$ kJ/mol), MFI-45.Table S.4.9. *Cis* 2-methylcyclohexanol (0.5 M) dehydration rates at different reaction temperatures, MFI-45.

T [°C]	T [K]	TOF [s ⁻¹]	rate [mol·g ⁻¹ ·s ⁻¹]	(T·R) ⁻¹ [(J·mol ⁻¹) ⁻¹]	ln rate	ln TOF
140	413	2.2·10 ⁻²	7.9·10 ⁻⁶	2.91·10 ⁻⁴	-11.74	-3.81
150	423	5.6·10 ⁻²	2.0·10 ⁻⁵	2.84·10 ⁻⁴	-10.81	-2.88
160	433	1.1·10 ⁻¹	4.1·10 ⁻⁵	2.78·10 ⁻⁴	-10.11	-2.18
170	443	2.5·10 ⁻¹	9.2·10 ⁻⁵	2.71·10 ⁻⁴	-9.30	-1.37
180	453	4.7·10 ⁻¹	1.7·10 ⁻⁴	2.65·10 ⁻⁴	-8.69	-0.76
190	463	8.4·10 ⁻¹	3.0·10 ⁻⁴	2.60·10 ⁻⁴	-8.11	-0.18

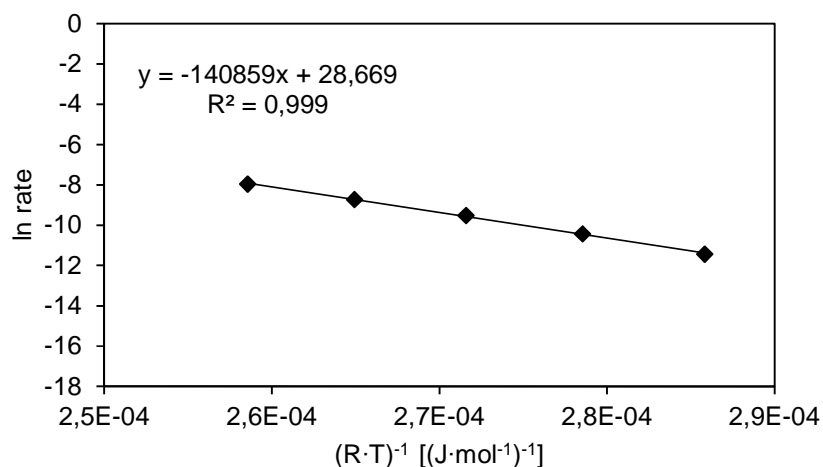
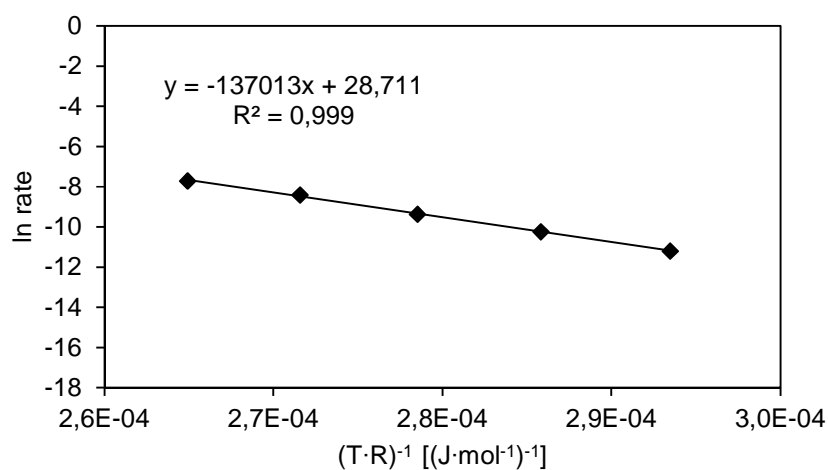
Figure S4.9. Arrhenius-plot: *Cis* 2-methylcyclohexanol (0.5 M) dehydration ($E_a \approx 141$ kJ/mol), BEA-83.

Table S4.10. *Cis* 2-methylcyclohexanol (0.5 M) dehydration rates at different reaction temperatures, **BEA-83**.

T [°C]	T [K]	TOF [s ⁻¹]	rate [mol·g ⁻¹ ·s ⁻¹]	(T·R) ⁻¹ [(J·mol ⁻¹) ⁻¹]	ln rate	ln TOF
150	423	9.2·10 ⁻²	1.1·10 ⁻⁵	2.84·10 ⁻⁴	-11.42	-2.39
160	433	2.5·10 ⁻¹	3.0·10 ⁻⁵	2.78·10 ⁻⁴	-10.41	-1.39
170	443	6.2·10 ⁻¹	7.4·10 ⁻⁵	2.71·10 ⁻⁴	-9.51	-0.48
180	453	1.4	1.6·10 ⁻⁴	2.65·10 ⁻⁴	-8.72	0.31
190	463	3.0	3.5·10 ⁻⁴	2.60·10 ⁻⁴	-7.95	1.08

**Figure S4.10.** Arrhenius-plot: *Cis* 2-methylcyclohexanol (0.5 M) dehydration ($E_a \approx 137$ kJ/mol), **BEA-15**.**Table S4.11.** *Cis* 2-methylcyclohexanol (0.5 M) dehydration rates at different reaction temperatures, **BEA-15**.

T [°C]	T [K]	TOF [s ⁻¹]	rate [mol·g ⁻¹ ·s ⁻¹]	(T·R) ⁻¹ [(J·mol ⁻¹) ⁻¹]	ln rate
140	413	4.9·10 ⁻²	1.4·10 ⁻⁵	2.91·10 ⁻⁴	-11.18
150	423	1.3·10 ⁻¹	3.6·10 ⁻⁵	2.84·10 ⁻⁴	-10.23
160	433	3.1·10 ⁻¹	8.6·10 ⁻⁵	2.78·10 ⁻⁴	-9.36
170	443	7.9·10 ⁻¹	2.2·10 ⁻⁴	2.71·10 ⁻⁴	-8.40
180	453	1.6	4.5·10 ⁻⁴	2.65·10 ⁻⁴	-7.70

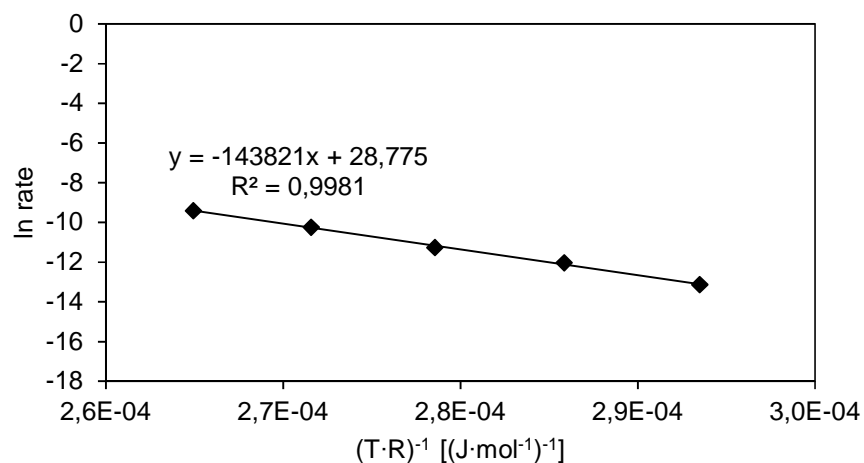


Figure S4.11. Arrhenius-plot: **Cis 2-methylcyclohexanol** (0.5 M) dehydration ($E_a \approx 144$ kJ/mol), **FAU-15**.

Table S4.12. **Cis 2-methylcyclohexanol** (0.5 M) dehydration rates at different reaction temperatures, **FAU-15**.

T [°C]	T [K]	TOF [s ⁻¹]	rate [mol·g ⁻¹ ·s ⁻¹]	(T·R) ⁻¹ [(J·mol ⁻¹) ⁻¹]	ln rate
140	413	5.2·10 ⁻³	2.0·10 ⁻⁶	2.91·10 ⁻⁴	-13.12
150	423	1.6·10 ⁻²	6.0·10 ⁻⁶	2.84·10 ⁻⁴	-12.02
160	433	3.4·10 ⁻²	1.3·10 ⁻⁵	2.78·10 ⁻⁴	-11.25
170	443	9.4·10 ⁻²	3.6·10 ⁻⁵	2.71·10 ⁻⁴	-10.23
180	453	2.1·10 ⁻¹	8.3·10 ⁻⁵	2.65·10 ⁻⁴	-9.40

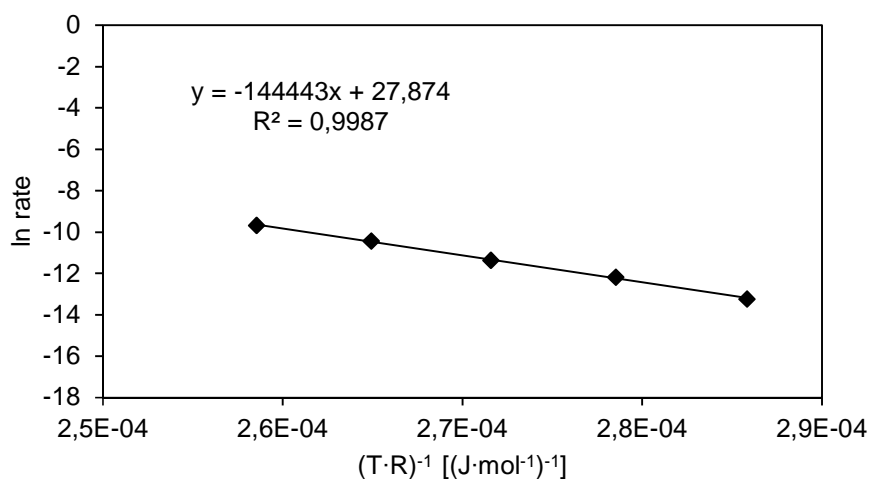
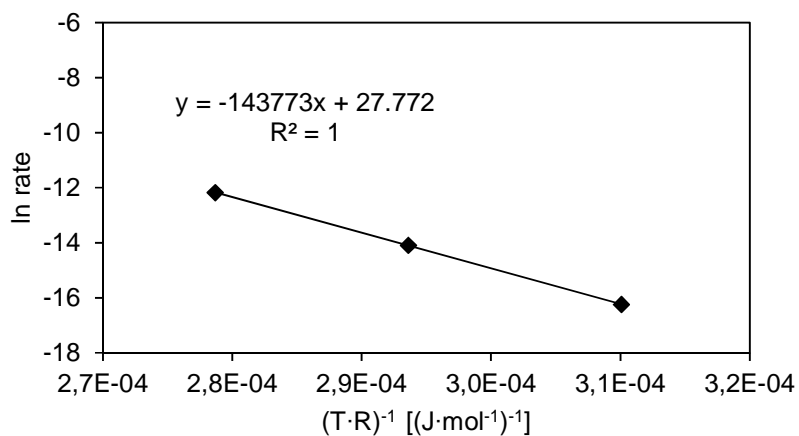


Figure S4.12. Arrhenius-plot: **Cis 2-methylcyclohexanol** (0.5 M) dehydration ($E_a \approx 144$ kJ/mol), **FAU-3**.

Table S4.13. *Cis* 2-methylcyclohexanol (0.5 M) dehydration rates at different reaction temperatures, FAU-3.

T [°C]	T [K]	TOF [s ⁻¹]	rate [mol·g ⁻¹ ·s ⁻¹]	(T·R) ⁻¹ [(J·mol ⁻¹) ⁻¹]	ln rate	ln TOF
150	423	5.4·10 ⁻³	1.8·10 ⁻⁶	2.84·10 ⁻⁴	-13.23	-5.23
160	433	1.6·10 ⁻²	5.2·10 ⁻⁶	2.78·10 ⁻⁴	-12.17	-4.17
170	443	3.5·10 ⁻²	1.2·10 ⁻⁵	2.71·10 ⁻⁴	-11.36	-3.35
180	453	8.9·10 ⁻²	3.0·10 ⁻⁵	2.65·10 ⁻⁴	-10.43	-2.42
190	463	1.9·10 ⁻¹	6.3·10 ⁻⁵	2.60·10 ⁻⁴	-9.67	-1.67

Dehydration of *trans* 2-methylcyclohexanol**Figure S4.13.** Arrhenius-plot: *Trans* 2-methylcyclohexanol (0.04 M) dehydration ($E_a \approx 144$ kJ/mol), MFI-45.**Table S4.14.** *Trans* 2-methylcyclohexanol (0.04 M) dehydration rates at different reaction temperatures, MFI-45.

T [°C]	T [K]	TOF [s ⁻¹]	rate [mol·g ⁻¹ ·s ⁻¹]	(T·R) ⁻¹ [(J·mol ⁻¹) ⁻¹]	ln rate	ln TOF
120	393	2.5·10 ⁻⁴	8.9·10 ⁻⁸	3.06·10 ⁻⁴	-16.24	-8.31
140	413	2.1·10 ⁻³	7.6·10 ⁻⁷	2.91·10 ⁻⁴	-14.09	-6.16
160	433	1.4·10 ⁻²	5.2·10 ⁻⁶	2.78·10 ⁻⁴	-12.17	-4.24

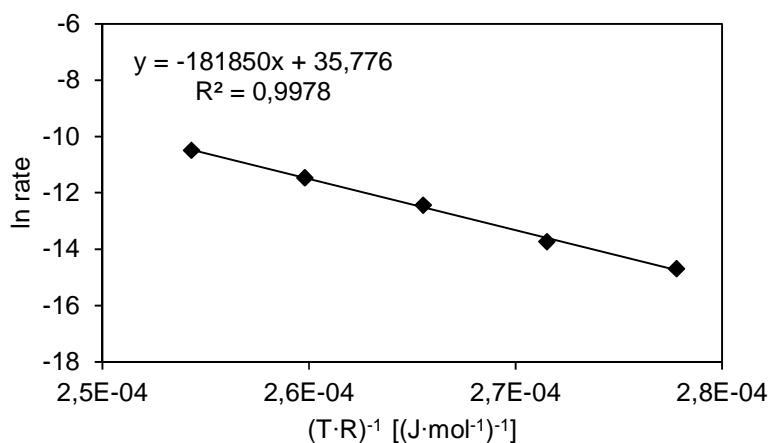


Figure S4.14. Arrhenius-plot: *Trans* 2-methylcyclohexanol (0.04 M) dehydration ($E_a \approx 182$ kJ/mol), **BEA-83**.

Table S4.15. *Trans* 2-methylcyclohexanol (0.04 M) dehydration rates at different reaction temperatures, **BEA-83**.

T [°C]	T [K]	TOF [s ⁻¹]	rate [mol·g ⁻¹ ·s ⁻¹]	(T·R) ⁻¹ [(J·mol ⁻¹) ⁻¹]	ln rate	ln TOF
160	433	3.5·10 ⁻³	4.2·10 ⁻⁷	2.78·10 ⁻⁴	-14.68	-5.66
170	443	9.1·10 ⁻³	1.1·10 ⁻⁶	2.72·10 ⁻⁴	-13.73	-4.70
180	453	3.3·10 ⁻²	4.0·10 ⁻⁶	2.66·10 ⁻⁴	-12.43	-3.41
190	463	8.8·10 ⁻²	1.1·10 ⁻⁵	2.60·10 ⁻⁴	-11.46	-2.43
200	473	2.3·10 ⁻¹	2.8·10 ⁻⁵	2.54·10 ⁻⁴	-10.48	-1.45

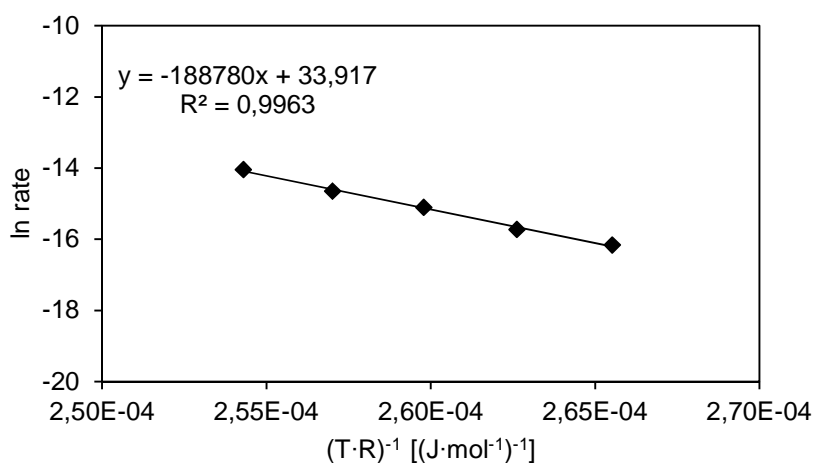
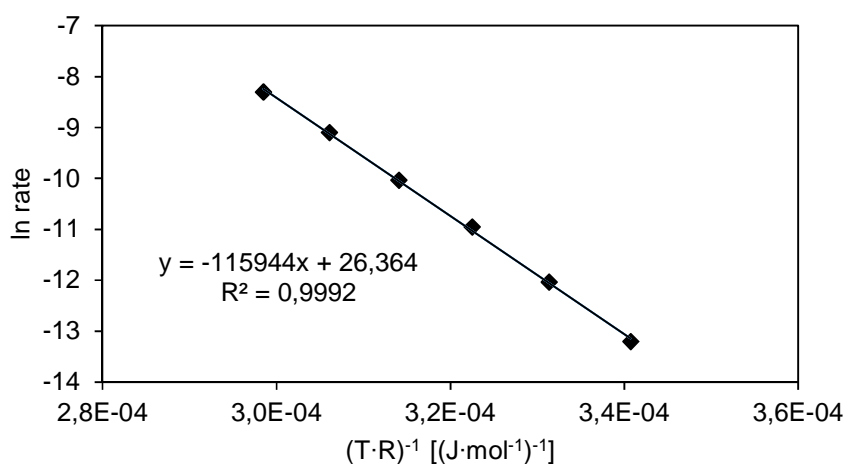


Figure S4.15. Arrhenius-plot: *Trans* 2-methylcyclohexanol (0.04 M) dehydration ($E_a \approx 189$ kJ/mol), **FAU-3**.

Table S4.16. *Trans* 2-methylcyclohexanol (0.04 M) dehydration rates at different reaction temperatures, FAU-3.

T [°C]	T [K]	TOF [s ⁻¹]	rate [mol·g ⁻¹ ·s ⁻¹]	(T·R) ⁻¹ [(J·mol ⁻¹) ⁻¹]	ln rate	ln TOF
180	453	2.9·10 ⁻⁴	9.6·10 ⁻⁸	2.66·10 ⁻⁴	-16.16	-8.16
185	458	4.4·10 ⁻⁴	1.5·10 ⁻⁷	2.63·10 ⁻⁴	-15.72	-7.72
190	463	8.2·10 ⁻⁴	2.8·10 ⁻⁷	2.60·10 ⁻⁴	-15.10	-7.10
195	468	1.3·10 ⁻³	4.4·10 ⁻⁷	2.57·10 ⁻⁴	-14.65	-6.64
200	473	2.4·10 ⁻³	7.9·10 ⁻⁷	2.54·10 ⁻⁴	-14.05	-6.05

Dehydration of 1-methylcyclohexanol

**Figure S4.16.** Arrhenius-plot: 1-methylcyclohexanol (0.5 M) dehydration ($E_a \approx 116$ kJ/mol), MFI-45.**Table S4.17.** 1-methylcyclohexanol (0.5 M) dehydration rates at different reaction temperatures, MFI-45.

T [°C]	T [K]	TOF [s ⁻¹]	rate [mol·g ⁻¹ ·s ⁻¹]	(T·R) ⁻¹ [(J·mol ⁻¹) ⁻¹]	ln rate	ln TOF
80	353	5.1·10 ⁻³	1.8·10 ⁻⁶	3.41·10 ⁻⁴	-13.21	-5.28
90	363	1.7·10 ⁻²	5.9·10 ⁻⁶	3.31·10 ⁻⁴	-12.03	-4.10
100	373	4.9·10 ⁻²	1.8·10 ⁻⁵	3.22·10 ⁻⁴	-10.95	-3.02
110	383	1.2·10 ⁻¹	4.4·10 ⁻⁵	3.14·10 ⁻⁴	-10.04	-2.11
120	393	3.1·10 ⁻¹	1.1·10 ⁻⁴	3.06·10 ⁻⁴	-9.10	-1.17
130	403	6.9·10 ⁻¹	2.5·10 ⁻⁴	2.98·10 ⁻⁴	-8.30	-0.37

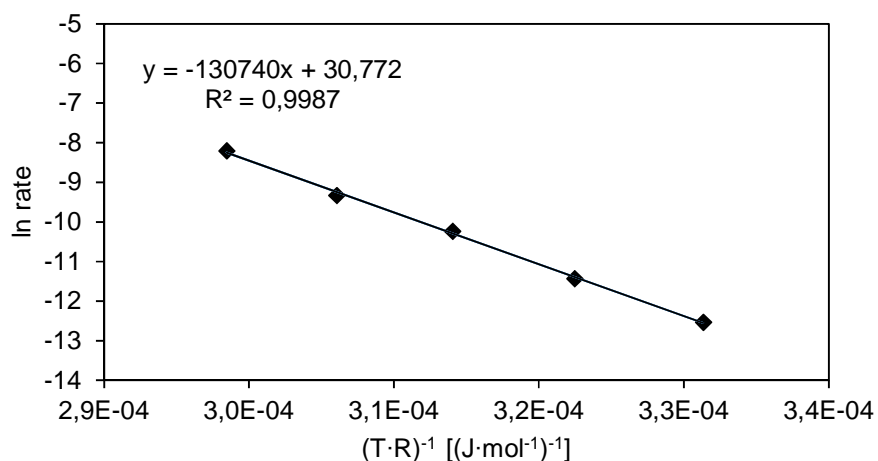


Figure S4.17. Arrhenius-plot: **1-methylcyclohexanol** (0.5 M) dehydration ($E_a \approx 131$ kJ/mol), **BEA-83**.

Table S4.18. **1-methylcyclohexanol** (0.5 M) dehydration rates at different reaction temperatures, **BEA-83**.

T [°C]	T [K]	TOF [s ⁻¹]	rate [mol·g ⁻¹ ·s ⁻¹]	(T·R) ⁻¹ [(J·mol ⁻¹) ⁻¹]	ln rate	ln TOF
90	363	3.0·10 ⁻²	3.6·10 ⁻⁶	3.31·10 ⁻⁴	-12.53	-3.50
100	373	9.1·10 ⁻²	1.1·10 ⁻⁵	3.22·10 ⁻⁴	-11.43	-2.40
110	383	3.0·10 ⁻¹	3.6·10 ⁻⁵	3.14·10 ⁻⁴	-10.23	-1.20
120	393	7.4·10 ⁻¹	8.9·10 ⁻⁵	3.06·10 ⁻⁴	-9.33	-0.30
130	403	2.3	2.7·10 ⁻⁴	2.98·10 ⁻⁴	-8.20	0.83

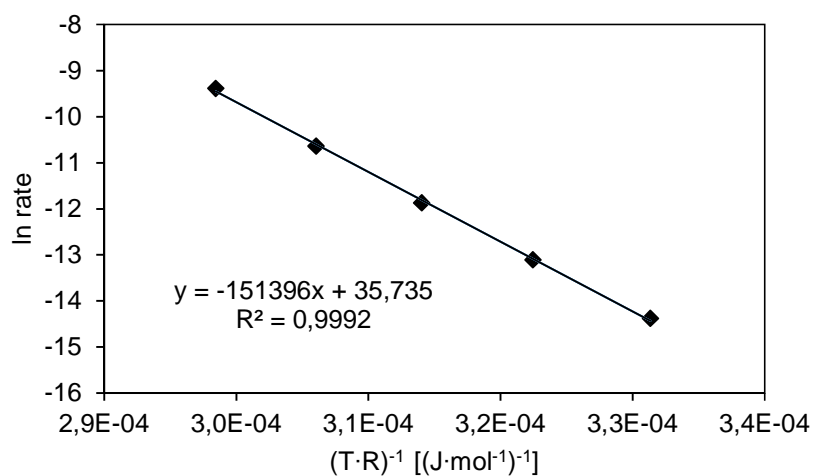
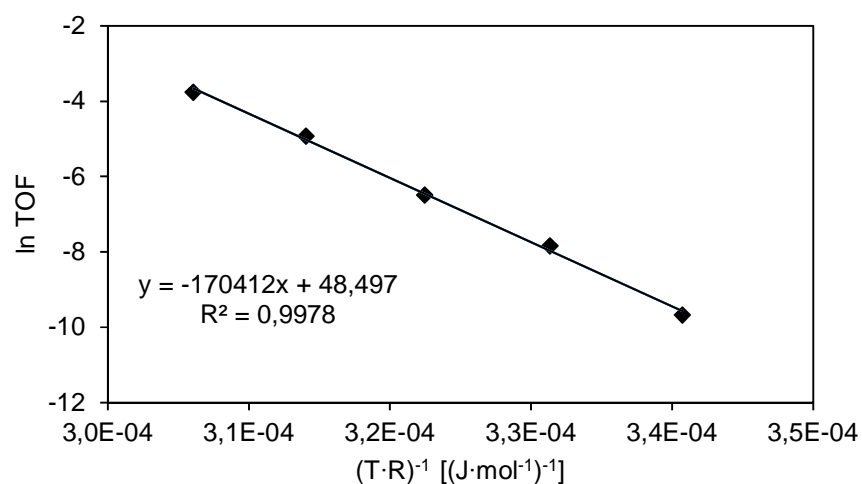


Figure S4.18. Arrhenius-plot: **1-methylcyclohexanol** (0.5 M) dehydration ($E_a \approx 151$ kJ/mol), **FAU-3**.

Table S4.19. 1-methylcyclohexanol (0.5 M) dehydration rates at different reaction temperatures, FAU-3.

T [°C]	T [K]	TOF [s ⁻¹]	rate [mol·g ⁻¹ ·s ⁻¹]	(T·R) ⁻¹ [(J·mol ⁻¹) ⁻¹]	ln rate	ln TOF
90	363	1.7·10 ⁻³	5.7·10 ⁻⁷	3.31·10 ⁻⁴	-14.38	-6.38
100	373	6.1·10 ⁻³	2.0·10 ⁻⁶	3.22·10 ⁻⁴	-13.11	-5.10
110	383	2.1·10 ⁻²	7.0·10 ⁻⁶	3.14·10 ⁻⁴	-11.87	-3.87
120	393	7.2·10 ⁻²	2.4·10 ⁻⁵	3.06·10 ⁻⁴	-10.64	-2.64
130	403	2.5·10 ⁻¹	8.4·10 ⁻⁵	2.98·10 ⁻⁴	-9.38	-1.38

**Figure S4.19.** Arrhenius-plot: 1-methylcyclohexanol (0.1 M) dehydration ($E_a \approx 170$ kJ/mol), H₃PO₄.**Table S4.20.** 1-methylcyclohexanol (0.1 M) dehydration rates at different reaction temperatures, H₃PO₄.

T [°C]	T [K]	rate [mol·s ⁻¹]	TOF [s ⁻¹]	(T·R) ⁻¹ [(J·mol ⁻¹) ⁻¹]	ln TOF
80	353	2.8·10 ⁻⁸	6.3·10 ⁻⁵	3.41·10 ⁻⁴	-9.67
90	363	1.6·10 ⁻⁷	4.0·10 ⁻⁴	3.31·10 ⁻⁴	-7.84
100	373	5.7·10 ⁻⁷	1.5·10 ⁻³	3.22·10 ⁻⁴	-6.49
110	383	2.5·10 ⁻⁶	7.3·10 ⁻³	3.14·10 ⁻⁴	-4.92
120	393	7.4·10 ⁻⁶	2.4·10 ⁻²	3.06·10 ⁻⁴	-3.75

Dehydration of 2-cyclohexylethanol

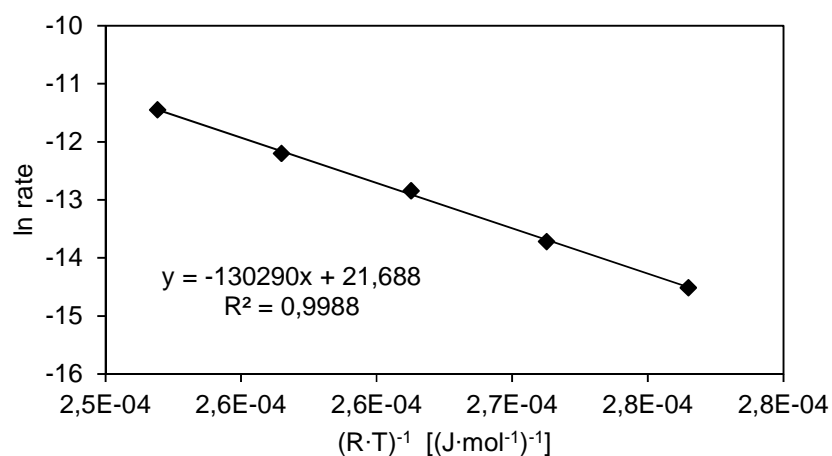


Figure S4.20. Arrhenius-plot: **2-cyclohexylethanol** (0.2 M) dehydration ($E_a \approx 130$ kJ/mol), **MFI-45**.

Table S4.21. **2-cyclohexylethanol** (0.2 M) dehydration rates at different reaction temperatures, **MFI-45**.

T [°C]	T [K]	TOF [s ⁻¹]	rate [mol·g ⁻¹ ·s ⁻¹]	(T·R) ⁻¹ [(J·mol ⁻¹) ⁻¹]	ln rate	ln TOF
160	433	1.39·10 ⁻³	5.00·10 ⁻⁷	2.78·10 ⁻⁴	-14.51	-6.58
170	443	3.07·10 ⁻³	1.11·10 ⁻⁶	2.72·10 ⁻⁴	-13.71	-5.79
180	453	7.39·10 ⁻³	2.66·10 ⁻⁶	2.66·10 ⁻⁴	-12.84	-4.91
190	463	1.41·10 ⁻²	5.06·10 ⁻⁶	2.60·10 ⁻⁴	-12.19	-4.26
200	473	2.97·10 ⁻²	1.07·10 ⁻⁵	2.54·10 ⁻⁴	-11.45	-3.52

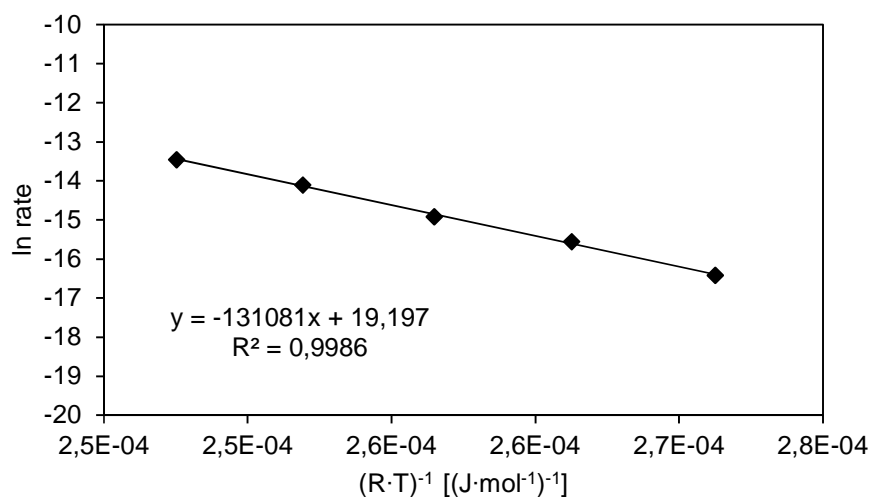
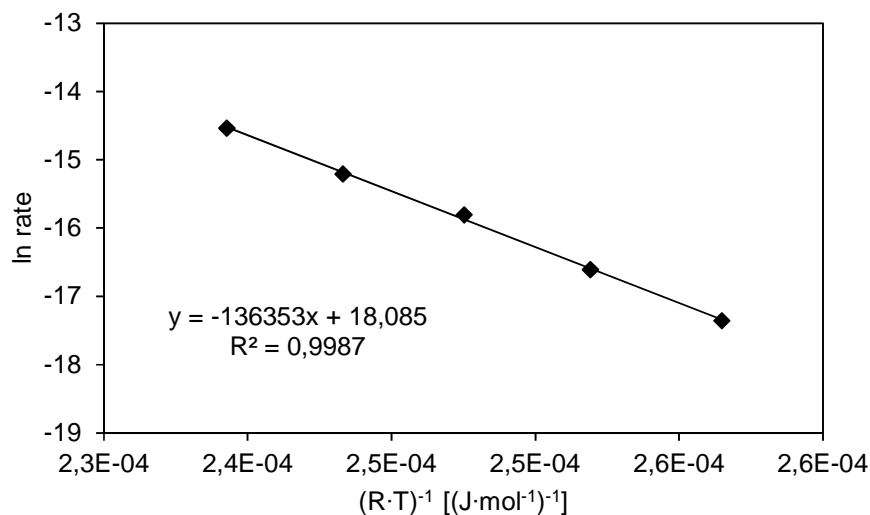


Figure S4.21. Arrhenius-plot: **2-cyclohexylethanol** (0.1 M) dehydration ($E_a \approx 131$ kJ/mol), **BEA-83**.

Table S4.22. 2-cyclohexylethanol (0.1 M) dehydration rates at different reaction temperatures, **BEA-83**.

T [°C]	T [K]	TOF [s ⁻¹]	rate [mol·g ⁻¹ ·s ⁻¹]	(T·R) ⁻¹ [(J·mol ⁻¹) ⁻¹]	ln rate	ln TOF
170	443	6.21·10 ⁻⁴	7.45·10 ⁻⁸	2.72·10 ⁻⁴	-16.41	-7.38
180	453	1.47·10 ⁻³	1.76·10 ⁻⁷	2.66·10 ⁻⁴	-15.55	-6.52
190	463	2.78·10 ⁻³	3.34·10 ⁻⁷	2.60·10 ⁻⁴	-14.91	-5.89
200	473	6.25·10 ⁻³	7.50·10 ⁻⁷	2.54·10 ⁻⁴	-14.10	-5.08
210	483	1.20·10 ⁻²	1.44·10 ⁻⁶	2.49·10 ⁻⁴	-13.45	-4.43

**Figure S4.22.** Arrhenius-plot: 2-cyclohexylethanol (0.1 M) dehydration ($E_a \approx 136$ kJ/mol), **FAU-3**.**Table S4.23.** 2-cyclohexylethanol (0.1 M) dehydration rates at different reaction temperatures, **FAU-3**.

T [°C]	T [K]	TOF [s ⁻¹]	rate [mol·g ⁻¹ ·s ⁻¹]	(T·R) ⁻¹ [(J·mol ⁻¹) ⁻¹]	ln rate	ln rate
190	463	8.67·10 ⁻⁵	2.91·10 ⁻⁸	2.60·10 ⁻⁴	-17.35	-9.35
200	473	1.84·10 ⁻⁴	6.15·10 ⁻⁸	2.54·10 ⁻⁴	-16.60	-8.60
210	483	4.10·10 ⁻⁴	1.38·10 ⁻⁷	2.49·10 ⁻⁴	-15.80	-7.80
220	493	7.43·10 ⁻⁴	2.49·10 ⁻⁷	2.44·10 ⁻⁴	-15.21	-7.20
230	503	1.45·10 ⁻³	4.87·10 ⁻⁷	2.39·10 ⁻⁴	-14.54	-6.53

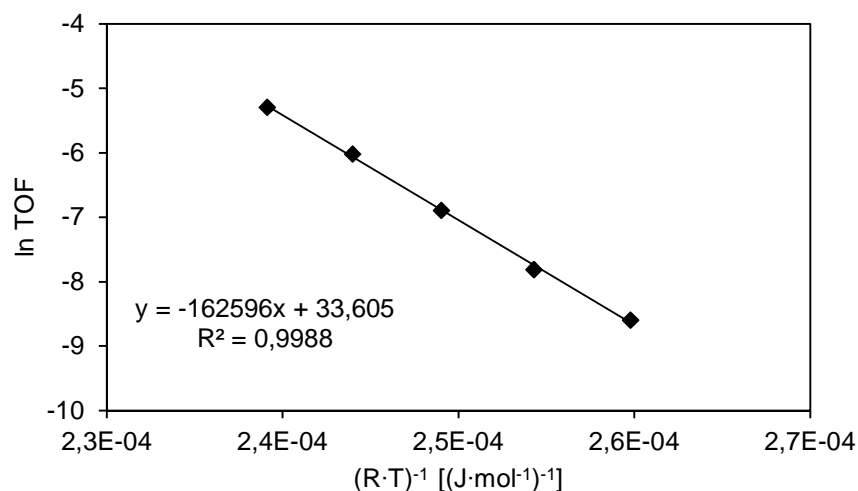


Figure S4.23. Arrhenius-plot: **2-cyclohexylethanol** (0.2 M) dehydration ($E_a \approx 163$ kJ/mol), H_3PO_4 .

Table S4.24. **2-cyclohexylethanol** (0.2 M) dehydration rates at different reaction temperatures, H_3PO_4 .

T [°C]	T [K]	n H ⁺ [mol]	TOF [s ⁻¹]	ln TOF	rate [mol·s ⁻¹]	(T·R) ⁻¹ [(J·mol ⁻¹) ⁻¹]
190	463	1.95·10 ⁻³	1.85·10 ⁻⁴	-8.59	7.22·10 ⁻⁸	2.60·10 ⁻⁴
200	473	1.76·10 ⁻⁴	4.06·10 ⁻⁴	-7.81	1.43·10 ⁻⁷	2.54·10 ⁻⁴
210	483	1.58·10 ⁻⁴	1.02·10 ⁻³	-6.89	3.22·10 ⁻⁷	2.49·10 ⁻⁴
220	493	1.42·10 ⁻⁴	2.44·10 ⁻³	-6.02	6.94·10 ⁻⁷	2.44·10 ⁻⁴
230	503	1.28·10 ⁻⁴	5.04·10 ⁻³	-5.29	1.29·10 ⁻⁶	2.39·10 ⁻⁴

Calculation of ΔH^\ddagger and ΔS^\ddagger

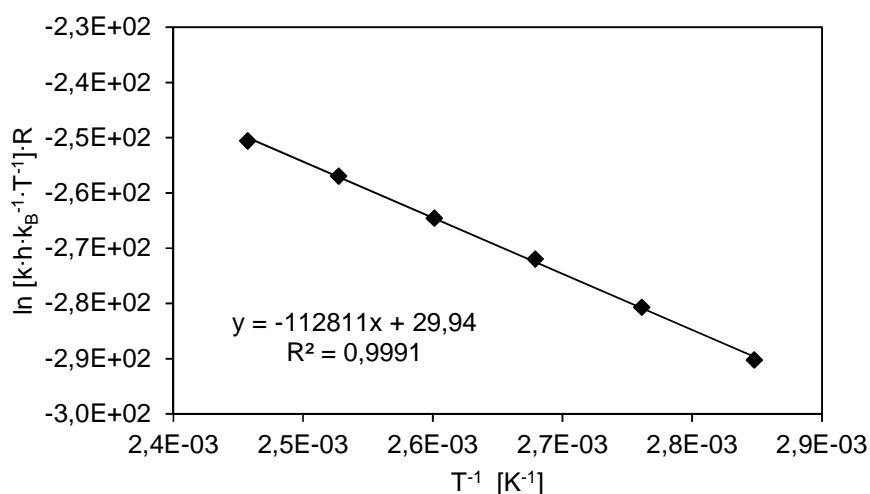
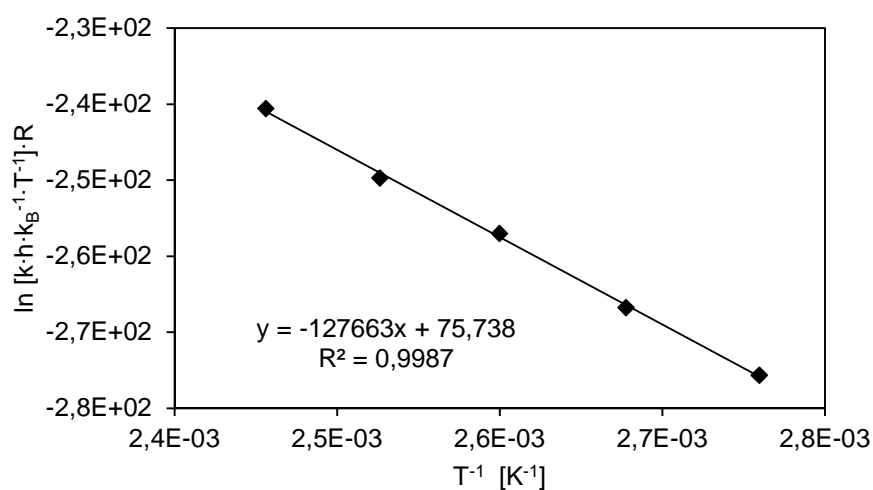


Figure S4.24. ΔH^\ddagger (113 kJ/mol) and ΔS^\ddagger (+30 J/(K·mol)) for **1-methylcyclohexanol** (0.5 M) dehydration, **MFI-45**.

Table S4.25. Kinetic data for **1-methylcyclohexanol** (0.5 M) dehydration, **MFI-45**.

T [°C]	rate [mol·g ⁻¹ ·s ⁻¹]	TOF [s ⁻¹]	T [K]	ln [k·h·k _B ⁻¹ ·T ⁻¹]·R	T ⁻¹ [K ⁻¹]
80	1.84·10 ⁻⁶	5.11·10 ⁻³	353	-290.2	2.83·10 ⁻³
90	5.94·10 ⁻⁶	1.65·10 ⁻²	363	-280.7	2.76·10 ⁻³
100	1.75·10 ⁻⁵	4.86·10 ⁻²	373	-271.9	2.68·10 ⁻³
110	4.38·10 ⁻⁵	1.22·10 ⁻¹	383	-264.5	2.61·10 ⁻³
120	1.12·10 ⁻⁴	3.11·10 ⁻¹	393	-256.9	2.55·10 ⁻³
130	2.48·10 ⁻⁴	6.89·10 ⁻¹	403	-250.5	2.48·10 ⁻³

**Figure S4.25.** ΔH^{\ddagger} (128 kJ/mol) and ΔS^{\ddagger} (+76 J/(K·mol)) for **1-methylcyclohexanol** (0.5 M) dehydration, **BEA-83**.**Table S4.26.** Kinetic data for **1-methylcyclohexanol** (0.5 M) dehydration, **BEA-83**.

T [°C]	rate [mol·g ⁻¹ ·s ⁻¹]	TOF [s ⁻¹]	T [K]	ln [k·h·k _B ⁻¹ ·T ⁻¹]·R	T ⁻¹ [K ⁻¹]
90	3.63·10 ⁻⁶	3.03·10 ⁻²	363	-275.6	2.75·10 ⁻³
100	1.09·10 ⁻⁵	9.08·10 ⁻²	373	-266.7	2.68·10 ⁻³
110	3.61·10 ⁻⁵	3.01·10 ⁻¹	383	-257.0	2.61·10 ⁻³
120	8.91·10 ⁻⁵	7.43·10 ⁻¹	393	-249.7	2.54·10 ⁻³
130	2.74·10 ⁻⁴	2.28	403	-240.6	2.48·10 ⁻³

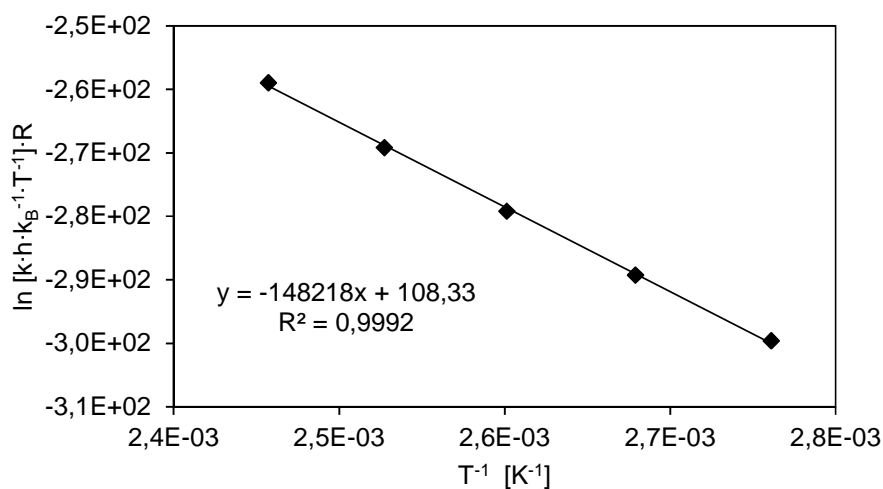


Figure S4.26. ΔH^{\ddagger} (148 kJ/mol) and ΔS^{\ddagger} (+108 J/(K·mol)) for **1-methylcyclohexanol** (0.5 M) dehydration, **FAU-3**.

Table S4.27. Kinetic data for **1-methylcyclohexanol** (0.5 M) dehydration, **FAU-3**.

T [°C]	rate [mol·g ⁻¹ ·s ⁻¹]	TOF [s ⁻¹]	T [K]	ln [k·h·k _B ⁻¹ ·T ⁻¹]·R	T ⁻¹ [K ⁻¹]
90	5.70·10 ⁻⁷	1.70·10 ⁻³	363	-299.6	2.76·10 ⁻³
100	2.04·10 ⁻⁶	6.07·10 ⁻³	373	-289.2	2.68·10 ⁻³
110	7.00·10 ⁻⁶	2.09·10 ⁻²	383	-279.1	2.61·10 ⁻³
120	2.40·10 ⁻⁵	7.16·10 ⁻²	393	-269.1	2.55·10 ⁻³
130	8.40·10 ⁻¹	2.51·10 ⁻¹	403	-258.9	2.48·10 ⁻³

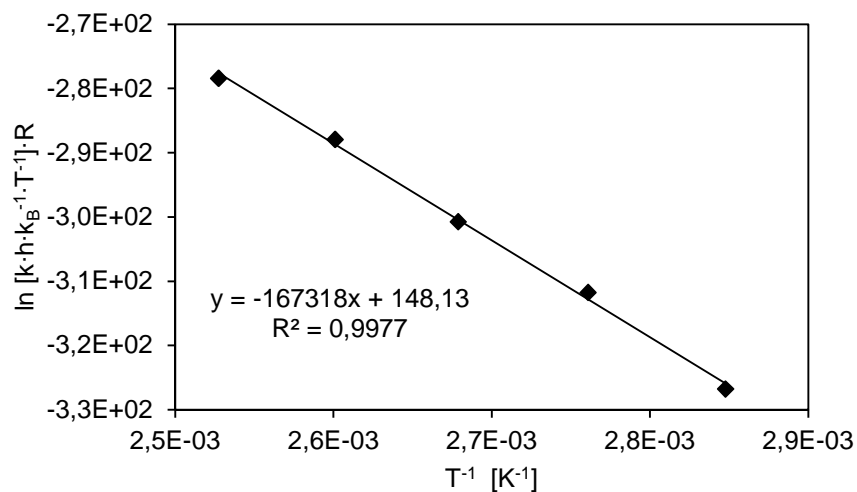
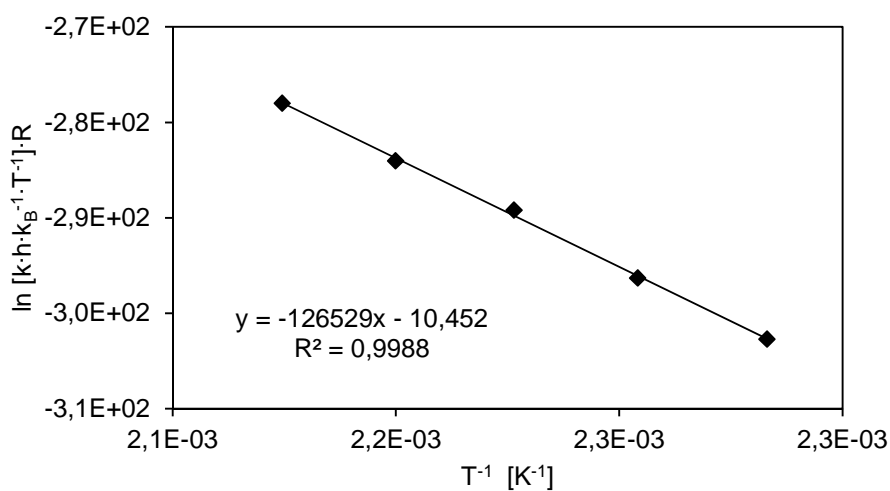


Figure S4.27. ΔH^{\ddagger} (167 kJ/mol) and ΔS^{\ddagger} (+148 J/(K·mol)) for **1-methylcyclohexanol** (0.1 M) dehydration, **H₃PO₄**.

Table S4.28. Kinetic data for **1-methylcyclohexanol** (0.1 M) dehydration, **H₃PO₄**.

T [°C]	rate [mol·s ⁻¹]	TOF [s ⁻¹]	T [K]	ln [k·h·k _B ⁻¹ ·T ⁻¹]·R	T ⁻¹ [K ⁻¹]
80	2.75·10 ⁻⁸	6.31·10 ⁻⁵	353	-326.7	2.83·10 ⁻³
90	1.60·10 ⁻⁷	3.95·10 ⁻⁴	363	-311.7	2.76·10 ⁻³
100	5.69·10 ⁻⁷	1.52·10 ⁻³	373	-300.7	2.68·10 ⁻³
110	2.51·10 ⁻⁶	7.28·10 ⁻³	383	-287.9	2.61·10 ⁻³
120	7.44·10 ⁻⁶	2.35·10 ⁻²	393	-278.4	2.55·10 ⁻³

**Figure S4.28.** ΔH^{\ddagger} (127 kJ/mol) and ΔS^{\ddagger} (-10 J/(K·mol)) for **2-cyclohexylethanol** (0.2 M) dehydration, **MFI-45**.**Table S4.29.** Kinetic data for **2-cyclohexylethanol** (0.2 M) dehydration, **MFI-45**.

T [°C]	rate [mol·g ⁻¹ ·s ⁻¹]	TOF [s ⁻¹]	T [K]	ln [k·h·k _B ⁻¹ ·T ⁻¹]·R	T ⁻¹ [K ⁻¹]
160	5.00·10 ⁻⁷	1.39·10 ⁻³	433	-302.7	2.31·10 ⁻³
170	1.11·10 ⁻⁶	3.07·10 ⁻³	443	-296.3	2.26·10 ⁻³
180	2.66·10 ⁻⁶	7.39·10 ⁻³	453	-289.2	2.21·10 ⁻³
190	5.06·10 ⁻⁶	1.41·10 ⁻²	463	-284.0	2.16·10 ⁻³
200	1.07·10 ⁻⁵	2.97·10 ⁻²	473	-278.0	2.11·10 ⁻³

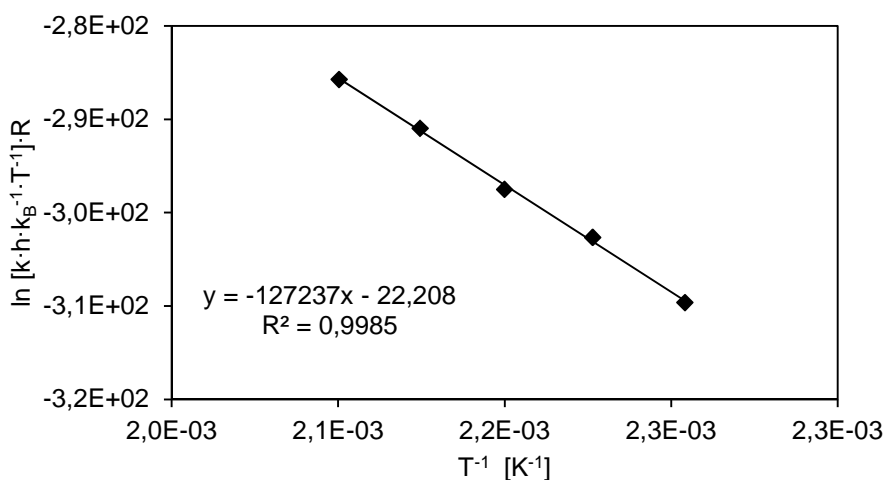


Figure S4.29. ΔH^{\ddagger} (127 kJ/mol) and ΔS^{\ddagger} (-22 J/(K·mol)) for **2-cyclohexylethanol** (0.1 M) dehydration, **BEA-83**.

Table S4.30. Kinetic data for **2-cyclohexylethanol** (0.1 M) dehydration, **BEA-83**.

T [°C]	rate [mol·g ⁻¹ ·s ⁻¹]	TOF [s ⁻¹]	T [K]	ln [k·h·k _B ⁻¹ ·T ⁻¹]·R	T ⁻¹ [K ⁻¹]
170	7.45·10 ⁻⁸	6.21·10 ⁻⁴	443	-309.6	2.26·10 ⁻³
180	1.76·10 ⁻⁷	1.47·10 ⁻³	453	-302.6	2.21·10 ⁻³
190	3.34·10 ⁻⁷	2.78·10 ⁻³	463	-297.5	2.16·10 ⁻³
200	7.50·10 ⁻⁷	6.25·10 ⁻³	473	-290.9	2.11·10 ⁻³
210	1.44·10 ⁻⁶	1.20·10 ⁻²	483	-285.7	2.07·10 ⁻³

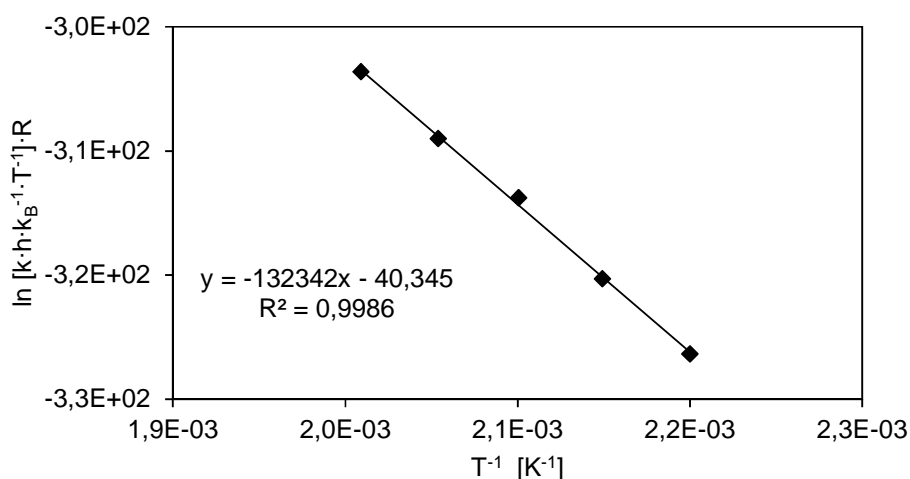
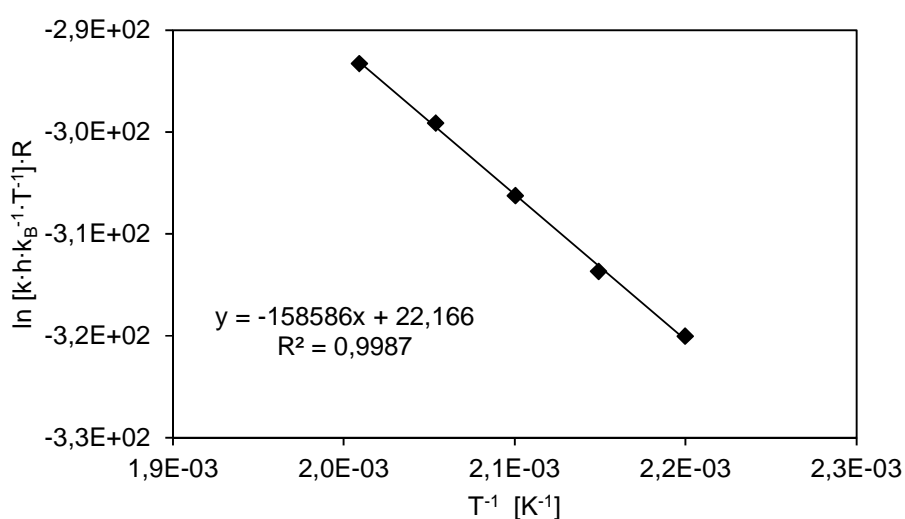


Figure S4.30. ΔH^{\ddagger} (132 kJ/mol) and ΔS^{\ddagger} (-40 J/(K·mol)) for **2-cyclohexylethanol** (0.1 M) dehydration, **FAU-3**.

Table S4.31. Kinetic data for **2-cyclohexylethanol** (0.1 M) dehydration, **FAU-3**.

T [°C]	rate [mol·g ⁻¹ ·s ⁻¹]	TOF [s ⁻¹]	T [K]	ln [k·h·k _B ⁻¹ ·T ⁻¹] ⁻¹ ·R	T ⁻¹ [K ⁻¹]
190	2.91·10 ⁻⁸	8.67·10 ⁻⁵	463	-326.2	2.16·10 ⁻³
200	6.15·10 ⁻⁸	1.84·10 ⁻⁴	473	-320.3	2.11·10 ⁻³
210	1.38·10 ⁻⁷	4.10·10 ⁻⁴	483	-313.8	2.07·10 ⁻³
220	2.49·10 ⁻⁷	7.43·10 ⁻⁴	493	-309.0	2.03·10 ⁻³
230	4.87·10 ⁻⁷	1.45·10 ⁻³	503	-303.6	1.99·10 ⁻³

**Figure S4.31.** ΔH^{\ddagger} (159 kJ/mol) and ΔS^{\ddagger} (+22 J/(K·mol)) for **2-cyclohexylethanol** (0.2 M) dehydration, **H₃PO₄**.**Table S4.32.** Kinetic data for **2-cyclohexylethanol** (0.2 M) dehydration, **H₃PO₄**.

T [°C]	rate [mol·s ⁻¹]	TOF [s ⁻¹]	T [K]	ln [k·h·k _B ⁻¹ ·T ⁻¹] ⁻¹ ·R	T ⁻¹ [K ⁻¹]
190	7.22·10 ⁻⁸	1.85·10 ⁻⁴	463	-320.2	2.16·10 ⁻³
200	1.43·10 ⁻⁷	4.06·10 ⁻⁴	473	-313.7	2.11·10 ⁻³
210	3.22·10 ⁻⁷	1.02·10 ⁻³	483	-306.2	2.07·10 ⁻³
220	6.94·10 ⁻⁷	2.44·10 ⁻³	493	-299.1	2.03·10 ⁻³
230	1.29·10 ⁻⁶	5.04·10 ⁻³	503	-293.2	1.99·10 ⁻³

5. Summary

The catalytic dehydration of substituted cyclohexanols (2-, 3-, 4-methylcyclohexanol, 2-, 4-ethylcyclohexanol and 2-propylcyclohexanol) was investigated in the presence of a MFI zeolite (Si/Al = 45) as well as a homogeneous acid (H_3PO_4). In experiments with pure *cis* and *trans* 2- and 4-methylcyclohexanol different dehydration reactivities of the isomers were identified.

Remarkable differences among the *cis* and *trans* isomers of 2-methylcyclohexanol were observed regarding the product distribution (1-methylcyclohexene (*Saytzeff*-product) and 3-methylcyclohexene (*Hofmann*-product)) and the activation parameters (E_a , $\Delta H^{\circ\ddagger}$ and $\Delta S^{\circ\ddagger}$). $^1\text{H-NMR}$ and GC-MS analysis gave further insights into the proceeding elimination mechanisms of the isomers of 2- and 4-methylcyclohexanol. It can be assumed that *cis* 2-methylcyclohexanol proceeds *via* a concerted elimination (E2), since no *trans* isomer was detected after the reaction. In case of *trans* 2-methylcyclohexanol as well as *cis* and *trans* 4-methylcyclohexanol as reactants the corresponding other isomer was formed with increasing conversion. The formation of both isomers is attributed to the nucleophilic attack of water to the carbocation intermediate *via* the E1 pathway. In all cases, the addition of H_2O to the double bond led to 1-methylcyclohexanol according to *Markovnikov's* rule (pathway *via* the most stable carbocation).

In agreement with racemic product distributions of reaction routes *via* carbenium ions, the E1 dehydration mechanism in case of *trans* 2-methylcyclohexanol showed a rather low product ratio (*Saytzeff/Hofmann*: 2/1). The concerted E2 dehydration led to a clear excess of the product with the higher substituted double bond (*Saytzeff/Hofmann*: 14/1). Furthermore, $\Delta S^{\circ\ddagger}$ proposed different reaction pathways. The stepwise E1 dehydration with a late and product-like transition state showed high entropy values ($\Delta S^{\circ\ddagger} = +42/+58 \text{ J}\cdot\text{K}^{-1}\cdot\text{mol}^{-1}$), whereas the early and reactant-like transition state of a concerted mechanism even led to negative entropic values ($\Delta S^{\circ\ddagger} = -8 \text{ J}\cdot\text{K}^{-1}\cdot\text{mol}^{-1}$) based on the complex arrangement of the proton, the alcohol and the abstracting base (water cluster). The E1 pathway for *trans* 2-methylcyclohexanol as well as *cis* and *trans* 4-methylcyclohexanol *via* the carbocation had a significant higher activation barrier of ca. $30 \text{ kJ}\cdot\text{mol}^{-1}$ in MFI zeolite ($E_a = 144 \text{ kJ}\cdot\text{mol}^{-1}$) compared to *cis* 2-methylcyclohexanol ($E_a = 116 \text{ kJ}\cdot\text{mol}^{-1}$).

In addition, the reactants 2- and 4-ethylcyclohexanol were investigated. The extension of the alkyl group led to different kinetic results for position 2. The trend of negative values for $\Delta S^{\circ\ddagger}$ was continued by the ethyl- and propyl-substituent ($\Delta S^{\circ\ddagger} = -25$ and $-43 \text{ J}\cdot\text{K}^{-1}\cdot\text{mol}^{-1}$). The complex

arrangement within the concerted mechanism of the *cis* isomer results in a loss of entropy by $-17/18 \text{ J}\cdot\text{K}^{-1}\cdot\text{mol}^{-1}$ for each further CH_2 -unit.

Moreover, the impact of the Brønsted acid site concentration was investigated on the different dehydration mechanisms. Based on previous results, two model compounds which follow different reaction pathways were identified. The dehydration of both isomers of 4-methylcyclohexanol proceed *via* a stepwise reaction pathway with a carbocation intermediate (E1), whereas *cis* 2-methylcyclohexanol is converted in a concerted way (E2). Various MFI zeolites of different Si/Al ratios (12, 15, 23, 32, 40, 45, 60 and 193) were investigated in the dehydration reaction of the two model compounds in aqueous phase. ^{27}Al -MAS-NMR and IR investigations qualitatively showed besides tetrahedrally also octahedrally coordinated aluminum ("extra-framework Al"). The latter was observed in considerable amounts in the two most acidic zeolite samples (Si/Al = 12 and 15) whereas in all other zeolites it was detected in negligible amounts.

These two catalysts showed different activation barriers and entropy values compared to all other samples. In case of (*cis*) 2-methylcyclohexanol the enthalpic barrier was ca. $10 \text{ kJ}\cdot\text{mol}^{-1}$ less ($\Delta H^{\ddagger} = 106 \text{ kJ}\cdot\text{mol}^{-1}$ and $\Delta S^{\ddagger} = -30/-39 \text{ J}\cdot\text{K}^{-1}\cdot\text{mol}^{-1}$) compared to zeolites with medium or high Si/Al ratios ($\Delta H^{\ddagger} = 116 \text{ kJ}\cdot\text{mol}^{-1}$ and $\Delta S^{\ddagger} = +2 - -19 \text{ J}\cdot\text{K}^{-1}\cdot\text{mol}^{-1}$). The activation barrier of *cis* and *trans* 4-methylcyclohexanol dehydration with the two most acidic zeolites was about $10 \text{ kJ}\cdot\text{mol}^{-1}$ higher ($\Delta H^{\ddagger} = 156/160 \text{ kJ}\cdot\text{mol}^{-1}$ and $\Delta S^{\ddagger} = +66/+77 \text{ J}\cdot\text{K}^{-1}\cdot\text{mol}^{-1}$) compared to the other MFI zeolites ($\Delta H^{\ddagger} = 146 \text{ kJ}\cdot\text{mol}^{-1}$ and $\Delta S^{\ddagger} = +48 - +60 \text{ J}\cdot\text{K}^{-1}\cdot\text{mol}^{-1}$). The influence of the octahedrally coordinated species was therefore inverse on the two dehydration mechanisms. After the removal of the extra-framework aluminum with ammonium hexafluorosilicate (AHFS) the effect on the activation barriers and ΔS^{\ddagger} disappeared. According to the observations it is assumed that the extra-framework aluminum species like AlOOH , AlO^+ or $\text{Al}(\text{OH})_3$ positively influences the concerted elimination mechanism by initiating the β -H abstraction. In case of the reaction pathway *via* carbocation, the electron accepting octahedrally coordinated aluminum has a negative effect on the electron deficient intermediate.

Moreover, the impact of the catalyst environment on the dehydration of an E1 (*trans* 2-methylcyclohexanol) and an E2 mechanism (*cis* 2-methylcyclohexanol) was investigated. Therefore, the dehydration reaction of both model compounds was examined by three zeolites of varying confinement (MFI, BEA and FAU). The Si/Al ratios of the zeolites were chosen according to the highest stability in hot liquid water (MFI: 45, BEA: 83 and FAU: 3). Additional investigations with less stable BEA and FAU zeolites (Si/Al = 15) revealed that the activation parameters are independent of the aluminum content.

In case of a stepwise dehydration *via* a carbocation species the decreasing zeolite confinement led to enormously higher enthalpic barriers (MFI: 140 → BEA: 178 → FAU: 185 kJ·mol⁻¹) as well as higher values for ΔS^{\ddagger} (MFI: +43 → BEA: +116 → FAU: +92 J·K⁻¹·mol⁻¹). Also for the concerted elimination the activation enthalpy (MFI: 112 → BEA: 137 → FAU: 141 kJ·mol⁻¹) as well as entropy (MFI: -8 → BEA: +56 → FAU: +42 J·K⁻¹·mol⁻¹) increased from the 10-membered to the 12-membered ring channel system. The different proceeding dehydration mechanism of *cis* and *trans* 2-McyOH are independent of the catalyst environment with constant differences in enthalpy ($\Delta\Delta H^{\ddagger} = 30 - 40$ kJ·mol⁻¹) and entropy of activation ($\Delta\Delta S^{\ddagger} = 50 - 60$ J·K⁻¹·mol⁻¹).

After a detailed analysis of secondary alcohols, the dehydration of a tertiary (1-methylcyclohexanol) and a primary alcohol (2-cyclohexylethanol) was investigated as a function of catalyst confinement. According to the high stability of a tertiary carbocation and the obtained high ΔS^{\ddagger} values an E1 dehydration pathway is highly likely in case of the tertiary alcohol. With increasing zeolite confinement the transition state is entropically constrained (H₃PO₄: +148 → FAU: +108 → BEA: +76 → MFI: +30 J·K⁻¹·mol⁻¹), while it is enthalpically stabilized (H₃PO₄: 167 → FAU: 148 → BEA: 128 → MFI: 113 kJ·mol⁻¹). The significantly higher dehydration rates in smaller zeolite channels are enthalpically favored. Based on the low stability of a primary carbocation and the low entropic values of the transition state a concerted E2 pathway for the dehydration of 2-cyclohexylethanol is assumed. The constant values for activation enthalpy in zeolite catalysis ($\Delta H^{\ddagger} = 127 - 132$ kJ·mol⁻¹) illustrate the absence of a positively charged intermediate. The higher TOFs in smaller zeolite pores are entropically favored in a concerted dehydration (FAU: -40 → BEA: -22 → MFI -10 J·K⁻¹·mol⁻¹).

6. Zusammenfassung

Die katalytische Dehydratisierung von substituierten Cyclohexanolen (2-, 3-, 4-Methylcyclohexanol, 2-, 4-Ethylcyclohexanol und 2-Propylcyclohexanol) wurde in der Anwesenheit eines MFI Zeoliths (Si/Al = 45) und einer homogenen Säure (H₃PO₄) untersucht. In Experimenten mit reinen *cis* und *trans* Isomeren von 2- und 4-Methylcyclohexanol wurden verschiedenen Reaktivitäten in der Dehydratisierung erkannt.

Es wurden bemerkenswerte Unterschiede zwischen den *cis* und *trans* Isomeren von 2-Methylcyclohexanol hinsichtlich der Produktverteilung (1-Methylcyclohexen (*Saytzeff*-Produkt) und 3-Methylcyclohexen (*Hofmann*-Produkt)) und der Aktivierungsparameter (E_a , ΔH^{\ddagger} und ΔS^{\ddagger}) beobachtet. ¹H-NMR und GC-MS Auswertungen gaben weitere Einblicke in die ablaufenden Eliminierungsmechanismen der Isomere von 2- und 4-Methylcyclohexanol. Man kann davon ausgehen, dass *cis* 2-Methylcyclohexanol über eine konzertierte Eliminierung (E2) verläuft, da kein *trans* Isomer nach der Reaktion beobachtet wurde. Für die Substrate *trans* 2-Methylcyclohexanol ebenso wie für *cis* und *trans* 4-Methylcyclohexanol entstand das jeweils andere Isomer mit fortschreitendem Umsatz. Es wird angenommen, dass die Bildung beider Isomere eine Konsequenz des nucleophilen Angriffs von Wasser an das Carbokation-Intermediat über den E1 Reaktionspfad ist. In allen Fällen führte die Addition von H₂O an die Doppelbindung zu 1-Methylcyclohexanol, gemäß der *Markovnikov*-Regel (Reaktionspfad über das stabilste Carbeniumion).

In Übereinstimmung mit racemischen Produktverteilungen von Reaktionswegen über Carbeniumionen, zeigte der E1 Dehydratisierungsmechanismus im Falle von *trans* 2-Methylcyclohexanol ein eher niedriges Produktverhältnis (*Saytzeff/Hofmann*: 2/1). Die konzertierte E2 Dehydratisierung führte zu einem klaren Überschuss des Produktes mit der höher substituierten Doppelbindung (*Saytzeff/Hofmann*: 14/1). Desweiteren verwies ΔS^{\ddagger} auf verschiedene Reaktionspfade. Die schrittweise E1 Dehydratisierung mit einem späten und produktähnlichen Übergangszustand zeigt hohe Entropiewerte ($\Delta S^{\ddagger} = +42/+58 \text{ J}\cdot\text{K}^{-1}\cdot\text{mol}^{-1}$), während der frühe und substratähnliche Übergangszustand des konzertierten Mechanismus sogar zu negativen Entropiewerten ($\Delta S^{\ddagger} = -8 \text{ J}\cdot\text{K}^{-1}\cdot\text{mol}^{-1}$), aufgrund der hoch strukturierten Anordnung von Proton, Alkohol und Base (Wassercluster), führte. Der E1 Reaktionspfad für *trans* 2-Methylcyclohexanol sowie *cis* und *trans* 4-Methylcyclohexanol über das Carbokation hat eine deutlich höhere Aktivierungsbarriere von ungefähr $30 \text{ kJ}\cdot\text{mol}^{-1}$ im MFI Zeolith ($E_a = 144 \text{ kJ}\cdot\text{mol}^{-1}$), verglichen mit *cis* 2-Methylcyclohexanol ($E_a = 116 \text{ kJ}\cdot\text{mol}^{-1}$).

Zusätzlich wurden die Substrate 2- und 4-Ethylcyclohexanol untersucht. Die Verlängerung der Alkylgruppe führte für Position 2 zu unterschiedlichen kinetischen Resultaten. Der Trend der negativen Werte für ΔS^{\ddagger} wurde durch den Ethyl- und Propylsubstituenten fortgesetzt ($\Delta S^{\ddagger} = -25$ und $-43 \text{ J}\cdot\text{K}^{-1}\cdot\text{mol}^{-1}$). Die hoch strukturierte Anordnung im konzertierten Mechanismus des *cis* Isomers bewirkt eine Entropieverringerng von $-17/18 \text{ J}\cdot\text{K}^{-1}\cdot\text{mol}^{-1}$ für jede weitere CH_2 -Einheit.

Zudem wurde der Einfluss der Brønsted-Säurezentrenkonzentration auf die unterschiedlichen Dehydratisierungsmechanismen untersucht. Mit den Ergebnissen des vorherigen Kapitels wurden zwei Modellverbindungen identifiziert, welche über verschiedene Reaktionspfade umgesetzt werden. Die Dehydratisierung beider Isomere von 4-Methylcyclohexanol verläuft entlang eines schrittweisen Reaktionspfades über eine Carbokation-Zwischenstufe (E1), während *cis* 2-Methylcyclohexanol konzertiert umgesetzt wird (E2). Zahlreiche MFI Zeolithe mit unterschiedlichen Si/Al-Verhältnissen (12, 15, 23, 32, 40, 45, 60 und 193) wurden bei der Dehydratisierung der beiden Modellverbindungen in wässriger Phase untersucht. ^{27}Al -MAS-NMR und IR Untersuchungen zeigten qualitativ neben tetraedrisch auch oktaedrisch koordiniertes Aluminium („extra-framework Al“). Letzteres wurde in beachtenswerten Mengen in den sauersten Zeolithen (Si/Al = 12 und 15) gefunden, während es in allen anderen Zeolithen in vernachlässigbaren Mengen detektiert wurde.

Diese zwei Proben zeigten unterschiedliche Aktivierungsbarrieren und Entropiewerte verglichen mit allen anderen Proben. In der Umsetzung von *cis* 2-Methylcyclohexanol war die enthalpische Barriere ca. $10 \text{ kJ}\cdot\text{mol}^{-1}$ geringer ($\Delta H^{\ddagger} = 106 \text{ kJ}\cdot\text{mol}^{-1}$ und $\Delta S^{\ddagger} = -30/-39 \text{ J}\cdot\text{K}^{-1}\cdot\text{mol}^{-1}$) verglichen mit Zeolithen mittlerer oder höherer Si/Al-Verhältnisse ($\Delta H^{\ddagger} = 116 \text{ kJ}\cdot\text{mol}^{-1}$ und $\Delta S^{\ddagger} = +2 - -19 \text{ J}\cdot\text{K}^{-1}\cdot\text{mol}^{-1}$). Die Aktivierungsbarriere der Dehydratisierung von *cis* und *trans* 4-Methylcyclohexanol mit den zwei sauersten Zeolithen war ca. $10 \text{ kJ}\cdot\text{mol}^{-1}$ höher ($\Delta H^{\ddagger} = 156/160 \text{ kJ}\cdot\text{mol}^{-1}$ und $\Delta S^{\ddagger} = +66/+77 \text{ J}\cdot\text{K}^{-1}\cdot\text{mol}^{-1}$) im Vergleich zu anderen MFI Zeolithen ($\Delta H^{\ddagger} = 146 \text{ kJ}\cdot\text{mol}^{-1}$ und $\Delta S^{\ddagger} = +48 - +60 \text{ J}\cdot\text{K}^{-1}\cdot\text{mol}^{-1}$). Der Einfluss der oktaedrisch koordinierten Spezies wirkte somit invers auf die beiden Dehydratisierungsmechanismen. Nach dem Entfernen des „extra-framework“ Aluminiums mit Ammoniumhexafluorosilikat (AHFS) verschwand der Effekt auf die Aktivierungsbarrieren und ΔS^{\ddagger} . Gemäß den Beobachtungen wird angenommen, dass die „extra-framework“ Aluminiumspezies wie AlOOH , AlO^+ oder $\text{Al}(\text{OH})_3$ den konzertierten Eliminierungsmechanismus positiv durch die Initiierung der β -H Abstraktion beeinflusst. Im Falle des Reaktionspfades über das Carbokation hat das elektronenakzeptierende, oktaedrisch koordinierte Aluminium einen negativen Effekt auf die elektronendefizitäre Zwischenstufe.

Außerdem wurde der Einfluss der Katalysatorumgebung auf die Dehydratisierung eines E1 (*trans* 2-Methylcyclohexanol) und eines E2 Mechanismus (*cis* 2-Methylcyclohexanol) untersucht. Deshalb wurde die Dehydratisierung beider Modellverbindungen mit drei Zeolithen unterschiedlicher Gitterstruktur (MFI, BEA und FAU) getestet. Die Si/Al-Verhältnisse der Zeolithe wurden gemäß der höchsten Stabilität in heißem Wasser ausgewählt (MFI: 45, BEA: 83 und FAU: 3). Zusätzliche Untersuchungen mit weniger stabilen BEA und FAU Zeolithen (Si/Al = 15) zeigten, dass die Aktivierungsparameter unabhängig vom Aluminiumgehalt sind.

Im Falle einer schrittweisen Dehydratisierung über eine Carbokation-Spezies, führen die größeren Reaktionskanäle der Zeolithe sowohl zu deutlich höheren enthalpischen Barrieren (MFI: 140 → BEA: 178 → FAU: 185 kJ·mol⁻¹) als auch zu höheren Werten für ΔS^{\ddagger} (MFI: +43 → BEA: +116 → FAU: +92 J·K⁻¹·mol⁻¹). Auch im Falle der konzertierten Eliminierung erhöhte sich die Aktivierungsenthalpie (MFI: 112 → BEA: 137 → FAU: 141 kJ·mol⁻¹) und -entropie (MFI: -8 → BEA: +56 → FAU: +42 J·K⁻¹·mol⁻¹) von einem 10-Ring zum 12-Ring Kanalsystem. Die unterschiedlich verlaufenden Dehydratisierungsmechanismen von *cis* und *trans* 2-McyOH sind unabhängig von der Katalysatorumgebung mit konstanten Unterschieden in der Aktivierungsenthalpie ($\Delta\Delta H^{\ddagger} = 30 - 40$ kJ·mol⁻¹) sowie in der -entropie ($\Delta\Delta S^{\ddagger} = 50 - 60$ J·K⁻¹·mol⁻¹).

Nach einer detaillierten Analyse sekundärer Alkohole wurde die Dehydratisierung eines tertiären (1-Methylcyclohexanol) und eines primären Alkohols (2-Cyclohexylethanol) als Funktion der Katalysatorumgebung untersucht. Gemäß der hohen Stabilität eines tertiären Carbokations und den erhaltenen hohen ΔS^{\ddagger} Werten verläuft mit hoher Wahrscheinlichkeit eine E1 Dehydratisierung, im Falle des tertiären Alkohols. Mit abnehmenden Zeolithporenradien wird der Übergangszustand entropisch eingeschränkt (H₃PO₄: +148 → FAU: +108 → BEA: +76 → MFI: +30 J·K⁻¹·mol⁻¹), während dieser enthalpisch stabilisiert wird (H₃PO₄: 167 → FAU: 148 → BEA: 128 → MFI: 113 kJ·mol⁻¹). Die deutlich höheren Dehydratisierungsraten in kleineren Zeolithkanälen sind enthalpisch begünstigt. Aufgrund der der niedrigen Stabilität eines primären Carbokations und den geringen Entropiewerten des Übergangszustandes wird ein konzertierter E2 Reaktionspfad für die Dehydratisierung von 2-Cyclohexylethanol angenommen. Die konstanten Werte für die Zeolith-katalysierte Aktivierungsenthalpie ($\Delta H^{\ddagger} = 127 - 132$ kJ·mol⁻¹) verdeutlichen die Abwesenheit eines positiv geladenen Intermediates. Die höheren Wechselzahlen in kleineren Zeolithporen sind entropisch begünstigt in der konzertierten Dehydratisierung (FAU: -40 → BEA: -22 → MFI: -10 J·K⁻¹·mol⁻¹).

7. List of publications

Journal contributions

“Hydronium ion catalyzed elimination pathways of substituted cyclohexanols”, P. H. Hintermeier, S. Eckstein, M. V. Olarte, D. M. Camaioni, E. Baráth, J. A. Lercher; ready for submission.

“Influence of acid site concentration and extra-framework aluminum in MFI zeolites on aqueous phase dehydration”, P. H. Hintermeier, S. Eckstein, Y. Liu, E. Baráth, J. A. Lercher; in preparation.

“Impact of confinement on aqueous phase dehydration of substituted cyclic alcohols”, P. H. Hintermeier, S. Eckstein, E. Baráth, J. A. Lercher; in preparation.

Oral presentations

P. H. Hintermeier, S. Eckstein, Y. Liu, E. Baráth, J. A. Lercher „*Zeolite catalyzed dehydration of cyclic alcohols in aqueous phase*“, 29. Deutsche Zeolith-Tagung, **2017**, Frankfurt am Main.

Poster presentations

P. H. Hintermeier, S. Eckstein, Y. Liu, E. Baráth, J. A. Lercher „*Aqueous phase dehydration of substituted cyclohexanols*“ (Poster Prize Winner), 50. Jahrestreffen Deutscher Katalytiker, **2017**, Weimar.

P. H. Hintermeier, S. Eckstein, F. M. Kirchberger, E. Baráth, J. A. Lercher „*Catalytic upgrading of pyrolysis bio-oil in aqueous phase – Deoxygenation of hydrogenated phenol derivatives*“, 49. Jahrestreffen Deutscher Katalytiker, **2016**, Weimar.

P. H. Hintermeier, S. Eckstein, E. Baráth, J. A. Lercher „*Zeolite catalyzed aqueous phase upgrading of pyrolysis oil*“, 27. Deutsche Zeolith-Tagung, **2015**, Oldenburg.

8. Curriculum vitae

Name: Peter Heinrich Hintermeier

Birth: 21.02.1987, Altötting

Citizenship: German

Education

- Since 11/2013 PhD candidate
Supervisor: Prof. Dr. Johannes A. Lercher
Lehrstuhl für Technische Chemie II
Technische Universität München
- 03/2016 – 04/2016 Free-lance lecturer
“Reaction Engineering and Catalysis”
TUM Asia, Singapore
- 10/2011 – 09/2013 Master of Science Chemistry
Subjects: Chemical Reaction Engineering and Organic Chemistry
Thesis: *“Influence of acid strength and localization of acid sites on catalytic cracking of 1-pentene”*
Technische Universität München
- 10/2008 – 09/2011 Bachelor of Science Chemistry
Thesis: *“Structural and mechanistic investigations on nickel catalysts”*
Technische Universität München
- 09/1998 – 06/2007 Abitur
Subjects: English, Economics and Law, Chemistry and Mathematics
Maria-Ward-Gymnasium, Altötting

Statutory declaration

I declare that I have authored this thesis independently and that I have solely used the declared (re)sources and that I have marked all material, which has been quoted either literally or by content from the used sources. At the beginning of each chapter all collaborators are named and their specific contribution is addressed.
